The fabrication of PLGA-Fe$_3$O$_4$-magnetic nanoparticles for targeted delivery of γ-secretase inhibitors to vascular stents

A dissertation submitted for the degree of PhD

by Roa Bashmail MSc.

Under the supervision of

Prof. Paul A. Cahill

March 2019

Vascular Biology & Therapeutics Lab

School of Biotechnology

Faculty of Science and Healthy

Dublin City University, Dublin 9, Ireland

Declaration

I hereby certify that this material, which I now submit for assessment on the programme of study leading to the award of PhD is entirely my own work, and that I have exercised reasonable care to ensure that the work is original, and does not to the best of my knowledge breach any law of copyright, and has not been taken from the work of others save and to the extent that such work has been cited and acknowledged within the text of my work.

Signed :

I.D. No: 13210189

Date: 29.3.2019

Dedication

This thesis is dedicated to my parents.

For Khalid Bashmail who taught me that '*never give up no matter what you can do it'*, and Fatimah Bashmail who reminded me that '*Patience is always the secret behind any successes"*.

Acknowledgements

First and foremost, I would like to express my sincere gratitude to Professor Paul Cahill for going beyond the call of any supervisor in providing continuous support, motivation, guidance and enormous knowledge throughout this whole process.

Next, I would like to thank the Vascular Biology and Therapeutics lab members in past and present. Particularly, Joseph Mackle, Dorota Kozlowska, Emma Fitzpatrick, Eimear Kennedy, Gillian Casey and Roya Hakimjavadi (along with Paul Cahill) for educating me nearly everything. To my colleague Claire Molony who a genuine friend to me was, thanks for always answering my questions. Thanks to Abi Olayinkai, who was and still there for me always, I am so grateful to you! Many thanks to Mariana Di Luca for always helping and solving problems. I am also grateful to the new students Eoin Corcoran, Denise Burtenshaw, Suzan Harman ,Yusof Gusti and Hissa bin Aqeel for their help, support and understanding with me through my last period!

I would like to acknowledge my brother Ahmed and my sisters; Reem, Rana and Ragad, also my relatives Hanan and Samar Bashmail for their compassion understanding and love they gave me through my difficult times.

I have special thanks to the people who supported me psychologically during my low moments, Hajer Salem and Dr Mohamd Alahmadi thanks for your massive support that gave me the courage to go until this point.

Lastly, I would like to thank my parents again for the love and support they gave me through my journey.

Table of Contents

Chapter 1

Introduction

Chapter 2 Materials & Methods

Chapter 3

The effects of gamma-secretase inhibitors (GSI's) on vascular smooth muscle and mesenchymal stem cell growth

Chapter 4
The effect of gamma-secretase inhibitors on myogenic differentiation of vascular stem cells

Chapter 5
Fabrication, characterisation and drug release kinetics of Fe$_3$O$_4$ PLGA-PVA magnetic nanoparticles

List of figures

List of Tables

List of Abbreviations

BMS	Bare Metal Stent
BSA	Bovine Serum Albumin
CAD	Coronary Artery Disease
cDNA	complementary Deoxyribose Nucleic Acid
Cnn1	Calponin1
CVD	Cardiovascular Disease
CO$_2$	Carbon dioxide
d.nm	diameter in nanometers
DAPI	4,6-diamidino-2-phenylindole
DAPT	N-[N-(3,5-Difluorophenacetyl)-L-alanyl]-S-phenylglycine t-butyl ester
DCM	Dichloromethane
ddSMC	De-differentiated SMC
DEPC	Diethylpyrocarbonate
DES	Drug-eluting stent
DLS	Dynamic Light Scattering
DM	Dulbecco's Modified Essential Medium
DMSO	Dimethylsulfoxide
DNA	Deoxyribose Nucleic Acid
dSMC	Differentiated SMC
EMEM	Eagle's Minimum Essential Medium
FACS	Fluorescence-activated cell sorting
FBS	Fetal Bovine Serum
Fc	fragment crystallizable
Fe$_3$O$_4$	Iron-oxide
FITC	Fluorescein Isothiocyanate
GSIs	Gamma Secretase inhibitors
hESCs	Human embryonic stem cells

HPLC	High-Performance Liquid Chromatography
Hes	Hairy enhancer of split
Hey	Hairy enhancer of split related with YRPW motif
ICC	Immunocytochemistry
IgG	Immunoglobulin
IMT	Intimal medial thickening
iPSC	induced Pluripotent Stem Cells
ISR	In-stent restenosis
Jag-1	Jagged ligand 1
MEM	Minimum Essential Medium
mRNA	messenger RNA
MNPs	Magnetic Nanoparticles
MSCs	Mesenchymal Stem Cells
MVSCs	Multipotent Vascular Stem Cells
Myh11	Myosin heavy chain 11
NICD	Notch Intracellular Domain
NP	Nanoparticle
PAH	Pulmonary arterial hypertension
PBS	Phosphate Buffered Saline
PCI	Percutaneous coronary intervention
PCR	Polymerase chain reaction
PCSK9	Proprotein convertase subtilisin/Kexin type 9
PDGF	Platelet-Derived Growth Factor
Pdi	Polydispersity index
PI	Propidium Iodide
PLGA	Poly (D,L-lactide-co-glycolide)
PS	Phosphatidylserine

PVA	Polyvinyl Alcohol
QRT-PCR	Quantitative Reverse Transcriptase Polymerase Chain Reaction
RNA	Ribonucleic Acid
RPM	Rotation per minute
RT	Reverse transcriptase
SEM	Scanning Electron Microscopy
SMA	Smooth Muscle Actin
SD	Standard deviation
SMCs	Smooth Muscle Cells
TEM	Transmission Electron Microscopy
TGFβ	Transforming Growth Factor Beta
UV	Ultra-violet
vSMCs	Vascular Smooth Muscle Cells

Units

°C	Degrees Celsius
cm	Centimetres
g	Grams
h	Human
M	Molar
m	Mouse
mg	Milligram
Min	Minute
mL	Millilitre
ng	Nanogram
nm	Nanometre
RPM	Revolutions per minute
x g	G force
μg	Microgram
μL	Microliter
μM	Micromoles

Presentations: Poster

Bashmail et al., (2015) The Generation of g-secretase inhibitor-loaded PLGA-Fe_3O_4-Magnetic Nanoparticles Research day, School of Biotechnology, DCU, Dublin Ireland.

Bashmail et al., (2018) The Generation of g-secretase inhibitor-loaded PLGA-Fe_3O_4-Magnetic Nanoparticles. Vascular Discovery: From Genes to Medicine 2018 Scientific Sessions San Francisco, California. ATVB 2018.

Bashmail et al., (2018) The Generation of g-secretase inhibitor-loaded PLGA-Fe_3O_4-Magnetic Nanoparticles. 21St Annual Meeting of the Scottish Cardiovascular Forum, Trinity College, DCU, Dublin Ireland.

Conference Presentations

Bashmail R et al., (2014) Generation of χ-secretase inhibitor-loaded PLGA-FE3o4 magnetic nanoparticles. Heart Mar 2018, 104 (Suppl 4) A9 A10; DOI: 10.1136/heartjnl-2018-SCF.24.

Published abstracts

R Bashmail, N Mckenna, C O'Shea, R Hakimjavadi, C Molony, D. Kozlowska Cahill PA. Generation of γ-secretase Inhibitor-loaded PLGA-Fe3O4-Magnetic Nanoparticles. Arteriosclerosis, Thrombosis, and Vascular Biology 2018: 38 (Suppl_1), A716-A716

R. Bashmail, N. McKenna, C. O'Shea, R. Hakimjavadi, C. Molony, D. Kozlowska and P. A. Cahill, Heart, 2018, 104, A9–A10.

Papers in preparation

R. Bashmail, N. McKenna, C. O'Shea, R. Hakimjavadi, C. Molony, D. Kozlowska and P. A. Cahill. Generation of γ-secretase Inhibitor-loaded PLGA-Fe3O4-Magnetic Nanoparticles

R. Bashmail, R. Hakimjavadi, C. Molony, D. Kozlowska and P. A. Cahill. Magnetic nanoparticles and drug delivery to vascular stents. Review

Author: Roa Bashmail

Project Title: The fabrication of PLGA-Fe3O4- magnetic nanoparticles for targeted delivery of γ-secretase inhibitors to vascular stents

Cardiovascular disease is the number one killer in Ireland and the wider EU. A hallmark of the disease is the obstruction to blood flow due to the build-up of neointimal vascular smooth muscle (SMCs)-like cells within the vessel wall. Several groups have shown SMC-like cells play important roles in the pathophysiological processes of arteriosclerosis, atherosclerosis, and in-stent restenosis [ISR]. Our lab and others have shown a putative role for re-capitulation of Notch signalling components in arteriosclerosis progression. Lately, multipotent vascular stem cells (MVSCs) have been isolated and shown to proliferate and differentiate into SMCs, causing vascular injury in animal models. Therefore, targeting these cells is an attractive therapeutic strategy for treating vascular remodelling disorders.

In-stent restenosis treatment options include percutaneous transluminal coronary angioplasty (PTCA) and intravascular stenting yet a significant number of stented vessels may become re-occluded due to ISR. While polymer-coated drug-eluting stents (DES) have significantly reduced the incidence of ISR, current DESs have limitations. This limitation can be overcome by combining magnetic targeting via a uniform field-induced magnetization effect and a biocompatible magnetic nanoparticle (MNP) formulation designed for efficient entrapment and delivery of a specific drug that targets resident multipotent vascular stem cells (MVSCs). Therefore, the overall aim of this thesis was to develop a method for targeting vascular stents using nanotechnology. Specifically, the aim was to (i) fabricate magnetic nanoparticles (MNP's) containing magnetite (Fe_3O_4) and functionalised with poly (DL-lactide-co-glycolide) polyvinyl alcohol [PLGA-PVA], (ii) characterise their functional properties, targeting to vascular stents and drug-release kinetics following the entrapment of two drugs, DAPT and Compound E, both of which are Ɣ-secretase inhibitors (GSI) of Notch target gene expression (iii) determine the effects of MNPs loaded with Ɣ-secretase inhibitors (DAPT and Compound E) on the growth and myogenic differentiation capacity of resident vascular stem cells under non-magnetic and magnetic conditions *in vitro.*

The DAPT-loaded MNPs had an average hydrodynamic diameter of 351 d.nm. Up to 68% and 98% of the drug was incorporated into MNPs after one week under magnetic

conditions. The Notch ligand, Jagged1 increased *Hey1* mRNA levels and promoted myogenic differentiation of MSCs *in vitro* by increasing SMC differentiation markers, myosin heavy chain 11 (Myh11) and calponin1 (CNN1) expression, respectively. This effect was significantly attenuated following treatment of cells with both MNP's loaded with DAPT and MNP's loaded with Compound E when compared to unloaded MNP's. These data suggest that Notch GSI loaded magnetic nanoparticles are functional at vascular stem cells *in vitro.*

Chapter 1

General Introduction

1. The Vasculature

The circulatory system consists of three independent systems that work together: the heart (cardiovascular); the lungs (pulmonary); and arteries, veins, coronary and portal vessels (system). The circulatory system as a whole is responsible for the flow of blood, nutrients, oxygen and other gases, and hormones to and from cells. The vasculature is considered one of the essential networks in the mammalian body. This is due to its formation in earliest stages of embryonic development, as primitive organs are first formed, and its role in the transfer of oxygen and nutrients and the removal of waste products from these early tissues. Understanding the development of the vascular system, as well as the signalling pathways responsible for vascular growth, is important as re-activation of these pathways can occur in cardiovascular disease (CVD). The vasculature refers to the arrangement and distribution of blood vessels throughout an organism. In accordance with this definition, there are different vasculatures corresponding to each organ, for example, the vasculature of the brain, lungs, etc (Mackay and Mensah 2004, Rossant and Howard 2002).

The blood from the heart is carried through the body by a complex network of blood vessels. The main artery is the aorta, which branches into other major arteries, which in turn take blood to different limbs and organs. These major arteries include the carotid artery, which takes blood to the brain; the brachial arteries, which take blood to the arms; and the thoracic artery, which takes blood to the thorax and then into the hepatic, renal, and gastric arteries for the liver, kidneys, and stomach respectively. The iliac artery takes blood to the lower limbs. The major arteries diverge into minor arteries, and then into smaller vessels called arterioles, to reach more deeply into the muscles and organs of the body (Charles Molnar 2015).

There are three distinct layers of the arterial wall: The Tunica Intima (innermost), the Tunica Media (middle), and the Tunica Adventitia (outermost) (Waugh and Grant 2007). The intimal layer is a lining of squamous endothelial cells and the extracellular matrix (collagen and proteoglycans). The Internal Elastic Lamina (IEL) separates the intimal layer from the medial layer. The medial layer is denser than the intimal layer and contains vascular smooth muscle cells (VSMCs) surrounded by elastin. The medial and adventitial layers are separated by the External Elastic Lamina (EEL) see (Figure 1.1.). The outer

adventitial layer covers the vessel in connective tissue with fibroblasts, vasa vasorum, pericytes and nerve endings (Waugh and Grant 2007).

All three of these layers are known to play a role in arteriosclerotic disease (Villablanca et al., 2010).
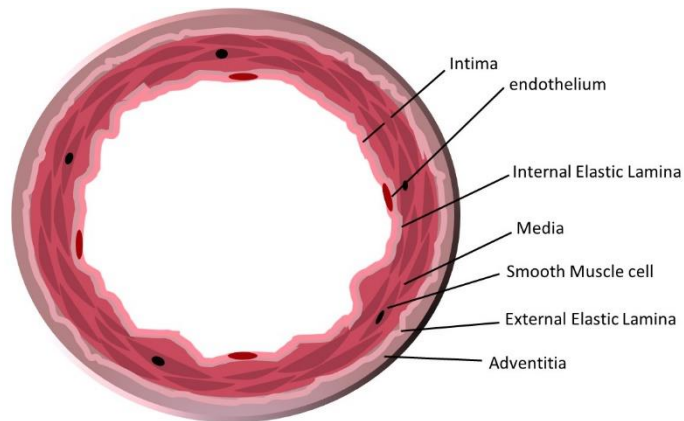
Figure 1.1. Anatomy of the vessel wall. Figure adapted from (Davis et al., 2003)
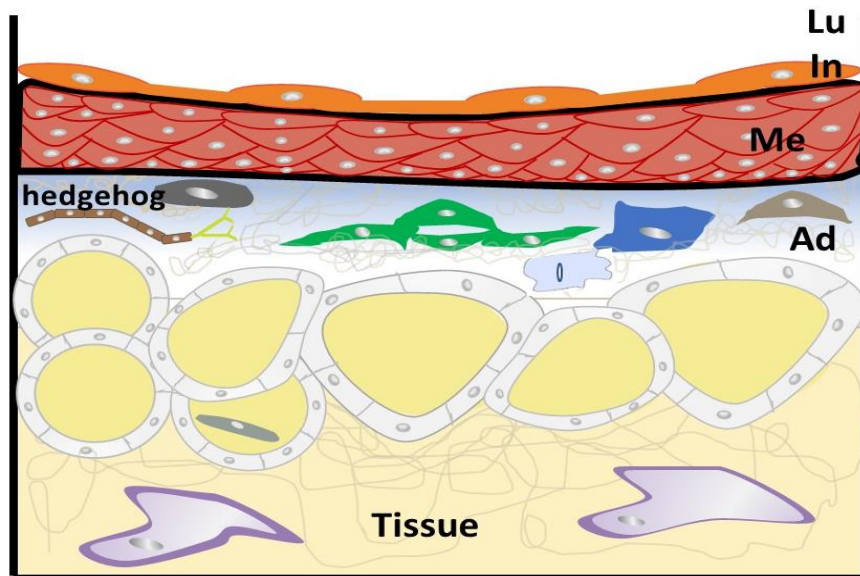
Figure 1.2. The arterial adventitia acts as the external connective tissue layer of the vessel. Lu indicates lumen; In, intima; Me, media; Ad, adventitia; Figure adapted from (Majesky et al., 2011)

Recent studies on the composition of the adventitial layer have revealed that in addition to fibroblasts and perivascular nerves, it also comprises macrophages (blue), mast cells (pale green), CD34/Sca1^{+} progenitor cells (dark green), T cells (grey) (Figure 1.2.), microvascular endothelial cells (light grey), pericytes (dark blue), and adipocytes

(yellow). In mice, these cells exist in a sonic hedgehog signalling domain (blue shaded) restricted to the adventitia (Majesky et al., 2011).

2.1 Cardiovascular Disease

Cardiovascular disease (CVD) is a class of diseases that affect the heart and blood vessels of an organism. Many of the mechanisms that underlie the wide spectrum of CVDs remain unknown. CVDs are the leading cause of global deaths in adults and the elderly. (WHO 2017, Naghavi et al., 2015, Everson-Rose and Lewis 2005).

Common CVDs include coronary heart disease, angina, heart attack, congenital heart disease, stroke, atherosclerosis, rheumatic heart disease, cardiomyopathies, cardiac arrhythmias, ischaemic stroke, heart failure, heart valve problems, cerebrovascular disease, peripheral arterial disease, rheumatic heart disease, deep vein thrombosis and pulmonary embolism.

During CVD progression, arteriosclerotic arteries become thicker and stiffer and thus restrict the passage of blood flow to organs and tissues. On the other hand, atherosclerosis, which is a specific type of arteriosclerosis, is caused by a build-up of fats and other molecules within the artery walls, also restricting the flow of blood. There are two major types of vessel remodelling; (i) symmetrical and (ii) asymmetrical thickening (Boudi et al., 2013).

2.2 CVD Statistics

By 2030 the number of deaths per year worldwide will rise to above 23.6 million. In addition to that, Current statistics from the United States reveal that 229 people die per every 100,000 because of CVD (Sans et al., 1997). CVD results in substantial disability and loss of productivity and contributes greatly to the escalating cost of health care, especially in the presence of an ageing population. One-third of adults throughout the world have been diagnosed with CVD, which makes it currently the greatest medical challenge to human health. The cost of the CVD represents a huge problem, with over US$863 billion spent in 2010 worldwide, with current estimates that this number will rise to $1 trillion by 2030 (WHO 2017).

2.3 Risk factors for cardiovascular disease

One type of CVDs is coronary heart disease. It is classified as an atherosclerotic disease of the blood vessels – a progressive thickening of the *intima* and *media* – due to a deposit of cholesterol and lipid molecules inside the walls of the vessels. Among major risk factors for coronary heart disease are high blood cholesterol levels, high blood pressure, excessive use of tobacco, and a blend of unhealthy diet and sedentary lifestyle, along with genetic risk factors (Mackay and Mensah 2004). It accounts for more than 50% of cardiovascular-related deaths (Kraemer et al., 2012). Stroke is considered another type of CVD, in which a lack of blood supply in a specific brain area can result in necrosis of the tissue. The symptoms of a stroke are highly dependent on the affected brain area and can affect the senses, short and long-term memory and even sleep patterns. Furthermore, among the most common symptoms of stroke is the paralysis of one side of the body. In the case of ischaemic stroke, there is a low blood supply to a specific brain area because of the obstruction of a blood vessel. This stroke usually results from an ischaemic thrombosis, which develops within an atherosclerotic lesion. Moreover, Peripheral Artery Disease (PAD) is caused by the presence of an atherosclerotic lesion in the peripheral circulation. The developmental process of PAD is like Coronary Artery Disease (CAD), and usually results from low oxygen delivery to the legs due to a decreased blood flow (Hirsch et al., 2001). (Kraemer et al., 2012). The primarily affected areas include the calves, but buttocks may also be impacted. In this case, a thickening of the artery walls results in a gradual narrowing of its upper and lower extremities. Specifically, the major cause of PAD is atherosclerosis, which is a progressive thickening of the *intima* and *media*, due to a deposit of cholesterol and lipid molecules inside the walls of the vessels (Lewis et al., 2016). A final type of CVDs is aortic aneurysm and dissection, which involves the dilation and even rupture of the aorta. Among the risk factors are increased age, long-standing high blood pressure, and the presence of Marfan's syndrome or other inherited disorders (Lewis et al., 2016).

3. Vascular remodelling

Vascular remodelling is a dynamic process of physical modification of the blood vessel wall. This includes modifications to four cellular processes: cell differentiation, cell death, cell movement, and the production of extracellular matrix (Renna et al., 2013). In general, vascular remodelling occurs as a result of a disease process that causes alterations in the cellular and non-cellular constituents of the vessel wall. These alterations result in deviations in cell growth and migration of vascular smooth (SMC)-like cells, dysfunction of the endothelial cell, progression of inflammation, and the deposition of extracellular matrix (Renna et al., 2013). The most common mechanism associated with vascular remodelling is cell growth and accumulation. In the beginning, the consequence of remodelling an artery might be adaptive; however, if this progresses too far, it has the opposite effect, leading to cardiovascular difficulties such as hypertension (Intengan and Schiffrin 2001).
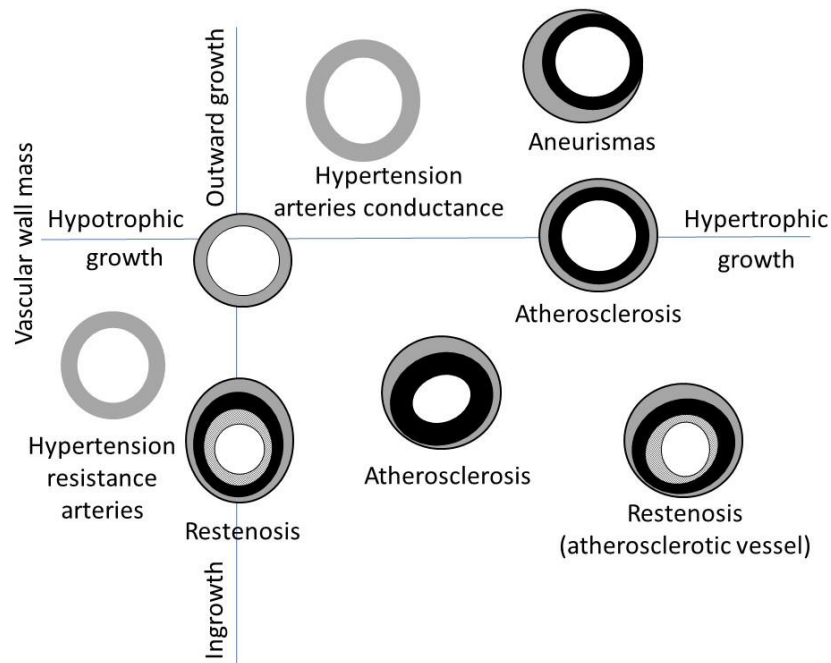
Figure 1.3. Diagram illustrating the structural modifications of the intima layer. intima layer helps the vascular wall remodelling. The outward remodelling compensates for the development of atherosclerotic plaque and through the stenosis. Figure adapted from (Renna et al., 2013)

3.1.1 Arteriosclerosis and Atherosclerosis

Arteriosclerosis is an irregular situation linked with stiffening and loss of elasticity in the walls of arteries and is broadly categorized as "hardening" of the arteries. Not all types of arteriosclerosis have the distinctive feature of fatty deposition. Atherosclerosis is a category of arteriosclerosis caused by lipid deposition in the arterial wall (Boudi et al., 2013). It is a systemic vascular disease distinguished by the presence of fatty acid deposits, cellular debris and cholesterol accumulation (ox-LDL), leading to stenosis of the vessel wall and resulting in an insufficient delivery of oxygenated blood to the heart, culminating in cardiac ischaemia (Owens et al., 2004) see (Figure 1.4.). Atherosclerosis is the primary cause of most cardiovascular events (Roger Véronique L et al., 2012).
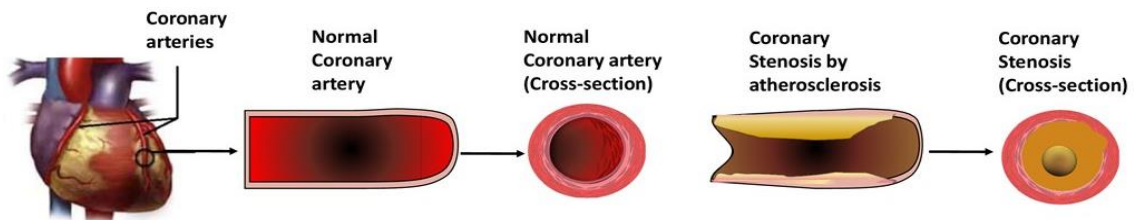
Figure 1.4. Coronary atherosclerosis and coronary stenosis. Figure adapted from (R. X. Yin et al., 2014).

The vessel wall is composed of the inner intima layer, the vascular media that contains the SMCs, and the outer adventitial surface that contains vasa vasorum, pericytes and nerve endings. Classically, VSMCs proliferation and migration from the media to the intima, through the internal elastic lamina, has been proposed to account for the development of arteriosclerotic lesions and atherosclerotic plaques, a situation facilitated in part by cytokines. During the atherosclerotic process, endothelial cells and/or additional circulating fats can contribute to the aggravation of the situation. This results in the growth of an initial atherosclerotic lesion, a fatty streak (aggregation of lipid-laden cells beneath the endothelium), expressive sub-endothelial build-up, and accumulation of lipids and LDL in the vessel wall. The atherosclerotic lesion (atheroma) is composed of the fatty streak, macrophages with T-cells, foam cells and lipid droplets. Ultimately, continuous inflammation will result in the translocation of leukocytes to the intima, via chemotactic stimuli by pro-inflammatory cytokines (Kalampogias et al., 2016).

After the formation of the lesion or plaque, various responses follow, such as vascular dilation, growth of a fibrous cap or lesion and vessel blockage. The latter results from thrombosis due to plaque rupture and platelet adhesion (Z. Tang et al., 2013). It is important to mention that the plaque is unstable, a phenomenon which easily leads to its rupture. The instability is due to the activation of specific cells in the core of the plaque by molecules and enzymes that degrade the cap. The latter is produced by immune cells that are found in large quantities in the thin and damaged fibrous cap (Hansson 2005). Both plaque rupture and endothelial deterioration are the primary sources of coronary thrombosis (Rajendran et al., 2013). Macrophages are important cellular elements of the inflammatory response prior to atherosclerosis. The mechanism of their action involves the presentation of scavenger receptors. This morphological change facilitates the conversion from macrophages to foam cells, resulting from the inability of macrophages to metabolize lipids. The mechanism that underlies this conversion results from the pickup of the lipoprotein particles and the produced foam cells continue to assemble in the intima. The outcome of a continuous inflammatory condition within the vessel wall will eventually cause the vessels to narrow or even block, and lead to atherosclerosis which comes after a complete loss of function (Kzhyshkowska et al., 2012).

3.1.2 Role of LDL in atherosclerosis

There is no doubt about the influence of risk factors such as ageing, gender, elevated blood pressure, smoking, high levels of Low-Density Lipoprotein (LDL) cholesterol, and low levels of High-Density Lipoprotein (HDL) cholesterol on CVD (Fruchart et al., 2004). In general, fatty streaks are the most common early signs of atherosclerotic lesions. Macroscopically, they appear as areas of yellow discolouration on the inner surface of the artery. They neither make protrusions in a significant manner into the arterial lumen nor affect blood flow. Even though it may sound surprising, fatty streaks exist as early as the age of 20 in most individuals. They are asymptomatic, occur in several locations throughout the vasculature, and may diminish over time (Nishizawa et al., 2014). During fatty steak formation, the accumulation of lipoproteins and further modifications are apparent. The role of the lipoproteins is to carry water-insoluble fats inside the bloodstream. The constituents of these particles are a lipid core which is surrounded by a hydrophilic phospholipid, a free molecule of cholesterol and apolipoproteins. The so-called apolipoproteins may present many classes of lipoprotein

molecules and can serve as the driving force of the system. The five principal classes of lipoproteins are classified by their relative densities, the lipids that they contain and finally their associated apolipoproteins. These classes are the chylomicrons, very-low-density lipoproteins (VLDL), intermediate-density lipoproteins (IDL), low-density lipoproteins (LDL) and high-density lipoproteins (HDL) (Ding et al., 2015). Since the endothelium cells can no longer function after been exposed to high shear stress. Their role as a barrier to the penetration of circulating lipoproteins is stopped, such lipoproteins can now enter the arterial wall. As a result, there is an increased endothelial permeability that favours the entrance of low-density lipoprotein (LDL) inside the intima, which can be further exacerbated by increased levels of circulating LDL concentration (such as in patients with hypercholesterolemia). In addition to dietary causes for elevated LDL concentrations, there are other factors including mutations of the LDL receptor and LDL accumulation which enhanced by the apolipoprotein B and Proprotein convertase subtilisin/Kexin type 9 (PCSK9) (protease with LDL receptor regulatory properties). When LDL enters the intima, it tends to accumulate and bind to various proteoglycans located at the extracellular matrix. With this 'trapping' mechanism, LDL manages to stay longer inside the vessel wall than usual, and lipoproteins can undergo chemical modifications that can facilitate the formation of atherosclerotic lesions. In cases of hypertension, this can further cause retention of lipoproteins inside the intima by increasing the production of LDL-binding proteoglycans by SMCs (C. Wu et al., 2012). Finally, oxidation of LDL is a major type of modification that occurs when LDL is inside the sub-endothelial space for extended periods of time. This can be the result of an action of oxygen species or pro-oxidant enzymes produced from activated endothelial cells or SMCs. Macrophages also produce oxygen species in this situation, after penetrating the vessel wall. Moreover, the microenvironment of the subendothelial space itself has the property of isolating oxidized LDL from antioxidants located in the plasma. Collectively, the biochemical changes of LDL can cause early alterations in the plaque and even contribute to long-term inflammatory mechanisms throughout the life of the plaque (Ding et al., 2015)

4. Neointimal Thickening

There are several important changes in the vascular wall during remodelling. For example, due to an increased deposition of collagen, the vascular wall becomes thicker, resulting in an increase in peripheral resistance and blood pressure (hypertension) (Renna et al., 2013).

There are numerous cell types present in atherosclerotic lesions, including macrophages, lymphocytes, neutrophils, endothelial cells, and vascular SMC-like cells that leads to intimal medial thickening (Owens et al., 2004). The origin of these neointimal cells continues to be a contentious issue (Herring et al., 2014). More than 20 years ago, several studies purported that differentiated SMCs (dSMCs) enter the cell cycle and begin to proliferate and migrate to the intima in response to arterial injury and become de-differentiated (Nemenoff et al., 2011). However, many recent studies have challenged this theory. This is because new studies have presented compelling evidence for a role of bone marrow-derived progenitors and resident vascular stem cells in contributing to the neointimal formation (Z. Tang, Wang, Yuan, Yan, Liu, Chu, Helms and Li 2012a). The probability of circulating and/or resident multipotent vascular stem cells derived from bone marrow may offer an increasing amount of diverse damaged cells including SMCs or SMC-like cells. Furthermore, as the main constituent of neointimal lesions and atherosclerotic plaques is de-differentiated VSMC-like cells proliferation, numerous sources of neointimal VSMC-like cells, such as resident progenitor cells, adventitial fibroblasts, blood and bone marrow-derived precursor cells, in addition to de-differentiated medial VSMCs have been reported (Moore and Tabas 2011).

Classically, differentiation of SMCs occurs in evolving organisms where multipotential cells attain distinct cell-specific features to be recognised from other cells (Owens et al., 2004). The de-differentiation of these cells during arteriosclerotic disease progression has many effects, including the reduction of protein expression, which is mandatory for the usual contractile process (Herring et al., 2014). To begin with, the remodelling of arteries in human cells suggests a remodelling of both the extracellular matrix and the attachment sites of extracellular–vascular SMC. This then results in the activation and the restructure of vascular SMCs due to adhesion molecules that attach to extracellular matrix components. These changes, in addition to the appearance of adhesion receptors, result in alterations in the connections between SMCs and matrix proteins and a general

9

reorganisation of SMCs and the vascular wall (Alexander and Owens 2012). Then SMCs begin to proliferate and migrate, with a direction from the media to the intima, in order to form a lesion, a procedure mainly provoked by endothelial-derived cytokines (H. Y. Park et al., 2014).

4.1 Smooth Muscle Cells

The main cell type within the tunica media of the blood vessel wall is the VSMC, the contractile component of the vessel wall (G. Wang et al., 2015). These cells are essential for regulating the flow and pressure of blood within the vascular system (Herring et al., 2014). SMCs play an important role in vascular development, including blood vessel morphogenesis, a process that involves a great degree of cell proliferation, migration, and deposition of extracellular matrix components. SMCs have many roles, one of which is maintaining the structural integrity of the vessel wall. Furthermore, these cells play a role in the adjustment of vascular tone, allowing them to control the pressure of the intravascular space and the perfusion of tissue (G. Wang et al., 2015). An intrinsic property of SMCs is that they are not considered terminally differentiated but instead may remain plastic. Specifically, the progression of vascular disease such as atherosclerosis results from an injury in response to extracellular signals and vascular interventions that lead to de-differentiation of SMCs (Herring et al., 2014). Furthermore, changes to the differentiated state of the VSMC is thought to be in part responsible for the accumulation of intimal SMCs. This accumulation leads to vessel obstruction, but also the expression of numerous proteases, inflammatory cytokines, and also the presentation of inflammatory cell markers, which contribute to inflammatory reactions, contractile protein expression and general contractility (Owens et al., 2004).

4.2 SMC-like pericytes

In atherosclerotic lesions, there is another group of cells termed as SMC-like pericytes, generated from dSMCs, resident vascular stem cells, or circulating bone-marrow-derived mesenchymal stem cells (MSCs). These cells may also lead to high-duration plasticity within the lesion (Alexander and Owens 2012).

As mentioned earlier, the SMCs migrate and proliferate to create the neointimal layer by migrating into the intima. In cases of balloon angioplasty and stent deployment, these

cells can lead to in-stent restenosis [ISR]. To prevent the formation of the coronary intimal hyperplasia, which results from coronary stenosis, it is important for the accumulation of these SMC-like cells to be inhibited. The process behind their proliferation involves N-cadherin, a specific marker of myofibroblasts (Hiruta et al., 2013).

4.3 Stem cells

Stem cells are found in the human embryo, as well as in adult animals. These cells are exclusive cell populations that have the capability to experience either self-renewal or differentiation (Kovtonyuk et al., 2016).

The classification of stem cells depends on the probability of their differentiation. The classifications are totipotent, pluripotent, or multipotent. Totipotent cells can create all tissues in the body. Pluripotent cells have the ability to generate most sorts of cells in the organism, but not all. Finally, stem cells that can only produce a restricted lineage of cells are called multipotent stem cells (Kovtonyuk et al., 2016). The broader categorization of native stem cells includes four distinct groups: adult stem cells, foetal stem cells, embryonic stem cells, and nuclear transplant stem cells (Kovtonyuk et al., 2016).

One example of adult stem cells is resident stem cells that are in general ready to appropriately respond to an inductive stimulus in order to regenerate tissue. The fundamental properties of the stem cells are that they keep their ability to divide throughout the life of the organism and produce new cells. With this pattern, blood vessel stem cells are able to produce blood vessels, but because of certain restrictions, there is no possibility of their giving rise to other cell types (Kovtonyuk et al., 2016).

Furthermore, the presence of adult stem cells in the blood vessels is of paramount importance for the proper function and regeneration of the organism. Blood vessels primarily distribute oxygen, nutrients, hormones and immune cells throughout the organism. It follows that continuous cell death and recovery cycle is necessary for maintaining these significant processes (Raiser et al., 2008).
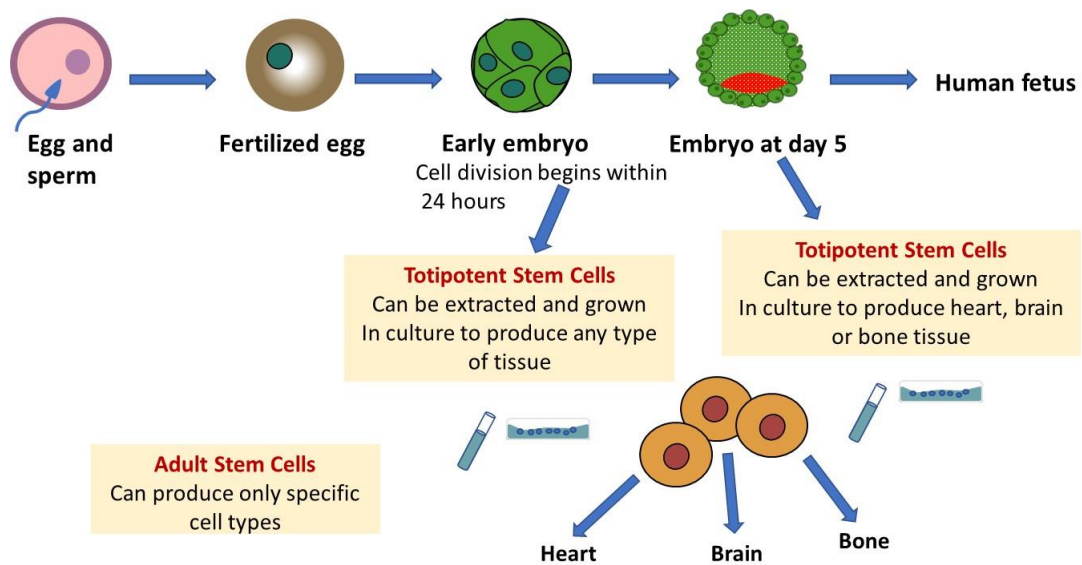
Figure 1.5. The origin of stem cells following fertilisation. Three basic types of stem cells originate from the fertilised egg and include totipotent stem cells, pluripotent stem cells and multipotent stem cells (including adult stem cells). Figure adapted from (Chadwick et al., 2003).
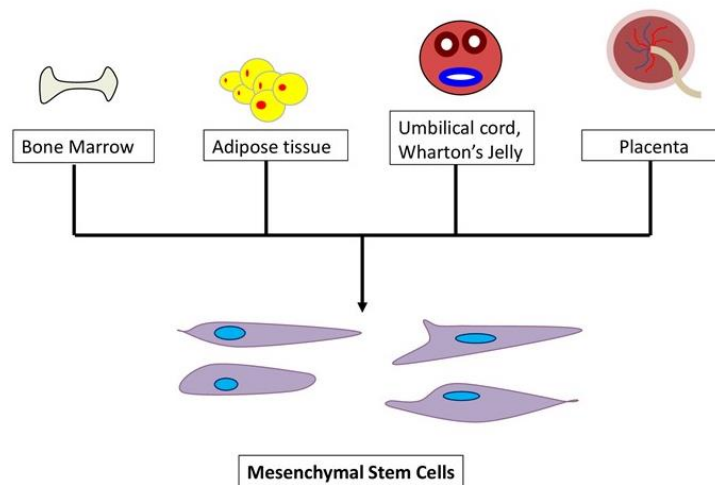
Figure 1.6. Sources of mesenchymal stem cells. MSCs can be obtained from various sources, including bone marrow, adipose tissue, the umbilical cord, Wharton's jelly, and the placenta. Figure adapted from (D. E. Lee et al., 2016)

Stem cells that derive from the bone marrow have a primary role in confronting inflammation. They achieve this by maintaining a balance of haematopoietic stem cells that is called an (HSCs) niche, a space with all the appropriate factors for their survival and long-term maintenance. Immune effector cells are generally involved in both innate

and adaptive immunity, and their lifespan is extremely limited. Exceptions to this rule are the memory B and T cells, which have a capacity to live for the entire duration of human life. As a result, due to the short life of most immune cells, they need to be replaced by haematopoietic stem cells (HSCs) and progenitor cells (HSPCs) that are located inside the bone marrow. The exact mechanism of HSC response during an inflammatory episode remains unknown (Kovtonyuk et al., 2016). As mentioned above, stem cells that derive from the bone marrow are significant in inflammatory processes. This is logical because, in contrast to the resident cells, which reside only in a specific tissue, there is a great need for cells that can migrate and deliver inflammatory molecules throughout the body. It is commonly recognised that both MSCs and human embryonic stem cells (hESCs) have the potentiality to differentiate into SMCs. However, the exact processes involved in these transitions remain unknown (Kurpinski et al., 2010a).

The existence of a newly identified type of stem cell in the blood vessel wall, named multipotent vascular stem cells (MVSCs), has been proposed. MVSC express markers, including Sox17, Sox10 and S100, show telomerase activity and the ability to differentiate into neural cells and MSC-like cells, which thereafter differentiate into VSMCs (Z. Tang et al., 2012a). There is also the participation of embryonic stem cell pluripotency genes through the revival SMC phenotypic switching in adult animals (Cherepanova et al., 2016).

Most of the adult tissue near or within blood vessels house an important location of resident vascular stem cells. There are two cell populations that have been implicated in vascular remodelling and intimal medial thickening. These populations are called pericytes and adventitial progenitor cells (APCs) (Lin and Lue 2013).

4.3.1 APCs

APCs are located within the adventitial layer of the vessel wall (Lin and Lue 2013). They habitually differentiate into pericytes *in vitro*. APCs also differentiate into vascular cells such as endothelial, SMCs and mesenchymal cells as well as bone, cartilage, and fat *in vitro* (Lin and Lue 2013).

4.3.2 MVSCs

Lin and Lue (2013) define resident vascular stem cells as cells that exist within the blood vessel wall and can differentiate into all cell types within the vessel wall. This includes endothelial cells and pericytes, which can come from the differentiation of the VSCs in the capillary. Moreover, in larger vessels, the VSCs can differentiate into smooth muscle and adventitial cells (Lin and Lue 2013). When a vascular injury occurs, there is substantial vascular remodelling and neointimal formation created by the proliferation and differentiation of MVSCs. These outcomes suggest that vascular remodelling and related diseases may be facilitated by the differentiation of MVSCs instead of de-differentiation of SMCs (Z. Tang et al., 2012a).

5.1 Cellular pathways involvement

Lineage tracing analysis has provided substantial evidence for the involvement of stem cell-derived progeny, in addition to 're-programmed' de-differentiated dSMCs, as well as SMC derived from endothelial-mesenchymal transition (EndMT) in progressing lesion formation (Z. Tang et al., 2012a); (Nemenoff et al., 2011); (H. Tang et al., 2017); (Cooley et al., 2014). These cells may become activated or re-programmed, differentiate down myogenic and myeloid lineages, and subsequently dictate, in part, vessel remodelling. Notch and Hedgehog pathways play a critical role in vascular development, stem cell self-renewal and myogenic and myeloid differentiation. Both are recapitulated in murine models of vessel remodelling, during ageing and in human arteriosclerotic vessels, whilst targeted inhibition of these pathways attenuates neointimal formation in mice (G. Wang et al., 2015).

5.2 Notch Pathway

The Notch pathway is known to play a pivotal role in the development of the vasculature, including the stimulation of morphogenesis. Within the developing vasculature, multiple notch ligands and receptors are expressed, and cell-to-cell signalling between receptors and ligands is regulated via the notch pathway. In adult vasculature, there is also strong evidence for a role for the notch in the conservation of the smooth muscle layer. Additionally, the notch may define SMCs fate (Rossant and Howard 2002).

In summary, there are four different Notch receptors (Notch1-4) that can be bound by five distinct ligands (Delta-like 1, 3, and 4 and Jagged 1 and 2). These receptors are transmembrane ligands and the Notch family of transmembrane receptors. Each of the new Notch receptors that are synthesized will be proteolytically cut in the Golgi apparatus and then transported to the cellular surface mediated by a furin-like protease. After this cleavage, the generation of a heterodimeric receptor follows, that consists of an extracellular portion (N^{EC}) which is non-covalently bound to another subunit. The latter contains an extracellular heterodimerization domain and also the transmembrane domain, which is the next part of the cytoplasmic region of the Notch receptor (N^{TM}). Each receptor's extracellular part may contain between 29 and 35 epidermal growth factor-like repetitions that are of high importance in the binding of the ligand. These repeats are also followed by three cysteine-rich LIN12 repeats, that have an inhibitory role in the ligand-independent activation. Furthermore, there is also a hydrophobic stretch of amino acids that permit heterodimerization between N^{EC} and N^{TM}. The tail of the receptor that resides within the cytoplasm is paramount regarding nuclear localization signals, and protein-protein interaction and transactivation domains (Costantini and Kopan 2010).
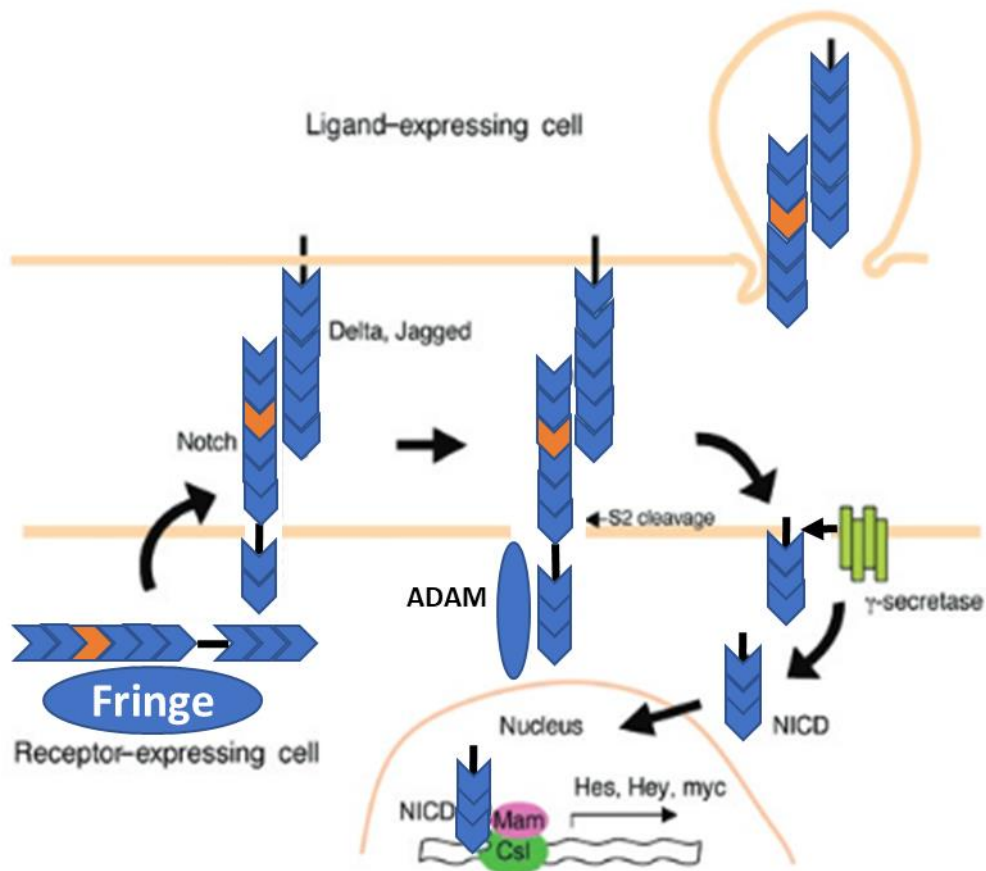
Figure 1.7. Basic elements of Notch signalling. Figure adapted from (Redmond et al., 2011).

A schematic view of two cells is presented, one presenting the receptor, Notch, and an adjacent cell presenting the ligand Delta or Jagged. The glycosyltransferase Fringe is demand for of Notch receptor Maturation. Followed binding to Delta or Jagged, with ADAM metalloproteases aid Notch is cleaved in order to release the extracellular domain, which will afterword endocytosed along with ligands. Following the cleavage happening by γ- secretase, the Notch intracellular domain (NICD) release occurred. Then, NICD will translocate into the nucleus (Dressler 2008) and interactions with transcription factor CBF-1 (also recognized as RBP-Jκ or CSL). Following the function of the co-activator, Mastermind-like (MAML) protein endorse the downstream effector's transcriptional activation. Started the notch vascular target gens which are the *Hes* and *Hey* [*Hey1, Hey 2* and *Hey L*] gene families (Redmond et al., 2011)

The membrane-bound ligands, Delta (D1) or Serrate (Ser) (Jagged in mammals) are responsible for the fate of the cell that is expressing them and for the neighbouring cell that expresses the Notch receptor. The interaction between the ligand and the receptor will lead to a cascade of proteolytic events that release the Notch intracellular domain (NICD) from the membrane. The NICD then moves into the nucleus where it forms a transcriptional complex with the help of the Mastermind (Mam) and the DNA-binding protein as in (Figure 1.7) (Costantini and Kopan 2010). There is a communication between notch receptors and five ligands including Delta-like (Dll) 1, 3, 4, Jagged1, and Jagged 2. The interaction occurs through the single-pass membrane-bound ligands which have EGF repeats that connect to the Notch receptors through a common DSL (Delta, Serrate, Lay) motif. The latter is located in the extracellular domain of the protein. The proteolytic cleavage of the intracellular domain of the receptor (NICD) due to ligand binding releases the NICD as a transcription factor. Following that, there is a stimulation of specific downstream target genes in the nucleus when the NICD complex enters it (Rossant and Howard 2002). In leukaemia, lymphoma, and diversity of solid tumours, the Notch pathway is dysregulated, and this has led to research of this pathway by scientists to invent a therapy for these tumours (Shah et al., 2013).

The expression of Notch receptors 1, 3 and 4 and ligands Dll4, Jagged1 and 2 has been found in the human arterial system. In addition, they are found to be vital for normal vascular structure, angiogenesis and vascular remodelling, conservation in physiological and pathological events (Qiao et al., 2012, Gridley 2010)

Fatal mortality due to Notch Signalling defects has reinforced the crucial roles of Notch systems. For instance, embryonic deaths triggered by (or as a result of) vascular remodelling, can either be a result of knockout of Notch1, Notch1 and Notch4, HERP1 and HERP2, Jagged1, DLL4, presenilin-1, or ceaseless expression of Notch4 (Miniati et al., 2009). Additionally, human diseases involving arteries like Alagille Syndrome has been linked to Jagged1 gene mutations, constriction of small pulmonary arteries and CADASIL Syndrome are linked to mutations of Notch3 gene, and gradual deterioration of the VSMCs have displayed gene mutations in the notch system (Roca and Adams 2007).

Li et al., depicted that the levels of mRNA and proteins of Notch 3 amplified recurrently in the lungs of idiopathic pulmonary hypertension (PH) patients, hypoxia-induced PH

mice and monocrotaline-induced PH rats (X. Li, Zhang, Leathers, Makino, Huang, Parsa, Macias, Yuan, Jamieson and Thistlethwaite 2009). The role of Notch Signalling pathway including Notch1, 3 and 4 was advocated as vital for the vascular remodelling in PH. Nonetheless, the operation of this pathway varies according to the cell types. The regulatory factors responsible for the development along with the vascular injury associated growth factors regulate the Notch system in the arteries (Bordonaro et al., 2011).

The generation, relocation, and accumulation of VSMCs, restrained VSMCs' apoptosis, uncontrolled cell cycle arrest and assisted conversion of endothelial cells, fibroblasts and SMCs are all regulated by Notch 1 and 3, as has been illustrated by (Qiao et al., 2012, Boucher et al., 2012).

5.2.1 Notch Ligands (Jagged and TGF-β1)

Notch-1 (Notch) is a cell-surface receptor which controls cell-fate arrangement in the evolving nervous system, and it could have a role in adult brain for synaptic plasticity. As mentioned previously, once the ligands (Delta and Jagged) binds the receptor, proteolytic cleavage occurs. The first cleavage will happen in the extracellular domain then in a transmembrane domain. The cleavage in the transmembrane domain achieved by presenilin-1 and the γ-secretase enzyme complex which lead to a liberation of NICD. The NICD will move to the nucleus as it will monitor the transcription (Arumugam et al., 2006). MSCs exposed to transforming growth factor-beta (TGF-β1) caused a reduction in JAG1 gene expression. This was performed to define whether JAG1 controls the smooth muscle gene response to TGF-β1. The markers of the smooth muscle which are promoted by TGF-β1 were considerably weakened, especially for α-actin (ACTA2) and myocardin (MYOCD) following exposure to TGF-β1 without JAG1 expression (Kurpinski et al., 2010). Because of these findings, the importance of JAG1 in the MSC response to TGF-β1 has been proposed. Parallel DNA microarray studies indicate that the upregulation of the Notch ligand Jagged 1 (JAG1) in MSCs is caused by the TGF-β1 activation. The Notch activation by TGF-β1 signalling during MSC differentiation into SMC was facilitated by JAG1 ligand expression. (Kurpinski et al., 2010). γ-secretase inhibitor can detach the notch receptor and ligand. Therefore by blocking the notch

signalling, using the γ-secretase inhibitor in medical applications becomes a promising approach (Chen et al., 2012).

5.2.2 Gamma secretase inhibitors (GSIs)

Gamma-secretase (GS) is a multimeric membrane protein complex composed of presenilin (PS), nicastrin, Aph-1 and, Pen-2 that is responsible for the intramembrane proteolysis of various type I transmembrane proteins, including amyloid beta-precursor protein and Notch. The direct labelling of PS polypeptides by transition-state analogue gamma-secretase inhibitors suggested that PS represents the catalytic centre of gamma-secretase. The major gamma-secretase inhibitors of dipeptidic type, N-[N-(3,5-difluorophenacetyl)-l-alanyl]-S-phenylglycine t-butyl ester (DAPT), target the C-terminal fragment of PS, especially the transmembrane domain 7. DAPT binding site as a novel functional domain within the PS C-terminal fragment that is distinct from the catalytic site or the substrate-binding site. Compound E selectively binds to the high molecular weight gamma-secretase complex in an activity-dependent manner (Morohashi et al., 2006).

There are more than 100 GSIs synthesized up to date and can be divided into three groups: peptide isosteres, azepines, and sulphonamides. As Notch and its ligands are overexpressed in breast cancer, γ-secretase inhibitors are used to efficiently block Notch activity by averting the Notch and its ligands cleavage at the cell surface. Therefore, utilizing the anti-Notch drugs in treatment could be a contribution to innovative medicine and provide more significant clinical approaches for women with breast cancer (Olsauskas-Kuprys et al., 2013).

Depending on the structure and binding sites, the GSIs are categorized into two categories:

(1) Aspartyl proteinase transition-state analogues as peptide isosteres that initiate the transition condition of substrate cleavage by γ-secretase and bind to the catalytic active position of presenilin.

(2) Small molecule non-transition-state inhibitors where the binding spot is diverse from the active spot, probably at the interface of the γ-secretase complex dimer.

It is widely acknowledged that the side effects of GSIs happen within the gastrointestinal tract. The small-molecule GSI classified as a tetralin imidazole PF-03084014 (Pfizer Inc.,

Groton, CT, USA) is in a Phase I pilot to treat breast cancer and other solid tumours which are in an advanced stage. This classification used when evaluated for Notch activity, PF-03084014 remarkably reduced tumour cell migration, decreased the capability of tumour cell self-renewal in vivo, and reduced mRNA expression of Notch target genes such as *HEY-2* in xenograft growths. Another small-molecule GSI containing dibenzoazepine core was used *in vitro* on a colon cancer cell line, and this molecule provided a significant diminution in mRNA levels of Notch target genes *HES-1, HES-4*, and *HEY-1*. In the murine model of ovarian cancer, it was found that GSIs had no impact on cellular proliferation with a remarkable reduction and alteration in the density of microvessel. Additionally, targeting Notch1 and inhibition of this pathway resulted in a weakness in the tumour growth in animal models of breast cancer and neuroblastoma. These discoveries lead researchers to examine the angiogenesis pathway and notch inhibition in relation to metronomic chemotherapy along with the most operative strategy of Notch inhibition in ovarian cancer (Shah et al., 2013). There are several GSIs including transition-state analogs based on hydroxyethylamines (such as L-685,458;(Y. M. Li et al., 2000)), helical peptides (Bihel et al., 2004), and dipeptide analogs (such as Compound E, DAPT (Lanz et al., 2006). Although they have diverse chemical structures and mechanisms of action, all these GSIs illustrate high specificity and potency along with the inhibition of γ-secretase (Olsauskas-Kuprys et al., 2013b, Groth and Fortini, 2012).

Notch receptor signalling has been targeted in vSMC proliferation and differentiation (Redmond et al., 2011, X. Li, Zhang, Leathers, Makino, Huang, Parsa, Macias, Yuan, Jamieson and Thistlethwaite 2009b). Specifically, N-[N-(3,5-difluorophenacetyl)-L-alanyl]-S-phenylglycine t-butyl ester (DAPT), a γ-secretase inhibitor which inhibits activation of Notch3 in vSMC demonstrating a mechanistic link between Notch3 receptor signalling through the Hairy Enhancer of Split (HES) genes and vSMC proliferation and a shift to a de-differentiated phenotype. This suggests the importance of the NOTCH3-HES5 signalling pathway in pulmonary arterial hypertension development (Li et al., 2009). It also represents the potential of therapeutic intervention by targeting this pathway (Li et al., 2009). Following Compound E administration, a definite inhibition of Notch signalling occurred and was verified by a decrease in both NICD levels and transcriptional downregulation of Notch1-responsive genes. (Groth and Fortini, 2012).

Therefore, a clinical approach using γ-secretase inhibitors (GSIs) in order to avert the final cleavage stage of the Notch receptor will reduce NICD levels and therefore may represent an innovative therapeutic approach to combat intimal thickening due to the accumulation of vSMCs (Olsauskas-Kuprys et al., 2013).

5.2.3 Notch and Cardiovascular Disease

Notch signalling controls tissue expansion and contributes to adult's innate and adaptive immunity (Fukuda et al., 2012). Moreover, there is strong chronological evidence for a role for the Notch pathway in numerous biologic systems. Notch activation dictates SMC differentiation. Significantly, it has been shown that the stimulation of TGF-β1 and the activation of Notch were enough to activate vascular, myogenic differentiation of MSCs. These findings support the role of Notch in regulating smooth muscle differentiation which can be useful for generating SMCs in vitro. (Kurpinski et al., 2010).

Many acquired types of heart disease that are apparent in adult life are due to chronic hypertension, myocardial ischemia and atherosclerosis. Especially for atherosclerosis, evidence has accumulated that *NOTCH* mutations or polymorphisms predispose as inherited forms of heart disease (Costantini and Kopan 2010). Normally, in each given cell, the stimulation of notch signalling regulates cell fate choice (Rossant and Howard 2002). It has been noted from several studies that the induction of smooth muscle gene/protein expression in MSCs arises from both TGF-β1 and Notch activation (Kurpinski et al., 2010). Notch signalling is also adequate to promote hESCs differentiation into SMCs. This supports the hypothesis that Notch activation may promote smooth muscle differentiation and could be the nexus between TGF-β1 signalling and the upregulation of SMC markers in MSCs (Kurpinski et al., 2010).

It is well known that in atheromatic and fat tissue in LDL-receptor–deficient mice, the increase of Notch ligand Delta-like 4 (Dll4) expression is due to the rise of a high-fat, high-cholesterol diet. This is because apolipoprotein B100-containing LDL transporting circulating cholesterol which causes an elevation of the circulating cholesterol. Consequently, this will promote atherosclerosis and CVD (Weber and Noels 2011). Moreover, utilizing anti-Dll4 antibody to inhibit Dll4-Notch signalling caused a reduction of the atherosclerosis growth, reduced plaque calcification, enhanced insulin

resistance, and declined fat accumulation. Triggering Notch signalling by Dll4 induces macrophages to have an inflammatory response *in vitro* (Fukuda et al., 2012).

6. Cardiovascular treatment options

If CVD has been identified in a patient, there are certain treatments which can be undertaken.

These approaches span wide from diet changes to using high-tech nanotechnology (Kalanuria et al., 2012). At times when the threats can't be downgraded by changes in diet or by increasing physical activities or by commencing other ways of modifying lifestyle like curbing smoking, targeted therapies including statins and other lipid-lowering drugs need to be instigated to keep the levels of lipoprotein under control. Medical therapy becomes utmost important in the secondary prevention/approach (S. Bergheanu et al., 2017).

6.1 Cardiovascular Therapeutics

CVD and/or the likelihood of any cardiovascular ailment can be prevented in women by using assertive handling of risk factors accompanied by positive transformations in lifestyle like quitting smoking, consuming a healthy diet with low saturated fats and more fruits and vegetables, intensifying the total amount of physical activities and ultimately maintaining a healthy weight. Hormone replacement therapy showed astonishing results in CHD risk. Cardiovascular incidences were increased by 50% in the first year, but in 3 to 5 years, the risks decreased dramatically for the therapy in recipient women, while the general impact of hormone replacement therapy in Heart and Estrogen/progestin Replacement Study (HERS), remained null (Afilalo et al., 2008). Coronary artery disease (CAD) is listed among the most common reasons for death throughout the world. Several important developments have been introduced in the treatments of CAD during the last decade. The level, seriousness and clinical aspects of the CAD determine the treatment method to be used which either can be medical or surgical or a combination. The co-occurring diseases like the hypercholesterolemia are treated along with the main ailment in CAD patients by using a combination of therapeutic, supportive and lifelong medications (Kandaswamy and Zuo 2018).

The prescription medicines are used to relieve heart trauma and symptoms. Various kinds of medicines exist for this purpose. Aspirin, clopidogrel and other antithrombotic

22

medications constitute a commonly used class of drugs for CAD patients (Kandaswamy and Zuo 2018). Statins have an important role in lowering cholesterol and hence is commonly used to decrease the cholesterol levels in CAD patients. Research has highlighted the role of statins in the reversal of plaque (Kalanuria et al., 2012). The impact of statin therapy on cardiovascular results has been demonstrated in numerous landmark trials. However, the side-effects of this therapy are an underrated issue in medical practice and have always stood in the way of full compliance. A study found 38% of the patients administered with high statin doses unable to perform even mild physical exertion due to muscular pains, while the other 4% were noted to be completely bedridden (S. Bergheanu et al., 2017). In accordance with the clinical trial results, statin therapy has been anticipated to be able to better prevent acute coronary incidences in the elderly than in young. Hence, considering the high, attributable and absolute risk associated with the statin therapy, it has been highly recommended in the elderly with CHD. Primary prevention clinical trials have shown that Statin treatment in addition to risk factor modifications can prevent coronary events in middle-aged adults. The fact that the middle-aged patients might already have well-established atherosclerosis which might not be symptomatic though makes these results more appreciable. (Afilalo et al., 2008)

6.2 Cholesterol absorption inhibitors

Ezetimibe diminishes the low-density lipoprotein cholesterol (LDL-C), by inhibiting the absorption of cholesterol. Ezetimibe therapy alone can control LDL-C up to the extent of about 15-22%, and it could generate a reduction of about 15-20% in LDL-C levels when used in combination with a statin. Unlike other therapies, no major side effects were observed for ezetimibe. In statin contradiction cases, statin tolerant patients and in patients where even the maximum tolerant limits of statin could not produce the expected results, use of ezetimibe has been advocated by several studies, for use as second-line therapy along with the statins (S. Bergheanu et al., 2017).

6.3 Mechanical revascularization

The alternate therapy methods for symptomatic patients include revascularization of the brachiocephalic and subclavian artery using balloon angioplasty, bypass grafting, atherectomy, and stenting (S. Bergheanu et al., 2017). Moreover, to accomplish a successful clinical outcome and to focus on recanalization as the main clinical endpoint, several clinical trials following revascularization procedures have been performed (Molina 2010). Although, revascularization trials may not adjust the natural history of multicentric plaque rupture (Gould et al., 2013), the study of patients in acute stroke who have been treated with mechanical revascularization present with a high recanalization rate and a low rate of periprocedural complications (Jeromel et al., 2013).

6.4 Coronary artery bypass graft surgery

One of the latest treatment methodologies for CAD patients is the robotically assisted hybrid coronary revascularization, which includes bypass graft as well as percutaneous coronary intervention (PCI). The least invasive nature of this procedure allows for additional benefits like reduced morbidity and shorter hospital stays (Kandaswamy and Zuo 2018). In 1998, cardiopulmonary bypass (CPB) and cardioplegic arrest were the most commonly used techniques in the cardio surgery sphere, for carrying out the coronary artery bypass grafting (CABG) (1). At least one or more than one complication, like atrial fibrillation, bleeding, myocardial infarction, sternal infection, stroke, or renal failure, is present in about 25% patients undertaking CABG. The avoidance of the gruesome complications of standard CPB-supported CABG is one of the most important goals of the minimally invasive CABG. minimally invasive direct coronary artery bypasses (MIDCAB), and off-pump coronary artery bypass (OPCAB) is the two most common minimally invasive CABG techniques (Wait, 2000).

6.5 Percutaneous coronary interventions

There's a known requirement of treatment in patients with hypercholesterolemia and established Coronary heart disease (CHD) to manage the secondary prevention of recurring coronary events. Other than the diabetics, primary prevention is debated for most patient groups due to the increased risk of CHD developing. The undertreated groups include the postmenopausal women, young adults and the elderly, in which the

young adults are often underdiagnosed too. The efficiency of various prevention and treatment methods for different patient groups can be better understood by numerous trials (Afilalo et al., 2008). The lipid-lowering revolutionary therapy that transformed the atherosclerosis treatment was advanced by the HMG-CoA reductase [(3-hydroxy-3-methyl-glutaryl-coenzyme A reductase, officially abbreviated HMGCR is the rate-controlling enzyme inhibitors, or statins (Cherng et al., 2008).

6.6 Surgical Robotics

Surgical robots have undoubtedly been the fascinating technological development to evade sternotomy. The heart can now be accessed by the surgeons without exposing the chest, by using the highly evolved robotic system, the da Vinci® Si HD Surgical System (Intuitive Surgical, Inc.; Sunnyvale, Calif). Unlike manual surgeries, the robotic instruments including a video scope can access the chest just by 4, one-half inch, incisions between the ribs. High definition, 3-D Optics is at the disposal of the surgeon to monitor the chest interiors while sitting at a robotic console. The inclusion of the robotic tech has made it possible to gain superhuman precision while eliminating the sense of touch. This capability is gained by courtesy of robotics, the unprecedented image magnification which allows the scaling and filtration of surgeon's movements. The LIMA can be reaped from the back of the sternum, open the pericardium, stabilize the segment of the LAD chosen for grafting, and perform the anastomosis between the LIMA and LAD on a beating heart by using the da Vinci system. Executing the real anastomosis is a far bigger challenge of this technique. Though new methods of automating this part of the process are being developed, none of these high-tech devices including the one with strong rare-earth magnet clips or locking nitinol frames could obtain the United States approval (Gummert et al., 2007). High costs and immaculate skill set requirements have been a limitation for the widespread use. This method can only be an option for CAD patients after future enhancements and simplification (Cohn 2010).

6.7 Angioplasty and Percutaneous Transluminal Coronary Angioplasty (PTCA)

Angioplasty and Percutaneous Transluminal Coronary Angioplasty (PTCA) are the present-day methods which include the insertion of a stent in the vessels. Despite the success of this treatment, up to 30 % of patients have the same problem again as they are

suffering from in-stent restenosis. Restenosis is the main limitation of percutaneous angioplasty techniques because it's the reaction to balloon angioplasty and stent deployment injury and is categorized by the unhindered accumulation of smooth muscle-like cells (SMC) and additional vascular inflammatory cells. In the evolution of this pathology, resident SMC and vascular stem cells have a multidimensional contributory role (R. X. Yin et al., 2014). Although intracoronary stents minimise the restenosis ratio in front of the balloon angioplasty ratio, nonetheless in-stent restenosis prevails (Kasaoka et al., 1998). In-stent restenosis occurs in about 30% of stented coronary arteries. Frequently, there is a demand to rerun the intravascular procedures and/or surgery in recurrent ischemic episodes (Woods and Marks 2004). Although the sirolimus-eluting stent treatment has accomplished substantial achievement in combatting coronary artery restenosis, incidents of restenosis continue after the treatment in numerous patients (Wong et al., 2013).

There are several factors in the stent that may have an impact on restenosis. These include elastic recoil of the dilated artery, platelet-mediated thrombus formation, the proliferation of smooth-muscle like cells and vascular remodelling (Fischman et al., 1994). Following the reduction in the elastin fibers of the inner and external elastic laminae, the coronary artery experiences elastic recoil which leads to a 40% lumen deprivation. This process happens minutes after the deflation of the balloon (Woods and Marks 2004). The dimension of the stent may impact its mechanical performance (Barragan et al., 2000). If the elastic recoil of the vessel and the sealing of the intimal flaps is reduced, this will result in a broader, smoother coronary lumen (Fischman et al., 1994).

Although the advantages of vascular patency which provided by bare-metal stents (BMS), these stents substantially cause an injury in the arterial wall. This will lead to neointimal hyperplasia and subsequently restenosis. Therefore, as a solution to this problem drug-eluting stents (DESs) had been invented. Regardless of the high efficiency of DES, they still have an adverse effect (Khan et al., 2012).
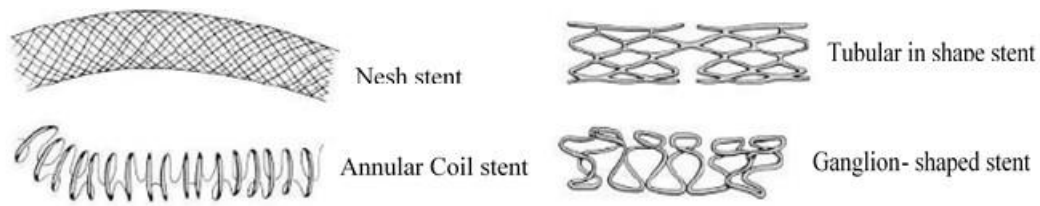
Figure 1.8. Types of the stents. Nesh stent, Tubular in shape stent, Annular Coil stent and Ganglion- shaped stent adapted from (Stanisławska 2014).

It has been found that post the DES, between 3 - 20 percent of patients have the in-stent restenosis. Therefore, numerous studies are ongoing in order to invent biodegradable/bioabsorbable stents with nanoparticle (NP) loaded with an antibody that induces endothelial progenitor cells (Ambesh et al., 2017).

6.8 Drug-Eluting Stent

The obstruction of blood flow is reduced by stent deployment, which assists the contraction of atherosclerotic plaque and expands the artery. Stents, 18mm in size and 3-3.5mm in diameter are small mesh tubes that assist the mechanical structure of the vessel in which it is placed. Paul and Sigwart used the stent for the first time in 1986 in the treatment of a human patient. The angioplasty balloon method is used to insert the stents into the aimed vessels. Though, Plain BMSs have shown a failure rate of 70% but in comparison to PTCA procedure, stents have shown a reduction in angiographic and clinical restenosis (Habara et al., 2015, S. C. Bergheanu et al., 2011) Advancements have given way to superior DESs with lower failure rates, which replaced the original BMS. Stents coated with either Sirolimus or Paclitaxel drugs are the main types of the stent that are used in present times. The stents can cost around 2500-2700$ each. Clopidogrel treatment may accompany the stent treatment in patients (Farkouh et al., 2012, M. S. Lee et al., 2010).

The formation of the neointima due to the migration and proliferation of vascular cells/progenitor cells leads to the restenosis. Drug-eluting stents (DES) coated with drug-delivery vehicles have been manufactured to solve this problem by supplying anti-proliferative therapeutics (Woods and Marks 2004). The preferred coating of choice for stents is non-biodegradable polymers. This is because the coating will make sure the

27

interaction between metallic stent strut and blood is minimal, thereby minimising restenosis due to thrombosis (R. X. Yin et al., 2014). Flexibility, ease of expansion, and possessing pores at the side struts all are present in the stent to make them more compliant (Serruys et al., 1994). In the initial group of DESs, stainless-steel stents were utilised as the stent platform (R. X. Yin et al., 2014). The improvements in the PCI using developed first-generation drug-eluting stents (DES) coated with anti-mitotic drugs, sirolimus and paclitaxel lead to a reduction in restenosis. These stents are very important because of their role in keeping the coronary vessels unobstructed at places that have been expanded (Inoue and Node 2009).

Nowadays there are controversial opinions about the long-term security of the first-generation DES, specifically after stopping the dual antiplatelet treatment, which could potentially lead to late stent thrombosis (Sheiban et al., 2008). Nevertheless, the DES has been a revolutionary improvement in the treatment of CAD. The improvement of drug-eluting stents demands to resolve the difficulty of exactly how to apply adequate concentrations of medication to the stent over time with proper release kinetics (Woods and Marks 2004).

In anti-restenosis therapy, delivering small molecular weight anti-proliferative and anti-inflammatory therapeutic agents can be achieved using targeted NP platforms. This delivery will inhibit in-stent neointimal formation. In the pro-healing strategy, the nanofibrous scaffold imitates extracellular matrix in vessels. This could facilitate the re-endothelialization, which improves the transport of cells to stent struts within magnetic fields by using magnetic nanoparticles (MNPs) (R. X. Yin et al., 2014). It is still unknown what promotes in-stent restenosis, but the involvement of vascular stem/progenitor cells in restenosis development appears to be a major factor.

Therefore, finding a drug that can efficiently target the stem cell pathways and inhibit the notch in order to prevent stem cells growth and accumulation is essential. DAPT and Compound E drugs were employed in this study; it is believed that these drugs could have a promising impact on the in-stent restenosis treatment.

6.9.1 γ-secretase inhibitors - **DAPT and Compound E**

The Notch 1-4 receptors' expression and downstream factors involved in PH development were examined by (Qiao et al., 2012). DAPT (N-[N-(3,5-difluorophenacetyl)- L-alanyl]-S-phenylglycine t-butyl ester) was used as an inhibitor of a Notch signalling pathway to narrow down the part that Notch signalling plays in the vascular remodelling of PH (pulmonary hypertension, (high blood pressure in the *lungs*) (Qiao et al., 2012). For instance, embryonic death due to vascular remodelling defects could be caused by either knockout of Notch1, Notch1 plus Notch4, HERP1 plus HERP2, Jagged1, DLL4, presenilin-1, or constant expression of Notch4 (Gridley 2010).

DAPT (the γ-secretase inhibitor) a cell-permeable dipeptide inhibits all four Notch receptors, resulting in the attenuation of the Notch signalling pathway. That is why DAPT is being considered as a potent treatment for several disorders (L. Jiang et al., 2011). DAPT has been shown to inhibit Notch signalling in studies of autoimmune diseases, such as cancer cell growth, angiogenesis, and differentiation of human-induced pluripotent stem cells (P Imbimbo and AM Giardina 2011). The attenuation of Notch action through the inhibition of notch receptors can be achieved by γ-secretase inhibitors, such as DAPT. These inhibitors have been shown to prevent the growth of renal cell carcinoma *in vitro* and *in vivo* (Mori et al., 2012). The substantial decrease in cell self-renewal and proliferation was seen after the incubation of cells with DAPT (L. Jiang et al., 2011). Recent studies succeeded in using DAPT to inhibit the activation of hepatic stellate cells. The activation and proliferation of these cells were found as a serious incidence in the hepatic fibrosis growth. Hepatic fibrosis is known by the accumulation of extracellular matrix when the response to the critical liver injury. Preservation of this fibrotic accumulation could generate a cure for liver diseases such as cirrhosis and hepatocellular carcinoma. This preservation can occur by targeting the carbon tetrachloride which inducing the hepatic fibrosis *in vivo*, DAPT significantly achieved to treat this by attenuating the carbon tetrachloride. Additionally, the inhibition of hepatocyte apoptosis *in vivo* happened by using DAPT (Chen et al., 2012). DAPT was used also to deduce the effect of TGF-β1 by reducing TGF-β1 expression in order to defend hepatocytes from apoptosis. This is because the latter was found as an apoptotic-inducing for hepatocytes and stimulator of extracellular matrix accumulation in hepatic

fibrosis. All these data proposed that inhibition of Notch signalling might be an innovative choice for hepatic fibrosis therapy (Chen et al., 2012). DAPT, also known as GSI IX and Compound 3 is the most broadly used in the laboratory. DAPT potentiated the apoptotic impacts of the DNA-damaging drug melphalan in breast cancer cells. In cell lines with chromosomal translocations, DAPT inhibited the proliferation of truncated Notch-1 expressing cleavage site. (Olsauskas-Kuprys et al., 2013a). Treatment with γ-secretase inhibitor, DAPT resulted in a noticeable inhibition of renal cell carcinoma development *in vitro* and *in vivo* and hindered the growth of pancreatic cancer cells *in vitro* by inhibition of Notch signalling. Also, there was a determination of DAPT effect on hindering Notch which leads to preventing the ovarian cancer stem cells formation. This is because it is known that Notch activity contributes to self-renewal of ovarian cancer stem cells. When using DAPT the γ-secretase inhibitor as the treatment this will result in inhibiting the proteolytic process of Notch receptors, and this instantly decreases the generation of NICD protein. Therefore, a decline of HES1 transcription and HES1 protein expression occurs and this proves that DAPT blocked the Notch signalling pathway. It is indicated that DAPT also hinders ovarian cancer stem cells stemness maintenance, reduce the subpopulation of stemness maintenance of ovarian cancer stem cells and in contrast raise the subpopulation of differentiated cells (L. Jiang et al., 2011).

There is systemic toxicity of GSI compounds, particularly cytotoxic effects on the gastrointestinal tract (Groth and Fortini, 2012). The main side-effect of GSIs is gastrointestinal toxicity (Barten et al., 2006). Nevertheless, this could be minimized by modulating Notch receptors expression using receptor antibody as pre-treatment before GSI treatment(Y. Wu et al., 2010). The existing generation of γ-secretase inhibitors has side effects, along with with intestinal goblet cell metaplasia in experimental animals (Milano et al., 2004). From the side effect standpoint though, it could be acceptable within the local and short-term administration of the drugs and has been considered for the probable treatment of Notch-induced cancers (van Es and Clevers 2005). Moreover, this could be used possibly for modulating the stem cell differentiation in vivo locally, within the context of future medicine recreation (J. Jiang et al., 2014). Patients who treated with GSIs had some substantial complications fluctuating from rising the occurrence of skin cancer to intestinal toxicity due to the goblet cell metaplasia happened because of all four Notch family members the inhibition (van Es et al., 2005). This could

be explained as the recent data have shown that diverse Notch family members perform different and occasionally contrasting roles within the same tissue and/or cell type (L. Yin et al., 2010). For instance, Notch1 has been demonstrated to function relying on the context as both an oncogene and a tumour suppressor (Radtke and Raj 2003). Therefore, the present work by (Z. Liu et al., 2011), has a specific interest in this context, as it revealed that long-term anti-Notch1 therapies usage requested a careful revision. Their results represent the notch 1 inhibition however DAPT and Compound E they are inhibiting Notch 3 receptor. Traditionally, Notch inhibitors are not cytotoxic drugs. This is because, in the current study, the cytotoxic effects of DAPT at 10 mol/l were relatively restricted. However, 10 μmol/l DAPT hindered the Notch signalling pathway and reduced the cancer stem cell (CSCs) proportion significantly (S. Yu et al., 2012).

To conclude, it has been demonstrated that notch signalling is crucial for self-renewal and proliferation of ovarian cancer stem cells and for their stemness maintenance. It is evident that DAPT is effective in inhibition of ovarian cancer stem cell-like cells from renewing and proliferating. Therefore, the treatment that targets ovarian cancer stem cells using the γ-Secretase inhibitors is considered as a very promising approach, and it could be utilized as anti-cancer drugs for ovarian cancer (L. Jiang et al., 2011). Commercial DAPT was used to inspect its effect on inhibiting notch pathway for the brain tumour stem cells which are known as glioma tumour initiating cells. There was an observation of a correlation between the glioma tumour initiating cells response to DAPT and the activity of their notch signalling. (Saito et al., 2014)

6.9.2 The impact of DAPT on Notch Signalling within the vasculature

In vascular strips from pulmonary hypertension (PH) (high blood pressure in the lungs) rats, the classic Notch signal pathway involves dual steps of enzymolysis, which is preceded by the binding of Notch ligands to Notch receptors. This leads to the release of the NICD, which then activates the Notch signalling by translocating to the nucleus. The hydrolysis of Notch NICD protein is inhibited by DAPT, which specifically inhibits the γ-secretase. The impact of DAPT administration on the expression of the Notch system was investigated and revealed that DAPT treatment, in comparison to control, did not affect Notch receptor mRNA levels. However, when compared with blank and DMSO control groups ($p<0.05$) DAPT significantly affected the expressions of Notch target genes HERP-1 and HERP-2 genes (Qiao et al., 2012).

In cultured vascular strips from PH rats, the thickness of the vascular wall increases in response to hypoxia, an effect that is decreased by the DAPT treatment (Qiao et al., 2012). A decrease of 30% was noted in the thickness of the vascular wall of PH rats when the cultured vascular strips of PH rats by hypoxia were treated with DAPT. There was also a considerable increase in the expression level of apoptotic factors whereby DAPT treatment inhibited cell proliferation and promoted apoptosis, in agreement with earlier studies (X. Li et al., 2009a). These results particularly emphasised the bax/caspase-3 pathway in the DAPT treatment-induced apoptosis. Though the DAPT reduced the mRNA levels of downstream effectors, HERP1 and HERP2, it did not affect the mRNA level of Notch receptors of the vascular strips. This implied that the inhibition of intracellular Notch signalling pathway is mediated by the DAPT without disturbing the expression of Notch receptors. Intriguingly, DAPT enhanced the mRNA levels of SM-MHC and SM22α appreciably, signifying Notch inhibition promoted the conversion of VSMC phenotype during vascular remodelling (Qiao et al., 2012). In this context, the lungs of humans and rodents with pulmonary hypertension have overexpression of Notch3 while the knock-out mice with a homozygous deletion of Notch3 did not develop pulmonary hypertension in response to hypoxic-induced pulmonary hypertension (X. Li et al., 2009a).

To summarize, the function of the Notch pathway in vascular remodelling is complicated. It was observed that the changes in the expressions of Notch1, Notch 3, and Notch4, after the development of PH occurs in a time-dependent pattern. The other observation was the inhibition of Notch signalling by DAPT could reverse the biological traits of VSMCs in PH rats including decreasing proliferation, increasing apoptosis, and the phenotypic transformation of VSMCs, finally inhibiting the pulmonary vascular remodelling. It was concluded that focusing on the Notch signalling pathway could be a beneficial approach for designing new therapy for PH because the role of Notch pathway has been found critical in pulmonary vascular remodelling in PH (Qiao et al., 2012)

Compound E is another cell-permeable non-competitive inhibitor of γ-secretase, and it is the chemical form is $C_{27}H_{24}F_2N_4O_3$. Studies indicate that γ-secretase is a multifunctional transmembrane protein complex that enzymatically catalyses the cleavage of single-pass transmembrane proteins. One of the most common substrates for this enzyme is the

amyloid precursor protein. Once cleaved, this protein produces amyloid plaques in brain tissue often seen in Alzheimer's disease (Crump 2013).

A number of studies have been performed in order to test the impact of γ-secretase inhibition on general cell proliferation or cell survival. The results show that although there was an assumption that γ-secretase inhibitors have cytotoxic and antiproliferative activity in breast cancer, lately this has been uncertain. This is because very specific inhibitors activity presented a nontoxic effect on the cells. This indicates that some nonspecific inhibitors may cause cell death within their activity to inhibit the enzyme instead of causing a γ-secretase activity blockage. Basal-like breast cancers cells were treated with two highly specific γ-secretase inhibitors and no cytotoxic activity post the treatment was detected. It is common in breast cancer subtype the existence of the notch pathway activation which can be blocked by γ-secretase inhibitors through their powerful capability to block the receptor cleavage and activation. Although the inhibition of the notch pathway is inadequate to defeat the basal-like breast tumour cell survival and proliferation, this inhibition revealed an important connection between these oncogenic pathways (Dong et al., 2010).

DAPT and compound E were also used to inhibit the Notch signalling in the retina in zebrafish to test the effect of the notch on maintaining Müller glial cell proliferation in the retina. Müller glial cells are considered as the main regenerative support cells for neurons in the vertebrate retina. Therefore, increasing the proliferation and the activation of these cells could be considered as a treatment for the damaged retina. The data suggest that blocking the notch pathways using DAPT and compound E is adequate to motivate other signalling pathways that are like those ones which are important for Muller Glia activation and proliferation in the light-damaged retina and propose that Notch signalling maintains multipotent cells in a quiescent state throughout the zebrafish nervous system (Conner et al., 2014).

Studies have shown that there's a correlation between the Notch1, Jagged1 levels and the tumour size, grade and tumour node metastasis stage, thus implying that there is a link between the Notch pathway and the oncogenesis process of renal cell carcinoma. DAPT was used on the renal carcinoma cell lines, and a decline in the cell's proliferation occurred along with an increase in cell apoptosis. This therapeutic impact of DAPT on

the tumour growth of the renal carcinoma cells suggests that DAPT would be an innovative therapeutic for renal carcinoma cell (K. Wu et al., 2014).

The γ-secretase inhibitor Compound-E decreased microvessel mass *in vivo*. The ovarian carcinogenesis cells treated with compound E presented a decline in the cell's proliferation. This experiment was repeated using DAPT, and the outcomes remained similar. This suggests that a wide choice of GSIs have a direct effect on cellular proliferation. However, in order to clarify the interaction between proliferation pathways of the abnormal cells and the γ-secretase inhibition efficiency, more studies need to be done (Shah et al., 2013).

Compound E inhibited the function of the notch in the ovarian tumour, and this resulted in a significant blockage for the growth of gonadotropin-dependent follicle up to the preovulatory phase of expansion. Additionally, it has been stated that using a higher dose of compound-E would cause an antitumor effect (Shah et al., 2013). This indicates that the proliferation of vascular cell is minimal at a control level in the animal's ovaries when treated with compound E. It has been proven through studies that compound E interrupts with theca layer endothelial cells accumulation with VSMCs and this interruption is adequate to destroy the growth of gonadotropin-dependent follicle (Jovanovic et al., 2013).
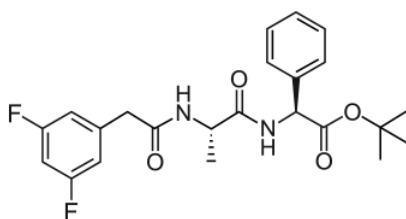
Figure 1.9. **Chemical structure of DAPT**.
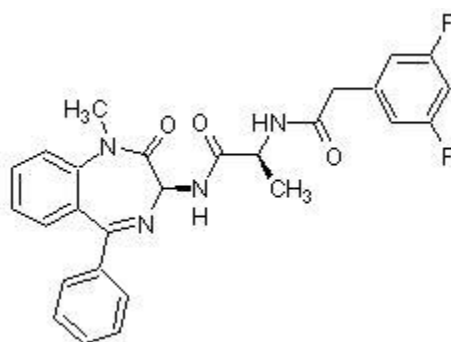
Figure 1.10. **Chemical structure of Compound E.**

7.1 Nanomedicine

The National Institutes of Health Research introduced the term Nanomedicine. Nanomedicine is a branch of medicine that applies nanotechnology on disease analysis, disease cure (Moghimi et al., 2005) and improved life science and health care (Tartaj et al., 2003). The results of the dramatic development of nanotechnology have led to an increase in the possibilities of applying engineered NPs for disease treatment (Naahidi et al., 2013). These new applications have enabled scientists, engineers, and physicians to work on a smaller scale like the molecular level (Tartaj et al., 2003). Also, they are able to include the identification of specific areas such as cells and receptors that might be responsible for the disorder in the body. This is achieved by choosing the proper nanocarrier to gain the needed responses with a lower percentage of side effects. There are many targets for nanotechnology applications. The most important ones are stem cells, endothelial cells, and cancers (tumour cells and tumour neovasculature) (Moghimi et al., 2005). It is believed that nanomedicine can enhance the CVD therapies using a combination of useful features of ultra-small sub–100-nm organic NPs and organised drug release (Chan et al., 2011). The mechanism is such that the atoms which construct a molecule with nanometre-scale size range and this molecule retains a unique property. These physical and chemical properties can alter or enhance because of their scaled downsize as a cluster of atoms (Moghimi et al., 2005).

7.2 Drug Delivery System

In order to enhance the pharmacological and remedial equities of a drug directed *in vivo*, drug delivery systems (DDS) such as lipid- or polymer-based NPs can be created. With trial and error of this system, several primary hitches that obstructed the use of the particulate DDS have been solved. Therefore, many DDS formulations of anticancer drugs nowadays have been officially approved for medical usage. Additionally, there is obvious attention to exploit the advantages of DDS to deliver new drugs and for their use with ligand-targeted therapeutics. This is because there are various pharmacological properties of free drugs that can be improved using DDS with its particulate carriers such as polymers with their linked carriers. There are two purposes for the currently constructed DDS, firstly to adjust the pharmacokinetics (PK) and biodistribution (BD) of their connected drugs and secondly as drug reservoirs. The DDS can have both or one of these purposes in the drug. The drug potency is considered as a very crucial property as well as the drug stability, solubility and its molecular weight. In general, if the DDS will carry low molecules which means low carrier ratio such as polymer conjugates the potency of the drug should be high. This is important to deliver therapeutically related amounts of the drug (Allen and Cullis 2004). For an effective anticancer drug carrier system, ideally, there are two requirements and NPs seem to own these requirements with satisfaction. One of the requirements is the ability to reach the targeted tumour tissues by penetrating the barriers in the body with as less as possible of their volume or activity loss within the blood circulation. Secondly, following the arrival to the tumour tissue, these drugs must have the selective ability for killing tumour cells with no harm on normal cells along with regulation of the release mechanism of active form. These two basic approaches are as well linked with enhancement in life quality and survival of patient by increasing the intracellular drug concentration and decreasing the dose-limiting toxicity (Cho et al., 2008).

7.3 Nanoparticles and stents

PLGA {poly (DL-lactide-*co*-glycolide)} based polymeric NP has been used to fabricate a drug delivery system. The prevalent use of biodegradable PLGA NPs is due to their advantages such as the capability to encapsulate water-soluble, encapsulate next-generation drugs (DNAs, oligonucleotides, proteins as anti-monocyte chemoattractant protein-1), improve cell membrane penetration via endocytosis and upsurge intracytoplasmic release. Moreover, the PLGA NP eluting stents have been proved safe for use in humans as neither did they raise the risk of thrombosis when tried in porcine coronary artery models nor did they work against the endothelial regeneration. (Nakano et al., 2009).

Curcumin-loaded PLGA NPs were used to demonstrate a novel drug delivery system that united localized drug delivery with controlled drug release. A natural emulsion method was used to load curcumin, an anti-proliferative natural product, into PLGA NPs. Conclusively, PLGA NPs proved to be an effective biodegradable barrier to anti-proliferative drug release while the electrophoretic deposition method was found to be highly reproducible, fast, flexible and reasonably economical coating method (Puranik et al., 2013).

This DDS trapped the hydrophilic agents like including the protein, DNA etc. and ultimately with endocytosis, the encapsulated therapeutic agents reach the cellular membrane and transported into the cellular cytoplasm (Niwa et al., 1994). A significant benefit of the NP-based drug delivery system over stent-based technologies is the ability to carry hydrophilic agents (Panyam et al., 2002). The PLGA used in this technology is biodegradable and hence safe for medical use. (Yamamoto et al., 2005).

The NP-based drug delivery system is far better than the systems that use non-NP polymeric DES coating technology. In porcine arteries, it was observed that water-soluble agents, including the oligonucleotides or plasmid DNA, could also be delivered using the NP eluting stents (Egashira et al., 2007). Hence, NP eluting stent system is a promising technique to deliver therapeutic agents for the treatment of CVD. (Lincoff et al., 1997). Thus, it becomes essential to think about the possible harms (toxicity) of using the NP eluting stent system to deliver the PLGA NP. When different types of polymer matrix materials used for stent coating were compared, the PLGA was found to be the

best option as it did not enhance the thrombosis instances in porcine coronary artery model (van der Giessen, Willem J et al., 1997). It has been observed that the bioabsorbable PLGA NP-eluting stent system can be used in human subjects without vascular toxicity. The stent-based platform, containing the delivery of proteins or genes that hinder inflammation, SMC proliferation, and thrombosis is considered as a new therapeutic strategy. (Miller et al., 1977). Another appealing strategy entails cell-specific delivery of NP into VSMC to block neointima formation or into endothelial cells to hasten endothelial regeneration. All the data points to the conclusion that in comparison to the dip-coated polymer eluting stent, bioabsorbable polymeric NP eluting stent system provides new features in novel electrodeposition coating technology, vascular compatibility and an efficient drug delivery system. This system is a promising method to deliver less invasive nanodevices as a CVDs treatment (Nakano et al., 2009).

Yang et al., 2013. achieved an improved drug release effect by mixing the grooves and the NPs. Bilayered PLGA (50/50) nanoparticles (BLPLGA NPs) were developed using a multistep emulsion technique. The outer layer of the BL-PLGA NPs consists of VEGF plasmids while the inner core contains paclitaxel. Vascular endothelial growth factor, i.e. VEGF, also known as vascular permeability factor (VPFs), is a kind of signal protein that is produced by the cells promoting the blood vessels formation. The rate and direction of flow and transport are usually determined using Rhodamine B which is a tracer dye within the water. It exhibits fluorescence and can be easily detected using fluorometers. Rhodamine B was loaded onto NPs- coated stent to verify the release of BL-PLGA NPs from the stent. A gradual decrease was observed in the intensity of fluorescence produced by rhodamine. However, it stayed detectable after shaking in PBS for 30 days. This indicated the slow-releasing effect and the stability of the BL-PLGA NPs coating layer. Using coaxial electrostatic spraying technology, a uniform NP stent was made by Hu et al., which could carry different kinds of drugs and provide a slow-release effect. (T. Hu et al., 2015).

7.3.1 Nanoparticle drug-eluting stents

The risk of late restenosis can be efficiently reduced by DESs. The present DESs operates through an organized and continuous release of the antiproliferative agents by using numerous biodegradable and non-erodible polymeric blends to coat the stent surface and to carry drugs. The existing stent technology can be further improved by using nanotechnology. Based on the therapeutic strategies, there can be two types of applications of nanotechnology, an anti-restenosis strategy to avert SMC proliferation and a pro-healing strategy to restore functional endothelium.

In the first strategy using anti-restenosis, NP-assisted delivery of small molecular weight antiproliferative and anti-inflammatory therapeutic agents can be used to prevent the in-stent neointima formation. Heat-induced ablation of inflammatory cells with light-activatable NPs can also serve the same purpose. In the latter strategy involving pro-healing, nanofibrous scaffolds or MNPs is employed. The nanofibrous scaffolds imitate the extracellular matrix in vessels while the MNPs use magnetic fields to increase the delivery speed of the cells to stent struts (Margolis et al., 2007, Danenberg et al., 2003).

A new prednisolone-encapsulated liposomal formulation that focused on chondroitin sulphate proteoglycans (CSPGs) was developed by (Joner et al., 2008b). They displayed that drugs localized especially to the stent-induced injury sites caused a reduction in the restenosis within atherosclerotic rabbits (Joner et al., 2008b). Similarly, collagen- IV-targeting, paclitaxel-encapsulated polymeric NPs called nano-burrs were developed by Chan et al.,   A considerable improvement was also reported in arterial stenosis when NP treatment was used in a rat carotid injury model (Chan et al., 2011).

A biocompatible, paclitaxel-loaded MNP was developed by (Chorny et al., 2012) which was drawn towards the stent struts and adjacent arteries in the presence of the magnetic field. This attraction allowed the NPs to be localized and inhibited the ISR (induced systemic resistance) at the same time (Chorny, Fishbein, Yellen, Alferiev, Bakay, Ganta, Adamo, Amiji, Friedman and Levy 2010a).

A bioactive stent was prepared by (Ceylan et al., 2011) by combining peptide amphiphile nanofibers with two products:

1. A REDV epitope which preferentially supports endothelial cell adhesion and spreading over SMCs and platelets. The REDV epitope has γ-4 β$_1$ integrins as a characteristic and has been shown to discriminatingly support the endothelial cell adhesion and spreading over smooth muscle cells (SMCs) and platelets. It also facilitated the selective growth of endothelial cells on the stainless-steel surface.
2. A Dopa (3,4-dihydroxyphenyl-L-alanine) molecule which immobilizes the nanofiber on stent surface by forming a strong hydrogen bond with hydrophilic surfaces of stainless steel.

7.3.2 Nanoparticle gene-eluting stents

As previously stated, nanotechnology strategies can be divided into two groups (i) inhibiting SMC-like proliferation; this strategy is called an anti-restenosis strategy and (ii) returning functional endothelium which calls for a pro-healing strategy (R. X. Yin et al., 2014). However, the utilisation of polymeric compounds in current drug-eluting stents may eventually limit their performance as well as their clinical applicability due to the potential induction of undesirable local reactions. Hence, using NP delivery of drugs, the extended-release of anti-proliferative agents can be accomplished (Lemos et al., 2013).

The stents are used as permanent supports by the Gene-eluting stents (GESs) to obtain the localized and continuous delivery of therapeutic genes to the affected vessel wall (Sharif et al., 2008). In recent times, the GESs has been recommended as an innovative method to avoid the issues caused by BMSs and DESs. In the current study, BMS displayed greater tendencies for neoatherosclerotic changes happening in the more proximal than DES distal lesions, thus representing different mechanisms by which neoatherosclerosis assign to DES could be more associated to incompetent and incomplete endothelialisation as contrasting to shear stress for BMS. These results in the BMS may be more similar to the atherosclerosis development in native coronary arteries and is most distinguished in the proximal areas of the coronary arteries (Davies 2009). The moderately earlier growth of neoatherosclerosis in DES than in BMS is possibly

associated with drug effects, which are also accountable for incomplete re-endothelialization. Previous animal studies of DES (Joner et al., 2008a) propose incomplete regeneration of the endothelial cell lining, and this could cause endothelial cell activation. The endothelial cell activation will lead to monocyte adherence with consequent subendothelial migration. Moreover, the present pathology study illustrates that there is a frequent presence of the neoatherosclerosis in DES, and happens significantly earlier in DES in comparing with BMS; nevertheless, BMS has more complications than DES. This could be as a result of the longer implant duration occurring in BMS (Nakazawa et al., 2011).

Restenosis and late stent thrombosis can be relieved by using nanotechnology and sustained and focused gene delivery, as they increase the speed of the regenerative ability of re-endothelization. The primary studies in the vascular gene therapy arena investigated the transport of both viral and non-viral gene factors using the catheters, such as the double-balloon, single lumen porous balloon, dispatch coil balloon, and Infiltrator nipple balloon catheters. But the modern studies are more interested in and favour the balloon-expandable GESs over catheters as a source for gene delivery. Moreover, using GESs to atherosclerotic coronary vessels is considered as an attractive method due to: first, an enhanced concentration of the therapeutic drug is made possible by the route immobilization (restriction) to stent struts, without spreading to non-target tissues and this avoids the system toxicity and raises the possibility of effective gene transfection to adjacent cells. Secondly, in mural thrombosis, vascular SMC proliferation and similar pathophysiological processes reflect the expected sites of therapeutic impact (Fishbein et al., 2008). Numerous methods of local gene delivery have been created and found effective in reducing restenosis in animal models. The four major molecular targets in focus are a reduction of neointimal hyperplasia; speeding up of re-endothelialization; restraining of thrombosis, and a decrease in inflammation. Among these, the most extensively studied method is the inhibition of restenosis via a reduction in neointimal (R. X. Yin et al., 2014).

There is a serious demand to innovate methods which are efficient to avoid the difficulties associated with BMSs and DESs. There are promising methods, including NP drug- and gene-eluting stents (R. X. Yin et al., 2014). A decrease in the risk of late restenosis was achieved by the drug-eluting stents (Lemos et al., 2013). To permit greater flexibility of

drug-release from DES, nanotechnology has been considered to allow for the best drug-tissue concentrations and continued drug delivery at the site of lesion facilitated by an external sheet of polymer (bioabsorbable or non-bioabsorbable) that coats metal stents and could be drug-loaded. Biodegradable polymers consist of poly-L-lactide (PLA), polyvinyl pyrrolidone, poly-lactide-co-caprolactone (PLC), and poly lactide-co-glycolide (PLGA) (Supralimus 181 And Infinium 181 stent, Sahajanand and Medical Technologies); or poly-L-lactic acid (PLLA) (Excel stent, JW Medical System). The difficulties related to polymer biocompatibility and polymer-induced infection can be reduced by the biodegradability of polylactic acid and polylactic-co-glycolic acid over a period. These two polymers are considered the greatest biodegradable polymers (Ho et al., 2016).

7.4 Polymers

Polymer Preparation is depending on the preparation method; the drug would be either captured physically in or linked covalently to the polymer matrix. Three possibilities of the producing compounds as they may have the:

– construction of capsules (polymeric NPs)
– amphiphilic core/shell (polymeric micelles)
– Polymeric NPs with hyperbranched macromolecules (polymer-drug conjugates).

Polymers such as albumin, chitosan, and heparin are known to be an optimal material for the oligonucleotide's delivery, DNA, and protein, in addition to the drugs (Ulbrich et al., 2016).

An NP fabrication of paclitaxel, where serum albumin is included and used as a carrier to generate nanometre-sized albumin-bound paclitaxel. There are several synthetic polymers such as the copolymer N-(2-hydroxypropyl)-methacrylamide (HPMA), polystyrene-maleic anhydride copolymer, polyethene glycol (PEG), and poly-L-glutamic acid (PGA). The first biodegradable polymer utilized for conjugate synthesis was PGA (Cho et al., 2008). Poly (lactic-co-glycolic acid) (PLGA) is a biodegradable polymer that has received FDA approval and allowed to be used in the treatment and therapeutic devices. PLGA coated NPs facilitates the prolonged release of hydrophobic drugs in

addition to extensive experimentations of PLGA NPs for DNA distribution in gene treatment (R. X. Yin et al., 2014).
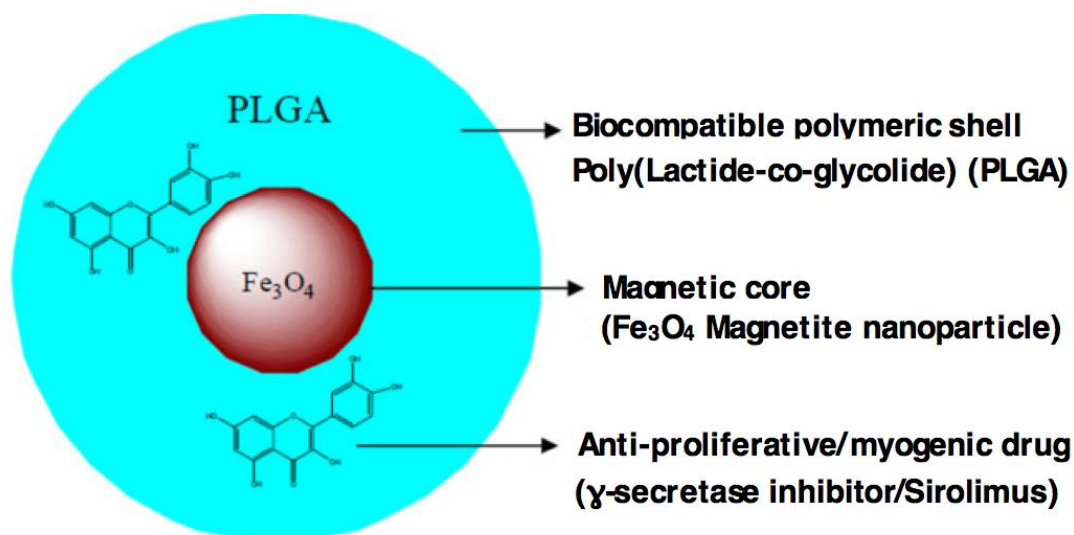
Figure 1.11. Schematic illustration of the ultrastructure of the nanoparticle. The magnetic core (nucleus, in red), incorporating the combination of two excipient carriers to allow penetration and release of the active agent. The PLGA has surrounded the core along with the γ-secretase inhibitors.

7.5.1 Magnetic nanoparticle

The NPs used in the drug delivery system are submicron-sized particles (3-200 nm), devices, or systems that can be formed by utilizing a diversity of resources along with:

– polymers (polymeric NPs, micelles, or dendrimers),
– lipids (liposomes),
– viruses (viral NPs)
– organometallic compound (Cho et al., 2008).

There is a very successful and alternative safe substitute approach to the present DES therapies. This strategy includes a combination of proficient drug carriers directed to the stented blood vessel and the continued drug discharge properties of the biodegradable polymer-based MNPs (Chorny et al., 2012). Freeman, Arrott et al., 1960 revealed a pioneering concept that fine iron particles can be carried through the vascular system and be located at a certain point in the body with the assistance of a magnetic field. The

purpose of using a drug delivery system is to localize the drug carriers to the linked place where the cell-specific ligands are located (Mamaeva et al., 2011).

Basically, drug localization to the area of interest using a magnetic field occurs due to the forces being put on the particles where the blood compartment is on one side and the magnetic field on the other side. Once the magnetic forces are over the linear blood influx average in arteries (10 cm s−1) or capillaries (0.05 cm s−1), this causes the magnetic particles to be retained at the wanted site and perhaps in the target tissue and these particles will be adopted by the endothelial cells of this tissue (Sun et al., 2008). Using the NPs for this application is preferred to the NPs transportation within the tissue and organs capillary system averting vessel embolism (Tartaj et al., 2003).

Superparamagnetic iron oxide NPs (SPION) have been extensively used in vivo such as magnetic resonance imaging, contrast improvement, repairing tissue, decontamination of biological fluids, drug delivery and in separating cells, etc. These entire applications need the NPs to be in a specific form. First, these NPs require to be with high magnetization, a size smaller than 100 nm with general narrow atom size delivery. As a result, the particles will have equal physical and chemical properties. Additionally, the magnetic particles are required to have a non-toxic and biocompatible coating surface which permits a targetable delivery of the particle to be localized in a precise area (Maleki et al., 2012).

Therefore, the MNPs can be attached to drugs, proteins, enzymes, antibodies, or nucleotides. Then these loaded MNP can be guided to an organ, tissue, or tumour with the help of an external magnetic field (Gupta and Gupta 2005) In details, the properties of MNPs differ depending on the usage. For instance, in biomedical utilization, it is favoured for particles to behave with superparamagnetic at room temperature (Bangs 1996).

7.5.2 Magnetic Nanoparticle Characteristics

Despite the numerous advantages provided by the NP as drug carrier systems, they still have many disadvantages, and a solution for these drawbacks need to be sought. These drawbacks include poor oral bioavailability, trembling in circulation, insufficient tissue

spreading, and toxicity. Therefore, in order to efficiently transport the drug to the desired tumour tissue, NPs should be capable of remaining in the bloodstream for a significant period without being disregarded. Additionally, the conventional surface of nonmodified NPs in circulation would be grasped by the liver or the spleen (reticuloendothelial system) according to the features of their size and surface. Consequently, regulating the NP's size and surface characteristics could lead to controlling the injected NP's fate (Cho et al., 2008). The following characteristics are required to ensure an effective carrier for the MNP loaded drug (Chorny et al., 2012) :

- the resilient magnetic reaction in case of nonappearance of magnetic memory because of the multiple small-sized iron oxide nanocrystals integrated into each individual particle
- The components must be entirely biocompatible and the appropriate dimension to reach the intravascular
- The chemically labile drug ($t_{1/2}$ ~8 h in aqueous solution at pH 7) should be protected from early disintegration
- Continued drug discharge

The process of endothelial repair and regeneration after damage can also be promoted by the time-based release of drugs that promote endothelial regeneration. For instance, the distribution of anti-proliferative agents to the vascular wall when neointimal proliferation is most active can be achieved with NPs. In addition, functionalised NPs can be directed to a specific location using ligands such as antibodies, peptides and minor particles in order to develop the drug delivery to locations of vascular damage (Chorny et al., 2012).

7.5.3 Magnetic nanoparticle benefits

The NPs facilitating drug delivery can be aimed at the stent themselves. There has been a development in the paclitaxel loaded MNP with the focus on the stent struts along with the arterial tissues that are close to the area. Imaging, sensing, tagging and separation, are all representation of the role of the MNP in the biomedical application. For instance, ferromagnetic iron oxide particles with poly-dispersive properties are being applied for emphasizing MRI contrast. Such polydispersity iron particles have decreased the NPs concentration that is essential for cell separation (Ambesh et al., 2017). There is a noticeable improvement in drug release profiles following incorporation of NPs into the

polymer coating layer on DESs. The long-lasting inhibition of cell growth is remarkable with moderate exposure to a short-term magnetic field (5 min), and a small dosage of Nano encapsulated paclitaxel (PTX), in contrast to the control treatments (Chorny et al., 2012). There is an important cell growth inhibition response that was produced by MNP treatment of cultured arterial SMCs with PTX-loaded MNPs. This effect was not detected under non-magnetic circumstances. There are also other advantages of MNPs: the substantial inhibition of in-stent restenosis with a low dosage of MNP-encapsulated PTX (7.5 µg PTX/stent). These advantages are due to the improved preservation of MNPs at object sites because of the uniform field-stimulated magnetization effect (Chorny et al., 2010).

7.5.4 Biomedical applications

There are two major biomedical applications for the use of MNPs; one *in vivo* and the other *in vitro*. *In vivo* applications include therapeutic strategies such as hyperthermia and drug-targeted delivery or diagnostic strategies such as nuclear magnetic resonance imaging (MRI). In contrast, the *in vitro* applications include diagnostic applications such as separation, selection and magnetorelaxometry (Tartaj et al., 2003). These diagnostic applications using MNPs are deployed for identifying very small molecules within tissues such as viral fragments that are undetectable under normal circumstances using classic diagnostics (Zhang et al., 2008).
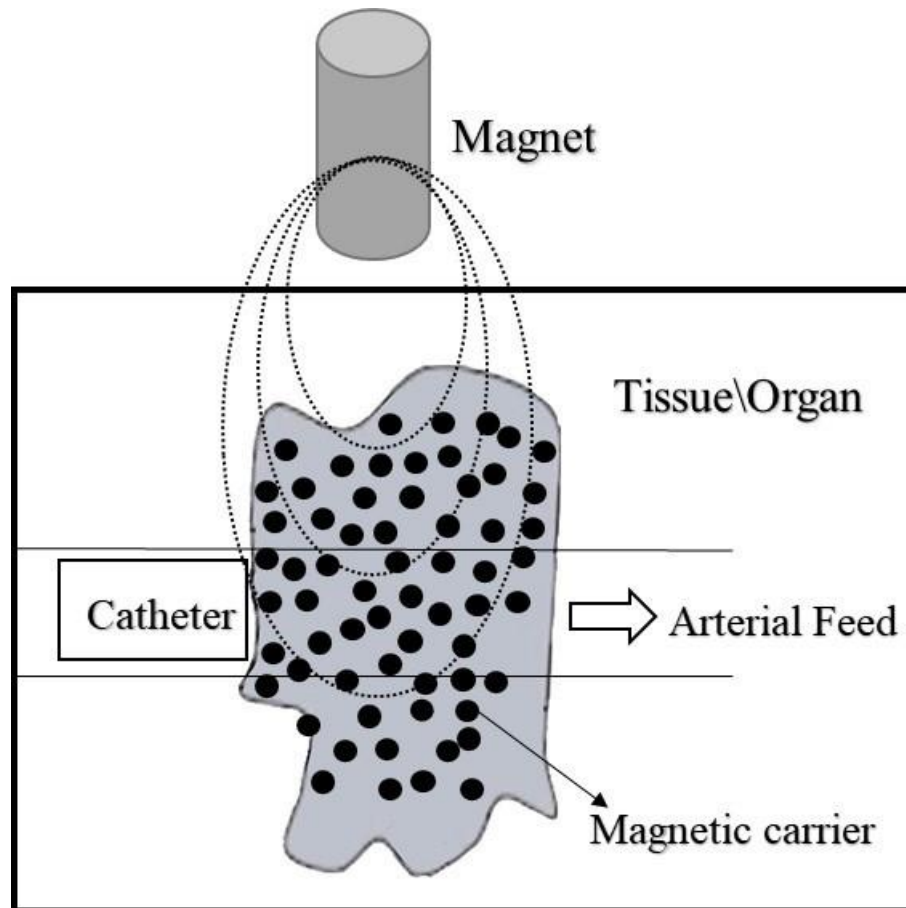
Figure 1.12. Schematic illustration of drug transport driven by a magnet to a precise area. A catheter is inserted into an arterial feed to the tumour, and a magnetic stand is located over the designated position. Figure adapted from (Tartaj et al., 2003).

Within the fabrication procedure of the MNPs to be used *in vivo,* a biocompatible polymer must be used to coat these particles. This is to avoid the creation of large aggregates, the alteration of the original structure and the biodegradation which could happen when these particles go through the biological system (Langer 1990). This biocompatible polymer is important as it is facilitating drugs binding by covalent attachment or entrapment on the particles (Denizot et al., 1999). The nature of the magnetically responsive component is used to detect the biocompatibility and toxicity of these particles. For example, these components are magnetite, iron, nickel, cobalt, neodymium–iron–boron or samarium–cobalt. Iron oxide particles such as magnetite (Fe_3O_4) or its oxidized form maghemite (γ-Fe_2O_4) are generally used for biomedical applications (Wormuth 2001). Regarding the NP size, the three leverages of having particles with a size smaller than 100 nm are first this will make their attachment to the ligands easier as their surface area become effectively higher, second their stability will be higher as the sedimentation rate will be

47

lower. Lastly, this small size will enhance the tissular diffusion (Portet et al., 2001). To conclude, the MNPs use in vivo biomedical application should be done with nontoxic and non-immunogenic material, and the size must be adequately small so after the injection of these particles, they will remain in the circulation and will not cause a vessel embolism when they go within the capillary systems of organs and tissues. Also, their magnetization must be high enough in order to monitor their flow in the blood using the magnetic field to point them nearby the pathologic tissue (Jordan et al., 2001).

On the other hand, the restriction for the particle size *in vitro* applications is not as important as *in vivo* applications. That is why even if the magnetic field is not present, the complexes containing superparamagnetic nanocrystals diffused in submicron diamagnetic particles with high sedimentation rates can be utilized. The positive aspect of adopting diamagnetic matrixes is that the superparamagnetic compounds can be effortlessly prepared with high effectiveness. The most challenges that occur during the fabrication of the nanomaterials is regulating the size and the shape of the particles in addition to their size distribution, their surface and their magnetic properties accordingly. If Ferri- and ferromagnetic materials such as Fe_3O_4 is prepared by grinding bulk, they may have uneven particles shapes. However, they can have round organized shape if they have been prepared with wet chemistry or from the aerosol and gas phases (Tartaj et al., 2003).

For the site-specific treatment of vascular disease, there is a targeted experimental approach now being developed by many laboratories. This approach includes the target delivery of drugs using polymer-coated MNPs loaded with the drug. Clinically, magnetic fields can do a lot. Normally, the content of these formulations is magnetically responsive NPs which are in steady connection with the drug. The targeting of this drug can be accomplished by one or more of the sources of the positioned magnetic field allowing the therapeutic agents to be targeted to an exact location in the body (Chorny et al., 2012).
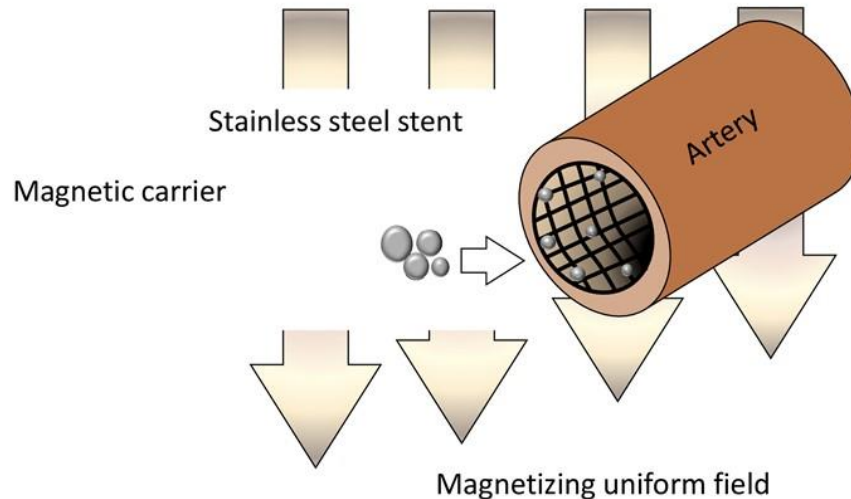
Figure 1.13. Magnetizing uniform field. The external magnetic field targets the magnetic nanoparticles (MNP's) to the area of the stent within the artery. Figure adapted from (Chorny et al., 2012).

Nanotechnology can be utilised in many areas in the cure of the CAD. Broadly, two treatment choices are available for the CAD: less aggressive ones using medications or aggressive ones, including mechanical revascularization, PCIs and coronary artery bypass graft surgery.

As a result of atherosclerotic lesion growth, necrotic lipid core and fibrous cap formation, the plaque deteriorates and ruptures resulting in intracoronary thrombosis formation, and this would cause myocardial ischemia and infarction in advanced cases. *In vivo*, it has been tested using Hirudin (a natural anti-thrombotic) encapsulated into micellar NPs for targeting the fibrin rich masses. The efficiency of this anti-thrombotic is under testing. Mouse models which have arterial thrombosis were used to test the NP loaded with irreversible thrombin inhibitor. This study suggested that intraarterial thrombosis decreased with the usage of anti-proliferative drugs. Also, delivering this drug could be achieved with ease using NPs targeting the PCIs with the recruitment of the endothelial cells. This inhibits neo-intimal hyperplasia and thrombogenesis formation. Additionally, in order to avoid arterial stenosis drug-loaded, NP has been tried. Paclitaxel is considered as a mitotic inhibitor with potent antiproliferative effects. Due to this, drug-eluting stents using Albumin-based- NP delivery of paclitaxel have been employed in a wide range to decrease proliferation and inhibit restenosis (Palekar 2015).

There is an irreversible binding that happens between albumin and paclitaxel. Moreover, albumin is attached to glycoprotein receptors on endothelial cells, and this is due to its natural affinity towards the vessel walls. According to the obtained data, it has been revealed that there is no significant toxic effect along with an optimal drug delivery while reducing the restenosis rates in the atherosclerotic rabbits. In addition, usage of the NPs loaded with paclitaxel in rat carotid injury models has been done and an anti-restenosis effect was observed (Ambesh et al., 2017).

7.5.5 γ-Secretase inhibitor magnetic nanoparticles

Drug-loaded particles conjugated to ligands promotes inhibition of notch activity *and* improvement of tumour retainment *in vivo*. A novel approach by Mamaeva et al., 2011 have used an imageable mesoporous silica nanoparticle (MSNPs) as a vehicle to deliver GSIs for notch signal blocking. Controlling of Notch activity in intestinal stem cells was achieved with the Oral administration of GSI-MSNPs. This proves the *in vivo* applicability of MSNPs to deliver GSI. MSNPs are discarded basically with the renal excretion as these particles are biocompatible and they do not reserve within the tumour. A communication occurs between the notch pathway and other oncogenic pathways; this leads to a resistance of the classic therapy approaches which targets these pathways. Additionally, the notch targeting therapy can be considered as an extraordinary potential cure choice. Recently, various medical experiments have been done to examine Notch inhibitors effectiveness and safety in cancer treatment. Furthermore, monitoring of stem cell fate and repair responses that happen by notch requires an evolved targeting strategy for regulating the period and the strength of Notch activity. This could be considered as an interesting curative in the field of developmental medicine (Mamaeva et al., 2011).

7.6 The challenges for nanomedicine:

The development of the NP has considered a challenge as the preparation steps for nanomedicines requires tremendous cleanliness. This is because the smallest impurities during the fabrication procedure could destroy the nano-infrastructure and this can be interpreted *in vivo* as an adversative outcome. In addition to the biological side effects, there's no up to date safety protocol for the NP as studies have only been done on a case by case basis. Therefore, the direct toxicity presents a major challenge, and there's the possibility of harm to the living cell due to the chemical used in the NP preparation. For

example, the carbon nanotube, the type of carbon isotope the surface coating and relative carbon tube concentrations all could be toxic in the body. Also, damage to the DNA has been observed as a result of using the NP. The mutation occurrence doubled following the multi-walled carbon nanotubes injection in mouse embryonic stem cells (Ambesh et al., 2017).

7.7 The future of nanomedicine in CAD therapy

The present nanomedicine has a promising potential in treating CAD. Following the stent placement, an endothelial regeneration is happening. It has been revealed that the drug-loaded MNPs represents a strong magnetic response and a possibility for therapeutic achievement. Despite the disadvantage of MNP as they could affect the cell proliferation, still, MNPs has presented a great value along with the magnetic targeting system in decreasing restenosis in rat vessels. The magnetic delivery of endothelial cells has been proven to be a favourable strategy in preventing the narrowing of the lumen. Ongoing studies have shown that there is remarkable progress in nanomedicine for the development of an effective nano-drug delivery system for CAD treatment (Ambesh et al., 2017).

1.8 Aims and Objectives

The specific aims of the thesis were:-

1. Determine the effects of ɣ-secretase secretase inhibitors (DAPT and Compound E) on VSMC and mesenchymal stem cell (MSC) proliferation and apoptosis *in vitro.*

2. Determine the effects of ɣ-secretase secretase inhibitors (DAPT and Compound E) on vascular, myogenic differentiation of mesenchymal stem cell (MSC) *in vitro.*

3. Fabricate PLGA-PVA MNP's loaded with ɣ-secretase secretase inhibitors (DAPT and Compound E)

4. Characterise PLGA-PVA MNP's loaded with ɣ-secretase secretase inhibitors (DAPT and Compound E) and determine their drug release kinetics *in vitro.*

5. Determine the effects of PLGA-PVA MNP's loaded with ɣ-secretase secretase inhibitors (DAPT and Compound E) on vascular, myogenic differentiation of mesenchymal stem cell (MSC) and resident vascular stem cells (MVSCs) *in vitro.*

Chapter 2

Materials and Methods

2.1   Materials

Material	Product Code	Company
2-Mercaptoethanol	M7522	Sigma-Aldrich, Arklow, Ireland
B27 Supplement	17504-044	Gibco/Bio-sciences, Dun Laoghaire
C$_3$H T10 1/2 Cells	ATCC-CCL-226	ATCC, Middlesex, UK
Mouse Smooth Muscle Cells	CRL-2797 Lot 58678387	American Type Culture Collection (ATCC) (United States)
DMEM	D5796	Sigma-Aldrich, Arklow, Ireland
DMEM	ATCC-30-2002	ATCC, Middlesex, UK
EMEM	ATCC-30-2003	ATCC, Middlesex, UK
FBS	F9665	Sigma-Aldrich, Arklow, Ireland
FBS	ATCC-SCRR-30-2020	ATCC, Middlesex, UK
Hanks Balanced Salt Solution	H6649	Sigma-Aldrich, Arklow, Ireland
Igg-Fc	110-HG-100	R&D, Abingdon, UK
Recombinant Jagged-1-Fc	599-JG-100	R&D, Abingdon, UK
Mouse Mesenchymal Stem Cells	S1502-01	Gibco/Bio-sciences, Dun Laoghaire
N2 Supplement	A13707-01	Gibco/Bio-sciences, Dun Laoghaire
Penicillin/Streptomycin	P4333	Sigma-Aldrich, Arklow, Ireland
Pierce™ Recombinant Protein G	21193	MSC, Mulhuddart, Ireland
Retinoic Acid	R2625	Sigma-Aldrich, Arklow, Ireland

Soybean Trypsin Inhibitor In Mem	10109886001	Roche, Dublin, Ireland
TGF-β1	7666-MB-05	R&D, Abingdon, UK
TrypleE Select	12563029	Thermo-fisher, Paisley, UK
MEM⁺glutamax media	32571028	Gibco/Bio-sciences, Dun Laoghaire. Ireland
Stem cell qualified FBS	12763025	Gibco/Bio-sciences, Dun Laoghaire. Ireland

Cell Characterization Antibodies and Reagents (ICC and FACS)

Material	Product Code	Company
anti-beta Actin	2228	Sigma-Aldrich, Arklow, Ireland
Anti-Calponin 1	ab46794	Abcam, Cambridge, UK
Anti-SM-MHC (Myh11)	sc-79079	Santa-Cruz Biotechnology, Heidelberg, Germany
Anti-smooth muscle Myosin heavy chain 11 antibody (Myh11)	AB683	Abcam, Cambridge, UK
BSA	A4503-50g	Sigma-Aldrich, Arklow, Ireland
DAPI	D9542-5 mg	Sigma-Aldrich, Arklow, Ireland
Goat Anti-Mouse Alexafluor488	A11030	Bio-sciences, Dun Laoghaire, Ireland
Goat Anti-Rabbit Alexafluor488	A11008	Bio-sciences, Dun Laoghaire, Ireland
Poly-L-Lysine	P9155	Sigma Aldrich
Tween-20	P1379	Sigma Aldrich
Glycine	G8898	Sigma Alrich
3.7% Formaldehyde	F8775	Sigma Aldrich

Myosin L-18: Myh11 Primary antibody	SC79078	Santa Cruz Biotechnology, Heidelberg, Germany
Triton-x-100	BP151500	Fischer Scientific
Fluoromount Aqueous Mounting medium	F4680	Sigma Aldrich
Alamarblue®	BUF012B	Bio-rad (United State)
Fluorescein Isothiocyanate (FITC) Annexin V Apoptosis Detection Kit I	556547	Becton Dickinson (Bd) Biosciences (United State)
DAPT	D5942	Sigma-Aldrich, Arklow, Ireland
Compound E	sc-221433	Santa-Cruz Biotechnology, Heidelberg, Germany

RNA Preparation

Material	Product Code	Company
Reliaprep RNA cell Miniprep system	Z6012	Promega
DNAse I, RNAse Free	89836	Thermo-fisher, Paisley, UK
Ultra-pure water with diethylpyrocarbonate (DEPC treated water)	750024	Thermo-fisher, Paisley, UK

Real Time q-PCR Reagents

Material	Product Code	Company
PrimeTime Calponin1 forward	PT.58.12652862	IDT Technologies, Leuven, Belgium
PrimeTime Calponin1 reverse	PT.58.12652862	IDT Technologies, Leuven, Belgium
PrimeTime Hey1	customised	IDT Technologies, Leuven, Belgium
PrimeTime mHPRT Forward	customised	IDT Technologies, Leuven, Belgium
PrimeTime mHPRT Reverse	customised	IDT Technologies, Leuven, Belgium
PrimeTime Myh11 forward	T9281	IDT Technologies, Leuven, Belgium
PrimeTime Myh11 reverse	T0565	IDT Technologies, Leuven, Belgium
Dynamag PCR Magnet	492025	Bio-sciences, Dun Laoghaire, Ireland
Quantitect mHPRT Primer	QT00166768	Qiagen, Hilden, Germany
Reliaprep RNA Miniprep spin columns	Z6012	IDT Technologies, Leuven, Belgium
Rotor-Gene SYBR® Green RT-PCR Kit	204174	Qiagen, Hilden, Germany
Sensifast SYBR no-rox	Bio-72005	MSC, Mulhuddart, Ireland
DNA Miniprep Kit	786-361	Qiagen, Hilden, Germany
Quantitect mCnn1 Primer	QT00105420	Qiagen, Hilden, Germany
Quantitect mHey1 Primer	QT0915094	Qiagen, Hilden, Germany
Quantitect mMyh11 Primer	QT01060843	Qiagen, Hilden, Germany

Nanoparticle Formulation & Analysis

Material	Product Code	Company
poly(lactic-co-glycolic acid) (PLGA	P2066	Qiagen, Hilden, Germany
dichloromethane	650463	Qiagen, Hilden, Germany
Iron (II)(III) Oxide in solution	700312	Qiagen, Hilden, Germany
Poly(vinyl)alcohol (PVA)	363138	Qiagen, Hilden, Germany
Supelco Discovery C18 Column	568523-U	Qiagen, Hilden, Germany
Acetonitrile	34851	Sigma-Aldrich, Arklow, Ireland
Dextran Magnet	2501008	Qiagen, Hilden, Germany

2.   Methods:

2.1.   Cell Culture

Cell Maintenance

The clean and sterile environment was used for all smooth muscle cell culture techniques using a Biosciences Air 2000 MAC laminar flow cabinet. Nikon Eclipse TS100 phase contrast microscope was used to visualise cells.

In this study, four cell lines have been employed:

i.   mouse smooth muscle cells (mSMCs) MOVAS ATCC ® CRL-2797™ Mus musculus aorta/smooth muscle was purchased from LGC Standards (UK)
ii.   mouse mesenchymal stem cells (mMSCs) purchased from Life Technologies.
iii.   mouse C3H/10T1/2 mesenchymal stromal cell line ATCC C3H/10T1/2, Clone 8 ATCC ® CCL-226™ was purchased from LGC Standards (UK)
iv.   mouse multipotent vascular stem cells (mMVSCs) derived from mouse aorta by explant

The mSMCs were grown in their complete growth medium which include 10% Fetal Bovine Serum (FBS) (Sigma) (v/v) with 1% penicillin/streptomycin (v/v) in Dulbecco's Modified Essential Medium (DMEM).

The mMSCs were grown in their complete growth medium which include 10% Mesenchymal Stem Cell Qualified FBS (Gibco S1502-01) (v/v) with 1% penicillin/streptomycin (v/v) in alpha Minimum Essential Medium (MEM) + Glutamax.

The C3H-10T1/2 cells were grown in their complete growth medium which includes 10% (v/v) heat-inactivated FBS (ATCC ESC) with 1% penicillin/streptomycin (v/v) in Eagles Modified Minimum Essential Medium (EMEM).

The mMVSCs were grown in their complete growth medium which include 1% FBS (ATCC ESC) (v/v), 1% penicillin/streptomycin (v/v), 1% N-2 Supplement (100X) (v/v), 2% chick embryo extract (v/v), 2% B-27 Supplement serum free (50X) (v/v), Recombinant Mouse basic Protein FGF (bFGF) (20 ng/μL), 100 nM Retinoic acid, 50 nM 2-Mercaptoethanol in DMEM. The cells were maintained in a Hera water jacket cell incubator at 37°C in an atmosphere humidified with 5% CO_2.

Trypsinisation of cells and subculture

Trypsinisation has required to subculture the cells. This is because all the cell lines used were adherent. Trypsin is a proteolytic enzyme that detaches cells from the surface they are cultured onto. Growth medium was removed from flasks/culture dishes and cells were washed twice using sterile Phosphate Buffered Saline (PBS) to ease the inhibition of α-2- macroglobulin, a constituent of FBS which prevents the trypsin activity. An appropriate volume of 1 X of trypsin added to the flask which was then incubated at 37°C for two to five minutes (depending on cell type). Regular cell growth medium containing FBS was added to neutralise the enzyme cleaving action of the trypsin. The mMSCs and mMVSCs were detached using Tryple E 1% (v/v) in PBS. The C3Hs detached by scraping. The cell suspension was placed in a 15ml centrifuge tube and cells spun down at 115 x g for five minutes at room temperature. Following centrifugation, the supernatant was carefully removed, and the pellet was re-suspended in 3ml of complete growth medium before the cells were counted using a haemocytometer.

2.1.1 Cell Counting

To ascertain the number of viable cells after trypsinisation or detachment, the cells were suspended in medium and cell number calculated using a haemocytometer. A 20μl of Trypan Blue was mixed at 1:1 with 20μl of the cell suspension before cells were counted. The unviable cells stain blue because their membrane is leaky. In contrast, the viable healthy cells do not absorb the dye and will turn up brighter under the microscope.

2.1.2 Cryogenic Cell Storage and Recovery of Cells

For freezing down, cells were split and trypsinised as described above, but the pellet was re-suspended in 10% Dimethylsulfoxide (DMSO) (v/v) with 20% (v/v) growth medium in addition to the complete growth medium. One mL of the suspension was transferred to sterile cryovials in a Nalgene Cryo freeze container and kept overnight in the -80˚C freezer. Then, for long-term storage, cells could be stored in liquid nitrogen. To defrost frozen cells, they are rapidly defrosted at 37˚C and re-suspended in 10mls of growth medium. The resultant suspension is centrifuged at 300 x g for five minutes and the resultant pellet is re-suspended in the fresh growth medium. Twenty-four hours later, a washing step can be done in the cells with PBS and medium changed.

2.2 Growth Studies

Alamar Blue Proliferation Assay

The cell proliferation alamarBlue® assay was performed to deliver a quick and accurate quantitative measure of cell proliferation and cytotoxicity in various cell lines. The alamarBlue® is an indicator dye, that integrates an oxidation-reduction (REDOX) indicator fluoresces and changes colour due to chemical reduction of the growth medium, resulting from cell growth. Continued growth maintains a reduced environment (Fluorescent, red). Inhibition of growth maintains an oxidizing environment (Non-fluorescent, blue). The colourimetric change was analysed by the Tecan Safire II. The wavelength was 530 λm for the excitation wavelength and 590 λm for the emission wavelength.

2.2.1 Cell Proliferation Assays using Alamar Blue Assay

For proliferation studies, cells were seeded at a density of 10,000 cells per well of 96 well plates (Thermo Scientific) and left for 24h in a complete growth medium. After this period the cells were quiesced with 0.5% FBS (v/v) with 1% penicillin/streptomycin (v/v) in DMEM. The following day, the cells were treated with the γ −secretase inhibitors DAPT and Compound E accordingly (Table 2.1 - 2.4).

After 3, 7 and 10 days, alamarBlue® was added at a concentration of 10% of the total well volume (i.e. 10μL in 100μL) followed by incubation at 37°C in the dark (using aluminium foil to cover the plate) for approximately three hours. Fluorescence was read on the Tecan Safire II at an excitation wavelength of 530 λm, the emission wavelength of 590 λm and bandwidth of mostly 10 λm and rarely 20 λm. The gain used was optimal.

Table 2.1. Serial Dilutions of DAPT using 30mM DAPT Stock

Desired Concentration (μM)	Previous Concentration (μM)	Volume of Previous Concentration (μL)	Volume of Medium (μL)	Total Volume
300	30000	30	2970	3000 μL
200	300	2000	1000	3000 μL
150	200	2250	750	3000 μL
100	150	2000	1000	3000 μL
80	100	2400	600	3000 μL
50	80	1875	1125	3000 μL
10	50	600	2400	3000 μL

Table 2.2. Serial Dilutions of DAPT using 12mM DAPT stock

Desired Concentration (μM)	Previous Concentration (μM)	Vol. of Previous Concentration (μL)	Volume of Medium (μL)	Total Volume
300	12000	100	3900	4000 μL
150	300	2000	2000	4000 μL
100	150	2667	1333	4000 μL
80	100	3200	800	4000 μL
50	80	2500	1500	4000 μL
10	50	800	3200	4000 μL

Table 2.3. Serial Dilutions of Compound E using 10.19mM Compound E Stock

Desired Concentration (μM)	Previous Concentration (μM)	Volume of Previous Concentration (μL)	Volume of Medium (μL)	Total Volume
300	1019	120	3880	4000 μL
200	300	2667	1333	4000 μL
150	200	3000	1000	4000 μL
100	150	2667	1333	4000 μL
90	100	3600	400	4000 μL
80	90	3556	444	4000 μL
70	80	3500	500	4000 μL
60	70	3429	571	4000 μL
50	60	3333	667	4000 μL
25	50	2000	2000	4000 μL
10	25	1600	2400	4000 μL

Table 2.4. Serial Dilutions of Compound E using 10.19mM Compound E Stock

Desired Concentration (μM)	Previous Concentration (μM)	Volume of Previous Concentration (μL)	Volume of Medium (μL)	Total Volume
100	1019	40	3960	4000 μL
50	100	2000	2000	4000 μL
45	50	3600	400	4000 μL
40	45	3556	444	4000 μL
35	40	3500	500	4000 μL
30	35	3429	571	4000 μL
25	30	3333	667	4000 μL
20	25	3200	800	4000 μL
10	20	2000	2000	4000 μL

Data analysis for Alamar Blue assay

The result was analysed in Excel and plotted using the relative fluorescent unit (RFU) vs. the drug concentrations using GraphPad Prism™.

2.2.2 Flow Cytometry

Fluorescent Activated Cell Sorting (FACS) or Flow cytometry is a technique to measure properties of cells as they move, or flow, in liquid suspension. All materials, including cells, will scatter light. In the flow cytometry, light scatters detectors are located opposite the laser relative to the cell. The measurements are made by these detectors: Forward light scatter (FSC) which provides information on the relative size of individual cells, and side light scatter (SSC) which provides information on the relative granularity of individual cells. If a cell is fluorescing for a particular protein, for example, Annexin-V-FITC, it will be excited by the laser and give off fluorescence which is picked up by the detector. BD FACS Aria-II instrument was used for these experiments and FLOWJO version 7.6.5 was used for FCS raw data analysis.

2.2.3 Apoptosis assay

In normal live cells, phosphatidylserine (PS) is located on the cytoplasmic surface of the cell membrane. However, in apoptotic cells, PS is translocated from the inner to the outer plasma membrane, thus exposing PS to the external cellular environment. The human anticoagulant, Annexin-V, has a high affinity for PS and can be used to identify apoptotic cells by binding to PS. Propidium iodide (PI) penetrates only damaged cellular membranes and then binds to double-stranded Deoxyribose Nucleic Acid (DNA).

AnnexinV-FITC/PI

The Annexin-FITC Apoptosis Detection Kit (Becton Dickinson) contains recombinant Annexin-V conjugated to the fluorochrome, FITC and the vital dye PI. Viable cells with intact membranes exclude PI, whereas the membranes of dead and damaged cells are permeable to PI. Cells that stain positive for Annexin-V and negative for PI are undergoing apoptosis. Cells that stain positive for both Annexin-V-FITC and PI are either in the end stage of apoptosis, are undergoing necrosis, or are already dead. Cells that stain negative for both Annexin-V-FITC and PI are alive and not undergoing measurable apoptosis. To perform the assay, cells were harvested and washed twice in ice-cold PBS. The cells were re-suspended in 1X Annexin-binding buffer at a concentration of ~1 x 10^6 cells/mL. A volume of 5 μL of Annexin-V-PE solution and 5 μL of the PI solution was added to 100 μL of cell suspension. The cells were incubated at room temperature for 15

minutes in the dark and 400 µL of 1X Annexin-binding buffer was then added and the samples were analysed within 1 h by flow cytometry.

2.2.4 Apoptosis Assay for Drug Dose Responses

A density of 5,000 or 10,000 cells/well was used to seed cells in a 6 well plate. Cells were left to grow overnight with 10% FBS (v/v) in growth medium in the Hera water jacket cell incubator at 37˚C in an atmosphere humidified with 5% CO_2. Cells were then quiesced with 0.5% FBS overnight in the same conditions. The cells were then treated after this period as per the table below (Table 2.5 – 2.6) and left for three and seven days before the level of apoptosis was assessed. Cells were washed with PBS and scraped from the 6 well plates and centrifuged at 1,500xg for five minutes, washed again with PBS and centrifuged. Then finally resuspended in 1x Annexin Binding Buffer -diluted with deionized water (dH2O)- and 5µL of Annexin-FITC and 2µL of Propidium Iodide (100µg/mL). The live/dead assay was carried out using the FACS Aria.

Table 2.5. Serial Dilution Table for Compound E using 10.19mM Compound E Stock

Desired Concentration (µM)	Previous Concentration (µM)	Volume of Previous Concentration (µL)	Volume of Medium (µL)	Total Volume
30	1019	32	10668	10700 µL
15	30	4500	4500	9000 µL
5	15	2667	5333	8000 µL
1	5	1400	5600	7000 µL

Table 2.6. Serial Dilution Table for DAPT using 58mM DAPT Stock

Desired Concentration (µM)	Previous Concentration (µM)	Volume of Previous Concentration (µL)	Volume of Medium (µL)	Total Volume
300	58000	36	6964	7000 µL
200	300	4667	2333	7000 µL
150	200	5250	1750	7000 µL
100	150	4667	2333	7000 µL
75	100	4500	1500	7000 µL
50	75	4000	2000	7000 µL
1	50	120	5880	7000 µL

FACs Data analysis

The results appear with four scatter plots the lower left quadrant shows healthy live cells lower right shows early apoptotic cells upper right shows necrotic cells and upper left shows late apoptotic cells. The percentage of the apoptotic cells and the necrotic cells were plotted by line graph using GraphPad Prism ™.
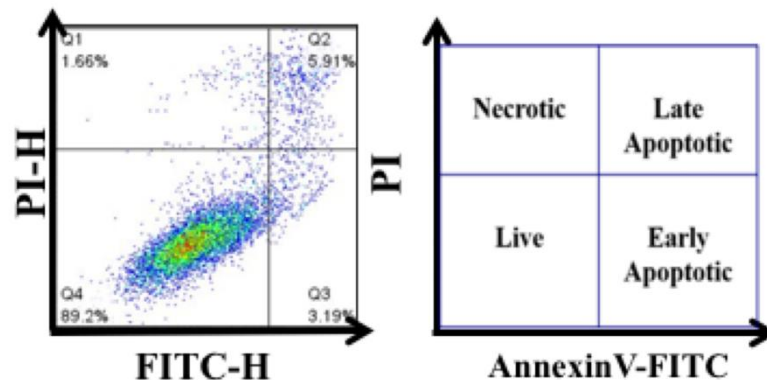
Figure 2.1. Typical FACS read-out for measuring apoptosis using the Vybrant™ Annexin V/propidium iodide assay

2.2.5 DAPI nuclear cell counting

DAPI is a high-purity form of (4′,6-Diamidino-2-phenylindole) dye is a classic nuclear counterstain for immunofluorescence microscopy of fixed cells. Due to the selectivity of DAPI for DNA and high cell permeability, it allows efficient staining of nuclei.

Cells were grown and treated with 25 µM of Compound E and 80 µM DAPT. Following treatment, cells were fixed with 3.7% formaldehyde (v/v) in PBS for a period of fifteen minutes. Following cell fixation, each well is washed with ice-cold PBS for five minutes and this is repeated three times. After three washes, cells were permeabilized with 0.1% Triton-X100 (v/v) in PBS. Again, the cells were washed three times with ice-cold PBS for five minutes each wash. Following that DAPI nuclear stain was added at a concentration of 1:1000 (i.e. 1µL in 1000 µL PBS) and the plate protected from light and incubated for 15 minutes at room temperature. The wells were then washed with ice-cold PBS for 5 minutes three times and the cells viewed under the Olympus 3000 Fluorescent Microscope. At least 5 high power field images were assessed for each treatment group and the cell nuclei counted in each image using Fiji Image J software ™.

Data analysis

Five images per sample are taken at magnification x10 before open-source software ImageJ™ (version 1.46r) was used to analyse each image. The number of cells in each image was used to determine the number of cells per well.

The number of cells / 0.00579373 (Area of 10 x of the microscope objective) multiplied by the 9.5 cm^2 (the well area in 6 well plate).

Then, the average cell count of this formula was taken and plotted in bars using GraphPad Prism™ and plotted DAPI nuclei positive cells vs drug concentrations. Results were presented as mean ± SD (where SD = standard deviation and n = number of cells). All statistical analysis was executed using one-way ANOVA or Kruskal Wallis t-tests based on the normality of the data. $p < 0.05$ was taken as a cut off value for significance.

2.3 Myogenic Differentiation Studies

Myogenic differentiation of mouse mesenchymal stem cells (mMSCs) and mouse multipotent vascular stem cells (mMVSCs) was performed following Notch activation as follows: First, 6 well plates were coated with protein G (MSC 21193) (50 μg/mL) overnight at 4°C. This step was necessary to immobilise Jagged-1(Jag-1) to a cell culture plate. Following the overnight incubation, a washing with sterile PBS was performed twice before blocking with 1% Bovine Serum Albumin (BSA) (v/v) in PBS for two hours at room temperature and then washed twice with PBS. An extra layer of coating was then done with 100 ng/mL for mMSCs and 500ng/mL for mMVSCs of Immunoglobulin (IgG)-Fc or Jag-1-Fc control for two hours. Plates were then washed with sterile PBS. Cells were then seeded at density of 20,000 cells/well for mMSCs, 50,000 cells/well for mMVSCs (for Quantitative Reverse Transcriptase Polymerase Chain Reaction (q-RT-PCR) or 5,000 cells/well (for all cell lines for immunocytochemistry (ICC) on glass coverslips) on these coated wells and incubated at 37°C for 24 hours for notch target genes marker Hey1 or more up until seven days for smooth muscle differentiation markers[calponin 1 (Cnn1) and myosin heavy chain 11 (Myh-11)]. Cells were then analysed for notch target genes Hey1 and for the smooth muscle differentiation markers expression (Cnn1) and (Myh-11) by ICC or q-RT-PCR.

Transforming Growth Factor Beta (TGF-β1 signalling pathway) was also used to induce myogenic differentiation. Cells were seeded at a density of 15,000 cells/well (for q-RT-PCR) or 6,000 cells/well (for ICC on glass coverslips) onto 6 well plates with the appropriate medium consisting of 10% (v/v) FBS and TGF-β1 (2-10ng/mL) or vehicle for 24 hours. Cells were then analysed for the smooth muscle marker expression (Myh-11) by q-RT-PCR.

The doses chosen to treat cells was chosen after initial studies determined the minimum dose that prompted a significant response which was then utilised for all similar experiments. The time selected for myogenic differentiation was also dependent on the subsequent method of analysis as the notch target genes expression occurred early while SMC differentiation protein and transcript marker protein expression take a longer time. The density of cells was chosen depending on the method used for analysis. Cells were seeded at low density for ICC as they were required to be seen under the microscope and countable for data processing and analysis. However, for harvesting cells to get high yield concentration of RNA, the number of cells was higher to detect the amplicons for specific genes through the q-RT-PCR.

2.3.1 Immunocytochemistry for SMC Markers

Cells were grown and treated as required for the experiment. Treated cells were then fixed with 3.7% formaldehyde (v/v) in PBS for 15 minutes. The cells were then washed three times with PBS. After fixation, cells were permeabilized with 0.1% Triton-X100 (v/v) in PBS. Another washing step was done on the cells three times. Cells were then blocked with 5% (BSA) (w/v) in 0.3% Glycine (w/v) in PBS with 7 PH for one hour at room temperature. The cells were then incubated overnight at 4°C with the appropriate primary antibody at the appropriate dilution (See Table 2.7). After the overnight incubation, the cells were washed three times as the day before and incubated with the appropriate secondary antibody (anti-rabbit for anti-calponin1 primary and anti-mouse for anti-myosin primary) at a dilution of 1:1000 for one hour at room temperature. After this period the cells were washed again three times and incubated for fifteen minutes with the cell nuclei stain (DAPI) at 1:1000. The cells were washed for the final time and viewed under the Olympus 3000 Fluorescent Microscope.

Table 2.7. Primary Antibody Dilutions for ICC

Primary Antibody	Dilution
anti- myosin SM-MHC (Myh11)	1:400
anti-calponin1	1:250

Data analysis

The number of positive cells was counted and divided by the number of negative cells to get the fraction of positive cells in each image and plotted using GraphPad Prism™ software.
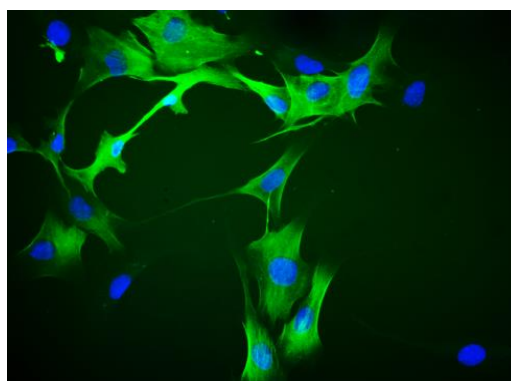
Figure 2.2. Sample immunocytochemical staining. Sample immunocytochemical readout with DAPI staining (blue) and Cnn1/alexafluor488 staining (green).

For capturing the images with the Olympus CK30 microscope Cell^F software was used. A threshold of background staining was distinct by using the secondary antibody control and exposure rates were restricted to avoid false positives. Minimum of five images were taken from the Olympus CK30 microscopy per slide. The images were analysed and cells were counted as described above.

2.3.2 RNA Extraction for RT-q-PCR

Two protocols were used from two different kits:

 Protocol 1: Ribonucleic Acid (RNA) was isolated from cultured cells using the MagCore® HF16 System of RBC Bioscience Corp. This instrument purifies Nucleic acids (RNA and DNA) from various tissue types, but for these experiments kit no. 610 was used for RNA extraction. The kit is a cartridge that contains various solutions/buffers pre-prepared that are essential for the isolation of RNA. These cartridges were slotted into racks within the machine. Two sets of racks are inside the machine, the smaller T-rack carried the samples and buffers prepared by the operator and the second larger rack carry the prepared cartridges. Pipette tips are added to well 2 and the raw sample is picked up and the RNA extracted by the machine. This allows everything to be carried out in a controlled, sterile environment. A protocol for tissue processing was provided by the instrument and this protocol was followed. In brief, Cells were trypsinised from 6-well plates and washed once using PBS. A solution of reaction buffer which includes 1% β-mercaptoethanol (v/v) in Ripa buffer that provided with the kit. Following that, 200μl of this solution was added to the cell pellet. The cell and buffer solution was mixed using a vortex until the cell pellet was resuspended. This suspension was added to well 4 on the rack. A DNase solution was prepared using DNase I and a DNase buffer solution provided with the kit, and this was added to well 3. The 610-option programme was run and the entire period for pure RNA extraction was 73 minutes. Samples were eluted in 60μl of Diethylpyrocarbonate (DEPC)-treated water into an elution tube inserted to Well 1. The RNA samples were kept at -80oC until they were analysed. RNA samples were qualified, and their purity was measured by using the Nanodrop 2000 spectrophotometer (Thermo Scientific). The purity was detected by the value attained at the 260nm and 280nm absorbance. A ratio of 2 is normally accepted as pure for an RNA sample (Wilfinger et al., 1997). Three readings were taken and averaged for each sample. Every sample had a suitable level of purity and the yield of isolated RNA was adequate to carry out qRT-PCR analysis.

 Protocol two: After 48 hour of exposure to treatment, cells were trypsinised and collected by centrifugation at 300 x g for five minutes. Cells were washed with ice-cold sterile PBS and re-suspended in 85μl of isopropanol. For each sample, filter cartridge was placed into the collection tube that was supplied with the kit. The aqueous layer mixture was pipetted onto the filter cartridge tube and centrifuged for 30 seconds at 12,000RCM

at 20º-25ºC. The resulted flow- through in the collection tube was discarded and the collection tube was reused for washing with RNA (500µl) wash solution followed by centrifugation for 30 seconds at 12,000RCM. Filter cartridge was then transferred into the clean new collection tube. To elute RNA from the filter, DNase 1 solution (24µl Yellow Core Buffer, 3µl MnCl$_2$ (0.09M) and 3µl DNase 1) was added to the centre of the filter and incubated for 15 minutes. Finally, 200µl of column wash solution was added followed by centrifugation for 15 seconds. The resulted elute was collected and stored at -80 C. The concentration and purity of RNA were identified using Nanodrop 2000 spectrophotometer (Thermo Scientific).

2.3.3 Realtime Quantitative Reverse Transcriptase Polymerase Chain Reaction

Realtime quantitative reverse transcription Polymerase Chain Reaction (RT-qPCR) is used when the initial material is RNA and it is amplifying DNA while quantifying the amount of DNA amplified at each cycle in real-time. This method in general means the amount of DNA expressed can be quantified and compared between different cell samples. In this method, RNA is first transcribed into complementary DNA (cDNA) by reverse transcriptase from total RNA or messenger RNA (mRNA). The cDNA is then used as the template for the qPCR reaction. RT-qPCR is used in a variety of applications including gene expression analysis and this type of Polymerase Chain Reaction (PCR) is a more precise method of quantification compared to older gel-based methods. All components required for this reaction are carried within the one tube. The concept behind this method is that the quantity of fluorescence measured is directly associated with the product amplification and this is proportional to the quantity of target gene existing in the sample. This method is used to quantify specific RNA target amplification using the designated primer sets. This procedure permits for streamlined samples and allows for higher throughput analysis, whereby reverse transcription and PCR take place sequentially in the same reaction tube. Q-RT-PCR was performed using the Rotor-Gene (RG-3000, Corvett Research) with the Quantitect™ Primer assay system using Quantitect mouse primers (Qiagen, Hilden, Germany with PrimeTime® Qiagen primers) or (the BioLine Sensifast with PrimeTime® IDT primers) -the sequence of the primer listed below- and the SYBR green PCR kit from Qiagen according to the manufacturers' instructions. The kit contains a master mix which contains: SYBR Green dye (the fluorescent component for the detection of the amplicon), a SYBR Green buffer containing a balanced combination of K+ and NH4+ ions (encouraging specific primer

annealing) and Taq polymerase. The kit also contains reverse transcriptase which is added to the sample reaction tubes only. Samples were done in triplicate with reverse transcriptase and a control sample for each sample was set up without the reverse transcriptase. HPRT was used as a reference housekeeping gene as a control for each PCR. The results were analysed using the comparative Ct method ($\Delta\Delta$Ct Method) described by (Livak and Schmittgen 2001) Rotor-GeneSYBR® Green RT-PCR Kit.

Table 2.8. Master mix Components

Component	Quantity
SYBR green	12.5μl
DEPC H$_2$O	4.75.4μl
Reverse transcriptase (RT) mix	0.25μl
Primer	2.5μl
RNA	5μl (50 ng)

The program used on the instrument for the different primer sets were as follows:

Hold 1: 45°C for 10 minutes

Hold 2: 95°C for 2 minutes

Denaturing Phase: 95°C – 10s

Annealing Phase: 68°C – 30 seconds with a touchdown step over 8 samples with the temperature dropping 1 degree per cycle

Elongation Phase: 72°C – 30 seconds

Table 2.9. IDT PrimeTime® primer sequences for q-RT-PCR.

Gene	Sequence
mHPRT	5'-GGC TAT AAG TTC TTT GCT GAC CTG -3' 5'- GCT TGC AAC CTT AAC CAT TTT GGG -3'
Myh11	5'-GCA GTG AGC TCT CAG TCA TC -3' 5'- AAC AGA GTT CTC CAT CAT CCA C -3'
Calponin1	5'-CTC AGC CCT CCT CAA TGA AGG -3' 5'- GCT TGT CTG CTG AAG TAA AGA AC -3'
Hey1	5'-CAC TTC TGT CAA GCA CTC TCG -3' 5'- GTA CCC AGT GCC TTT GAG AA -3'
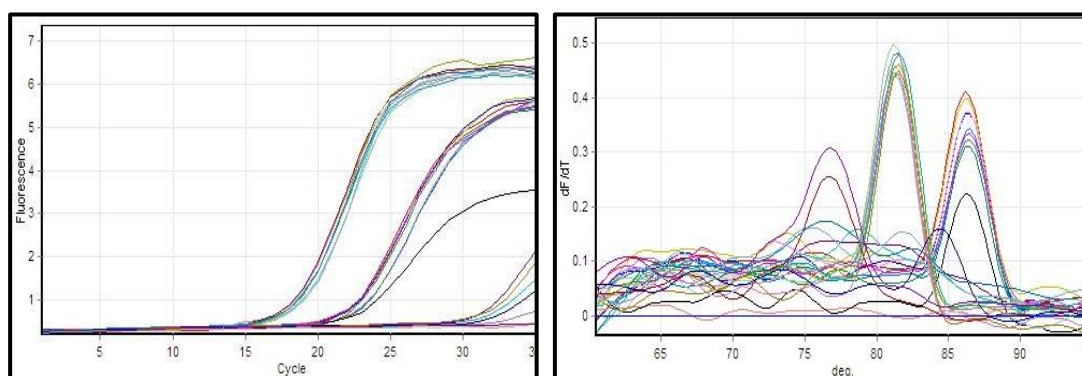
Figure 2.3. Sample cycling amplification curve and melting curves. HPRT and Cnn1 mRNA transcript for TGF-β1, maintenance medium and differentiation medium on mouse mesenchymal stem cells.

Data analysis:

Each sample was run in triplicate with a no-reverse transcriptase control and no template control. Ct values were obtained by using the Roter Gene 6000 series software. Ct values were then analysed using an excel template programme for analysis of fold changes by calculating the ratio to the efficiency of the genes then the ratio plotted using GraphPad Prism™ software.

2.4. Fabricating Nanoparticles

2.4.1 Preparation of PLGA-Fe$_3$O$_4$-DAPT-MNPs

The preparation of blank and drug-loaded polymeric magnetic nanoparticles (MNPs) was developed in a technique adapted from (McCall and Sirianni 2013). All the glassware to be used was cleaned, dried and washed with dH$_2$O. 3mg of a toluene-solvent was evaporated under nitrogen gas to receive free magnetite Iron-oxide (Fe$_3$O$_4$). The Polyvinyl Alcohol (PVA) was prepared at two concentrations. The first concentration was 450μL of 5% PVA (w/v) in dH$_2$O and the second was 10ml of 0.3% PVA (w/v) in dH$_2$O. Following this preparation, the two tubes were boiled at 90°C until dissolved completely (approximately 45 minutes). The Fe$_3$O$_4$ was dissolved in 1ml of dichloromethane (DCM) and vortexed. Poly lactic-co-glycolic acid (PLGA) (P2066) was weighed out to 22.5 mg and placed in a 13mm X 100mm test tube. Then 225μL of DCM was added to PLGA crystals to dissolve and the top of the tube was sealed with parafilm. The polymer was left to dissolve overnight after marking the level of the solvent. Following that, 50 mL conical flask was used to place the 10 mL 0.3% PVA solution and 16mm X 150mm test tube was used to place the 5% solution. Then the dissolved PLGA in DCM was added to the dried MNPs to dissolve them in the polymer complex. This was vortexed for 10 seconds to guarantee to mix. For the drug-loaded samples, the drug was added at the required concentration at this point to the polymer. Then Fe$_3$O$_4$-NP mixed and vortexed for another 10 seconds. The PLGA DCM Fe$_3$O$_4$NP Drug solution was dropped gently to the 5% PVA whilst under vortex. The solution was vortexed for 15 seconds and naturally, an emulsion would occur. The emulsion was put in a flask container with ice for sonication. The sonication occurred using the sonicator probe at 40% amplitude for 10 seconds three times with 5 seconds interfere in between. For the fluorescently mAB-loaded PLGA-MNPs, the fluorescent agents were added at this step. The resulting emulsion was then added to the 0.3% PVA and shaken overnight to allow the organic solvents to evaporate.

Figure 2.4. Sample MNP image. Representative image of freshly formulated PLGA/PVA coated Fe_3O_4-MNPs.

The blank and drug-loaded PLGA-MNPs were then recovered and washed via centrifugation with the Sorvall SA-600 rotor at (17,000g, 30 minutes, 4°C). This step was done twice by resuspending the pellet in 10 mL dH_2O and the supernatants from each time was collected and kept for High-performance liquid chromatography analysis to determine the concentration and quantity of drug incorporated into the nanoparticles (MNPs). The MNPs solution was then aliquoted out into 10 x 1 mL aliquots. Then these 10 x 1 mL aliquots were centrifuged again at 17000 x g for 1 hour. The MNPs pellets were then placed in the "DNA Speed Vac DNA110" for four hours to remove excess liquid and then stored at -80°C.
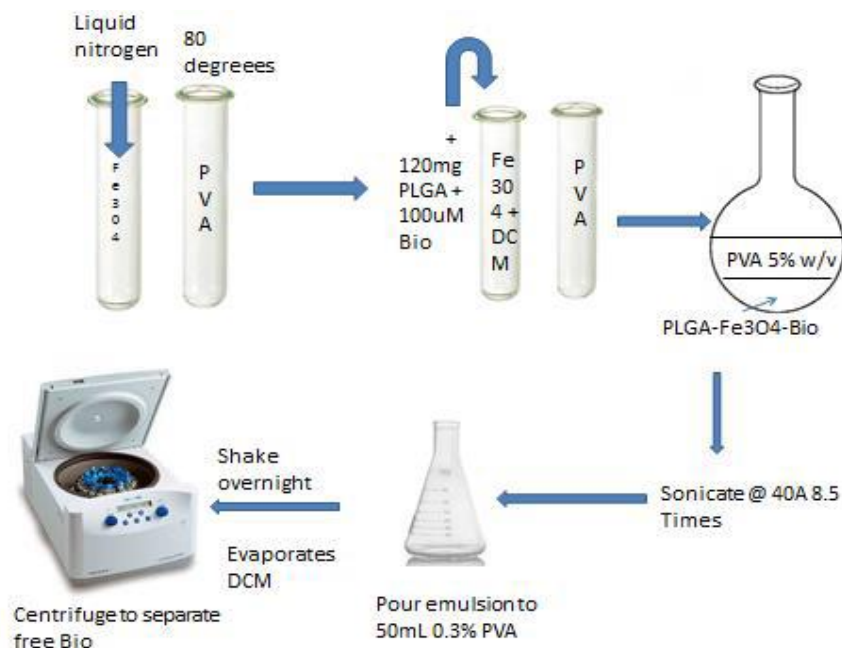
Figure 2.5. Schematic of the preparation of MNPs by oil-in-water emulsification.

2.4.2 High-performance liquid chromatography (HPLC)

Reversed-phase HPLC was used to determine the levels of drug released from each MNP preparation. The Agilent 1100 HPLC system was used in combination with the silica packed Supelco Discovery C18 Column to separate the molecules in the supernatant samples. The Supelco Discovery C18 column has porous silica beads packed within, separation depends on the reversible adsorption/desorption of the molecules, which have varying degrees of hydrophobicity, to a hydrophobic stationary matrix.

Retention time is the time at which it takes for a molecule to be eluted and detected from the column. The transportation of the mobile phase through the system is controlled by the High-pressure pumps and pump meters which regulates the flow rate typically in millilitres per minute (mL/minutes). The mobile phase usually consisted of either 50:50 or 70:30 acetonitrile (ACN):dH2O depending on the hydrophobicity of the drug. The flow rate was between 0.5 mL/minute to 1 mL/minute. An injector gets the sample to be analysed and injects it into the mobile phase stream where it will be separated by the column. Once it passes through the column it is then detected usually by an Ultra-violet (UV) or fluorescence detector, which sends an electrical signal to the computer to make a chromatogram.

Table 2.10. HPLC Settings used

Equipment	Agilent 1100 series HPLC system
Column	Supelco Analytical Discovery HS C18 column, 25cm x 4.6mm, 5μm
Detector	Diode array detector at wavelength range 190nm - 600nm
Injection volume	30μl
Temperature	Room temperature
Flow rate	1ml/min
Software	Chemstation version B.02.0-SR1
Mobile Phase	Filtered and degassed mixture of 50% ACN, 50% ultra-pure water and 0.1% trifluoroacetic acid

Figure 2.6. Typical HPLC Chromatogram for DAPT (100μM) as it appears by HPLC at 234 nm.

HPLC Data Analysis:

The repeated peak area at the same retention time for each concentration of the drug was taken and plotted as a line to generate a standard curve.

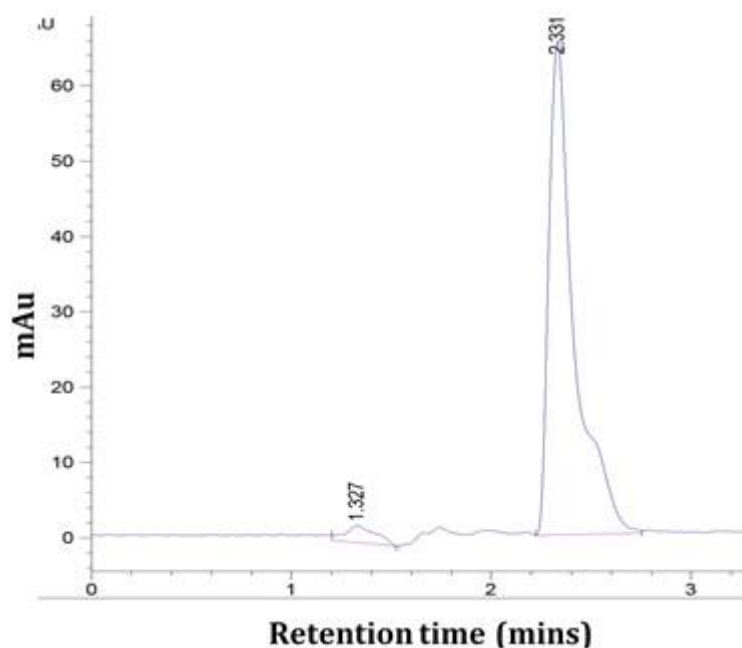## 2.4.3 Analysis of drug incorporation by HPLC

The incorporation of drug into the MNPs was determined by measuring the levels in the collected supernatants during purification. These supernatants were analysed by HPLC using a standard curve for each drug. The concentration of drug released from each MNP preparation was measured in the supernatant was then subtracted from the known total drug concentration loaded to give the concentration of drug incorporated. The listed equation was then used to calculate the drug incorporation: (Concentration of drug incorporated/extrapolated concentration of drug from the standard curve) X 100 = % of drug incorporated.

2.4.4 Drug release studies

To measure the release of drug from the MNPs, 1 mL of dH_2O was used to re-suspend the stored MNPs pellets. The resuspended pellets in dH_2O were then left for up to seven days at 37°C in the presence or absence of constant magnetization (Min et al., 2013) using the LifeSep™ 96F magnetic separator (Dexter Magnetic Technologies) according to the previously published protocol (Chorny et al., 2010a). The MNPs were centrifuged at 17000 x g after 48 hours and seven days and the supernatants were analysed by HPLC to detect the drug present in the supernatant. The cumulative release was expressed as the ratio of drug released by a given time point to the total amount of drug determined.

Data analysis

The percentage of drug released at each time point in the absence or presence of constant magnetisation using the LifeSep™ 96F magnetic separator was calculated using this formula: (Concentration of drug in supernatant/known concentration of drug incorporated) X 100 = % of drug released from the nanoparticle. Total percentage drug released at each time point was calculated as the percentage released at each time point. Then these values were plotted in GraphPad Prism™ v6 using the time as x axis and the percentage as y axis.

2.4.5 Dynamic Light Scattering

The size and colloidal stability of the MNPs were assessed using Dynamic Light Scattering (DLS) (Malvern Zetasizer Nano). DLS is a laser-based system which sends a laser beam through a polariser to the suspension or solution and measuring the random changes in the intensity of the scatter light and determined particle or molecules size of the samples in a solution. For these measurements, 100µl of the MNPs were added to 900µl of dH_2O and this was filtered through 0.45µM filter. This was then positioned in a polystyrene cuvette for size determination. The Z-average value of the MNPs was measured by following the automated protocol for magnetite in the water on the Zetasizer software. 12 reads at 30 seconds each were completed for each sample. This was done in triplicate for each sample and averaged. The polydispersity index (pdi) value was also documented.
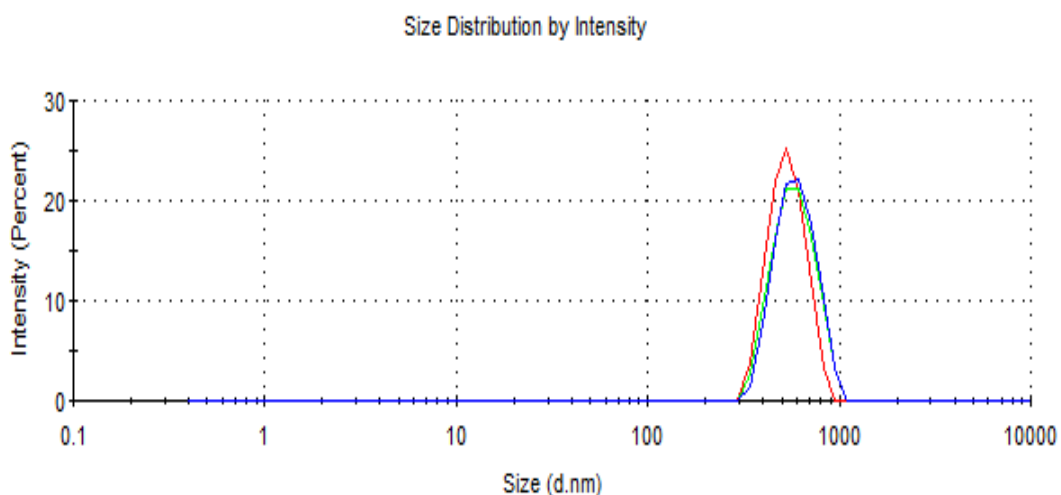
Figure   2.7. DLS Sizing Peaks. Sample DLS triplicate reading of loaded MNPs.

Data analysis

The data was performed in triplicate and analysed by reading and comparing the size of each peak.

2.4.6 Transmission Electron Microscopy (TEM) and Scanning Electron Microscopy (SEM)

A 100µL of MNPs was pipetted and placed onto carbon-coated copper TEM grids for Transmission electron microscopy (TEM). TEM analysis was performed at the University of Limerick and Fe- SEM (Hitachi S5500 FeSEM) images were recorded in the NRF DCU.
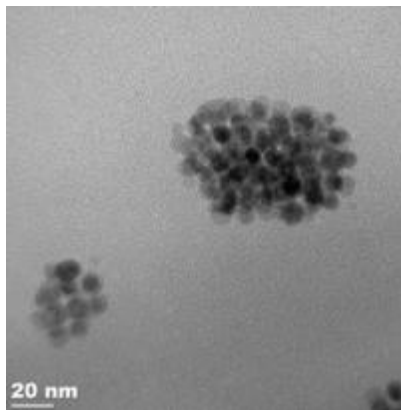
Figure 2.8. TEM image. The representative TEM image of blank MNPs.

2.4.7: Attachment of IgGAlexa488-Fe$_3$O$_4$-PLGA-MNPs to stents

A series of 96-well plates were used to perform this experiment. One plate was placed on the LifeSep™ 96F magnetic separator (Dexter Magnetic Technologies). Stents were positioned into the wells and covered in IgGAlexa488-Fe$_3$O$_4$-PLGA-MNPs (100µl), and IgGAlexa488 (12.6µg/mL, 100µl). Plates were incubated at room temperature for two hours. Following that stents were washed with H$_2$O (200µl) up to five times, and pictures were taken before the wash and after each wash using the Fluorescent Microscope.

Statistical Analysis

Data are presented as the mean ± SEM and are representative of at least three independent experiments. Statistical analysis was performed with GraphPad Prism™ v6 software package using t-test or a one-way analysis of variance (ANOVA) for parametric data or a Kruskal Wallis t-tests for non-parametric data.

Chapter 3

The effects of gamma-secretase inhibitors (GSI's) on vascular smooth muscle and mesenchymal stem cell growth

3.1 Introduction

The differentiation of vascular stem cells into vascular smooth muscle cells (VSMCs) plays a major role in cardiovascular diseases (CVD). Transforming Growth Factor-β (TGF-β1) and Notch signalling pathways mediate stem cell myogenic differentiation into smooth muscle cells and are central signalling pathways in vascular pathology (Kurpinski et al., 2010a).

Vascular disease is one of the biggest killers in the Western world, including heart attack and stroke. Thus, an improved understanding of the response of resident vascular stem cells to Notch activation is of major medical importance. Notch signalling is a fundamental pathway involved in the modulation of cell proliferation, survival and in overall stem cell maintenance (Rizzo and Ferrari 2015). Notch receptors and their ligands play a major role in the modulation of a plethora of biological functions of macrophages, endothelial, and vascular smooth muscle cells, particularly under inflammatory conditions and affect the biology of each cell type involved in atheromatous plaque formation (Rizzo and Ferrari 2015). Recent genome-wide association studies (GWAS) studies have also implicated the Notch pathway genes in lesion formation and coronary artery disease (Mäkinen et al., 2014).

Our lab and others have used lineage tracing analysis to confirm the role of resident vascular stem cells in contributing to intimal medial thickening (IMT) associated with arteriosclerotic lesion development (F. Yuan et al., 2017, Z. Tang, Wang, Yuan, Yan, Liu, Chu, Helms and Li 2012b).

Importantly, as stem cells proliferate, they self-renew and give rise to daughter cells that are also committed to lineage-specific differentiation through asymmetric cell division whereby they segregate cell fate determinants into only one of the two daughter cells (Knoblich 2008). The molecules involved are highly conserved in vertebrates and include the Notch pathway. Therefore, experiments were designed to address the central role and potential therapeutic targeting of Notch signalling in controlling mesenchymal stem cell growth and later myogenic differentiation using $\gamma-$secretase inhibitors (DAPT and Compound E).

3.2   Objectives of this chapter

The main aims of this chapter were: -

To investigate the modulatory effects of two pharmacological γ −secretase inhibitors, (GSI's) DAPT and Compound E on mouse aortic smooth muscle cell's (mSMC) and mouse mesenchymal stem cell's (mMSC) growth (balance of proliferation and apoptosis) and myogenic differentiation *in vitro*. Specifically,

- Determine the dose-dependent effects of DAPT and compound E on mSMC and mMSC proliferation *in vitro.*
- Determine the dose-dependent effects of DAPT and compound E on mSMC and mMSC apoptosis *in vitro.*
- Determine the IC_{50} for DAPT and compound E in controlling mSMC and mMSC growth *in vitro* and establish their optimal concentrations for inhibition of myogenic differentiation.

3.3   Strategy

In the present study, experiments were designed to determine potential growth inhibitory effects of the two pharmacological γ −secretase inhibitors, DAPT and compound E which are known to prevent the generation of the intracellular domain of Notch molecules and suppress the Notch activity.

Mouse smooth muscle cells (mSMCs) and mesenchymal stem cell (mMSCs) were used to determine the temporal effects of both GSI's on cell proliferation using an Alamar blue assay of metabolic activity, nuclei counting by DAPI nuclear staining and cell apoptosis by FACS analysis using annexin V/propidium iodide staining in the absence or presence of increasing concentrations of γ −secretase inhibitors, DAPT and compound E. The optimal concentration of the γ −secretase inhibitors (IC_{50}) that were not toxic or growth inhibitory was established for subsequent examination of myogenic differentiation.

3.4   Results

3.4.1   Cell Proliferation using AlamarBlue® Assays

To validate the cell proliferation assay and cell line suitability for the drug treatment experiments, a cell number titration assay was performed using AlamarBlue®. AlamarBlue® cell viability reagent functions as a cell health indicator by using the reducing power of living cells to quantitatively measure the proliferation of various cell lines, thereby establishing relative cytotoxicity of agents within various chemical classes. When cells are alive they maintain a reducing environment within the cytosol of the cell. Resazurin, the active ingredient of AlamarBlue® reagent, is a non-toxic, cell-permeable compound that is blue in colour and virtually non-fluorescent. Upon entering cells, resazurin is reduced to resorufin, a compound that is red in colour and highly fluorescent. Viable cells continuously convert resazurin to resorufin, increasing the overall fluorescence and colour of the medium surrounding cells. One-way ANOVA was used to using the GraphPad Prism™ software and $p < 0.05$ to establish significance.

Murine mSMCs were seeded at different densities in 96-well plates (as described in Materials and Methods section 2.2.1, Chapter 2) and the fluorescent absorbance measured after three days (Figure 3.1). There was a linear relationship between cell density and Alamar Blue absorbance. These results suggested that the AlamarBlue® assay is valid to measure cell proliferation.

The growth inhibitory effect of fetal bovine serum (FBS) deprivation was also investigated by culturing two cell lines mSMC and mMSCs in maintenance medium (MM) supplemented with 0.5%, 5% and 10% FBS (v/v). Cell viability assay using AlamarBlue® was performed after a period of three days (Figure 3.2). a.   In order to compare the effectiveness of DAPT and Compound E to inhibit cell proliferation, the half-maximal inhibitory concentration (IC50) was measured. The IC50 is a measure of the effectiveness of a substance in inhibiting a specific biological or biochemical function. The IC50 for DAPT and Compound E at inhibiting cell proliferation was evaluated and determined to be 80µM and 25 µM, respectively.
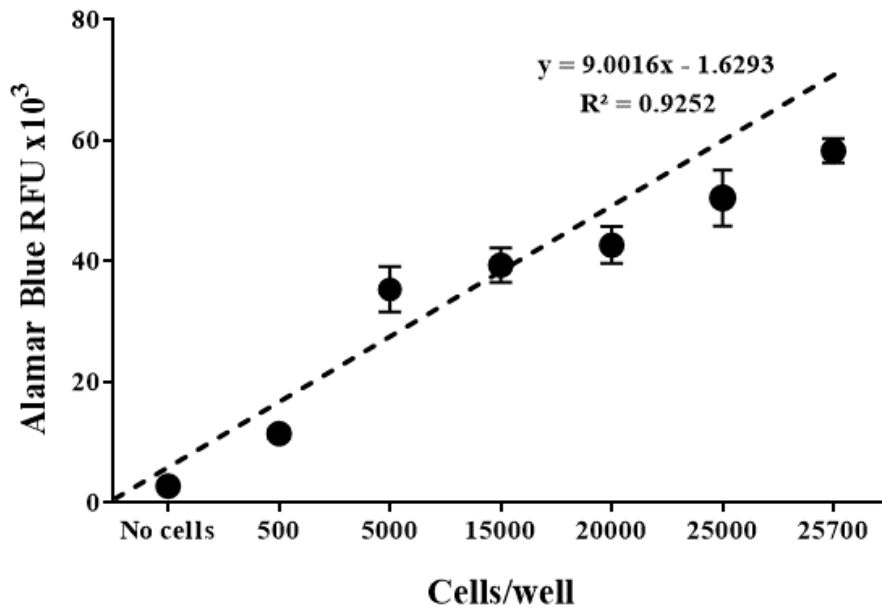
Figure 3.1. Titration of cell number for validating mSMCs proliferation by AlamarBlue® assay. The mMSCs were seeded at various cell densities from 500 to 25,700/ well in 6 well plates. Using an AlamarBlue® assay the fluorescent intensity at 590nm was measured after three days. RFU = relative fluorescent unit. Data are representative of 3 wells/group and analysis was performed by ANOVA using the GraphPad Prism™ software and p<0.05 ****p<0.001 all considered significant.
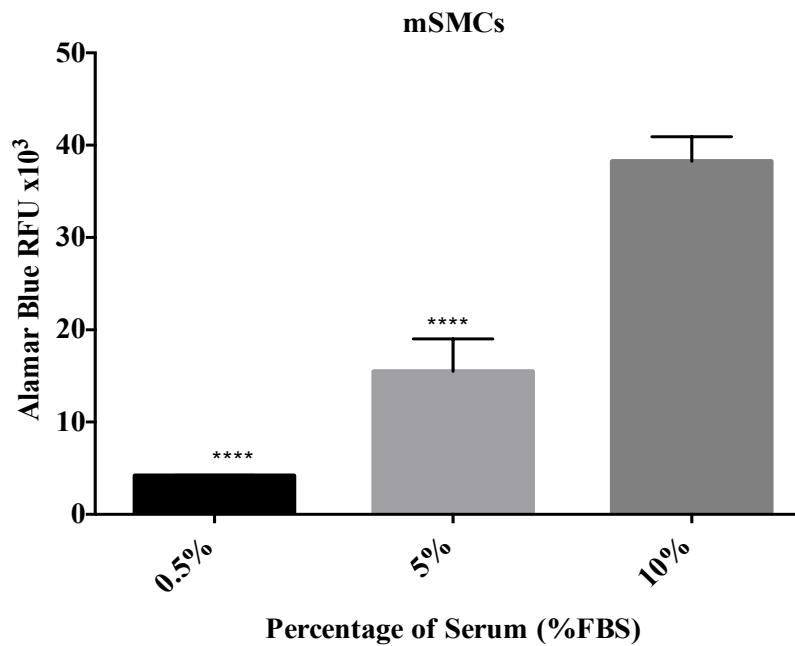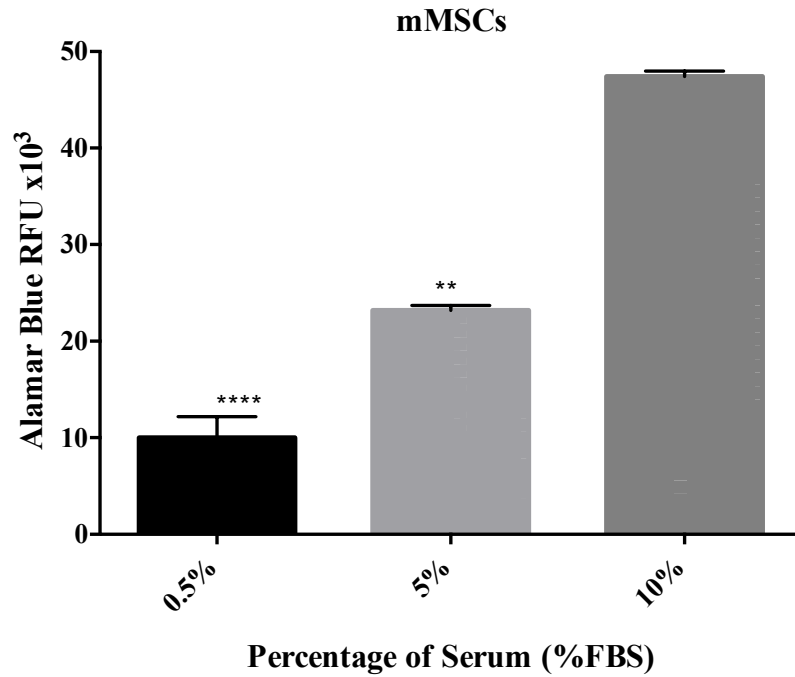
Figure 3.2. The effect of different concentrations of serum on mSMCs and mMSCs proliferation. The mSMCs and mMSCs were seeded at density of 10,000 cells/well and grown in the presence of either 0.5 % or 5% or 10 % FBS (v/v). Using an AlamarBlue® assay the fluorescent intensity at 590nm was measured after three days. RFU = relative fluorescent unit. For mSMCs data analysis was performed by ANOVA with the GraphPad Prism™ software and $p < 0.05$ ****$p < 0.0001$ all considered significant. For mMSCs data was analysed by Kruskal Wallis analysis using GraphPad Prism™ software and $p < 0.05$, **$p < 0.005$, ****$p < 0.0001$ all considered significant.

Mouse smooth muscle cells (mSMCs) and mouse mesenchymal cells (mMSCs) were treated with varying concentrations of DAPT and compound E to determine the anti-proliferative effects of these pharmacological γ−secretase inhibitors. The cell was treated with drug vehicle (DMSO $< 0.01\%$) and with various concentration of DAPT (10-300 μM) in 10% FBS and for the duration of three days. Using the AlamarBlue® assay, the fluorescent intensity of cells for each concentration was plotted as a bar chart (Figure 3.3 and 3.4).

The growth-inhibitory and anti-proliferative effect of Compound E were investigated by treating 10,000 mSMCs (Figure 3.5) and mMSCs (Figure 3.6) with various concentration of Compound E (10- 300 μM) and (10 -100 μM) respectively and with the drug vehicle (DMSO<0.01%). Two different range of concentration were used as concentrations above 100 μM led us to use lower concentration. Cells were cultured in maintenance medium (MM) supplemented with 10% FBS (v/v). Cell viability assay using AlamarBlue® assay was performed after three days. The fluorescent intensity for each concentration including the drug vehicle was plotted as a bar chart (Figure 3.5 and 3.6).
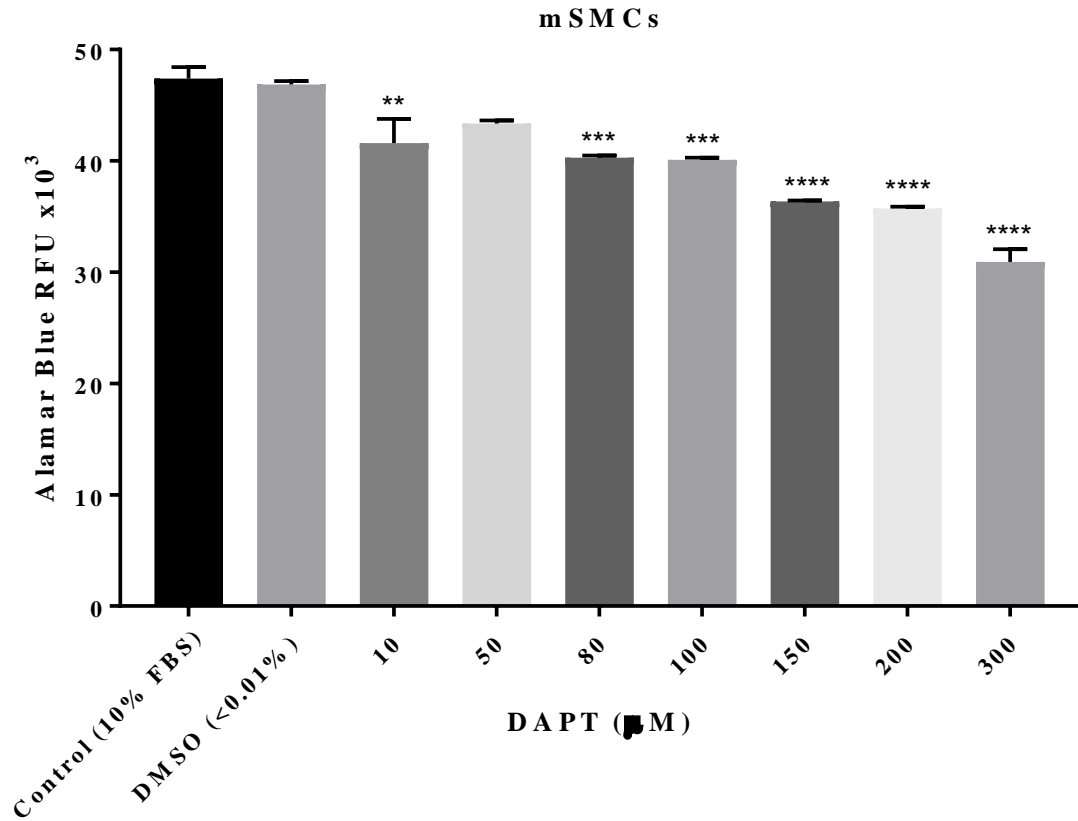
Figure 3.3. The effect of DAPT on mSMCs proliferation. The mSMCs were seeded at a density of 10,000 cells / well and treated with various concentrations of DAPT ranging from 10 to 300 µM in DMEM supplemented with 10% FBS (v/v). Using an AlamarBlue® assay the fluorescent intensity at 590nm was measured after three days. RFU = relative fluorescent unit. Data were analysed by ANOVA using GraphPad Prism™ software and $p < 0.05$ **$p < 0.005$; ***$p < 0.001$,****$p < 0.0001$ were all considered significant vs. control, n=4.
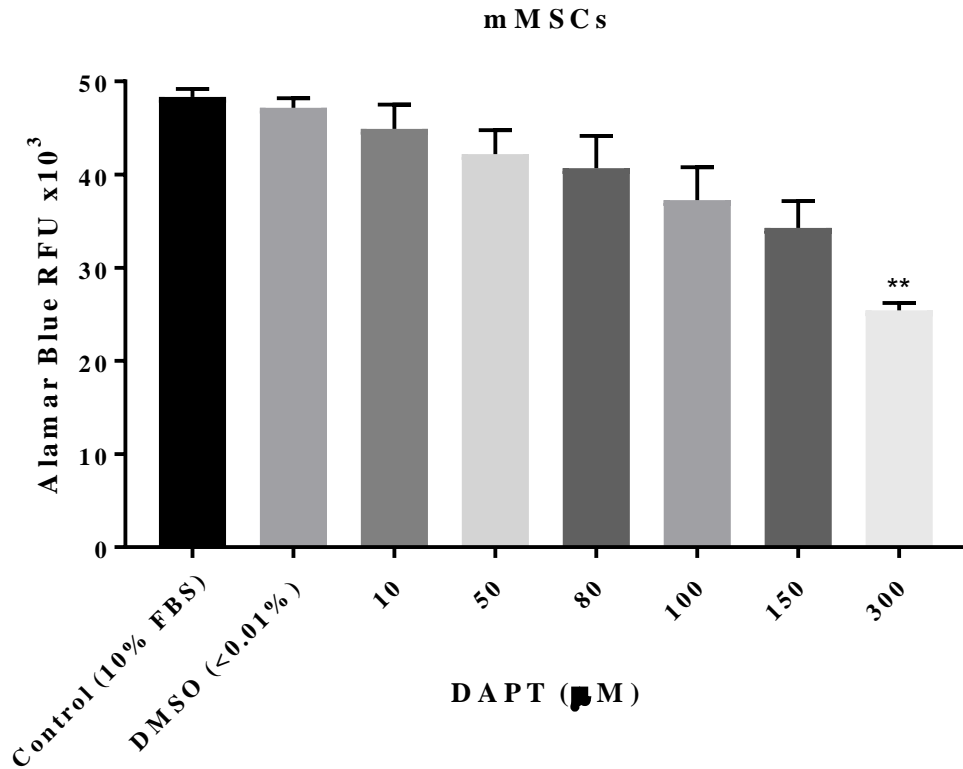
mMSCs

Figure 3.4. The effect of DAPT on mMSCs proliferation. The mMSCs were seeded at a density of 10,000 cells/well and treated with various concentrations of DAPT ranging from 10 to 300 μM in MM supplemented with 10% FBS (v/v). Using an AlamarBlue® assay the fluorescent intensity at 590nm was measured after three days. RFU = relative fluorescent unit. Data were analysed by Kruskal Wallis analysis using GraphPad Prism™ software as the data was not normally distributed (non-parametric) and $p < 0.05$, **$p < 0.005$ was considered significant vs. control, n=3.
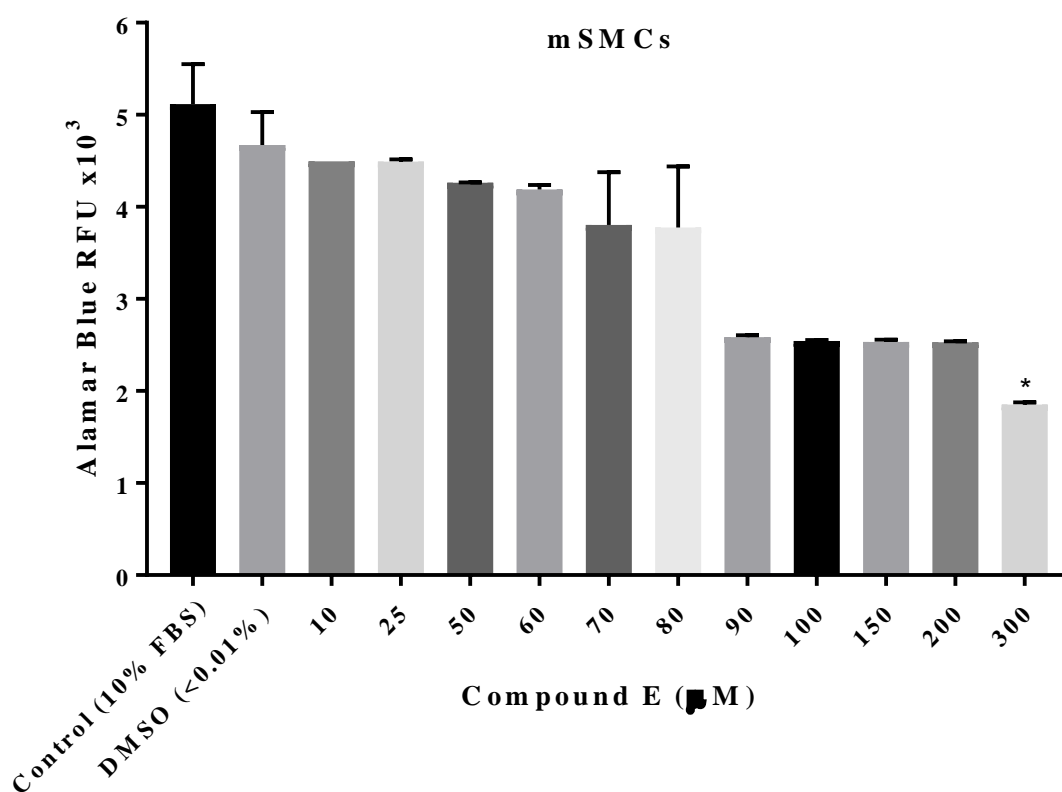
Figure 3.5. The effect of Compound E on cell proliferation. The mSMCs were seeded at a density of 10,000 cells/well and treated with various concentrations of Compound E ranging from 10 to 300 µM in DMEM supplemented with 10% FBS (v/v). Using an AlamarBlue® assay the fluorescent intensity at 590nm was measured after three days. RFU = relative fluorescent unit. The data were analysed by Kruskal Wallis using GraphPad Prism™ software as the data was not normally distributed (non-parametric) and $p < 0.05$, *$p < 0.005$ was considered significant vs. control, n=3.
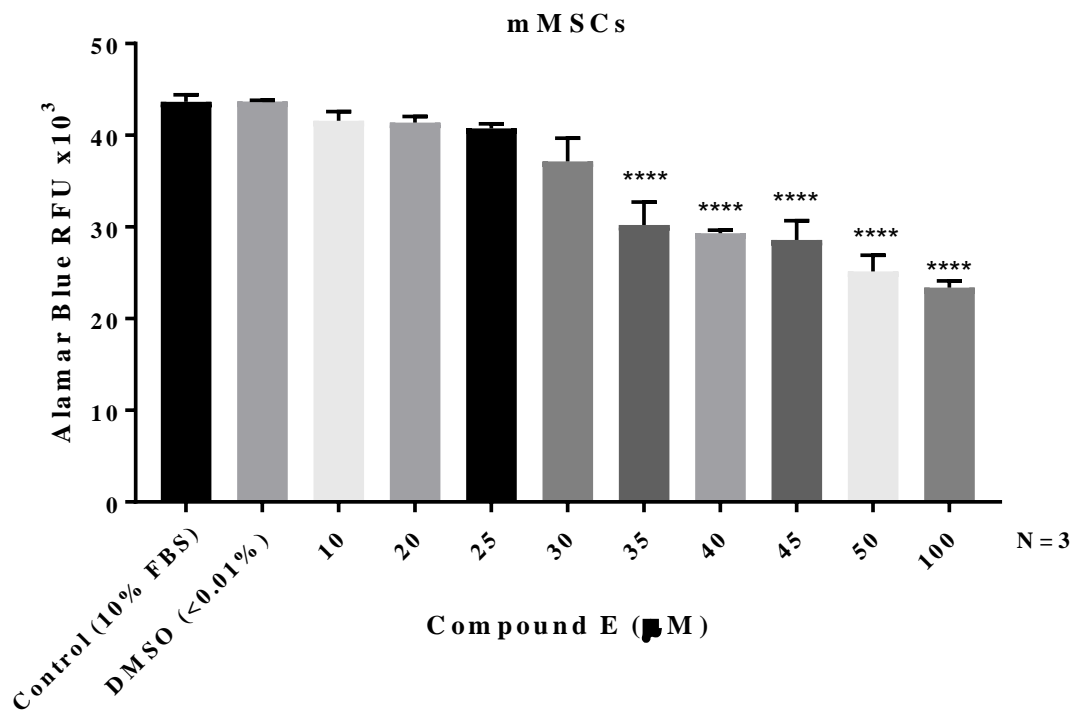
Figure 3.6 The effect of Compound E on mMSCs proliferation. The mMSCs were seeded at a density of 10,000 cells/well and treated with various concentrations of Compound E ranging from 10 to 100 µM in MM supplemented with 10% FBS (v/v). Using an AlamarBlue® assay the fluorescent intensity at 590nm was measured after three days. RFU = relative fluorescent unit. Data analysis was performed by ANOVA using GraphPad Prism™ software and $p < 0.05$, ****$p < 0.0001$ was considered significant vs. control, n=3.

3.4.2 Growth study by DAPI staining

To confirm the growth inhibitory effect of DAPT and Compound E at low concentrations, two different cell densities of mMSCc were first seeded in 6 well plates before the cells were treated with DAPT and Compound E for varying time periods (3, 7 and 10 days). The number of cells was assessed by counting the number of DAPI stained fixed cell nuclei in each plate following treatments.

Five separate images were taken for each treatment group using an Olympus fluorescent microscope as outlined in Materials and Methods, Chapter 2 section 2.2.5. Cells were counted using the particle counting function on ImageJ™ Fuji software.

Treatment of mMSCs with DAPT (80µM) for 3 days did not result in any significant inhibition of cell growth whereas Compound E (25 µM) resulted in a significant reduction in cell number (Figure 3.7).

Treatment of mMSCs with DAPT (80µM) or Compound E for 7 days did not result in any significant inhibition of cell growth (Figure 3.8).

In contrast, treatment of mMSCs with DAPT (80µM) or Compound E for 10 days resulted in significant inhibition of cell growth (Figure 3.9).
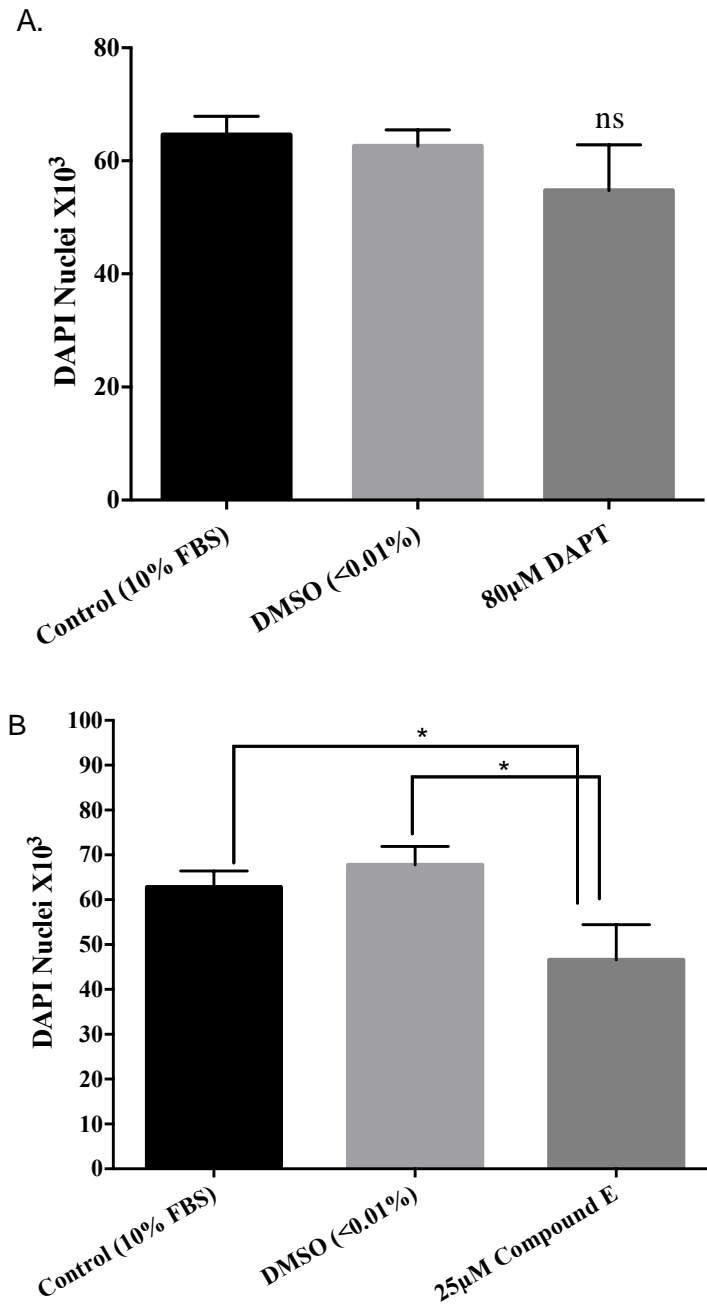
Figure 3.7. The effect of Compound E and DAPT on mMSCs growth after three days. The mMSCs were seeded at density of 1,000 cells/well and treated with (A) DAPT (80μM) and (B) Compound E (25μM), respectively. Using DAPI staining the number of DAPI nuclei was examined after three days. Data analysis was performed by ANOVA with the GraphPad Prism™ software and *$p<0.05$, n=3 was considered significant vs. control.
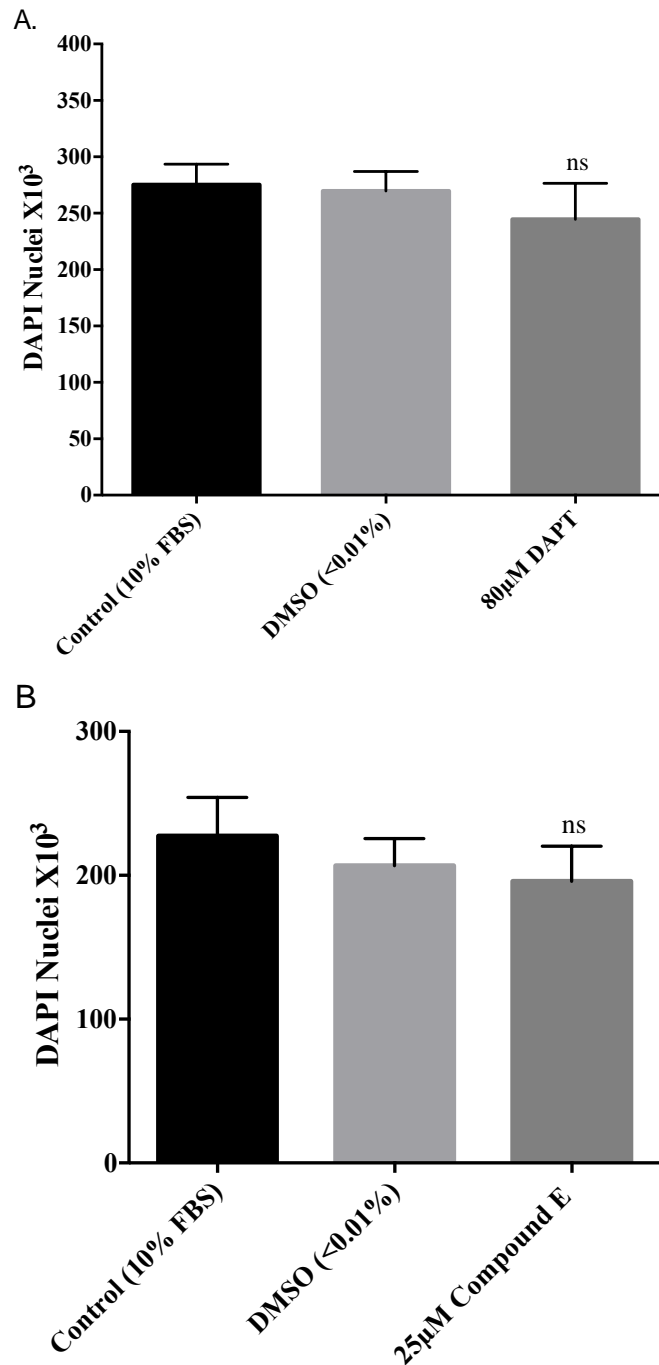
Figure 3.8. The effect of Compound E and DAPT on mMSCs growth after seven days. The mMSCs were seeded at density of 1,000 cells/well and treated with (A) DAPT (80µM) and (B) Compound E (25µM), respectively. Using DAPI staining the number of DAPI nuclei was examined after seven days. Data analysis was performed by ANOVA with the GraphPad Prism™ software and was considered not significant vs. control, n=3.
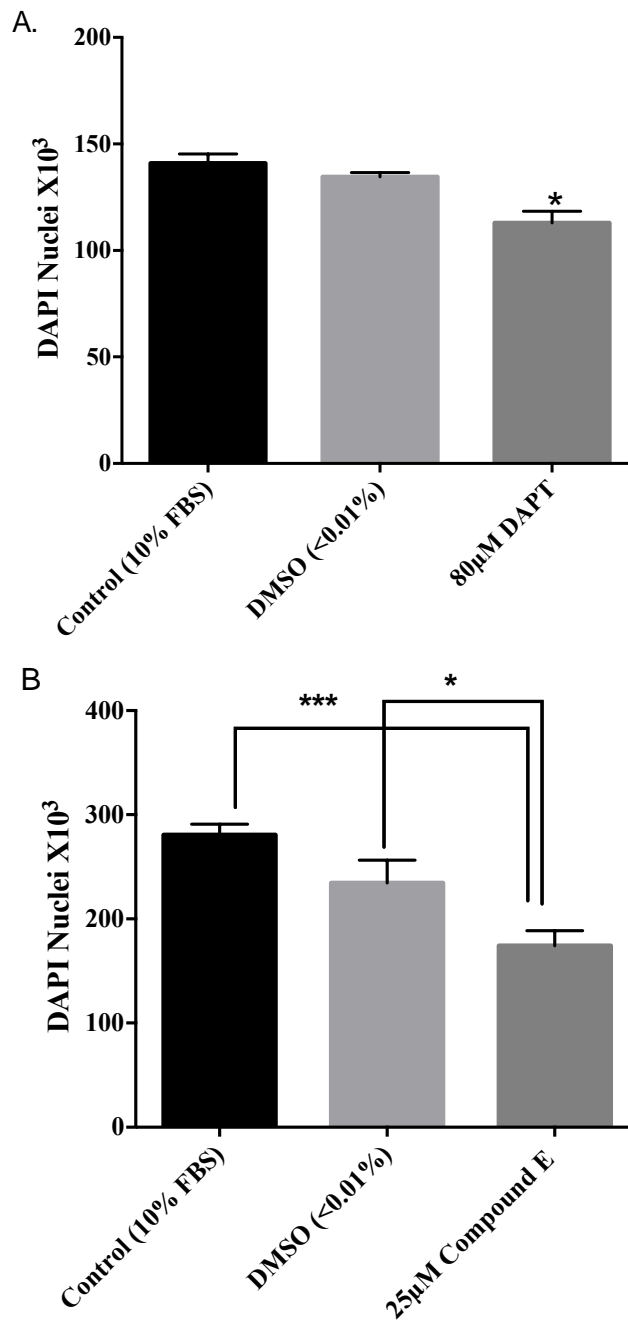
Figure 3.9. The effect of DAPT and Compound E on mMSCs growth after ten days.
The mMSCs were seeded at density of 1,000 cells/well and treated with (A) DAPT (80µM) and (B) Compound E (25µM), respectively. Using DAPI staining the number of DAPI nuclei was examined after ten days. Data analysis was performed by ANOVA with the GraphPad Prism™ software and $*p<0.05$, $***p<0.001$ n=3 was considered significant vs. control.

3.4.3 Apoptotic activity measurement by Flow Cytometry

Cell-based fluorescence-activated cell sorting (FACS) of cells using Annexin V-FITC/propidium iodide (PI) to stain apoptotic and necrotic cells, respectively was used to measure the number of early/late apoptotic cells and the number of necrotic cells following DAPT and Compound-E treatment. To validate the FACS analysis, mSMCs (6,000 cells/well) were cultured under three different conditions (10% FBS (v/v), 0% FBS and hydrogen peroxide (H_2O_2 $800\mu M$) in 10% FBS) in 6-well plate before cells were stained with Annexin V-FITC/PI and examined by FACS. Cell profiles were analysed after three days of treatment. Quadrant markers were based on stained/unstained controls. Cells in lower left quadrant are viable (PI$^-$/Annexin V$^-$), cells in lower right quadrant are early apoptotic (PI$^-$/Annexin V$^+$), cells in upper right quadrant are late apoptotic (PI$^+$/Annexin V$^-$) and cells in upper left quadrant are necrotic/mostly nuclear debris (PI$^+$/Annexin V$^+$). A bar chart representation of each experimental group is shown in Figure 3.10.

The number of apoptotic cells dramatically increased in cells grown in 0% FBS and cells exposed to H_2O_2 when compared to control (10%FBS) cells while the number of live cells decreased reciprocally (Figure 3.10).

MSCs (10,000 cells/well) were treated with various concentrations (0, 1, 5, 15, 30 μM) of Compound E in complete media containing 10% FBS for three and seven days before the number of apoptotic and necrotic cells were assessed by FACS analysis. The percentage of apoptotic and necrotic cells per concentration of Compound E did not significantly increase following treatment after three and seven days respectively (Figure 3.11 and 3.12).

Mouse MSCs (10,000 cells/well) were treated with various concentrations (0, 1, 50, 75, 100, 150, 200 and 300 μM) of DAPT for three and seven days, respectively. Cells were stained with Annexin V-FITC/PI and analysed by FACS. The percentage of apoptotic and necrotic cells per concentration of DAPT was then assessed (Figure 3.13 and 14). While the level of apoptosis and necrosis was higher than cells treated with Compound E, there was no significant difference in the percent apoptosis and necrosis across the does range (Figure 3.11, Figure 3.12).

97
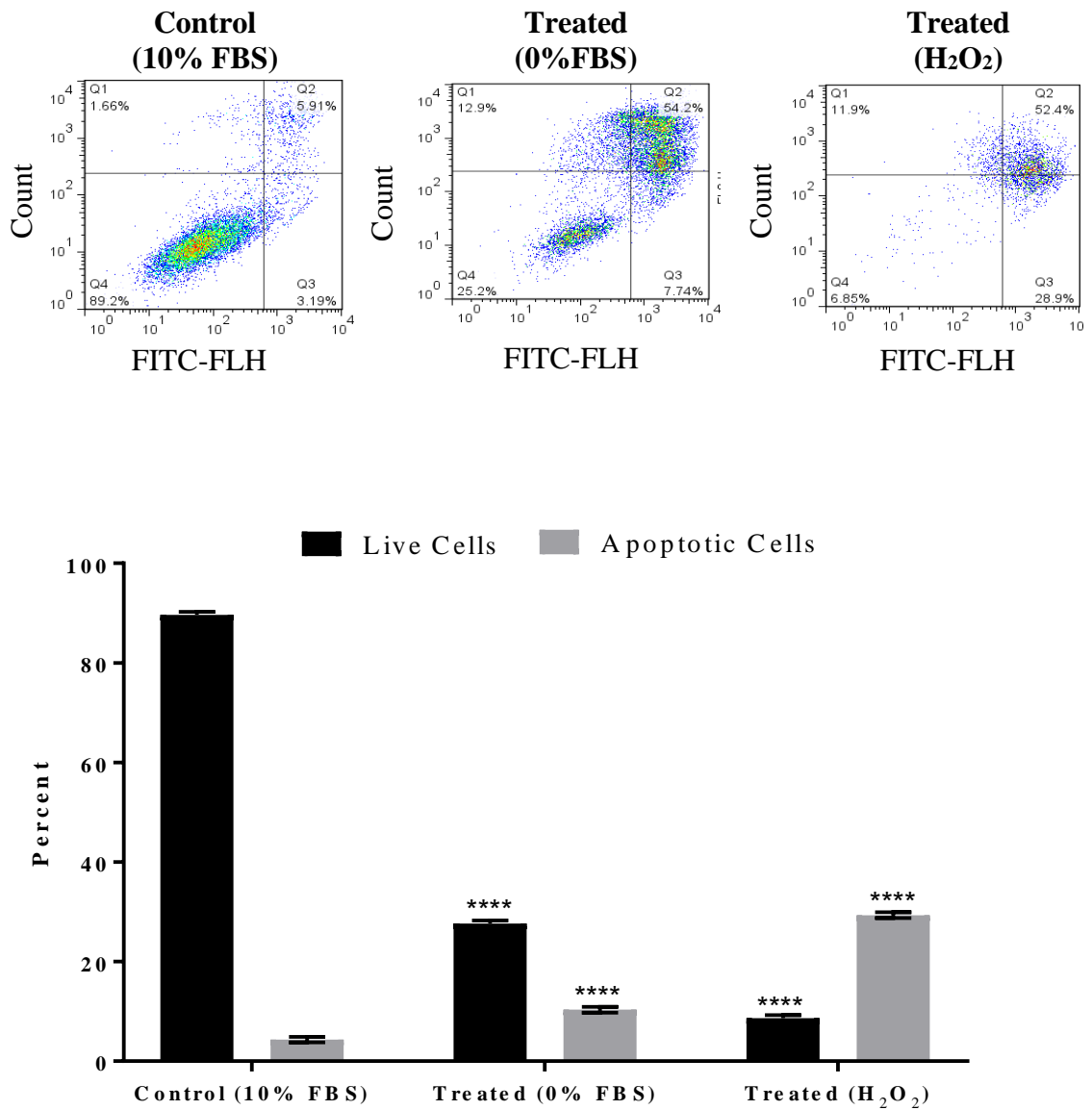
Figure 3.10. Annexin V-FITC/PI apoptosis assay validation. The mSMCs were seeded at a density of 6,000 cells /well and treated with 800μM H_2O_2 and medium without or without serum. The percentage of apoptotic (early and late) and necrotic cells was measured after three days using FACS. Data analysis was performed by ANOVA with the GraphPad Prism™ software and ****$p<0.0001$, n=3 was considered significant vs. control.
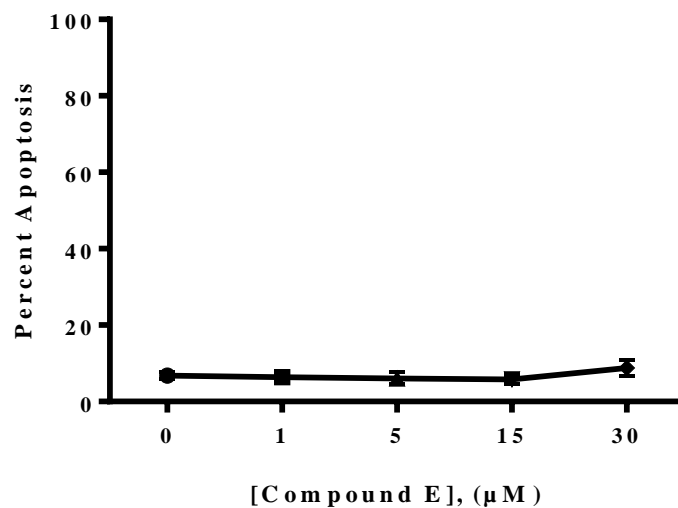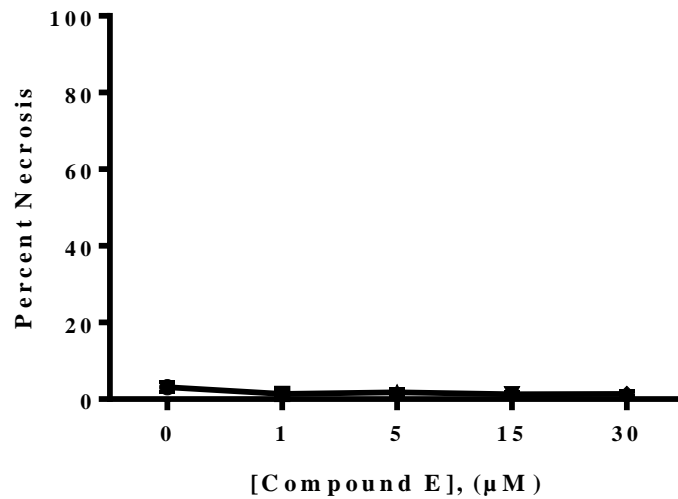
Figure 3.11. The percent apoptotic and necrotic cell following Compound E treatment of mMSCs after three days. The mMSCs were seeded at 10,000 cells / well density and treated with various concentrations of Compound E ranging from 1 to 30 µM. The percentage of apoptotic and necrotic cells was measured after three days using flow cytometer.
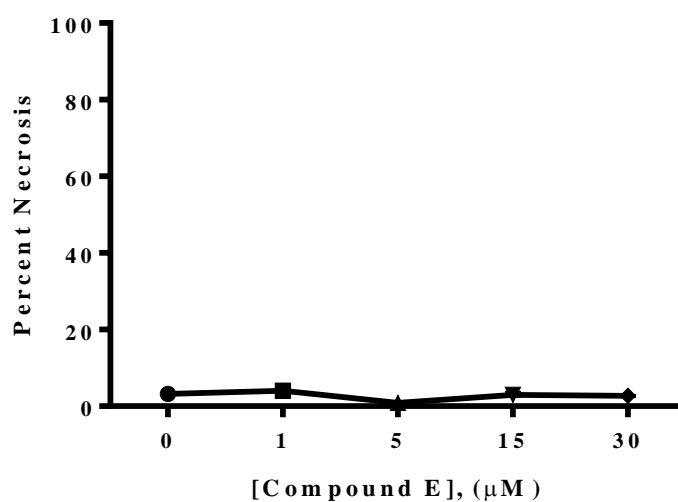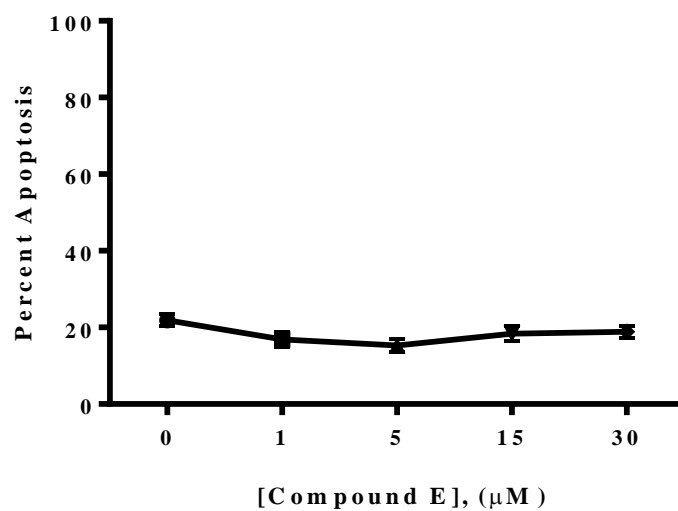
Figure 3.12. The percent apoptotic and necrotic cell following Compound E treatment of mMSCs after seven days. The mMSCs were seeded at 10,000 cells / well density and treated with various concentrations of Compound E ranging from 1 to 30 µM. The percentage of apoptotic and necrotic cells was measured after seven days using flow cytometer.
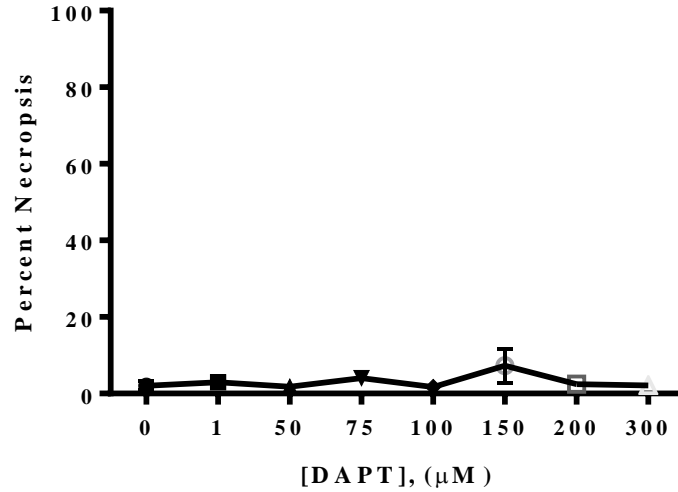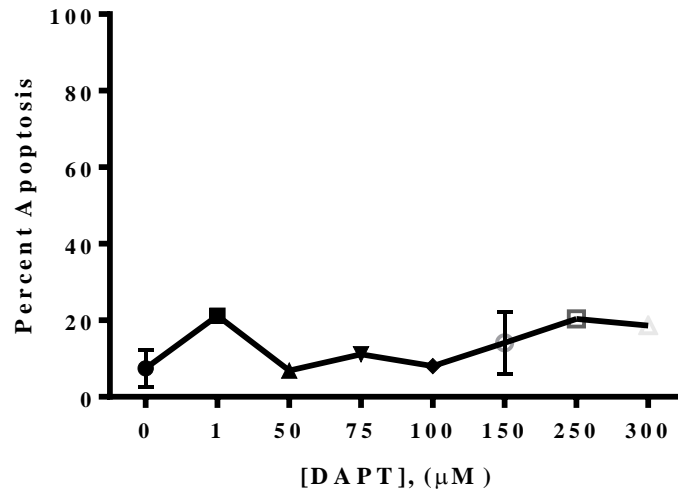
Figure 3.13. The percent apoptotic and necrotic cell following DAPT treatment of mMSCs after three days. The mMSCs were seeded at 10,000 cells / well density and treated with various concentrations of DAPT ranging from 1 to 300 µM. The percentage of apoptotic and necrotic cells was measured after three days using flow cytometer.
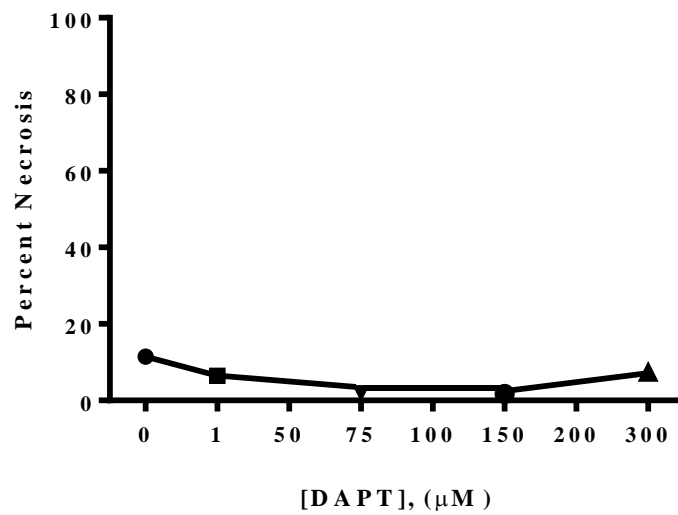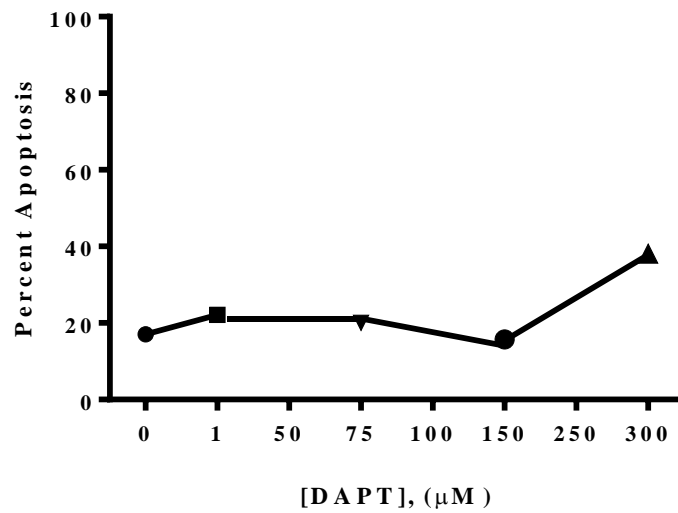
Figure 3.14. The percent apoptotic and necrotic cell following DAPT treatment of mMSCs after seven days. The mMSCs were seeded at 10,000 cells / well density and treated with various concentrations of DAPT ranging from 1 to 300 µM. The percentage of apoptotic and necrotic cells was measured after seven days using flow cytometer.

3.5   Discussion

The development and normal functioning of cells depend on interactions with molecules in their microenvironment. The major classes of molecules that regulate cellular development and function include growth and differentiation factors, cell adhesion molecules, and the components of the extracellular matrix (ECM). The Notch signalling pathway is one such major class of molecule regulating stem cell growth and differentiation (J. Liu et al., 2010). As stem cells divide, they undergo asymmetric division. The ability of stem cells to divide asymmetrically to produce one stem and one non-stem daughter cell is considered to be one of the defining characteristics of stemness (Shahriyari and Komarova 2013). Differentiation and proliferation decisions are under control of numerous signals emanating from the surrounding tissue and, in particular, the stem cells themselves. Indeed, cell cycle regulation is thought to play a key role in the orchestrating of stem cell renewal (Shahriyari and Komarova 2013). Quantitative analysis of long-term lineage-tracing data has revealed that the rate of stem cell replacement is comparable to the cell division rate, implying that symmetric cell divisions contribute significantly to stem cell homeostasis (A. M. Klein and Simons 2011). Moreover, adult stem cells are often lost (e.g. by differentiation) and replaced in a stochastic manner in addition to the more traditional concept of the stem cell as an immortal, slow-cycling, asymmetrically dividing the cell. In addition, symmetrically-dividing stem cells may respond to injury thus ensuring a robust mechanism of tissue homeostasis. In doing so, symmetric divisions may be "switched on" in response to a sudden stem cell loss, and the asymmetric division strategy is employed in the course of normal homeostasis. Hence the effect of local cues on stem cell growth (balance of proliferation and apoptosis) and differentiation is of critical importance in vascular homeostasis.

The aim of this chapter was to assess the proliferative and apoptotic effects of two chemically dissimilar ɣ -secretase Notch inhibitors on mSMCs and mMSCs *in vitro* in an effort to evaluate what concentrations of both inhibitors would be suitable at inhibiting myogenic differentiation of resident vascular stem without adverse effects on SMCs when GSI's are loaded on a functionalised magnetic nanoparticle.

The optimal seeding cell density for determination of cell proliferation studies by Alamar Blue and DAPI nuclear staining was first assessed and validated. The ideal cell

concentration for AlamarBlue® assay was 10,000 cells/well of 96 well plate and 2,000 cells/well of 6 well plate for DAPI nuclear staining technique. The data generated from cells grown in medium supplemented with different concentration of serum confirmed a linear relationship between the percentage of FBS in culture medium and the number, cell viability and growth.

The γ −secretase inhibitors, DAPT and compound E, both inhibited mSMC and mMSC cell growth *in vitro* in a dose and time-dependent manner, Both AlamarBlue® fluorescence activity and DAPI nuclear staining were significantly inhibited at higher concentrations of these inhibitors. Previous studies have shown that inhibition of Notch signalling with γ −secretase inhibitors attenuated both Notch ligand and NICD stimulation of vascular cell proliferation (X. Yuan et al., 2015, Sweeney et al., 2004). This change in cell growth was independent of apoptosis as FACS analysis did not reveal any significant apoptotic or necrotic effect of Compound E and DAPT on mMSCs over the same dose range.

Analysis of the dose-response curves for DAPT and Compound E revealed that both inhibitors had a similar potency at inhibiting cell growth but that mMSCs were more resistant to the anti-proliferative effects of DAPT and Compound E when compared to mSMCs. The IC50 for DAPT (80μM) and Compound E (25 μM) was determined using Alamar Blue and validated using DAPI nuclei staining with DAPI after ten days in culture. These doses will be deployed for subsequent studies on the myogenic differentiation of stem cells (Chapter 4).

Overall, these results suggest that Notch signalling is critical for stem cell proliferation since γ-secretase inhibitors that prevent the proteolysis of Notch receptors and suppress the Notch activity significantly decreased cell growth. Previous *in vivo* studies revealed a similar concentration of DAPT blocked activation of Notch3 in pulmonary vascular SMCs through the Hairy and enhancer of Split-5 (HES-5) protein and a shift to an undifferentiated SMC phenotype (X. Li et al., 2009a). These results suggest that Notch signalling is crucial for the development of pulmonary arterial hypertension and may provide a target pathway for therapeutic intervention when SMC/Stem cell proliferation persists.

Chapter 4

The effect of gamma-secretase inhibitors on myogenic differentiation of vascular stem cells

4.1 Introduction

The putative role of resident and/or circulating vascular stem cells in cardiovascular diseases has attracted a lot of attention in recent years. This is because current studies provide compelling evidence that diverse resident vascular stem cell populations including bone marrow-derived mesenchymal stem cells (MSCs) categorized by various specific markers and behaviours, participate in the vascular remodelling post vascular injury (F. Wang et al., 2018, C. Wang et al., 2008). Additionally, several studies have revealed the participation of similar stem cell populations during the progression of in-stent restenosis (Forte et al., 2007). This is in contrast to previous studies that purport migration and proliferation of neighbouring endothelial cells (ECs) and/or SMCs is responsible for the renewal of the wounded endothelium and the SMC-like cell accumulation leading to intimal medial thickening in arteries after injury (Wakeyama et al., 2003).

The contractile functions of the vascular SMCs are linked to changes in morphology, proliferation and the appearance of various lineage-specific protein markers. These markers are exclusive smooth muscle cells (SMCs) marks in adult cells and include calponin-h1 (Cnn1) and myosin heavy chain 11 (Myh11) which are myofibrillar thin filament, actin-binding proteins. The appearance of SMC-like cells within the vessel wall following vascular injury or in-stent restenosis leads to a significant reduction in the expression of these lineage-specific markers within neointimal cells. The origin of these cells has been addressed by many studies using lineage tracing analysis and includes (i) differentiated SMCs that de-differentiate and re-programme to various phenotypes (Newman et al., 2018) (ii) bone-marrow-derived MSCs that partially differentiate to SMC-like cells (N. F. Huang and Li 2008) (ii) resident vascular stems cells (F. Yuan et al., 2017, Z. Tang, Wang, Yuan, Yan, Liu, Chu, Helms and Li 2012c) that partially differentiate to SMC-like cells and (iv) endothelial cells that undergo endothelial-mesenchymal stem cell transition to SMC-like cells (F. Yuan et al., 2017, Kovacic et al., 2012).

Numerous types of SMC-related vascular progenitors within the blood vessel wall have been documented (F. Wang et al., 2018). In the tunica media, several

mesenchymal-like stem cells (MSCs) have been isolated (Z. Tang et al., 2012c). One of these cell populations is termed mouse multipotent vascular stem cells (mMVSCs) and they can differentiate into neural cells, mesenchymal stem cell-like cells and vascular SMCs. Recent studies have revealed that the myogenic differentiation of MVSCs to SMC-like cells may contribute in part to intimal medial thickening and vascular remodelling during disease development. MVSCs appear different from the adventitial layer of the aorta in the previously published "side population" isolated (Y. Hu et al., 2003). More importantly, MVSCs respond to Notch activation by transitioning to a vascular myogenic lineage (Z. Tang et al., 2012c); (Mooney et al., 2015a, Regan 2010).

Previous studies have shown that multipotent mesenchymal C3H 10T1/2 (10T1/2) cells may differentiate into muscle, fat, cartilage, and bone cells in response to the appropriate lineage inductive cue (Taylor and Jones 1979). Expression of myosin heavy chain II (Myh-11) appears subsequent to myogenic differentiation (Rosen and Spiegelman 2000). Many physical and chemical agents can be used to transform the phenotype of these cells (Tomei et al., 1993). Additionally, these cells are commonly used as a model for examining myogenic differentiation (Singh et al., 2003, Taylor and Jones 1979).

Transforming Growth Factor-β1 (TGF-β1) and Notch signalling pathways are both important regulators of myogenic vascular differentiation into smooth muscle cells and are central signalling pathways in vascular pathology (Kurpinski et al., 2010). Studies have revealed TGF-β1 family members regulate diverse cellular activities including growth, adhesion, migration, apoptosis, and (more specifically in smooth muscle cell) differentiation (G. Xue et al., 2015).

Notch signalling cascade has an essential role in regulating numerous important cellular processes such as proliferation, stem cell maintenance and differentiation during embryonic and adult growth (Borggrefe and Oswald 2009). Four Notch family receptors have been identified in mammals: NOTCH1 through to NOTCH4. Notch receptors interact with Notch ligands (Jagged (JAG1 and JAG2) and Delta-like (DLL1, DLL3 and DLL4) expressed on neighbouring cells ref (Costantini, Kopan 2010). The best-described Notch target genes in mammals are the transcription factors Hes1, Hes5 and Hey1.

106

Jagged1 (JAG1), a Notch ligand, stimulation of the Notch target gene HES1 is routinely used to confirm activation of the Notch pathway (Kurpinski et al., 2010a). Moreover, γ-secretase cleavage of the Notch receptor is vital for Notch signalling (Yang et al., 2004). It has been shown that the mice with interrupted *Notch*-related molecules present numerous irregularities in blood vessel creation, such as proliferation and migration of endothelial cells, smooth muscle differentiation, vascular remodelling progressions (Chiba 2006). These studies clearly demonstrate that notch receptors and ligands are involved in vascular formation (Y. Xue et al., 1999). In the vascular system, the candidate Notch targets are Hey1, Hey2, and Hey L (Iso et al., 2003). Indeed, it has been shown that a relationship exists between the presence of *Hey1* and *Hey2* and the aberrations in the heart and vasculature (Fischer et al., 2004). Additionally, the differentiation and maturation of vascular SMCs, particularly, arterial cells involve Notch signalling, (Domenga et al., 2004). Mutations to JAG1 are accountable for the abnormality of the heart observed in the Alagille syndrome (an autosomal-dominant human disorder). (Oda et al., 1997) (Chiba 2006).

In this Chapter, the role of γ-secretase inhibitors (DAPT and Compound E) in modulating Notch putative control of myogenic vascular differentiation was investigated using bone marrow-derived mesenchymal stem cells, C3H 10 T1/2 mesenchymal stem cells and resident MVSC vascular stem cells.

4.2   Objectives:

The main aims of this chapter were:

1- To first validate the induction of myogenic vascular differentiation in mouse mesenchymal stem cells (mMSCs), C3H cells and mouse multipotent vascular stem cells (mMVSCs)

2- To determine the effect of DAPT and Compound E on the myogenic differentiation in mouse mesenchymal stem cells (mMSCs), mC3H 10T1/2 cells and mouse multipotent vascular stem cells (mMVSCs).

4.3   Strategy:

The main objective of this chapter was to determine the effect of DAPT and Compound E on mMSCs, C3H mMVSC myogenic of vascular differentiation. To achieve this MSCs were cultured with Dulbecco's Modified Essential Medium (DM) supplemented with 10% FBS to induce myogenic differentiation. C3H cells and mMVSCs were cultured in maintenance medium (MM) with Jagged1 to induce myogenic differentiation. The cells were then treated with DAPT (80 µM) and Compound E (25µM) in the absence or presence of FBS or Jagged1. Myogenic differentiation was confirmed by measuring SMC differentiation marker mRNA expression (Myh11 and Cnn1) by real-time qRT-PCR and protein levels by fluorescence microscopy following immunocytochemical staining of these markers. Notch target gene expression was confirmed by measuring Notch target Hey 1 gene expression.

Data analysis was carried out using the GraphPad Prism™™ software and one-way ANOVA tests for parametric data and Kruskal Wallis t-tests for non-parametric data.

4.4 Results

4.4.1 γ−secretase inhibitors significantly reduce myogenic differentiation induced by serum-supplemented cell culture medium.

Maintenance Medium (MM) is formulated to retain cells in a specific state without inducing differentiation whereas, differentiation Medium (DM) is formulated to promote cells to change from one type to another.

Mouse mesenchymal stem cells were cultured in maintenance medium (MM) and differentiation medium (DM) for three days. In parallel cultures, mMSCs were treated with 80μM of DAPT in differentiation medium (DM) for the same period. The γ−secretase inhibitor, DAPT is known to prevent the generation of the intracellular domain of Notch molecules and suppress the Notch activity. Cells were stained for Myosin Heavy Chain 11 (Myh-11), the mature smooth muscle marker, and cell nuclei were stained by DAPI. Five images were taken/slide by fluorescence microscopy (Figure 4.1(a)) and positive cells stained for *Myh-11* filaments (green) were counted and divided by total cell count (DAPI positive cells) and relative cell differentiation was plotted as a bar chart (Figure 4.1(b)). The ratio of differentiated cells (Myh-11$^+$) to undifferentiated cells (Myh-11$^-$) increased in the presence of differentiation medium when compared to maintenance media (MM). Moreover, DAPT significantly reduced myogenic differentiation by decreasing the number of Myh-11$^+$ cells (Figure 4.1(b)).

Mouse MSCs cultured in maintenance medium (MM) and differentiation medium (DM) supplemented with 10% FBS were treated with DAPT (80μM) for seven days. Following treatment, total RNA was harvested from mMSCs and compared to an internal control mouse aorta RNA, as the aortic SMCs are enriched for the smooth marker (*Myh-11*). *Myh-11* mRNA levels were assayed in triplicate and normalised to a constitutive housekeeping gene, *HPRT*. Relative quantification levels were calculated relative to the control untreated cells cultured in Maintenance Medium (Figure 4.2). Differentiation medium (DM) significantly increased the mRNA expression levels of *Myh-11* compared to maintenance medium (MM). DAPT significantly reduced the levels of *Myh-11* mRNA in differentiation medium (DM) (Figure 4.2).

Mouse MSCs cultured in maintenance medium (MM) and differentiation medium (DM) supplemented with 10% FBS were treated with Compound E (25μM) for two days. Following treatment total RNA was harvested from mMSCs and mouse aorta. *Myh-11* mRNA levels were assayed in triplicate and normalised to *HPRT*. Relative quantification levels were calculated relative to the control (untreated cells cultured in Maintenance Medium (MM) (Figure 4.3). Differentiation medium (DM) significantly increased the mRNA expression levels of *Myh-11*compared to maintenance medium (MM). Compound E significantly reduced the levels of *MyH-11*mRNA in differentiation medium (DM) (Figure 4.3).

Mouse MSCs cultured in maintenance medium (MM) and differentiation medium (DM) supplemented with 10% FBS were treated with Compound E (25μM) for two days. Following treatment total RNA was harvested from mMSCs and mouse aorta. *Cnn1* mRNA levels were assayed in triplicate and normalised to *HPRT*. Relative quantification levels were calculated relative to the control (untreated cells cultured in Maintenance Medium (MM) (Figure 4.3). Differentiation medium (DM) significantly increased the mRNA expression levels of *Cnn1* compared to maintenance medium (MM). Compound E significantly reduced the levels of *Cnn1* mRNA in differentiation medium (DM) (Figure 4.4).

The effects of DAPT and Compound E on differentiation medium induced *Cnn1* mRNA levels were also compared. Mouse MSCs cultured in maintenance medium (MM) and differentiation medium (DM) supplemented with 10% FBS were treated with DAPT (80μM) and Compound E (25μM) for three days. Following treatment total RNA was harvested from mMSCs. *Cnn1* mRNA levels were assayed in triplicate and normalised to *HPRT*. Relative quantification levels were calculated relative to the control untreated cells cultured in Maintenance Medium (MM). Differentiation medium significantly increased the *Cnn1* mRNA expression levels compared maintenance medium (MM). This effect was significantly reduced in the presence of both Compound E (25μM) and DAPT (80μM) (Figure 4.5).

(a)
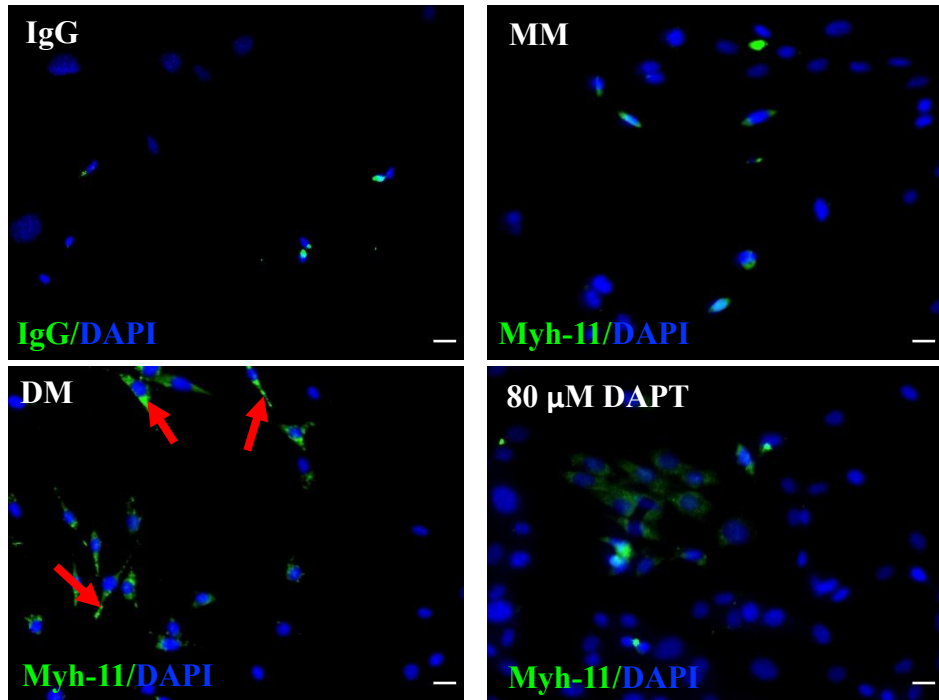
(b)
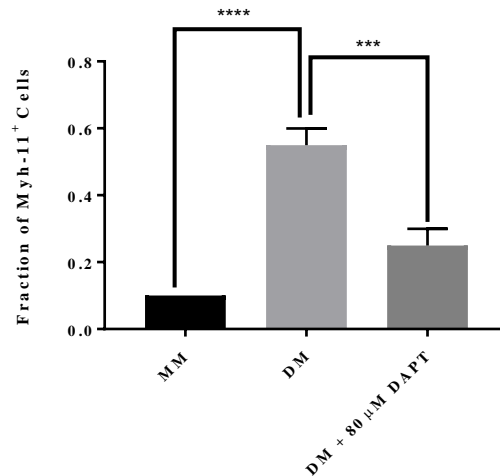
Figure 4.1. The inhibitory effect of DAPT on mouse mesenchymal stem cell (mMSC) myogenic differentiation. The mMSCs were seeded at a density of 3,000 cells/6 well and treated with DAPT (80μM) in differentiation medium (DM) for three days. (a) Representative immunocytochemical analysis of Myh-11$^+$ cells; red arrow depicts the Myh-11 staining (green) around the nuclei and DAPI nuclei staining (blue) was used to analyse the fraction of Myh-11$^+$ cells. (b) Positive cells were counted and averaged and compared to the maintenance medium (MM). Scale bars were set to 100μm. Data analysis was performed by ANOVA using the GraphPad Prism™ software and $p<0.05$, ****$p<0.0001$ and ***$p<0.001$ all considered significant.

111
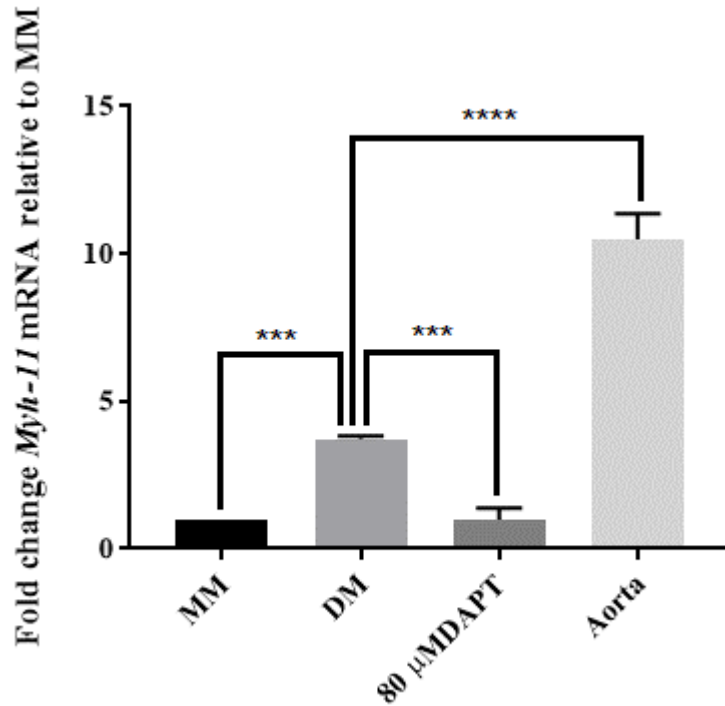
Figure 4.2. The effect of DAPT on *Myh-11* mRNA levels by qRT-PCR. The mMSCs were seeded at a density of 15,000 cells/well and treated with DAPT (80μM) in differentiation medium (DM) supplemented with 10% FBS for seven days. Following treatment, total RNA was harvested from mMSCs and mouse aorta. *Myh-11* mRNA levels were assayed in triplicate and normalised to *HPRT*. Relative quantification levels were calculated relative to the control (untreated cells cultured in Maintenance Medium (MM)). Data analysis was performed by ANOVA using the GraphPad Prism™ software and $p<0.05$, ***$p<0.001$ and ****$p<0.00001$ all considered significant n=6 wells.
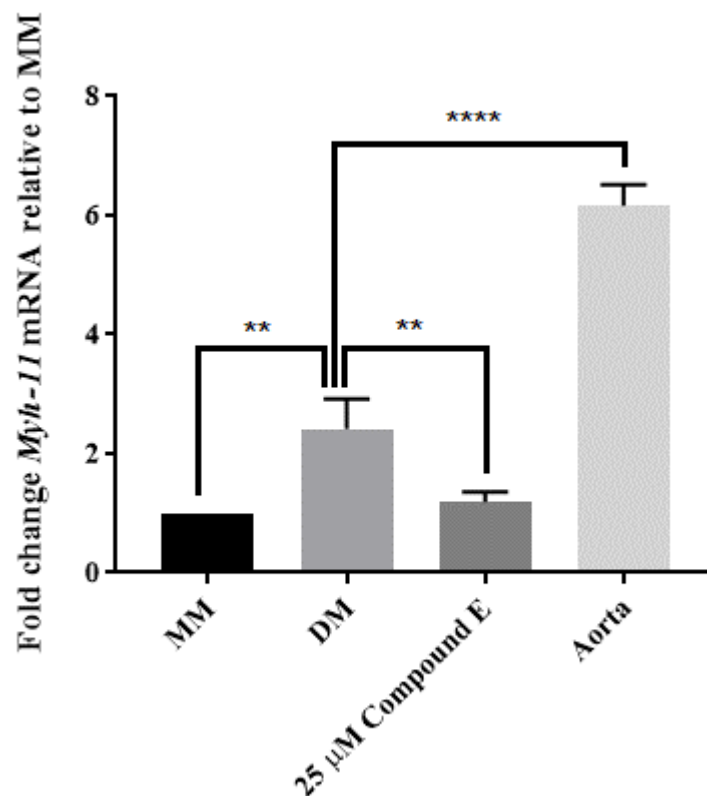
Figure 4.3. The effect of Compound E on *Myh-11* mRNA levels by qRT-PCR. The mMSCs were seeded at a density of 15,000 cells/well and treated with Compound E (25μM) in differentiation medium (DM) supplemented with 10% FBS for two days. Following treatment, total RNA was harvested from mMSCs and mouse aorta. *Myh-11*mRNA levels were assayed in triplicate and normalised to *HPRT*. Relative quantification levels were calculated relative to the control (untreated cells cultured in Maintenance Medium (MM)). For mMSCs data analysis was performed by Kruskal Wallis using the GraphPad Prism™ software and p<0.05, **p<0.001 ****p<0.00001 all considered significant n=6 wells.
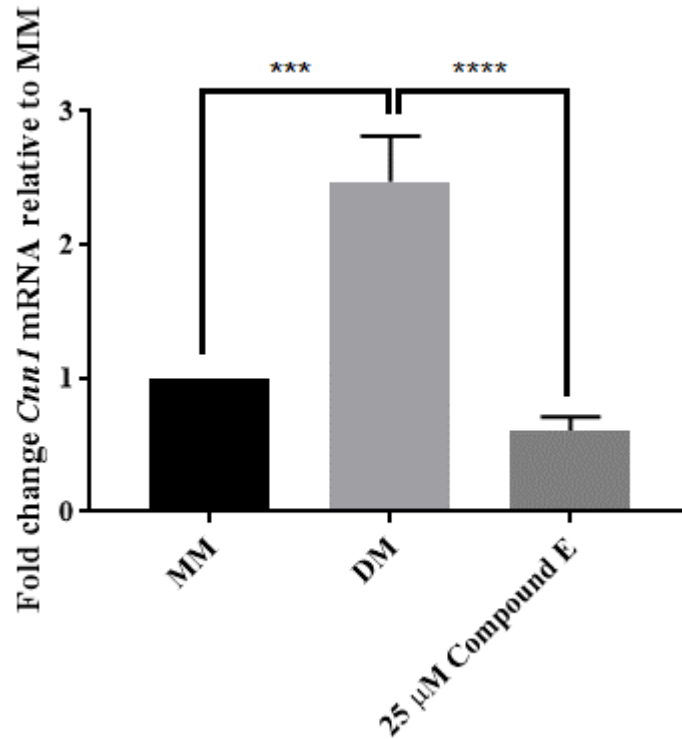
Figure 4.4. The effect of Compound E on *Cnn1* mRNA levels by qRT-PCR. The mMSCs were seeded at a density of 15,000 cells/well and treated with Compound E (25 μM) in differentiation medium supplemented with 10% FBS for two days. qRT-PCR was used to analyse the fold change in the *Cnn1* gene expression, compared to the maintenance medium (MM). Data analysis was performed by ANOVA using the GraphPad Prism™ software and p-value summary is **** p <0.0001.***p<0.001 and ****p<0.00001 all considered significant n=6 wells.
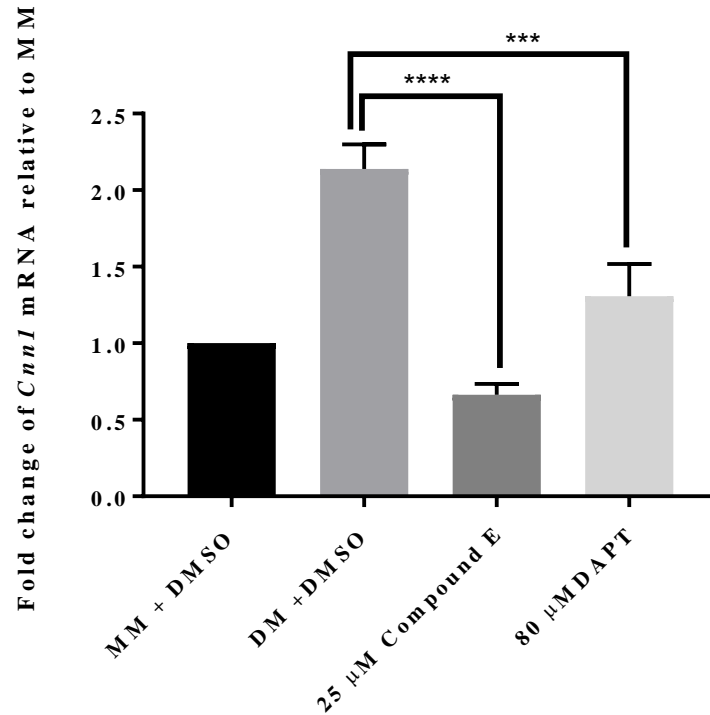
Figure 4.5. Comparison of effects of DAPT and Compound E on *Cnn1* mRNA levels by qRT-PCR. The mMSCs were seeded at a density of 15,000 cells/well and treated with DAPT (80μM), or Compound E (25μM) in differentiation medium supplemented with 10% FBS for both drugs for three days. qRT-PCR was used to analyse the fold change in the *Cnn1* gene expression, compared to the maintenance medium (MM). Data analysis was performed by ANOVA using the GraphPad Prism™ software and p-value summary is **** $p < 0.0001$.****$p<0.0001$ and ***$p<0.001$ all considered significant, n=9 wells.

4.4.2 TGF-β1 medium stem cell differentiation into the smooth muscle cell

Mouse MSCs were cultured in maintenance medium (MM) and differentiation medium (DM) supplemented with 10% FBS. Cells cultured in differentiation medium were treated with 4 ng/mL of TGF-β1 for two days. Following treatment, total RNA was harvested from mMSCs and *Myh1-11* mRNA levels assayed in triplicate and normalised to *HPRT*. Relative quantification levels were calculated relative to the control untreated cells cultured in Maintenance Medium (Figure 4.6). The mRNA expression levels of *Myh-11* increased following stimulation of differentiation medium (DM) and further increased following stimulation of TGF-β1 compared to when cells were cultured in the control Maintenance medium (MM).
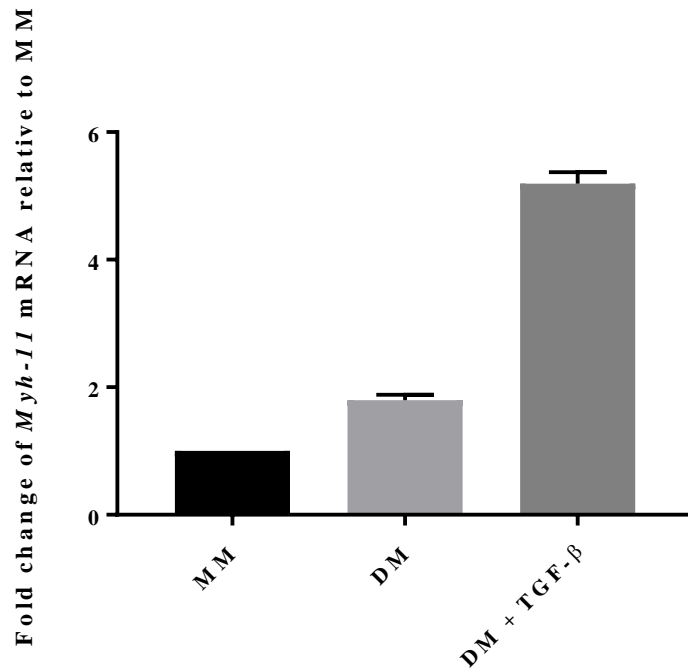
Figure 4.6. *Myh-11* **mRNA relative quantification by RTqPCR**. The mMSCs were seeded at a density of 10, 000 cells /well and treated with maintenance medium (MM), differentiation medium (DM) and TFG-β1(5 ng/mL) for two days. Representative qRT-PCR analysis of the fold change in the gene expression *Myh-11*comparing to the MM (n=3 wells).

4.4.3 Jagged 1 (JAG1) medium ted activation of Notch signalling pathway

In these set of experiments, the aim was to target and control Notch signalling using the Notch ligand, Jagged 1. Jagged-1-Fc (JAG1-Fc) and Fc specific fragment antibody (IgG-Fc-Control) were immobilised on the surface of culture plates as described in Materials and Methods section 2.3.1. Jagged-1 was used to induce myogenic differentiation of mouse C3H 10T1/2 cells (mesenchymal stromal cell line). C3H cells were stimulated with JAG1-Fc or control-FC in maintenance medium (MM) for seven days before cells were immunostained for Myh-11 and the fraction of positive cells stained for Myh-11 filaments (green) counted and divided by total cell count (DAPI positive cells) before the relative number of Myh-11$^+$ cells were plotted as a bar chart (Figure 4.7). JAG1-Fc stimulated myogenic differentiation by increasing the fraction of Myh11$^+$ cells compared to cells treated with the IgG-Fc-control (Figure 4.7).

The results confirmed that JAG-1 but not the Fc control fragment promoted myogenic differentiation of C3H stem cells into smooth muscle cells. Consistent with this, the addition of Notch inhibitor DAPT (80μM) caused a significant decrease in the number of JAG-1-Fc stimulated Myh-11$^+$ cells after three days (Figure 4.8). The ratio of differentiated cells (Myh-11$^+$) to undifferentiated cells (MyH-11$^-$) increased in the presence of JAG1-Fc while DAPT (80μM) significantly reduced the number of Myh-11$^+$ cells in the presence of JAG1-Fc (Figure 4.8).

In a similar manner, myogenic differentiation was induced with JAG1 in the absence or presence of DAPT (80µM) and the relative vehicle (DMSO <0.01%) before cells were immunostained for Cnn1 after seven days (Figure 4.9). JAG1-Fc stimulated myogenic differentiation by increasing the fraction of Cnn1$^+$ cells compared to cells treated with the IgG-Fc-control (Figure 4.9). This effect was significantly inhibited with DAPT (80µM) when compared to vehicle control (Figure 4.9).

(a)
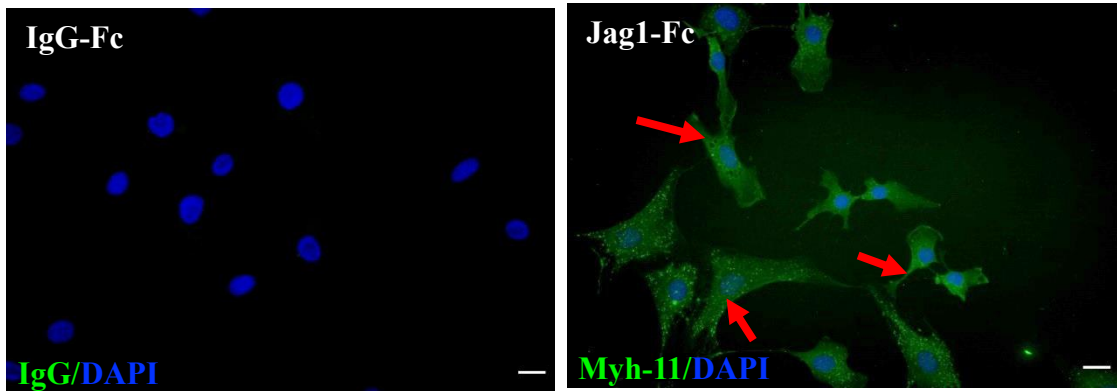
(b)
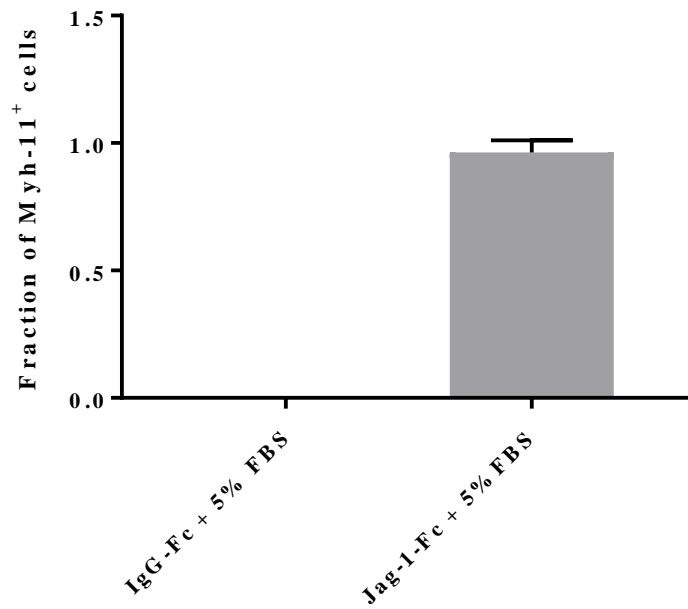
Figure 4.7. Jagged 1 induced myogenic differentiation of C3H 10T1/2 cells. The C3H cells were seeded at a density of 2, 500 cells/well and treated with IgG-Fc (100 ng/mL) and Jag1-Fc (100 ng/mL) in maintenance medium (MM) for seven days. (a) Representative immunocytochemical analysis and (b) fold change in the number of Myh-11 positive cells. Data are representative of one experiment performed in triplicate.

(a)

IgG-Fc
Myh-11/DAPI

Jag-1-Fc
Myh-11/DAPI

Jag-1-Fc + 80µM DAPT
Myh-11/DAPI

(b)
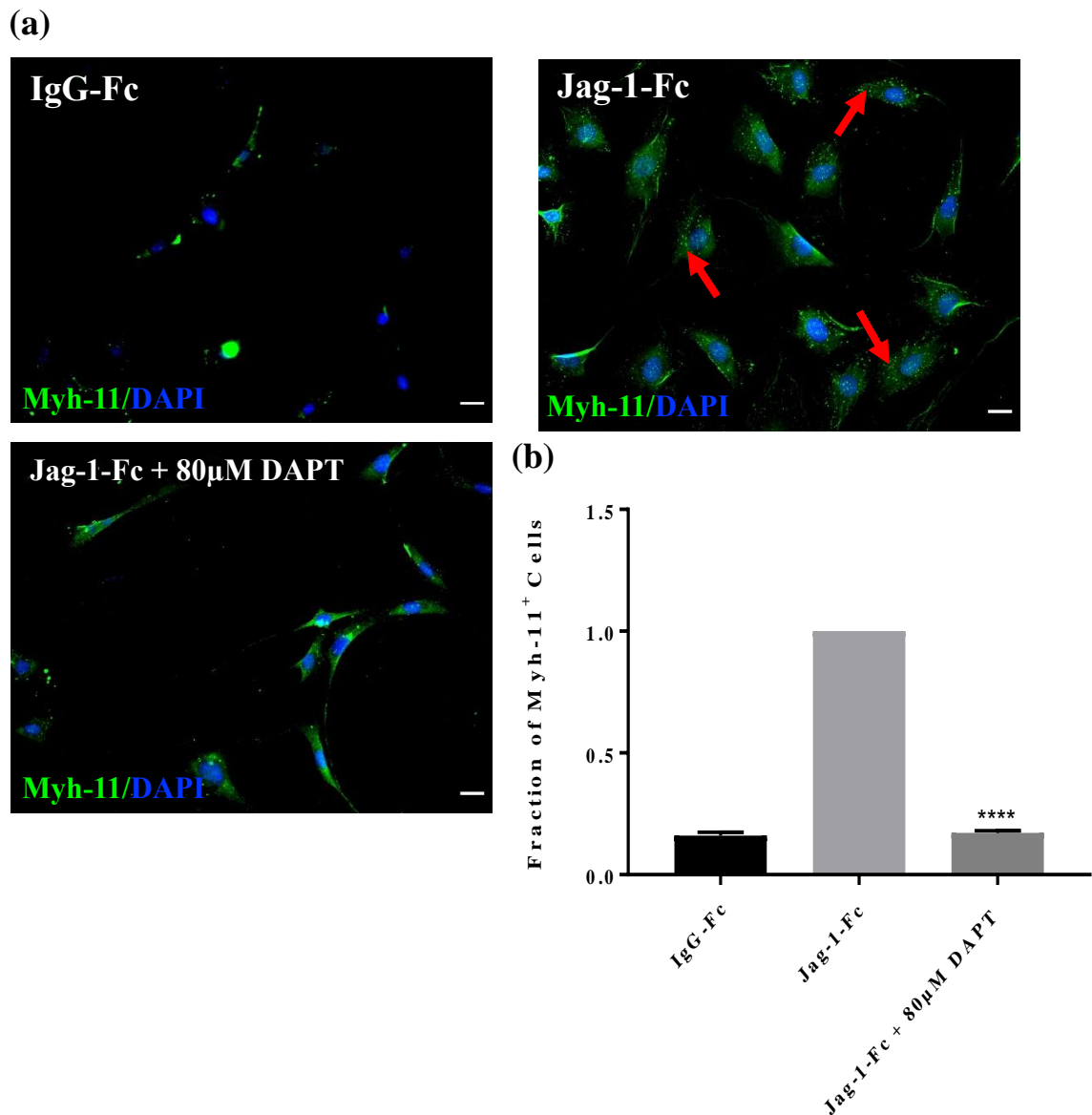
Figure 4.8. The effect of DAPT on Jagged1 induced myogenic differentiation. The C3H were seeded at a density of 2,500 cells/well and treated with IgG-Fc (100 ng/mL), Jag-1-Fc (100 ng/mL) in the absence or presence of DAPT (80µM) for three days. (a) Representative immunocytochemical analysis and (b) the fold change in the number of Myh-11 positive cells. Data analysis was performed by ANOVA using the GraphPad Prism™ software and p-value summary is **** p <0.0001.****p<0.0001 all considered significant vs. Jag1-Fc (n= 3).

(a)
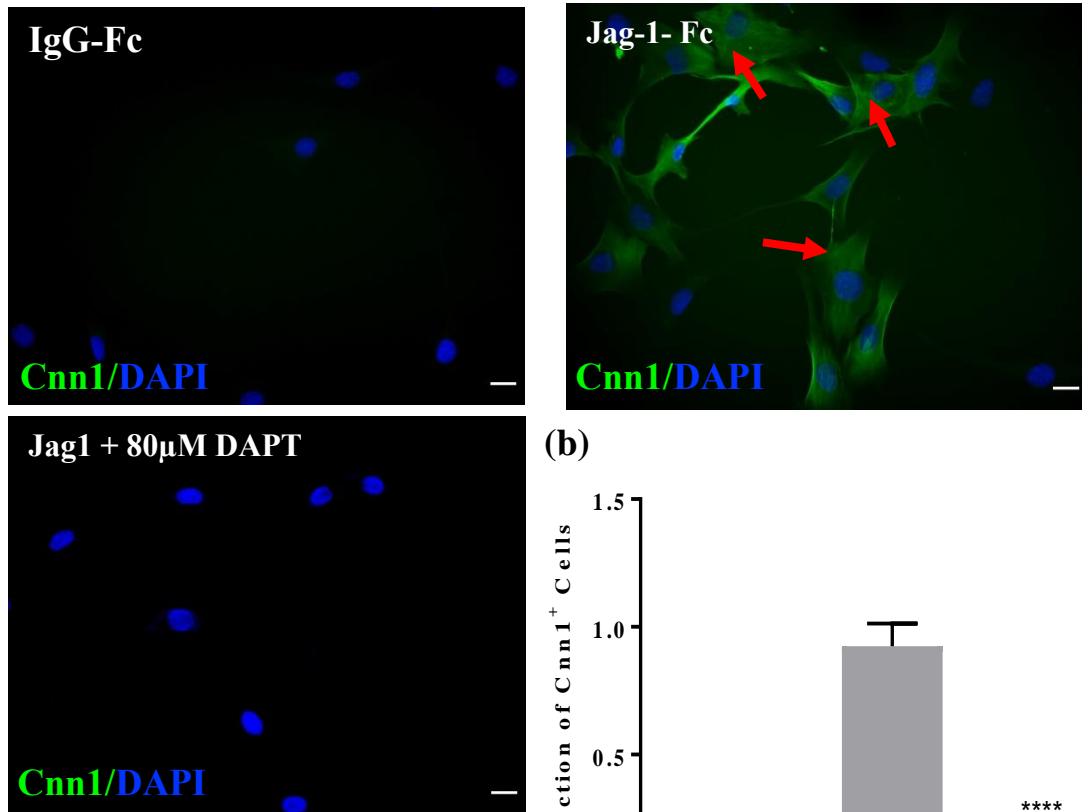
(b)

Figure 4.9. The effect of DAPT on Jag1 induced myogenic differentiation. The C3H were seeded at a density of 2,500 cells/well and treated with IgG-Fc (100 ng/mL), Jag-1-Fc (100 ng/mL) in the absence or presence of DAPT (80μM) for seven days. (a) Representative immunocytochemical analysis and (b) the fold change in the number of Cnn1 positive cells. Data analysis was performed by one-way ANOVA using the GraphPad Prism™ software and **** $p < 0.0001$ considered significant vs. Jag1-Fc (n=3).

4.4.4 γ−secretase inhibitors reduce Jagged1 induced myogenic differentiation of mMVSCs

Mouse Multipotent Vascular Stem Cells (mMVSCs) were seeded in plates with immobilised JAG-1-Fc and Fc specific fragment antibody (FC-control) in maintenance medium (MM) before the effects of DAPT on myogenic differentiation were evaluated. JAG1-Fc treated cells were treated with DAPT (80μM) (Figure 4.10) for three days. Activation of Notch target gene expression was confirmed by measuring *Hey1* mRNA levels normalised to *HPRT*. Relative quantification levels were calculated relative to the Fc-control untreated cells cultured in Maintenance Medium (MM). JAG1-Fc increased the mRNA expression levels of *Hey1* compared to when cells were cultured in the presence of IgG-Fc control (Figure 4.10). This effect was significantly reduced in the presence of DAPT (Figure 4.10).

The ability of GSI inhibitors, DAPT and Compound E to inhibit Notch target gene expression was evaluated. Mouse Multipotent Vascular Stem Cells (mMVSCs) were seeded in plates with immobilised JAG1-Fc and Fc-Control in maintenance medium (MM) before the effects of DAPT and Compound E on Myh11 and *Hey1* mRNA expression was evaluated. The Notch target gene *Hey1* mRNA levels were assayed in triplicate and normalised to *HPRT*. Relative quantification levels were calculated versus control untreated cells cultured in Maintenance Medium with Fc-control fragment (Figure 4.11). JAG1-Fc increased the mRNA expression levels of *Hey1* compared to the IgG-Fc control an effect significantly attenuated with DAPT (80μM) and Compound E (25μM), respectively (Figure 4.11).

The effect of GSI inhibitors, DAPT and Compound E on myogenic differentiation of MVSCs was assessed. Mouse MVSCs were stimulated with JAG1-Fc or control-Fc coated plates in the absence or presence of DAPT (80μM) or Compound E (25μM) for seven days. Smooth muscle differentiation marker *Myh-11* mRNA levels were determined in triplicate and normalised to *HPRT*. Fresh aortic SMCs were used as a positive control. Relative quantification levels were calculated relative to the control Fc-untreated cells cultured in Maintenance Medium with Fc-control fragment (Figure 4.12). JAG1-Fc increased *Myh-11* mRNA expression levels compared to IgG-Fc control, but these levels were substantially lower than observed in fresh aortic SMCs and were

reduced in the presence of DAPT (80µM) and Compound E (25µM), respectively (Figure 4.12).

In a similar manner, mouse MVSCs were stimulated with JAG1-Fc or control-Fc coated plates in the absence or presence of DAPT (80μM) for seven days before smooth muscle differentiation marker *Cnn1* mRNA levels were determined in triplicate and normalised to *HPRT*. JAG1-Fc increased *Cnn1* mRNA expression levels compared to IgG-Fc control, an effect that reduced in the presence of DAPT (80µM) (Figure 4.13).

Mouse MVSCs were also stimulated by plating on JAG1-Fc or control-Fc coated plates. Stimulated and unstimulated cells were treated with DAPT (80μM) and Compound E (25μM). Cells were immunostained for Cnn1 after seven days. The ratio of differentiated cells Cnn1$^+$ to undifferentiated cells Cnn1$^-$ increased in the presence of JAG1-Fc, and the effect that was significantly reduced in the presence of $\gamma-$secretase inhibitors, DAPT (80μM) and Compound E (25μM) (Figure 4.14)

In a similar manner, mouse MVSCs were also stimulated by plating on JAG1-Fc or control-Fc coated plates in the absence or presence of DAPT (80μM) before cells were immunostained for Myh-11 after seven days. The ratio of differentiated cells Myh-11$^+$ to undifferentiated cells Myh-11$^-$ increased in the presence of JAG1-Fc, and the effect that was significantly reduced in the presence of $\gamma-$secretase inhibitors, DAPT (80μM) (Figure 4.15).
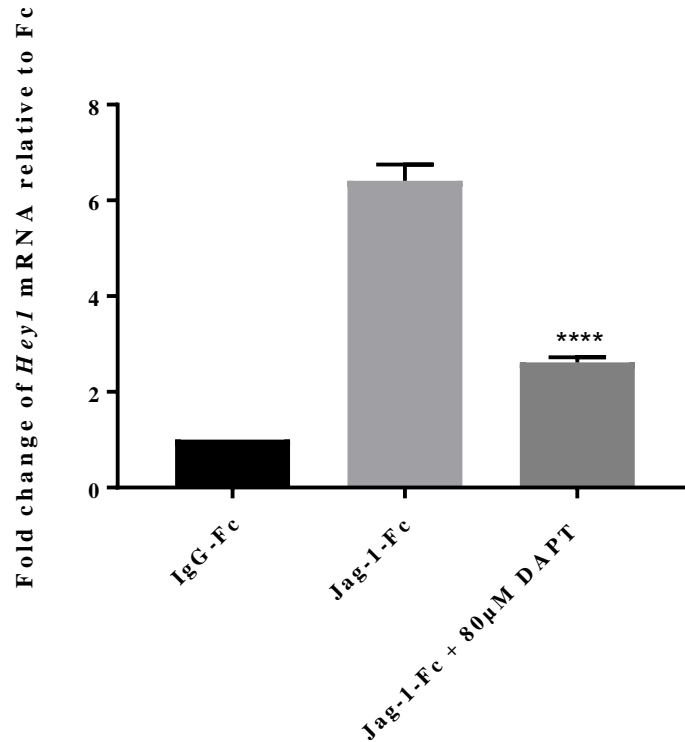
Figure 4.10. Jagged1 stimulation of *Hey1* mRNA levels in mMVSCs by qRT-PCR. The MVSCs were seeded at density of 10,000 cells/well and treated with IgG-Fc (500 ng/mL), Jag-1-Fc (500 ng/mL) in the absence or presence of DAPT (80μM) in maintenance medium (MM) for three days before qRT-PCR was used to analyse the fold change in *Hey1* gene expression when compared to the maintenance medium. Data analysis was performed by ANOVA using the GraphPad Prism™ software and **** p <0.0001 considered significant vs. Jag1-Fc (n=6 wells).
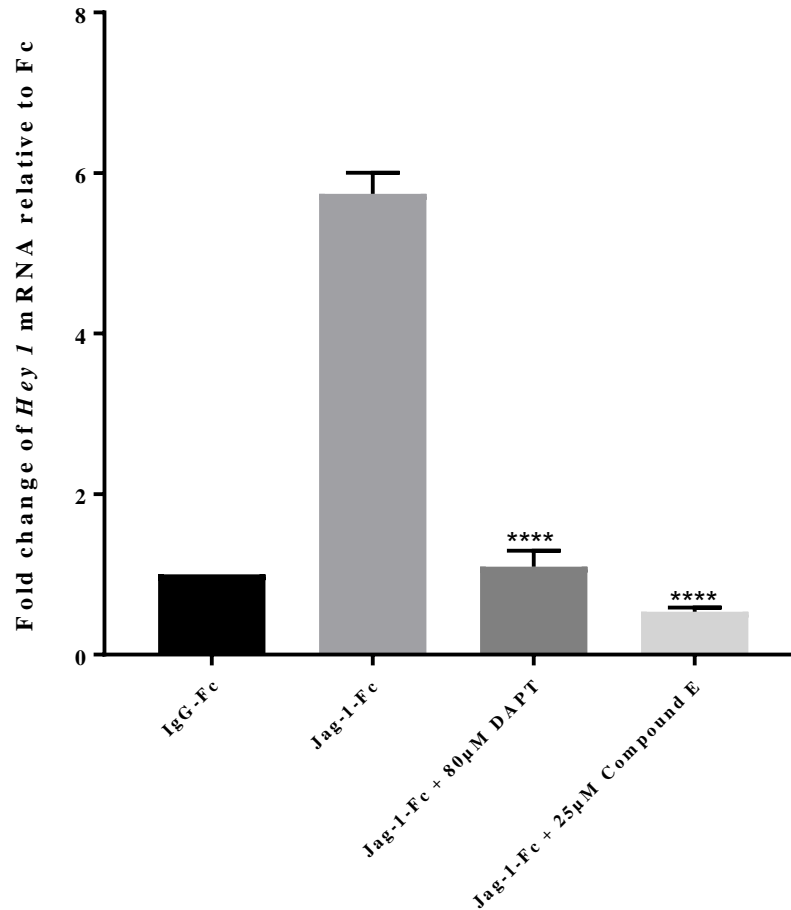
Figure 4.11. DAPT and Compound E attenuated Jagged1 stimulation of *Hey1* mRNA levels in mMVSCs. The mMVSCs were seeded at a density of 10,000 cells/well and stimulated with Fc- control (500 ng/mL), Jag-1-Fc (500 ng/mL) in the absence or presence of DAPT (80µM) or Compound E (25µM) for three days. Following treatment, total RNA was harvested from mMVSCs. *Hey1* mRNA levels were assayed in triplicate and normalised to *HPRT*. Relative quantification levels were calculated relative to the control untreated cells cultured in Maintenance Medium (MM). Data analysis was performed by ANOVA using the GraphPad Prism™ software and **** p <0.0001 all considered significant vs. Jag1-Fc (n=3).
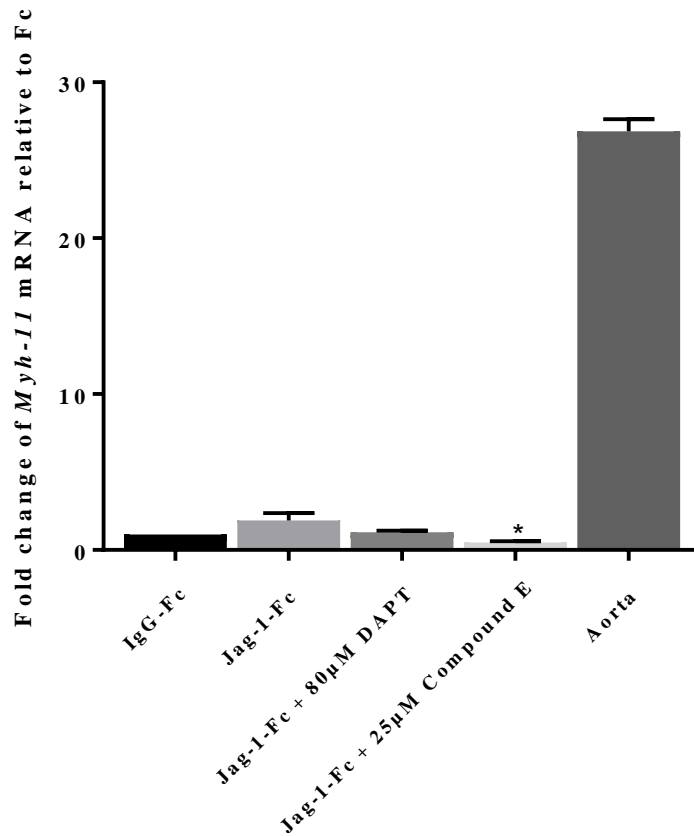
Figure 4.12. DAPT and Compound E attenuate Jagged1 stimulation of *Myh-11* mRNA levels in mMVSCs. The mMVSCs were seeded at density of 10,000 cells/well and treated with IgG-Fc (500 ng/mL), Jag-1-Fc (500 ng/mL) in the absence or presence of DAPT (80μM) or Compound E (25 μM) in maintenance medium for seven days before the levels of *Myh-11* were assessed by qRT-PCR and compared to aortic *Myh-11* levels. mRNA levels were assayed in triplicate and normalised to *HPRT*. Relative quantification levels were calculated relative to the control IgG Fc-untreated cells. Data are the mean and SEM of three wells. Data analysis was performed by ANOVA using the GraphPad Prism™ software and * p <0.05 all considered significant vs. Jag1-Fc. (n=3).
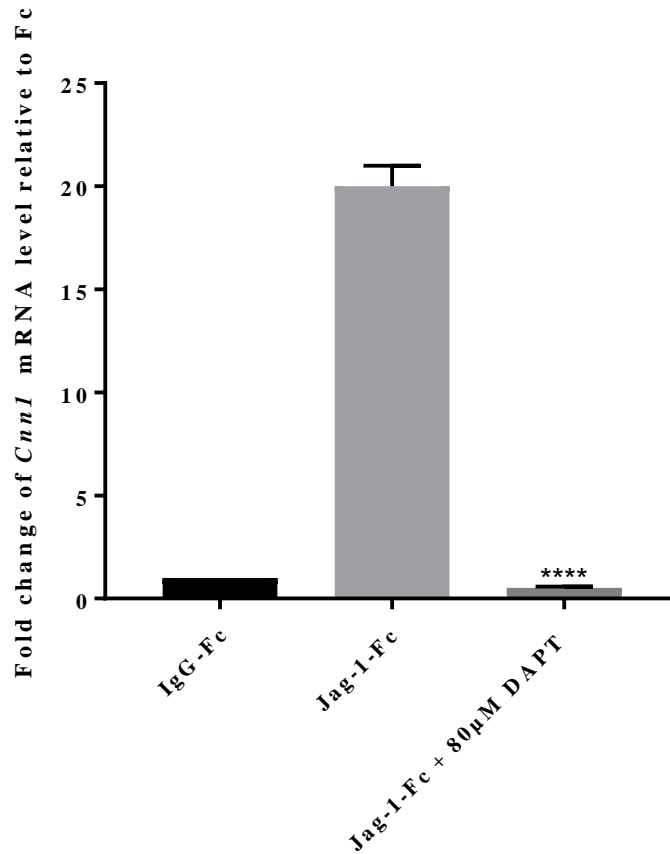
Figure 4.13. DAPT attenuates Jagged1 stimulation of *Cnn1* mRNA levels in mMVSCs. The mMVSCs were seeded at a density of 10^5cells/well and treated with IgG-Fc (500 ng/mL), Jag-1-Fc (500 ng/mL) in the absence or presence of DAPT (80μM) in maintenance medium (MM) for seven days. qRT-PCR was used to analyse the fold change in *Cnn1* gene expression compared to the Fc-control. Data analysis was performed by ANOVA using the GraphPad Prism™ software and ****p <0.0001 all considered significant vs. Jag1-Fc (n=4).

(a)
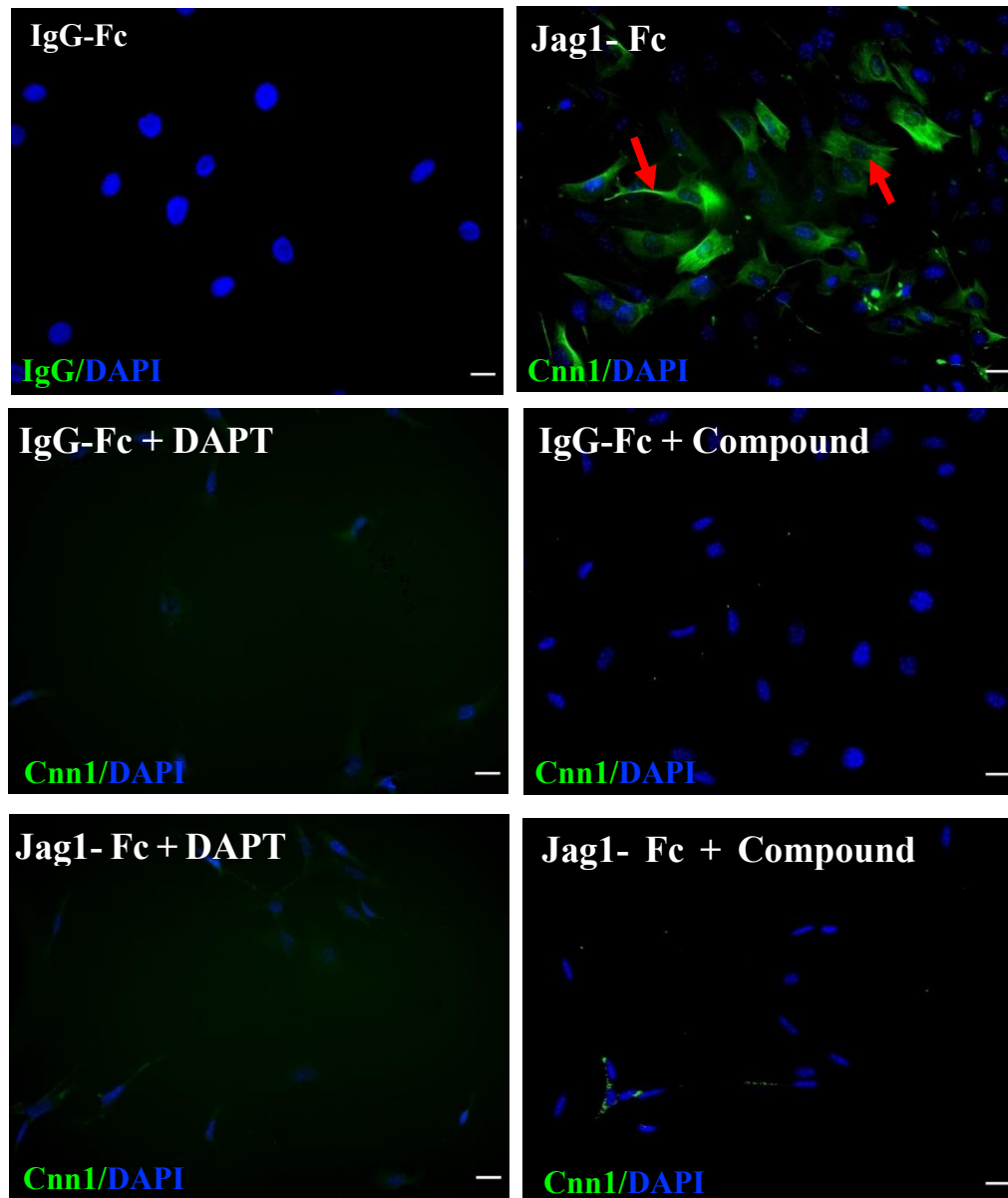
Figure 4. 14. (a) The effect of γ −secretase inhibitors on the number of Cnn1⁺ mMVSCs. The mMVSCs were seeded at a density of 2,500 cells/well and treated with and treated with IgG-Fc (500 ng/mL), Jag-1-Fc (500 ng/mL) in the absence or presence ofDAPT (80µM) and Compound E (25µM) in maintenance medium for seven days. Representative immunocytochemical analysis.

128

(b)
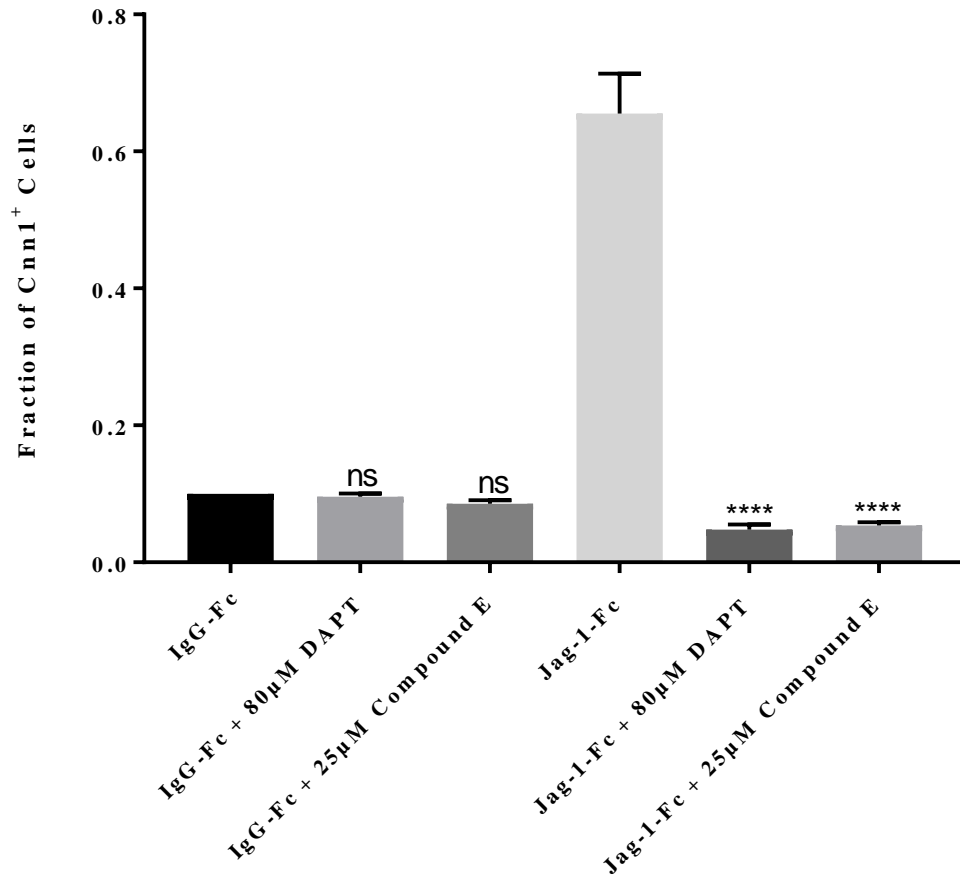
Figure 4. 14. (b). The effect of γ −secretase inhibitors on the number of Cnn1⁺ mMVSCs. The mMVSCs were seeded at density of 2,500 cells/well and treated with and treated with IgG-Fc (500 ng/mL), Jag-1-Fc (500 ng/mL) in the absence or presence ofDAPT (80μM) and Compound E (25μM) in maintenance medium for seven days before the fold change in the number of Cnn1 positive cells was evaluated. Data analysis was performed by ANOVA using the GraphPad Prism™ software and **** p <0.0001 all considered significant vs. Jag1-Fc (n= 6 wells).
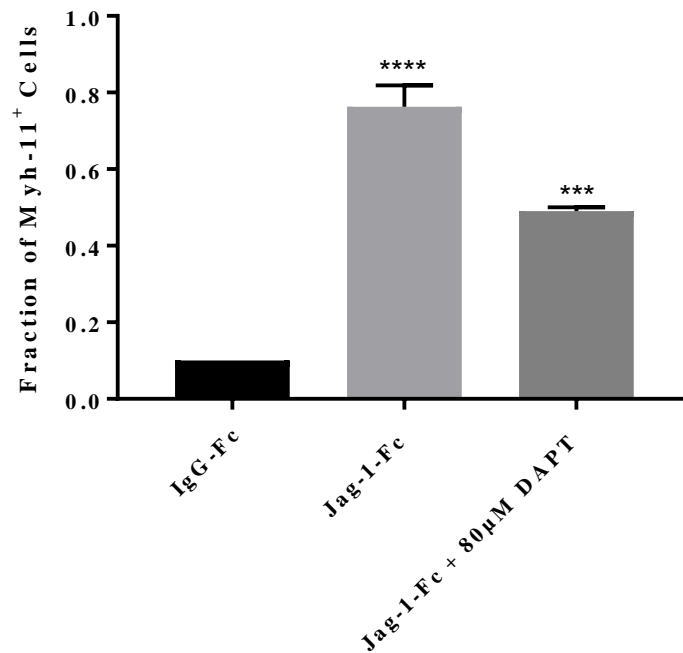
Figure 4.15. The effect of DAPT on Jag-1-Fc stimulation of Myh-11+ mMVSCs: The mMVSCs were seeded at density of 2,500 cells/mL density and treated with (i) Fc control (500 ng/mL), (ii) notch activation using Jagged-1 (500 ng/mL) and (iii) notch inhibition using DAPT (80μM) in maintenance medium for seven days. Immunocytochemistry was used to analyse the percentage of the positive cells. Positive cells were counted and averaged for the gene expression Myh-11 (images have not shown). The fold change in the number of Myh-11 positive cells. Data analysis was performed by ANOVA using the GraphPad Prism™ software **** p <0.0001 and ***p<0.001 all considered significant (n=3).

4.5 Discussion

Mouse stem cells exhibit the two basic characteristics of stem cells: self-renewal and the potential to differentiate. Mouse MSCs, MVSCs and C3H/10T1/2 maintain their stemness in maintenance medium (MM) and undergo myogenic differentiation to SMCs only when cultured in differentiation medium supplemented with the appropriate myogenic inductive cues.

Several signalling pathways and transcription factors are important in dictating the phenotypic state of vascular SMCs, some of which include: serum response factor (SRF)/myocardin (Manabe and Owens 2001), PDGF (Marmur et al., 1992), TGF-β1 (Ikedo et al., 2003), GATA-6 (Sun-Wada et al., 2000), IGF-I (Thömmes et al., 1996), FGF-2 (Segev et al., 2002), endothelin-1 (Hahn et al., 1992), and nitric oxide (GRANGE et al., 2001).

Strong evidence has now emerged supporting a pivotal role for Notch receptors/ligands in dictating the phenotypic state of SMC (Boucher et al., 2012, H. Tang et al., 2008, Campos et al., 2002). Studies investigating the function of Notch signalling in SMC have yielded conflicting results, describing both anti-differentiation (Morrow et al., 2008, Proweller et al., 2005) and pro-differentiation functions for Notch (Boucher et al., 2011, H. Tang et al., 2008, Domenga et al., 2004). These discrepancies are the result of a highly context-dependent nature and tight Spatio-temporal regulation of Notch pathway components during development, in the adult vasculature, and in response to physiological changes *in vivo* (Boucher et al., 2012).

It is clear from the data in this Chapter that Notch ligands promote myogenic differentiation of undifferentiated mouse stem cells (mMSCs, mMVSCs and C3H 10T1/2 cells) since Jag1-Fc not only increased SMC differentiation marker mRNA expression (Myh11 and Cnn1) levels but also the fraction of Myh11$^+$ and Cnn1$^+$ in these cells following treatment. In agreement with previous studies, smooth muscle phenotype was identified by marked expression of *Myh11* and/or *Cnn1* as (Simper et al., 2002, Shimizu et al., 2001). Moreover, MSCs were shown capable of differentiating into SMCs phenotype (Kobayashi et al., 2004). TGF-β1 is known for its effect on the cells including the activation of the SMC genes such as Myh11 (Simper et al., 2002). Stimulating stem

cells through Jagged-1 Notch activation promoted the expression of the Notch signalling target gene, *Hey1* (Zavadil et al., 2004) and significantly induced stem cells to differentiate into SMC-like cells (Doi et al., 2006). In addition, it is known that mMSCs obtained from 5 different strains of mice expand more rapidly if plated at very low density, formed single-cell-derived colonies and readily differentiated into various lineages depending on their media requirements for optimal growth, rates of propagation, and presence of the surface epitopes CD34, stem cell antigen-1 (Sca-1), and vascular cell adhesion molecule 1 (VCAM-1) (Peister et al., 2004). Hence the culture conditions for murine stem cells may ultimately dictate the level of responsiveness of these cells to various lineage-specific inductive cues.

γ-Secretase is a multi-subunit, intramembrane-cleaving protease that is now being considered as a therapeutic target for several diseases (Dong et al., 2010). Potent, orally bioavailable γ-secretase inhibitors (GSIs) have been developed and tested in humans with Alzheimer's disease (AD) and cancer. Of the more than 100 GSIs synthesized to date, most can be divided into three classes: peptide isosteres, azepines, and sulphonamides (Olsauskas-Kuprys et al., 2013a). The azepines (DAPT and Compound E) and sulfonamides are the most popular. DAPT and Compound E have previously been shown to inhibit Notch signalling in basal-like breast cancers cells because Notch1 has been revealed to be precisely hyperactivated in these cells (C. W. Lee et al., 2008). Both DAPT and Compound E inhibited *Hey1* Notch target gene expression in murine stem cells while concomitantly inhibiting Jag1-Fc stimulated myogenic differentiation by reducing the number of Myh11$^+$ and Cnn1$^+$ cells and decreasing the levels of *Myh11* and *Cnn1* mRNA. The inhibition of myogenic differentiation with DAPT and Compound E occurred at concentrations that did not significantly alter baseline growth (proliferation and apoptosis) of these cells suggesting that the decrease in myogenic differentiation was more likely due to a direct result of inhibiting Jag-1-Fc induced asymmetric division and differentiation to SMC-like cells. The data from these studies also demonstrate that at these concentrations of DAPT and Compound E attenuated myogenic differentiation of murine stem cells from 3 different sources (bone-marrow, adventitial fibroblasts and resident multipotent medial stem cells) without any marked effect on SMC growth (Chapter 3, Figure 3.3 and 3.5).

The Notch signalling pathway is a crucial regulator of stem cell behaviour and in lineage-specific differentiation and injury-induced tissue repair (Z. Liu et al., 2009). Following vascular injury, resident multipotent stem cells within the vessel wall may become activated and switch from an undifferentiated quiescent phenotype to a migratory, proliferative SMC-like phenotype which contributes to lesion formation and vascular occlusive disease. Important regulators of SMC-like cell phenotype include serum response factor and its cofactor myocardia, growth factors, Krüppel-like factors, microRNA-143/145 and Notch signalling. Knockout mouse models of most of the Notch ligand and receptor components display early embryonic lethality due to abnormal vasculogenesis, indicating their essential role in cardiovascular development. Following injury, the vascular remodelling response incorporates unique contributions from several of the Notch ligand and receptor components (Gridley 2010).

The importance of Notch in contributing to the neointimal formation has been addressed in mice. Using a tamoxifen-inducible, cell-specific Cre recombinase strain to delete the Notch2 gene in SMCs, vessel morphometric analysis and immunohistochemical staining revealed that loss of Notch2 in SMC does not significantly alter overall lesion morphology or cell proliferation (Peterson et al., 2018). In contrast, deletion of SMC Notch1 receptor resulted in significant attenuation of neointimal lesion formation in mice following carotid artery injury suggesting that Notch1 receptors are in part responsible for this phenotype (Y. Li et al., 2009). In agreement, studies using local perivascular delivery of siRNA duplexes to deplete the Notch1 receptor confirmed that Notch1 contributes in part to the neointimal formation in mice (Morrow et al., 2014).

Taken together, the data in this chapter reveals that the Notch ligand, Jag-1 promotes myogenic differentiation of murine stem cells derived from murine bone-marrow, adventitial and medial sources and that this effect is attenuated by γ-secretase inhibitors, DAPT and Compound E at concentrations that do not significantly inhibit baseline SMC and stem cell proliferation and offer a potential therapeutic avenue for inhibiting the accumulation of stem cell-derived SMC-like progeny within vascular lesions following injury or in-stent restenosis.

Chapter 5

Fabrication, characterisation and drug release kinetics of Fe$_3$O$_4$ PLGA-PVA magnetic nanoparticles

5.1   Introduction

Polymer coated drug-eluting stents (DESs) have been recognised as the leading therapeutic strategy at decreasing the risk of restenosis post stenting (Chorny, Fishbein, Yellen, Alferiev, Bakay, Ganta, Adamo, Amiji, Friedman and Levy 2010b). There has been a significant evolution in the development of coronary stents in order to avoid both restenosis and thrombosis. Improvements have led to changes in the design and conformation of metallic or resorbable structures, with an adequate balance between trackability and radial force, the development of antiproliferative drugs and the polymers to control release and allow adequate endothelialisation and optimal duration of the antiplatelet regimen. However, concerns still remain.

Current concerns with DES include
- the non-specificity of therapeutics
- incomplete endothelialisation leading to late thrombosis
- the need for long-term antiplatelet agents
- local undesired immune response to polymer delivery matrices
- they lack the fundamental capacity for:

    I.   adjustment of the drug dose and release kinetics and the
    II.   ability to replenish the stent with a new drug on depletion

Polymer coated drug-eluting stents (DESs) have however these desired properties:
- Biodegradable
- Biocompatible
- Prolonged drug release

For many years, the controlled delivery of therapeutics has been the goal of nanomedicine. Among the wide amount of drug nanocarriers, magnetic iron oxide nanoparticles (IONs) are robust nanoplatforms that can achieve high drug loading as well as targeting abilities due to their magnetic and biological properties (Vangijzegem et al., 2019). These applications require the precise design to attain the highest therapeutic efficacy. By precisely shaping the structural properties of the iron oxide nanoparticles (MNPs), drugs loaded onto the nanoparticles can be efficiently guided and selectively

delivered toward targeted locations, in particular, to vascular stents. With these goals in mind, the pharmacokinetics along with *in vivo* behaviour of these nanocarriers must be addressed. It is essential to characterize the size distribution precisely within the nanoparticle suspension (Hoo et al., 2008). This is because the chemical and physical properties are strongly related and dependent upon diameter. Particularly, one of the exclusive structures of an MNP is its high-surface-to-volume ratio and this property is linked inversely proportional to the MNP dimeter which means the larger the surface is, the smaller the MNP. Accordingly, there will be additional loading locations for applications as drug delivery (Berne and Pecora 2000). Additionally, it is a high priority to know the effect of the sonication, which is applied to assist in particle dispersal and solution mixture (Hood 2004).

It is imperative to assess the impact of the nanoparticle on biological activity; hence, an exact characterization of these ingredients is important in order to recognize the properties of the nanoparticles at a basic level which detect their biological effects. (Powers et al., 2006). Furthermore, various methods for characterizing the nanomaterial have been used including dynamic light scattering (DLS) (Powers et al., 2006). DLS has been utilized as a simple system for suspension steadiness analysis (Williams et al., 2006, Brown et al., 1975) and defining the particle size within colloidal suspension (Hoo et al., 2008). Also, this technique is useful for evaluating the particle size, size distribution, and the zeta potential of nanomaterials in solution (Powers et al., 2006). DLS delivers the hydrodynamic radius (radius of a sphere that has a similar distribution coefficient within the equivalent viscid atmosphere of the particles) on a collective average (Berne and Pecora 2000). Therefore, DLS has been broadly utilized to detect the hydrodynamic size of numerous MNPs(Lim et al., 2013)

Transmission electron microscopy (TEM) is used in conjunction with DLS to acquire nanoparticle morphology by examining the nanoparticle following the suspension in water and consequent deposition onto formvar/carbon-coated TEM grids. The general morphology of the nanoparticles is obtained by the AMT software for the digital TEM (Murdock et al., 2008). TEM is one of the utmost powerful tools because of its ability to provide straight MNPs structure and size information (Lim et al., 2013, Berne and Pecora 2000)

Another important analysis tool for drug release from MNPs is high-performance liquid chromatography (HPLC) (Lloyd et al., 2010). HPLC has a strong separation procedure that can resolve mixtures with many alike analytes and this separation happen in short period of time (Meyer 2013) and drug quantitation and their metabolites in biological models (Holčapek et al., 2008, Xu et al., 2007). Moreover, HPLC is applied effectively to determining drug entrapment efficiency (Song et al., 2008).

Lastly, MNPs exposed to a magnetic field is also essential for targeting. This is because these particles follow the Coulomb's law which means the outside magnetic field gradient would be used for manipulating these particles. This 'action at a distance', along with the essential penetrability of the magnetic fields within the human tissue, turning on various implementations including the magnetic nanoparticles transportation and/or magnetic nanoparticles immobilization. Because of the magnetic nanoparticle's nature, they can be prepared to have a resonant respond to a time-varying magnetic field. This is a beneficial outcome associated with the energy transferring from the exciting field to the nanoparticle. (Pankhurst et al., 2003). Preparing the NPs with iron oxide will conduct an NPs with a higher saturation magnetisation than any other NPs that prepared with other methods with parallel composition and size. (Fox 2014). Additionally, as the external magnetic field can be monitored to navigate the particle accumulations and distribution of drugs, this process can be targeted to the lesion location (Sun et al., 2008). Moreover, it is not considered an invasive therapeutic procedure (Nowak 2007).

In the present study, experiments were therefore designed to overcome the current DES limitations by fabricating MNP's functionalised with PLGA/PVA. Poly (lactic-co-glycolic acid) (PLGA) is a biodegradable polymer that has received FDA approval which allows it to be used in the treatment and therapeutic devices. PLGA coated nanoparticles (NPs) facilitate the prolonged release of hydrophobic drugs. Fe_3O_4 PLGA-PVA magnetic nanoparticles were therefore fabricated, characterised and functionalised with DAPT and Compound E *in vitro.*

5.2   Objectives:

The main aims of this chapter were:

1- To fabricate Fe_3O_4 PLGA-PVA magnetic nanoparticles

2- To characterize the size and morphology of blank and drug-loaded MNPs

3- To evaluate drug entrapment into the MNPs and subsequent release overtime under magnetic and non-magnetic conditions.

5.3   Strategy:

The main objective of this chapter was to fabricate blank and GSI drug-loaded MNPs and determine their characteristics, including particles size and morphology before drug entrapment and release kinetics, were assessed under magnetic and non-magnetic conditions. MNPs were prepared as described in Materials and Methods, Chapter 2, (Section 2.4.1). Lyophilised MNPs were resuspended before size and morphology characterisation was assessed using DLS and STEM microscopy for size and morphology characteristics, as described in Materials and Methods, Chapter 2, (Section 2.4.5 and 2.4.6).

The percentage of drug entrapment was assessed by HPLC from standard curves of the two drugs (DAPT and Compound E) and analysing the concentration of drug in the supernatant fractions following purification of the MNPs. Using the retention time data, the concentration of the drug not incorporated into the MNPs was first assessed in the supernatant fractions before the concentration entrapped was extrapolated by subtracting this value from the concentration loaded to reveal:-

% Drug incorporated = (Concentration of drug incorporated/theoretical drug-loaded) X 100

The concentration of drug released under magnet and non-magnetic conditions for various time points (24 hours, 48 hours 3 days and 7 days) and different temperature (0°C, 22°C and 37°C) was assessed by HPLC following purification of MNP's at each time interval and temperature before the concentration of the drug not incorporated into the MNPs was assessed in the supernatant fractions during purification and extrapolated from the standard curve to reveal :-

The concentration of drug in supernatant fraction/concentration of drug incorporated) X 100 = % of drug released from the nanoparticle.

In general, the strategy was to combine magnetic targeting via a uniform field-induced magnetization effect and a biocompatible magnetic nanoparticle (MNP) formulation designed for efficient entrapment and delivery of specific drugs.

Data analysis for the data was carried out using the GraphPad Prism™ software and one-way ANOVA tests for parametric data and Kruskal Wallis t-tests for non-parametric data.

5.4   Results

5.4.1 Nanoparticle preparation

Polylactide-based GSI drug-loaded MNPs formulated using a modified emulsification-solvent evaporation approach were first assessed by microscopy as described in Materials and Methods, Chapter 2, (Section 2.4.1). A 100 μL of nanoparticles was pipetted on carbon-coated copper TEM grids. TEM images were recorded in the University of Limerick and the FeSEM (Hitachi S5500 FeSEM) images were recorded in the NRF DCU.

High power TEM images indicate the grouping of the small 50nm and 100nm PLGA/PVA coated Fe_3O_4-NPs together to form a larger nanoparticle that would be encapsulated by the polymer for functionalization (Figure 5.1).

High power TEM images indicate the grouping of the small 10nm MNPs together to form a larger nanoparticle that would be encapsulated by the polymer for functionalization (Figure 5.2). High power TEM images indicate the grouping of the small 50nm and 500nm Compound E PLGA/PVA coated Fe_3O_4-NPs together to form a larger nanoparticle that would be encapsulated by the polymer for functionalization (Figure 5.3).
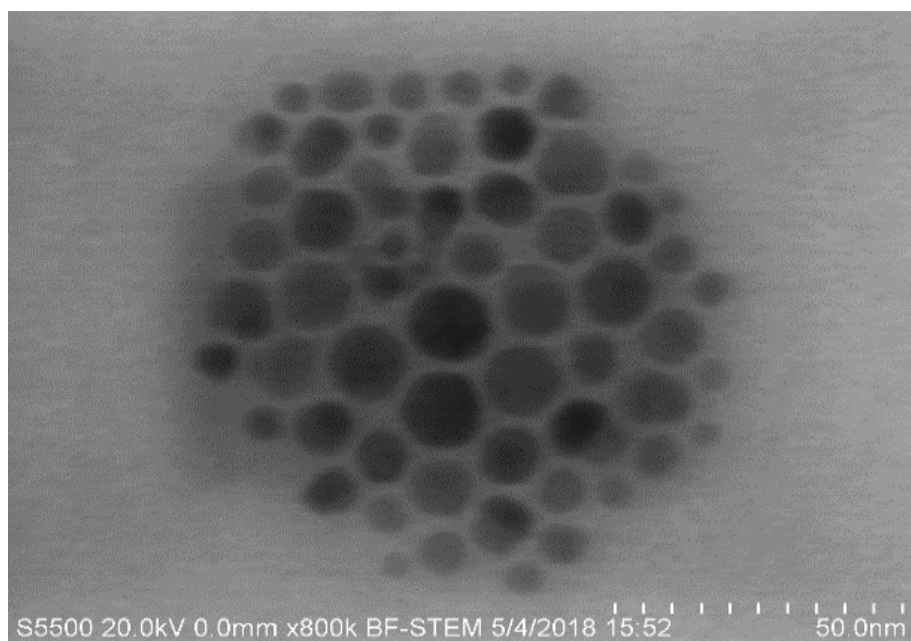
Figure 5.1. TEM images of polymer-coated MNPs. The TEM image of PLGA/PVA coated Fe$_3$O$_4$-NPs at 500 KX.
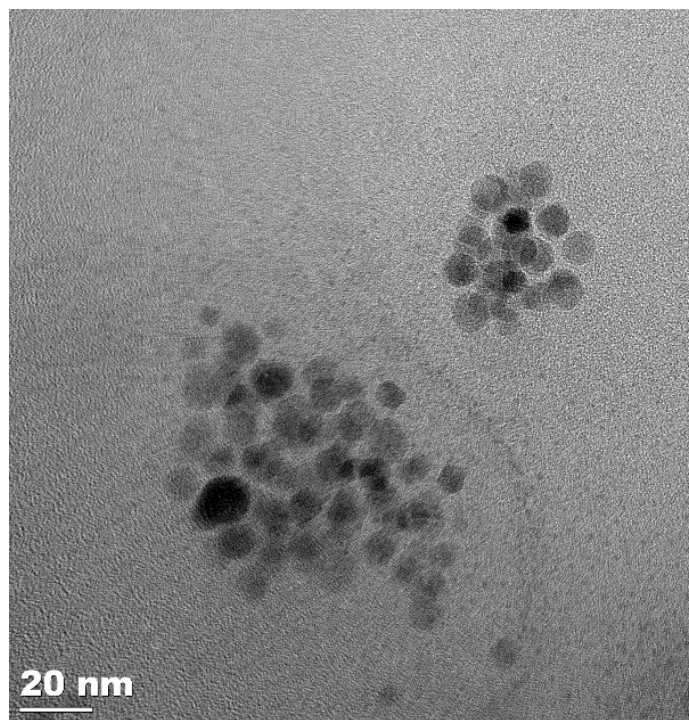
Figure 5.2. TEM images of polymer-coated MNPs. The TEM image of PLGA/PVA coated Fe_3O_4-NPs at 100KX.
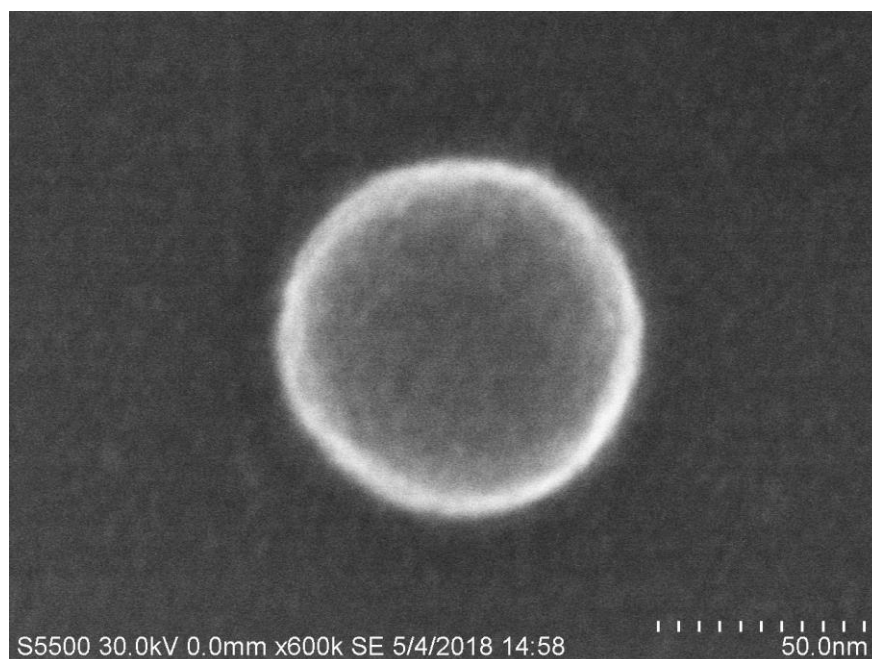
Figure 5.3. TEM images of Compound E loaded MNPs. The TEM image of Compound E PLGA/PVA coated Fe_3O_4 -NPs at 110KX.

5.4.2 Dynamic Light Scattering of MNPs

The Fe_3O_4 NPs, Fe_3O_4 PLGA-PVA blank and GSI drug-loaded MNPs were analysed using a Zetasizer nano Z system at room temperature. The particles were all a uniform size and exhibited little aggregation (Figure 5.4).

The dynamic light scattering (DLS) measurements of Fe_3O_4 nanoparticles had an average hydrodynamic diameter of the magnetite (Fe_3O_4) was 446.4 diameter in nanometre (d.nm) with the polydispersity index (pdi) value of 0.514 (Figure 5.4).

The blank PLGA-PVA MNP's had a decrease average hydrodynamic diameter value of 222.7 d.nm and pdi value of 0.299 (Figure 5.5).

The DAPT-loaded PLGA-PVA MNP's had an increased average hydrodynamic diameter value of 351.4 d.nm and a pdi value of 0.220, following the addition of DAPT (Figure 5.6).

The Compound E-loaded PLGA-PVA MNP's had an increased average hydrodynamic diameter value than the blank and less than DAPT-loaded PLGA-PVA MNP's as it exhibited a value of 256.2 d.nm and a pdi value of 0.321, following the addition of Compound E (Figure 5.7)

		Size (d.nm):	% Volume:	St Dev (d.nm):
Z-Average (d.nm): 446.4	Peak 1:	0.9592	100.0	0.5333
Pdl: 0.514	Peak 2:	0.000	0.0	0.000
Intercept: 0.0529	Peak 3:	0.000	0.0	0.000
Result quality Refer to quality report				

Size Distribution by Volume

Record 4: 02_05_proteoliposomes_1um_size 1
Record 5: 02_05_proteoliposomes_1um_size 2
Record 6: 02_05_proteoliposomes_1um_size 3
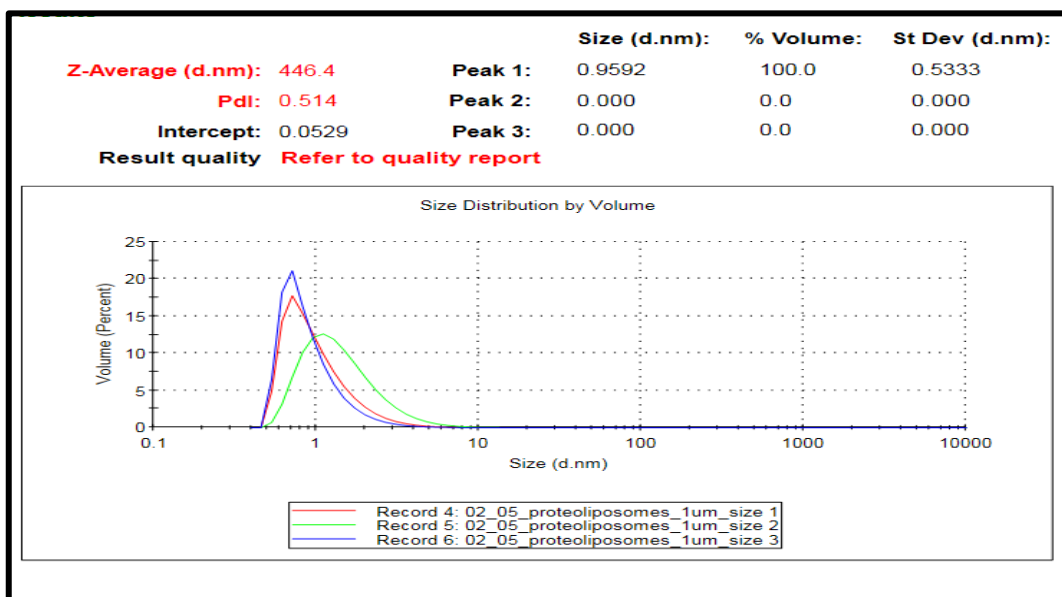
Figure 5.4. DLS Chromatogram of Fe$_3$O$_4$ magnetic nanoparticles. Size measurement of Fe$_3$O$_4$ (magnet) as samples was re-suspended in ultra-pure water and the Zetasizer nano Z system analysed the Fe$_3$O$_4$ (magnet) particles in triplicate peaks readings. The Fe$_3$O$_4$ (magnet) particles size-distribution analysis revealed that particle size was 446.4 d.nm and the pdi was 0.514.
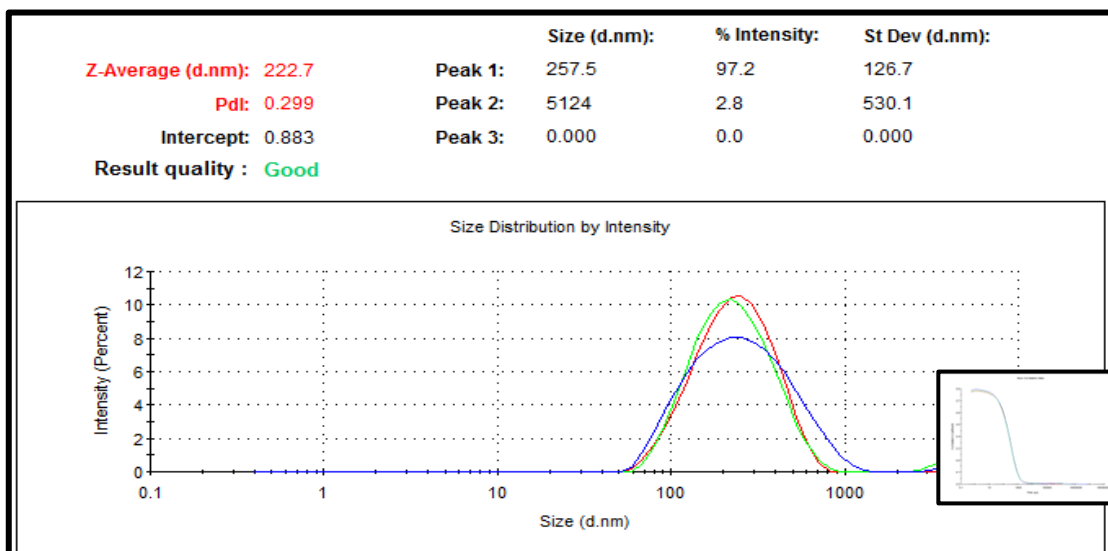
Figure 5.5. PLGA-MNP DLS Chromatogram. DLS size measurements of blank PLGA-PVA magnetic nanoparticles. Samples were re-suspended in ultra-pure water and the Zetasizer nano Z system analysed the PLGA-MNPs in triplicate peaks readings. The blank PLGA-MNP size-distribution analysis revealed that particle size was 222.7 d.nm and the pdi was 0.299.
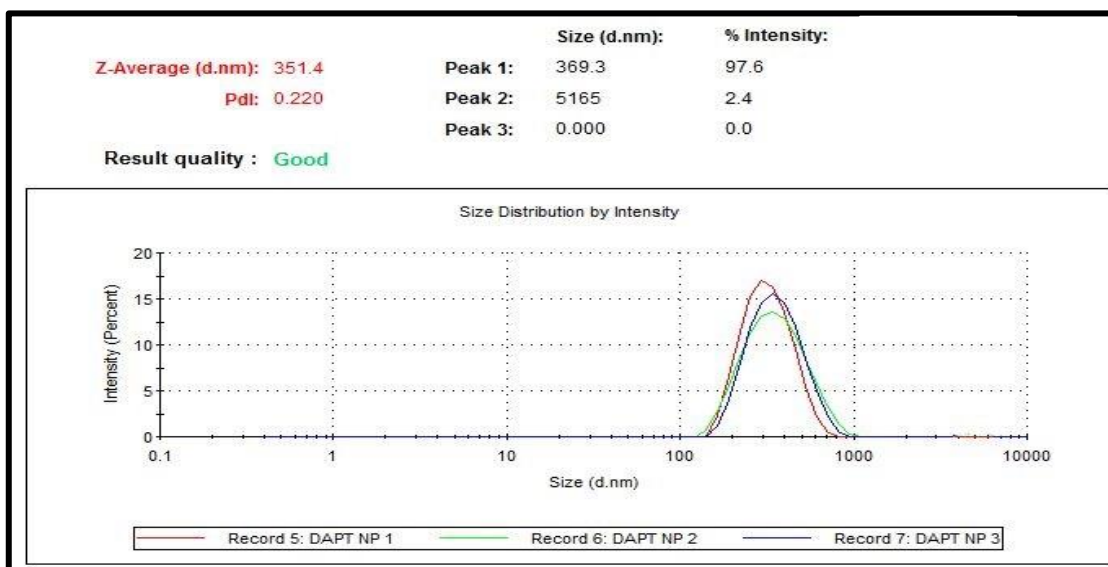
Figure 5.6. DAPT-loaded PLGA-MNP DLS Chromatogram. DLS size measurements of DAPT-loaded PLGA-magnetic nanoparticles. Samples were re-suspended in ultra-pure water and the Zetasizer nano Z system analysed the DAPT-loaded PLGA-MNPs in triplicate peaks readings. The blank PLGA-MNP size-distribution analysis revealed that particle size was 351.4 d.nm and the pdi was 0.220.
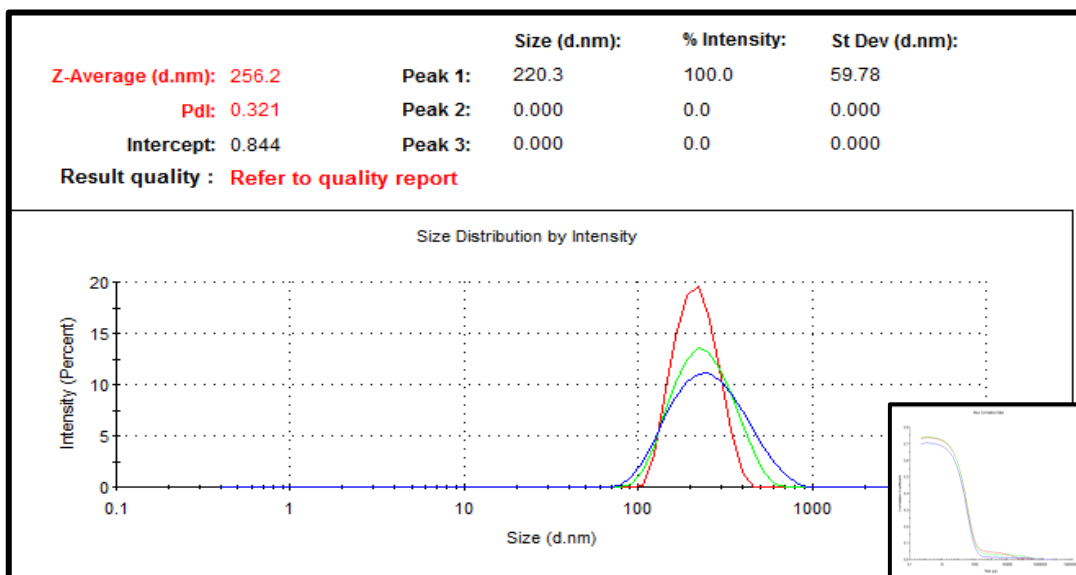
Figure 5.7. Compound E-loaded PLGA-MNP DLS Chromatogram. DLS size measurements of Compound E -loaded PLGA-magnetic nanoparticles. Samples were re-suspended in ultra-pure water and the Zetasizer nano Z system analysed the Compound E -loaded PLGA-MNPs in triplicate peaks readings. The Compound E-loaded PLGA-MNP size-distribution analysis revealed that particle size was 256.2 d.nm and the pdi was 0.321.

5.4.3   HPLC Characterisation of γ-Secretase inhibitors

High-performance liquid chromatography (HPLC) was deployed as described in Materials and Methods, Chapter 2, (Section 2.4.3), in order to separate, identify and quantify the amount of GSI's, DAPT and Compound E entrapped within the MNPs by measuring the levels in the supernatant fractions during their fabrication and purification. A standard curve was used to extrapolate the amount of each GSI in each preparation. The drug entrapment efficiency was then assessed and expressed as the ratio of the drug amount determined in MNPs to that initially used for their preparation.

A wavelength of 234 nm was used with a diode array detector with a wavelength range of 190 nm – 600 nm. The standard curve was created by plotting DAPT concentration (μM), versus peak areas (%), then an R^2 value was calculated. Increasing peak areas corresponds to increasing concentrations of DAPT (Figure 5.8) and Compound E (Figure 5.9).

5.4.3.1   HPLC Characterisation of DAPT

HPLC analysis was carried out on the serial dilutions of DAPT, ranging from 0 µM to 90 µM, using a wavelength of 234 nm. A peak was detected at 4.8 minutes for each sample.

DAPT Concentration (µM)	0	10	20	30	40	50	60	70	80	90
Peak Area (%)	0	24.3	29.7	52.5	87.7	101.2	123.8	135.8	143.5	170.8
Retention Time (minutes)	0	4.808	4.806	4.805	4.799	4.805	4.806	4.806	4.087	4.806
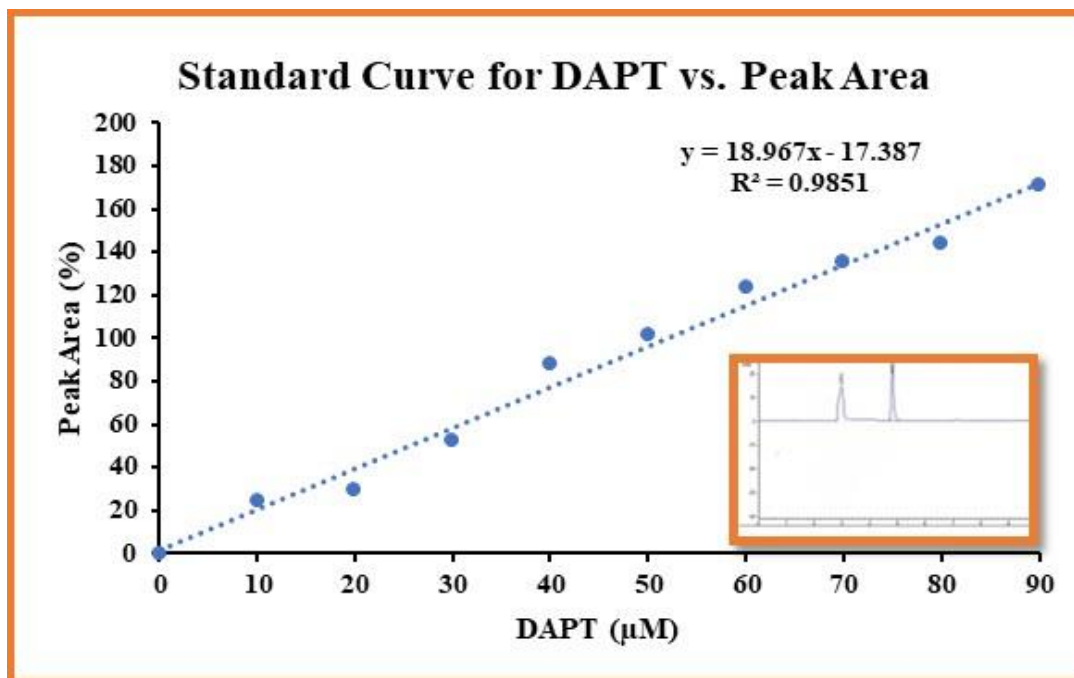
Figure 5.8. HPLC detection of DAPT. A wavelength of 234 nm was used. The standard curve was created by plotting DAPT concentration (0 -90 µM), versus peak areas (%) that were obtained from HPLC readings [Lower right chromatograph which has two peaks the first is the drug vehicle (DMSO) and the second is for the DAPT].

5.4.3.2 HPLC Characterisation of Compound E

HPLC analysis was carried out on the serial dilutions of Compound E, ranging from 1μM to 100μM, using a wavelength of 234nm. A peak was detected at 12 minutes for each sample.

Compound E Concentration (μM)	0	1	10	25	50	100
Peak Area (%)	0	87.1	189.8	464.5	921.8	1934.2
Retention Time (minutes)	0	12.318	12.323	12.324	12.324	12.331
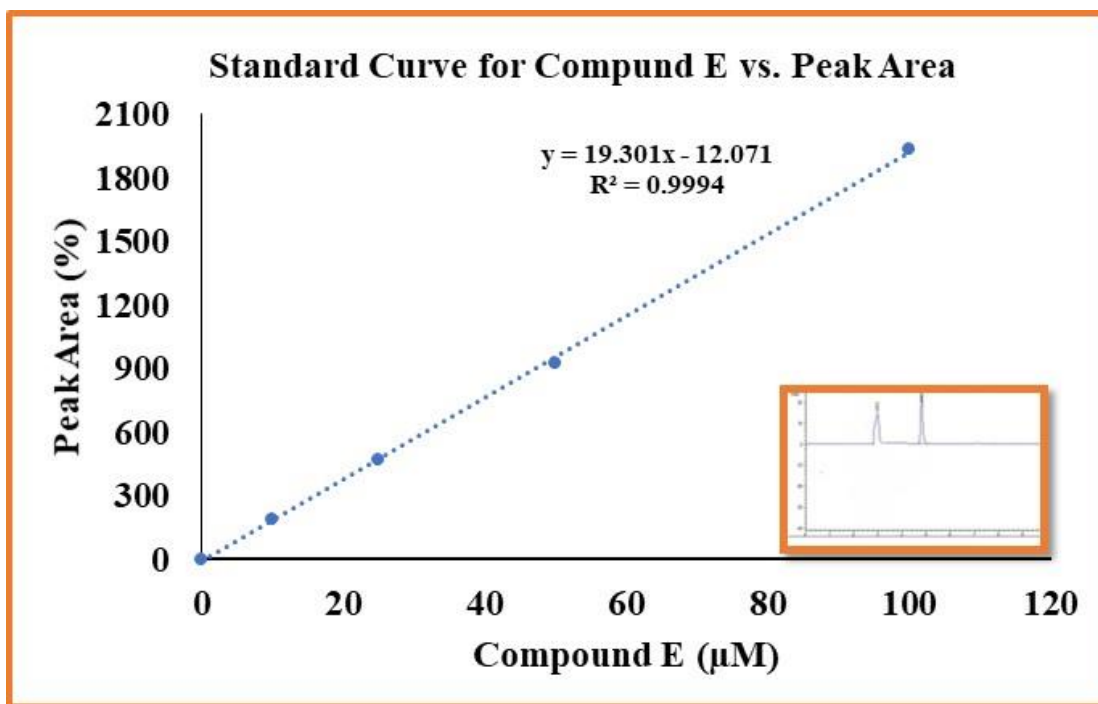
Figure 5.9. HPLC detection of Compound E. A wavelength of 234 nm was used. The standard curve was created by plotting Compound E concentration (1 -100 µM), versus peak areas (%) that were obtained from HPLC readings [Lower right chromatograph which has two peaks the first is the drug vehicle (DMSO) and the second is for the Compound E].

5.4.4   Drug Incorporation Efficiency

To establish the incorporation efficiency of the drugs (DAPT and Compound E) into the drug-loaded PLGA/PVA-MNPs, the supernatant fractions from washing and purification of MNPs during fabrication were collected and subjected to HPLC. The peak area of the drug from the two supernatants was compared to the peak area of the drug in the standard curve performed on the same day to determine the concentration of drug from the supernatant fractions. The concentration of drug detected in the supernatant was then divided by the theoretical drug-loaded to give the concentration of drug incorporated. The following equation was then used to calculate the incorporation efficiency:

(Concentration of drug in supernatant/concentration of drug incorporated) X 100 = % of drug released from nanoparticle.

 (Concentration of drug released during the incubation/theoretical drug-loaded) X 100 = % of drug incorporated.

DMSO (drug vehicle) supernatants had a peak area of 0.46 % for supernatant one and supernatant two had a peak area of 0.34% both at retention times of 5.15 minutes.

For DAPT loaded MNP's, supernatant one had a peak area of 18.3% and supernatant two had a peak area of 13.4%, both at retention times of 4.7 minutes. These results corresponded to ~ 32% (48μM) of the added DAPT (150μM) not incorporating to the PLGA-MNPs [Figure 5.10]. 68% (102μM) of DAPT was incorporated onto the DAPT-loaded PLGA-MNPs [Figure 5.12].

For Compound E loaded MNP's, supernatant one had a peak area of 0.5% and supernatant two had a peak area of 7.2% both at retention times of 2.34 minutes. These results corresponded to ~8% (4μM) of the added Compound E (60μM) not incorporating to the PLGA-MNPs [Figure 5.11] suggesting that ~92% (56μM) of Compound E was incorporated onto the Compound E -loaded PLGA-MNPs [Figure 5.12].

The loss of some drug during fabrication required that higher concentrations of drug were added during formulation to compensate for this loss.

153
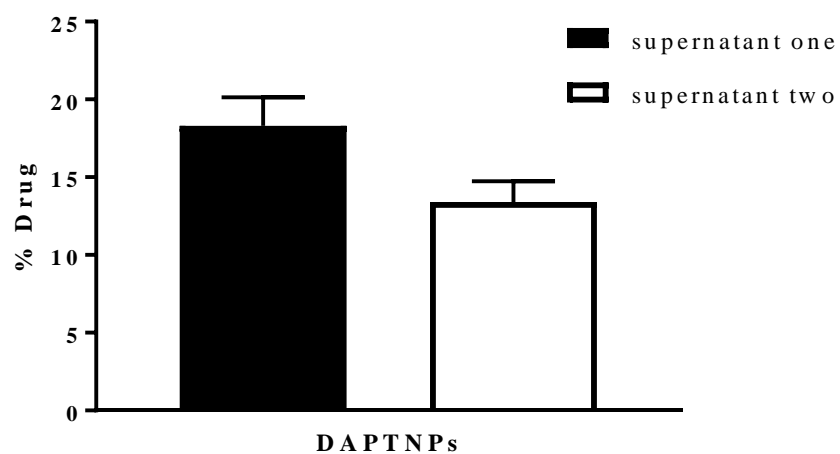
Figure 5.10.   HPLC analysis of the entrapment of DAPT in MNPs. The amount of
drug from the two supernatants was determined by HPLC using a standard curve before
the amount was divided by the known amount of drug-loaded prior to fabrication to give
the percentage of drug incorporated into the MNP's.
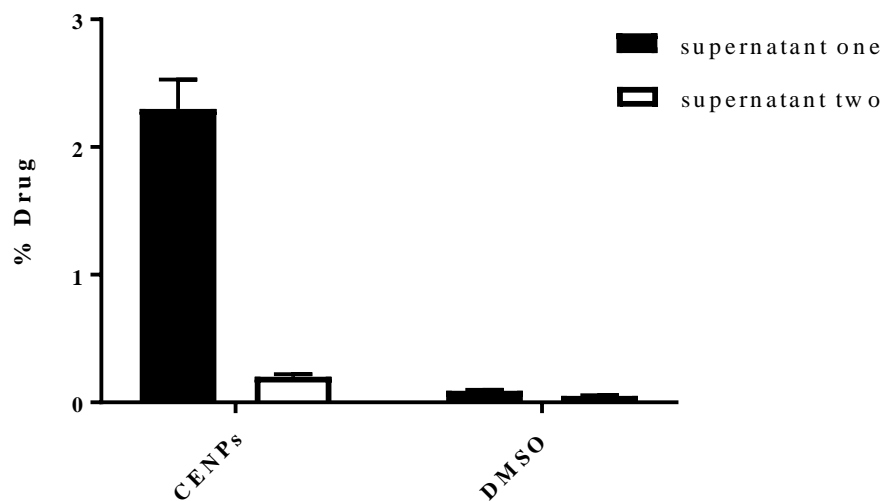
Figure 5.11. HPLC analysis of the entrapment of Compound E in MNPs. The amount of drug from the two supernatants was determined by HPLC using a standard curve before the amount was divided by the known amount of drug-loaded prior to fabrication to give the percentage of drug incorporated into the MNP's.
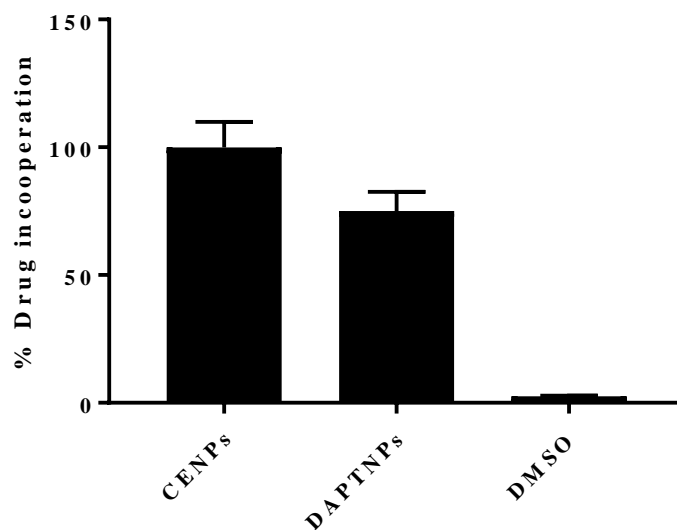
Figure 5.12. HPLC analysis of the entrapment of Compound E and DAPT in MNPs. The amount of drug from the two supernatants was determined by HPLC using a standard curve before the amount was divided by the known amount of drug-loaded prior to fabrication to give the percentage of drug incorporated into the MNP's.

5.4.5 Drug release Kinetic studies:

To study the release of drug from the nanoparticles, the stored nanoparticle pellets were re-suspended in 1 mL of distilled H_2O and were left for up to 7 days at different temperature ranges (0 $^{\circ}$C, 22 $^{\circ}$C and 37 $^{\circ}$C) (Figure 5.13). The nanoparticles were centrifuged at 17,000 x g after 24 h, 48 h, 7 days and the supernatants were analysed by HPLC for the presence of the drug in the supernatant. The percentage of drug released at each time point was calculated as follows:

(Concentration of drug in supernatant/concentration of drug incorporated) X 100 = % of drug released from nanoparticle.

Total percentage drug released at each time was simply calculated as the percentage released at that time point plus previous time points. No release of DAPT detected after 24 h at different temperatures (Table 5.1 A). There was no drug detected at 0 $^{\circ}$C after 48 h; however, an increase in temperature did lead to drug release at this time point (Table 5.1 B). After 7 days, there were significant amounts of DAPT released, almost double that at 22 $^{\circ}$C and 37 $^{\circ}$C compared to the previous time point (Table 5.1 C).

Follow up studies assessed the release of DAPT and Compound E from the MNPs at 37 $^{\circ}$C after 48 hours and 7 days in the absence or presence of an external magnetic field. Both DAPT and Compound E release was significantly increased in the presence of a magnetic field, especially after 7 days for both drugs [Figure 5.14 and 5.15].

Table 5.1 DAPT release from MNPs: Percentage peak area for DAPT-PLGA-loaded MNPs at 4, 22 and 37^0C over 24 hours, 48 hours and 7 days.

(A)

24 Hours	% Peak Area	µM	% Drug Release
4^0C	0	0	0
22^0C	0	0	0
37^0C	0	0	0

(B)

48 Hours	% Peak Area	µM	% Drug Release
4^0C	0	0	0
22^0C	36	18.15	30
37^0C	50	25.53	43

(C)

7 Days	% Peak Area	µM	% Drug Release
4^0C	26	12.87	21
22^0C	74	38.18	64
37^0C	111	57.69	96

% **Drug release vs.Temp. for DAPT-PLGA-MNPS**
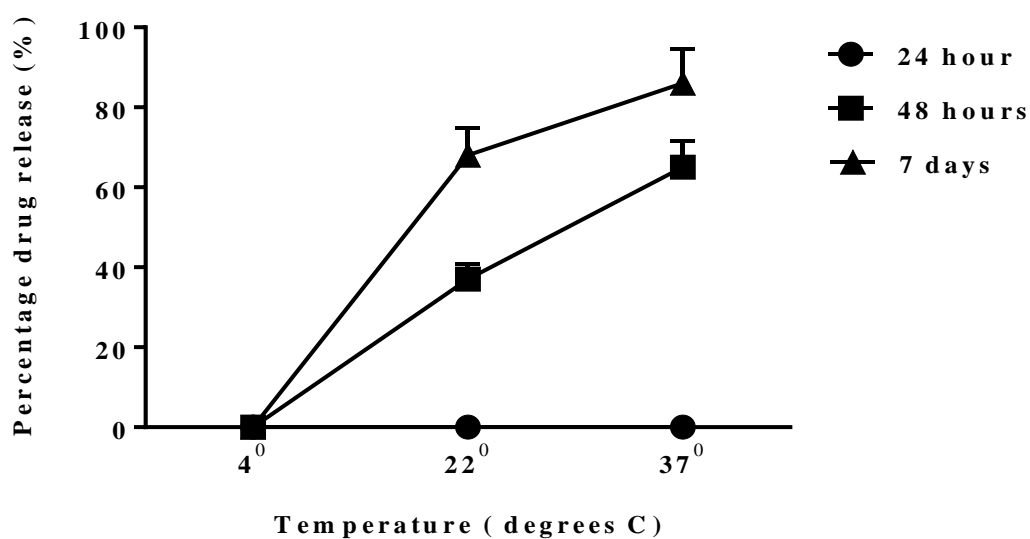
Figure 5.13. HPLC detection of DAPT-release from PLGA-MNPs. Percentage drug release of DAPT from DAPT-PLGA-loaded MNPs at 4ºC, 22ºC and 37ºC after 24 hours, 48 hours, and 7 days under magnetic field conditions. MNPs were re-suspended in ultra-pure water and the supernatants obtained were analysed using HPLC.
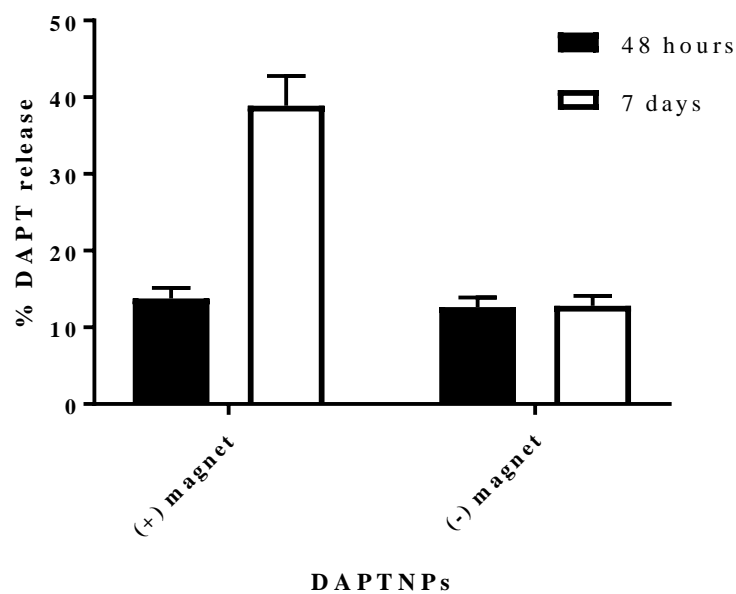
Figure 5.14. HPLC determination of DAPT release. Percentage drug release of DAPT from DAPT-PLGA-loaded MNPs at 37ºC after 48 hours and 7 days in the absence or presence of a magnetic field. MNPs were re-suspended in ultra-pure water and the supernatants obtained were analysed using HPLC. A wavelength of 234 nm was used.

160

Figure 5.15. HPLC determination of Compound E release. Percentage drug release of Compound E from CE-PLGA-loaded MNPs at 37ºC after 48 hours and 7 days in the absence or presence of a magnetic field. MNPs were re-suspended in ultra-pure water and the supernatants obtained were analysed using HPLC. A wavelength of 234 nm was used.

5.5   Discussion

In this chapter, polylactide-based GSI drug-loaded MNPs were successfully fabricated using a modified emulsification-solvent evaporation approach. The DLS and microscopic analysis indicated that these nanoparticles were round, relatively uniform in size and stable.

The TEM analysis of the Fe_3O_4 revealed the size of the nanoparticles were 5nm and the blank PLGA/PVA nanoparticles were between 5-17 nm and the DAPT and Compound E PLGA/PVA nanoparticles were 20 nm. Previous studies have reported that iron oxide nanoparticles range in size between 6-16 nm (X. Wang et al., 2009). DLS was used in this study to measure the size of the magnetite (Fe_3O_4) [Figure 5.4] which was 446.4 d.nm and this size has decreased to the half when the Fe_3O_4 loaded with PLGA/PVA [Figure 5.5] as it becomes 222.7 d.nm. This decrease in the size could be due to the diluted PLGA/PVA Fe_3O_4 while the magnetite itself (Fe_3O_4) was concentrated therefore the size was higher. Increasing the Fe_3O_4 concentration can impact the size of the nanoparticle (Tan et al., 2010). The size of the GSI drug-loaded nanoparticles increased slightly.

Despite DAPT and Compound E containing conjugated double bonds, the DAPT and Compound E in DMSO solution were colourless. Therefore, UV detection that can detect low wavelengths (less than 250nm) was required to detect DAPT and Compound E. DAPT and Compound E were detected using the UV-Vis spectrometer connected to the HPLC system as it was able to measure compounds with 190 nm wavelength. The optimization of the wavelength for DAPT and Compound E was performed before the drug entrapment and kinetic studies were optimised using HPLC.

The nanoprecipitation technique for preparation of nanoparticles can suffer the drawback of poor incorporation of water-soluble drugs. However, various formulation parameters to enhance the incorporation of a water-soluble drug (procaine hydrochloride) into poly(dl-lactide-co-glycolide) (PLGA) nanoparticles has been reported (Govender et al., 1999). Drug release from the MNPs appears to consist of two components with an initial rapid release followed by a slower exponential stage.

The initial incorporation efficiency of DAPT and Compound E into the PLGA-MNP was high due to the low percentage of DAPT and Compound E in the supernatant fractions

during purification of the MNPs. The temperature dependency study for DAPT drug release under magnetic conditions suggests that little DAPT was released overtime at 4 $^{\circ}$C. However, an increase in the temperature to a more physiological state resulted in significant drug release over time such that, after 7 days, there were significant amounts of DAPT released at 22 $^{\circ}$C and 37 $^{\circ}$C.

Previous studies assessing paclitaxel release from PLGA-MNPS at different time points (4 hours and 11 days) suggests that little drug is released within the first 4 hrs drug but this significantly increases to 75 % by 11 days (Danhier et al., 2009). On the other hand, tamoxifen release was significant after 24 hours (Chawla and Amiji 2002). The quicker release of tamoxifen in comparison to the DAPT and Compound E could be due to the molecular weight as tamoxifen has a lower molecular weight. Indeed, previous studies have suggested that the burst of drug release could be linked with the drying situations, the low molecular weight of the drug, and the minor size of the particles (X. Huang and Brazel 2001). Moreover, the burst of drug-release from PLGA MNPs is reduced as the molecular weight of the polymer was increased. Also, the fast release of tamoxifen may be due to the fact that the tamoxifen was released from the surface of the nanoparticle (Chawla and Amiji 2002). Previous studies have also highlighted the dual role played by the biodegradable hydrophobic polyester, polylactide, in facilitating efficient drug entrapment and release. In addition to providing a sustained release depot for the encapsulated drug, the polymer maintains the composite particle structure with the multiple magnetite grains embedded in the solid polymeric matrix, thus enabling the high magnetic susceptibility of the formulation achieved without the loss of the superparamagnetic properties characteristic of ultra-small-sized crystallites (B. Lee et al., 1999, M. Lee et al., 1996).

Using an external magnetic field, the attraction of the therapeutic agent's delivery towards a specific site can be facilitated (Sun et al., 2008). The effect of a magnetic field on Fe_3O_4 MNPs has been determined and clearly demonstrates that Fe_3O_4 MNPs can be detached from the suspension in the presence of the external magnetic field (Mahdavi et al., 2013). In this study, the effect of the magnetic field was to significantly increase the release of both DAPT and Compound E when compared to non-magnetic conditions. In this regard, the functionalised MNPs loaded with GSIs are capable of releasing a sufficient amount of drug (150 µM DAPT and 60 µM Compound E) to impact on stem

cell fate once targeted to a vascular stent using a uniform magnetic field or alternatively deploying a magnetic stent following balloon angioplasty (Räthel et al., 2012).

Chapter 6

The effects of MNPs loaded with gamma-secretase inhibitors on myogenic differentiation of vascular stem cells

6.1   Introduction

Several pioneering studies using MNPs have been reported (S. C. McBain et al., 2008). These include significant use of magnetic nanoparticles in pharmacy, particularly to improve drug kinetics and delivery to target sites (Tran et al., 2012). In particular, MNPs prepared using oil-water emulsification increased Fe_3O_4 particle size due to the long-time of the reaction and the higher-water content (Laurent et al., 2008). In water-oil microemulsions, an aqueous phase is formed such due to the scattering of the aqueous phase. A monolayer of surfactant molecules may then enclose the nanodroplets as the hydrocarbon phase continues. The surfactant molecule decreases the interfacial strain between water and oil which leads to the creation of a transparent solution. The water pool has a spherical form and the nanodroplet walls are enclosed by surfactant molecules. The nanodroplet wall acts as a cage for the rising particles leading to a reduction in the regular size of the particles (Tran et al., 2012).

For guided therapies, multifunctional nanoparticles have been successfully developed for drug delivery. Nanoparticles have the ability to migrate eclectically towards the damaged tissue (Fang et al., 2011) and nanoparticle therapy is capable of increasing the drug dose at the site of tissue damage (Matsumura and Maeda 1986). Polymeric NPs are widely considered beneficial nanotechnology platforms for anticancer agents controlling and targeting delivery of therapeutic molecules including molecular drugs and macromolecules such as genes and proteins. Moreover, in order to control the release of anticancer drugs encapsulated within magnetic-core silica nanoparticles, the external magnetic field can be utilized for this purpose (Thomas et al., 2010). Therefore, NPs are suitable for long-term therapeutic delivery (B. Lu et al., 2016). Once the nanoparticles are functionalised with therapeutics drugs or dyes, absorption of these nanoparticle occurs the inside targeted cell.

Improvements in diagnostic measures for biomedical applications have also been investigated in various studies using nanoparticles for better interpretations of biological abnormalities and several medical conditions (Felton et al., 2014). The use of imaging techniques, such as magnetic resonance imaging (MRI), is widespread and becoming a standard procedure for such specialized applications. A major avenue being studied in MRI is the use of magnetic nanoparticles (NPs) as contrast agents (CAs). Among various approaches, current research also incorporates the use of superparamagnetic iron oxide NPs and manganese-based NPs with biocompatible coatings for improved stability and

reduced biodegradation when exposed to a biological environment (Felton et al., 2014). Due to the nanoscale topographical features on cell culture substrates, cells can also be directed through all their biological functions (cell counting, cell behaviour, polarity, proliferation and differentiation). For instance, the nontopographical differences in cell adhesion substance can regulate human mesenchymal stem cell differentiation towards adipocytes or osteocytes (Ahn et al., 2014).

A magnetic targeting strategy has been widely used to target MNPs to damaged tissue. This is achieved by exposure to an external magnetic field in order to regulate the MNPs localization (S. McBain et al., 2008). This includes directing high tendency magnetic fields prompting the highly magnetically MNPs to accumulate at the target site. Lately, this approach was effectively applied in a medical trial to deliver the chemotherapeutic, doxorubicin, to hepatocarcinoma cells (Wilson et al., 2004). Despite the success of this approach, there are some drawbacks. This is because it is restricted to the targeted tissue being close to the body's surface as the magnetic field strength is lost the further the distance from the magnetic source (Debbage and Jaschke 2008)(Veiseh et al., 2010).

Therefore, while magnetic targeting has shown promise to improve the efficacy and safety of different classes of therapeutic agents by enabling their active guidance to the site of disease and minimizing dissemination to nontarget tissues, its translation into the clinic has proven more difficult. The inherent limitations of deep tissue targeting in human subjects underscore a need for developing well-characterized and fully biocompatible magnetic carrier formulations. A novel magnetic targeting scheme based on the magnetizing effect of deep-penetrating uniform fields has been reported as an example of a strategy providing a potentially clinically viable solution for preventing injury-induced re-stenosis of stented blood vessels (in-stent restenosis) (Chorny et al., 2010a).

The design of optimised magnetic carrier formulations and experimental results showing the feasibility of uniform field-controlled targeting for site-specific vascular delivery of small-molecule pharmaceuticals in the context of anti-restenotic therapy has evolved (Dorans 2010). The versatility of this approach prompts exploring the utility of uniform field-mediated magnetic stent targeting for combination therapies with enhanced efficiencies and improved safety profiles.

6.2   Objectives of this chapter

- To optimize the (DAPT/Compound E)-loaded PLGA -PVA MNPs effective functional dose or volume or dilution
- To assess the effect of (DAPT/Compound E)-loaded PLGA -PVA MNPs on stem cell growth and myogenic cell differentiation
- To assess the effect of the magnetic field on the attachment of the fluorescently labelled IgGAlexa-488-Fe_3O_4-PLGA-MNPs within the stent

6.3   Strategy

The main objective of this chapter was to optimise the drug-loaded MNPs effective dose. To achieve this, MNPs were fabricated with GSI's and serially diluted before mMVSC were treated with varying concentrations of blank or GSI-loaded MNPs under magnetic and non-magnetic conditions in the absence of presence of Jagged-1-Fc (Jag-1-Fc), a Notch ligand that promotes cell growth and myogenic differentiation. The RNA was then isolated before Notch target gene expression (Hey1) was determined by qRT-PCR to confirm that GSI-loaded MNPs were functionally active at a given dose.

The second objective was to assess the effect of MNPs effect on cell growth (using DAPI nuclear staining) and myogenic cell differentiation by measuring SMC differentiation markers, Myh-11 and Cnn1 (using q-RT-PCR) and immunocytochemistry using specific antibodies against these markers.

Finally, to determine the impact of the external magnetic field on MNP localisation to vascular stents fluorescently labelled MNPs (IgGAlexa488-Fe_3O_4-PLGA-MNPs and control IgGAlexa488) were assessed for their attachment to the stents under magnetic and non-magnetic conditions.

Data analysis for the data was carried out using the GraphPad Prism™ software and one-way ANOVA tests for parametric data and Kruskal Wallis t-tests for non-parametric data.

6.4 Results

6.4.1 (DAPT/Compound E)-loaded PLGA -PVA MNPs optimisation

The aim of these experiments was to determine the best dilution of the GSI drug-loaded MNPs at inhibiting Notch target gene expression and myogenic differentiation *in vitro*. To assess this, the levels of Notch target gene expression (*Hey1*) and SMC differentiation marker expression (*Myh-11* and *Cnn1*) were determined by qRT-PCR in MVSCs following treatment of cells with Jagged-1-Fc (Jag-1-Fc) and Fc specific fragment antibody (Fc-Control) in the absence or presence of serial dilutions of DAPT- and Compound E loaded-MNPs under magnetic and non-magnetic conditions.

Jag-1-Fc and control IgG-Fc were immobilised on the surface of culture plates (as described in Materials and Methods, Chapter 2 section 2.3.3 and 2.4.1). Jag-1-Fc was then used to induce Notch target gene (*Hey1*) expression for three days and myogenic differentiation after seven days (*Myh-11, Cnn1*) in maintenance media under magnetic and non-magnetic conditions. MVSCs were stimulated by plating the cells on Jag-1-Fc and IgG-Fc coated plates in the absence or presence of serial dilutions of DAPT-MNPs and Compound E-MNPs in maintenance media before Notch target gene expression (*Hey1*) and SMC differentiation gene expression (*Myh-11* and *Cnn1*) were assessed by qRT-PCR.

The serial dilutions were as follows : for DAPT MNPs; 102 µM (i.e., 1 mL of media and 1 mL of DAPT MNPs), 76 µM (i.e., 1.25 mL of media and 0.75 mL of DAPT MNPs) ,51 µM (i.e., 1.5 mL of media and 0.5 mL of DAPT MNPs) and 25 µM (i.e., 1.75 mL of media and 0.25 mL of DAPT MNPs).

For Compound E MNPs; 56µM (i.e., 1 mL of media and 1 mL of DAPT MNPs), 42 µM (i.e., 1.25 mL of media and 0.75 mL of DAPT MNPs), 28 µM (i.e., 1.5 mL of media and 0.5 mL of DAPT MNPs) and 14 µM (i.e., 1.75 mL of media and 0.25 mL of DAPT MNPs).

Jag-1-Fc stimulation increased the mRNA expression levels of *Hey1* compared to IgG-Fc control after three days. The levels of Jag-1-Fc stimulated *Hey1* mRNA were reduced

under magnetic conditions in the absence of DAPT-MNPs (Figure 6.1). Nevertheless, *Hey1* mRNA levels were significantly attenuated in the presence of increasing concentrations of DAPT-MNPs under both magnetic and non-magnetic conditions (Figure 6.1). In parallel cultures, Jag-1-Fc stimulation promoted myogenic differentiation and increased *Myh-11* mRNA expression levels compared to IgG-Fc control after seven days. The levels of Jag-1-Fc stimulated *Myh-11* mRNA were also reduced under magnetic conditions in the absence of DAPT-MNPs (Figure 6.2). Nevertheless, *Myh-11* mRNA levels were significantly attenuated in the presence of increasing concentrations of DAPT-MNPs under both magnetic and non-magnetic conditions (Figure 6.2).

In a similar manner, the levels of Jag-1-Fc stimulated *Hey1* mRNA were reduced under magnetic conditions in the absence of Compound E-MNPs (Figure 6.3). Nevertheless, *Hey1* mRNA levels were significantly attenuated in the presence of increasing concentrations of compound E-MNPs under both magnetic and non-magnetic conditions (Figure 6.3). In parallel cultures, Jag-1-Fc stimulation promoted myogenic differentiation and increased both *Myh-11* and *Cnn1* mRNA expression levels compared to IgG-Fc control after seven days. The levels of Jag-1-Fc stimulated *Cnn1* mRNA were also reduced under non-magnetic conditions in the presence of Compound E-MNPs (Figure 6.4) as were the levels of Jag-1-Fc stimulated *Myh-11* mRNA under magnetic conditions in the presence of Compound E-MNPs (Figure 6.4 and 6.5).

For all future experiments, the 1:2 dilution of MNPs (i.e., 1 mL of media and 1 mL of DAPT MNPs) corresponding theoretically to (150 µM DAPT and 60 µM Compound E) was deemed the optimum choice to treat the mMVSCs.
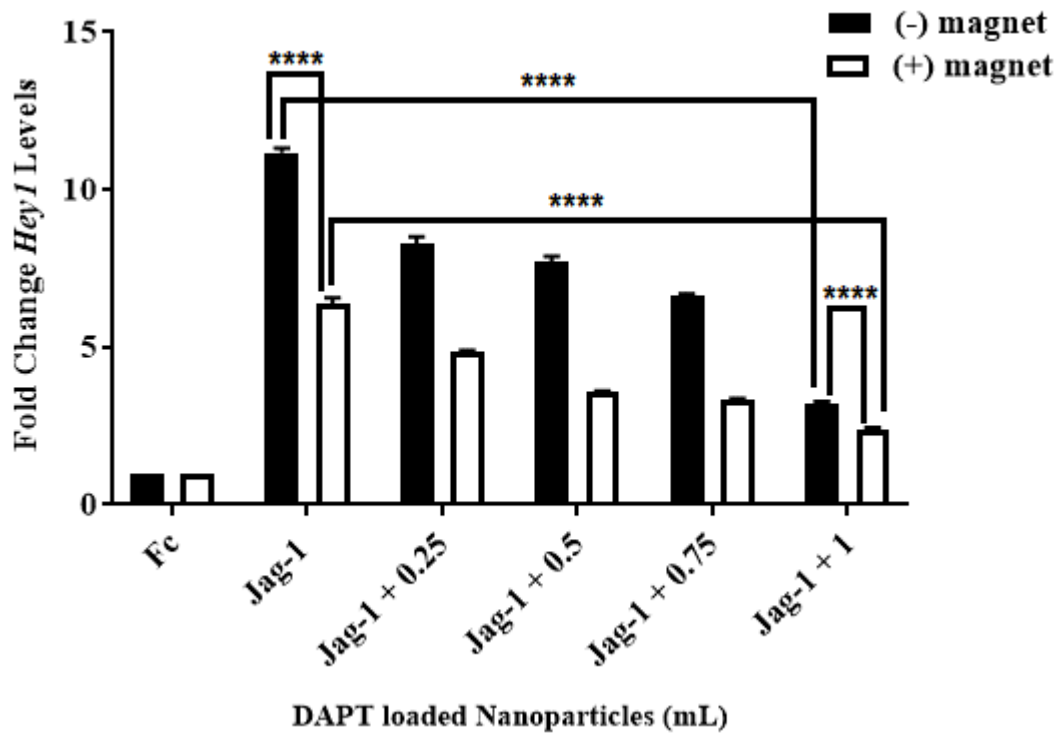
Figure 6.1. The effect of serial dilutions of DAPT-MNPs on Jag-1-Fc stimulation of Notch target expression under magnetic and non-magnetic conditions. The mMVSCs were seeded at 10^3 cells/well density and treated with IgG-Fc (500 ng/mL) control, Jag-1-Fc (500 ng/mL) and Jag-1-Fc (500 ng/mL) plus serial dilutions of DAPT-MNPs for three days in the absence or presence of an external magnetic field. qRT-PCR was used to analyse the fold change in *Hey1* gene expression compared to the control. Data analysis was performed by two-way ANOVA using the GraphPad Prism™ software and ****$p<0.0001$ all were considered significant.
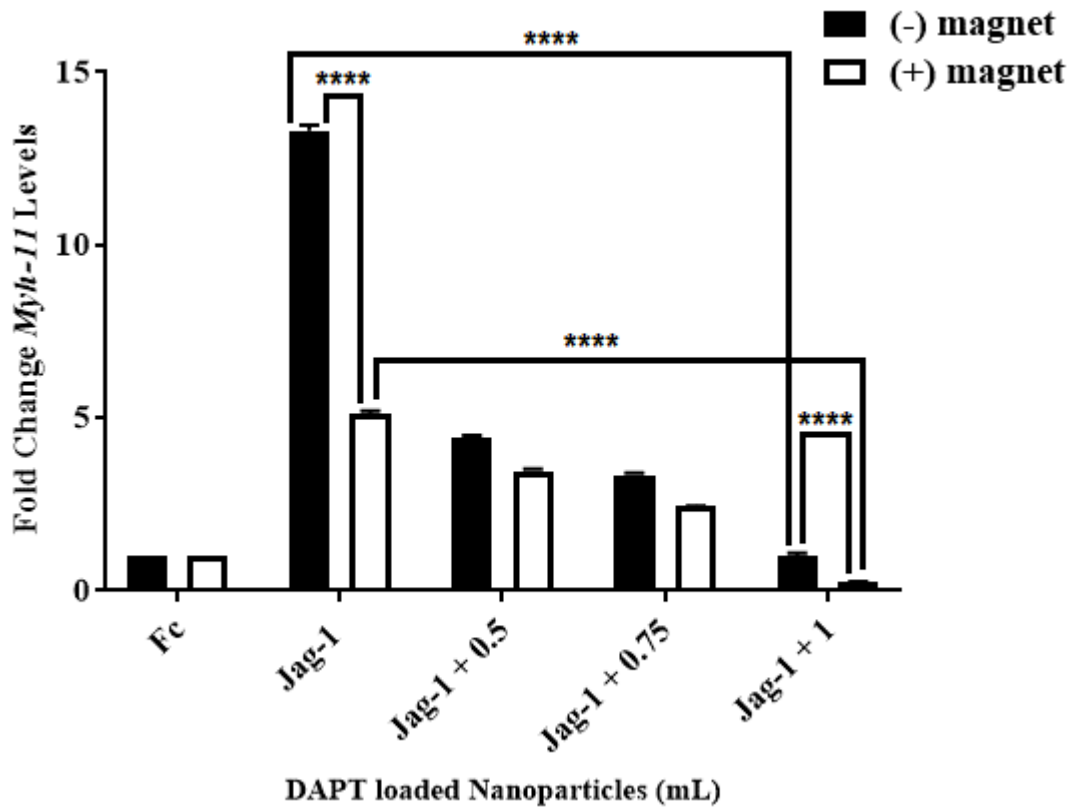
Figure 6.2. The effect of serial dilutions of DAPT-MNPs on Jag-1-Fc stimulation of myogenic differentiation under magnetic and non-magnetic conditions. *Myh-11* mRNA relative quantification was assessed by qRT-PCR**.** The mMVSCs were seeded at 10^3 cells/well density and treated with IgG-Fc (500 ng/mL) control, Jag-1-Fc (500 ng/mL) and Jag-1-Fc (500 ng/mL) plus serial dilutions of DAPT-MNPs for seven days in the absence or presence of an external magnetic field. qRT-PCR was used to analyse the fold change in the *Myh-11* gene expression compared to the control. Data analysis was performed by two-way ANOVA using the GraphPad Prism™ software and ****$p<0.0001$ all were considered significant.
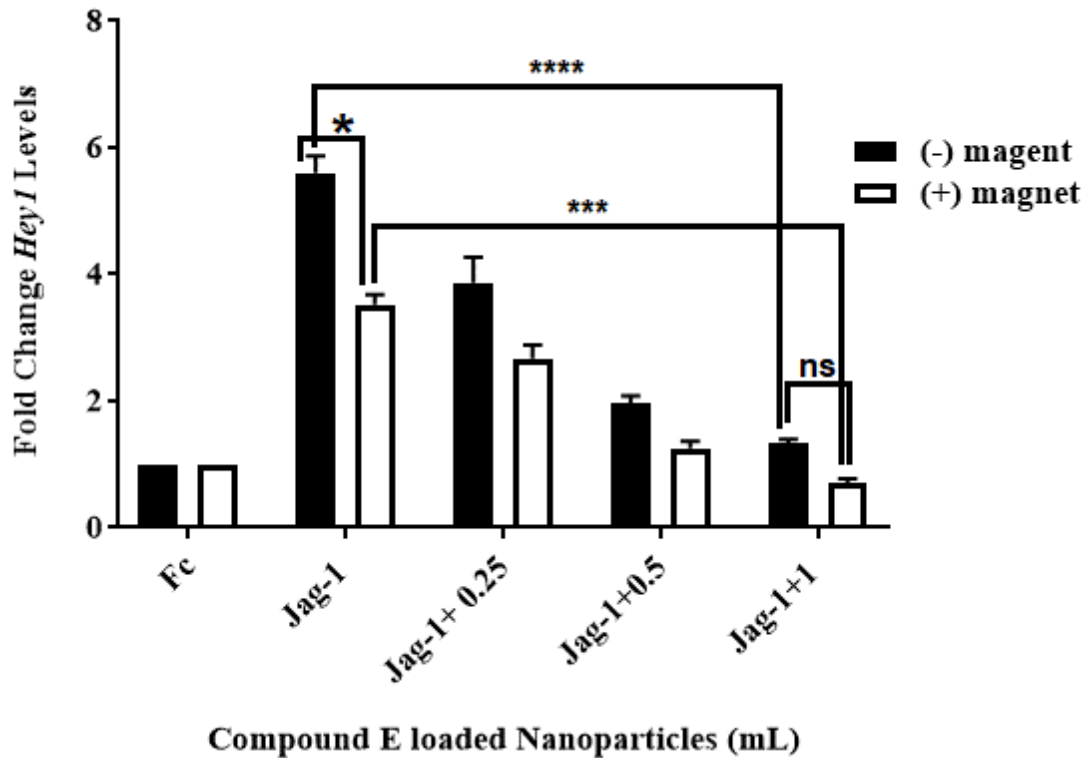
Figure 6.3. The effect of serial dilutions of Compound E-MNPs on Jag-1-Fc stimulation of Notch target expression under magnetic and non-magnetic conditions. *Hey1* mRNA relative quantification was assessed by qRT-PCR. The mMVSCs were seeded at 10^3 cells/well density and treated with IgG-Fc (500 ng/mL) control, Jag-1-Fc (500 ng/mL) and Jag-1-Fc (500 ng/mL) plus serial dilutions of Compound E-MNPs for three days in the absence or presence of an external magnetic field. qRT-PCR was used to analyse the fold change in the gene expression *Myh-11*, compared to the control. Data analysis was performed by two-way ANOVA using the GraphPad Prism™ software and * $p < 0.05$, ***$p<0.001$ and ****$p<0.0001$ all were considered significant.
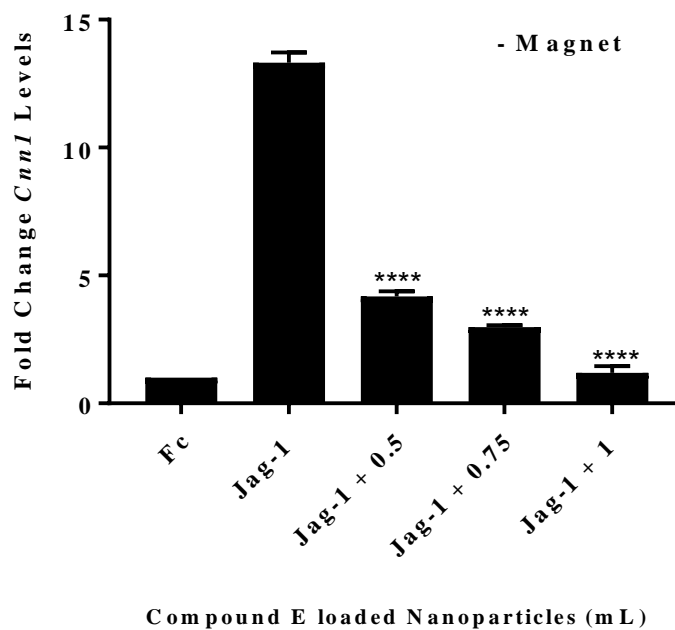
Figure 6.4. The effect of serial dilutions of Compound E-MNPs on Jag-1-Fc stimulation of myogenic differentiation under non-magnetic conditions. *Cnn1* mRNA relative quantification was determined by qRT-PCR**.** The mMVSCs were seeded at 10^3 cells/well density and treated with IgG-Fc (500 ng/mL) control, Jag-1-Fc (500 ng/mL) and Jag-1-Fc (500 ng/mL) plus serial dilutions of Compound E-MNPs for seven days in the absence of an external magnetic field. qRT-PCR was used to analyse the fold change in *Cnn1* gene expression, compared to the control. Data analysis was performed by ANOVA using the GraphPad Prism™ software and $p<0.05$, ****$p<0.0001$ all considered significant vs. Jag-1.

Compound E loaded Nanoparticles (mL)
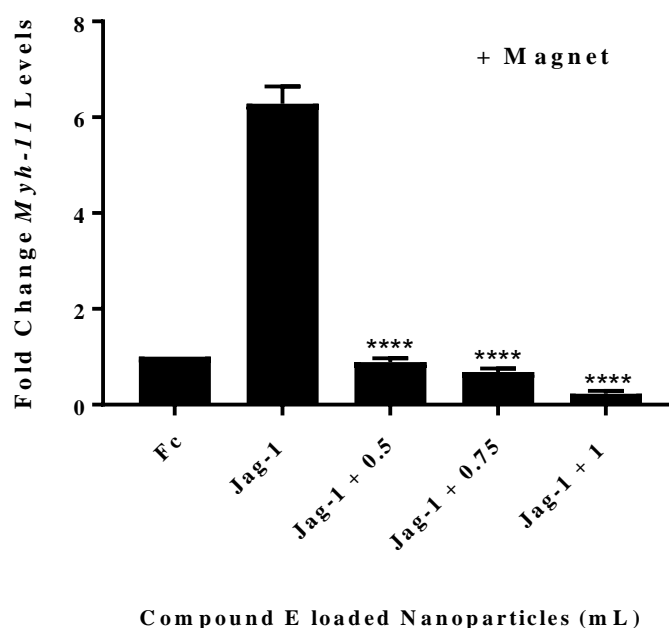
Figure 6.5. The effect of serial dilutions of Compound E-MNPs on Jag-1-Fc stimulation of myogenic differentiation under magnetic conditions. *Myh-11* mRNA relative quantification was determined by qRT-PCR. The mMVSCs were seeded at 10^3 cells/well density and treated with IgG-Fc (500 ng/mL) control, Jag-1-Fc (500 ng/mL) and Jag-1-Fc(500 ng/mL) plus serial dilutions of Compound E-MNPs for seven days in the presence of an external magnetic field. qRT-PCR was used to analyse the fold change in *Myh-11* gene expression, compared to the control. Data analysis was performed by ANOVA using the GraphPad Prism™ software and p<0.05, ****p<0.0001 all considered significant vs. Jag-1.

6.4.2   The effects of DAPT – and Compound E- MNPs on MVSCs cell growth.

   Mouse MVSCs were cultured in maintenance medium (MM) and the plates were coated with Control IgG Fc and Jag-1-Fc in the absence or presence of drug-loaded MNPs (Compound E and DAPT) at a dilution of 1:2 for seven days. Following treatment, the cells were fixed and stained with the nuclear stain, DAPI for cell counting. Five images were taken per slide by fluorescent microscope and all the nuclei were counted, averaged and plotted.

Jag-1-Fc treatment resulted in a significant increase in the number of DAPI stained nuclei (and hence cell number) after seven days when compared to IgG-Fc control (Figure 6.7). Treatment of cells with blank MNPs did not significantly affect Jag-1-Fc stimulation of cell growth whereas, treatment of cells with a similar dilution of DAPT- and Compound E-MNPs cause a significant reduction in the number of DAPI nuclei (Figure 6.7).

(a)
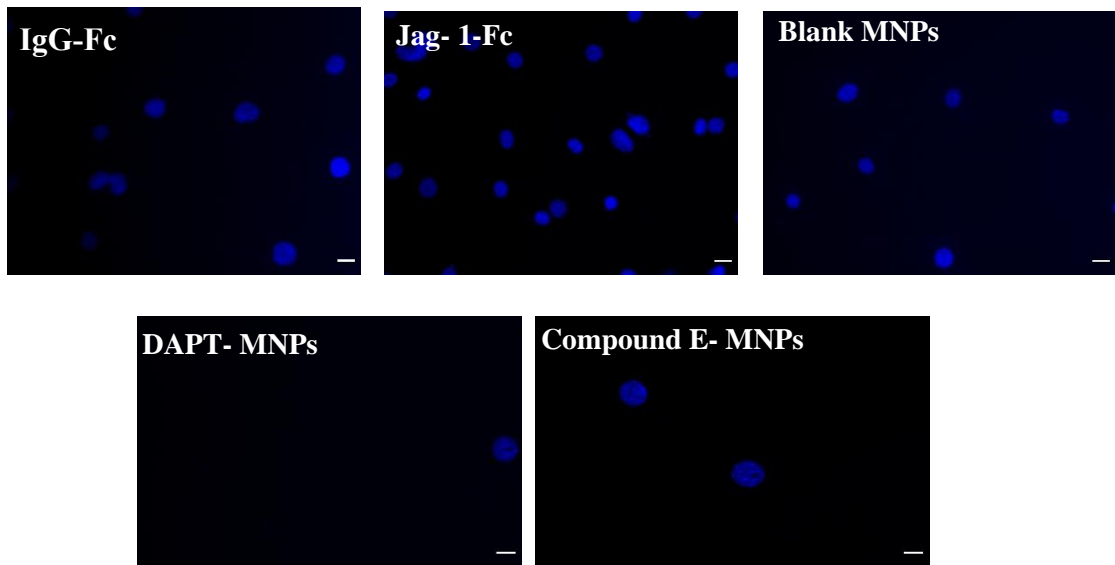
(b)
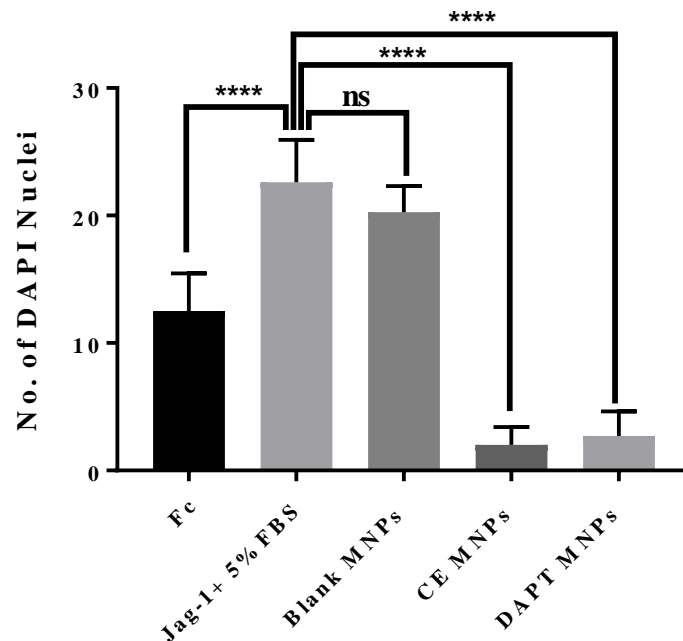
Figure 6.6. The inhibitory effect of DAPT/ Compound E MNPs on mouse multipotent vascular stem cell growth. The mMVSCs were seeded at 2200 cells/well and treated with IgG-Fc (500 ng/mL), Jag-1-Fc (500 ng/mL) and Jag-1-Fc (500 ng/mL) in the presence of blank PLGA-MNPs and DAPT MNPs (1:2 dilution) in maintenance medium for seven days under magnetic conditions (a) DAPI staining was used to analyse the number of cells (b) Cells were counted and averaged. Data analysis was performed by ANOVA using the GraphPad Prism™ software and ****$p < 0.0001$ was considered significant.

### 6.4.3 The effect of DAPT- and Compound E-loaded MNP's on myogenic differentiation

To determine whether DAPT- and Compound E- loaded into Fe_3O_4 PLGA/PVA-MNPs preserved their anti-myogenic effect when compared to blank Fe_3O_4 PLGA/PVA-MNPs, mSMCs (10^3cells/well) and mMVSCs (10^4cells/well) were treated with IgG-Fc and Jag-1-Fc in the absence or presence of (i) blank Fe_3O_4 PLGA/PVA-MNPs, (ii) DAPT-loaded Fe_3O_4 PLGA/PVA-MNPs and (iii) Compound E loaded Fe_3O_4 PLGA/PVA-MNPs before the Notch target gene, *Hey1* and the SMC differentiation genes, *Myh-11* and *Cnn1* mRNA levels and the number of Myh-11$^+$ and Cnn1$^+$ cells were evaluated by qRT-PCR and ICC, respectively.

The mRNA expression level of Notch target gene, *Hey1* and the smooth muscle marker gene, *Cnn1* were assayed in triplicate using mSMCs and normalised to *HPRT* mRNA level. Relative quantification levels were calculated versus the cells which were cultured in plates coated with IgG-Fc and treated with blank Fe_3O_4 PLGA/PVA-MNPs. Jag-1-Fc stimulation increased the mRNA expression levels of *Hey1* compared to when cells were cultured in the presence of IgG-FC control with blank MNPs. This effect was reduced in the presence of DAPT-PLGA-MNPs (Figure 6.8). In a similar manner, Jag-1-Fc stimulation increased *Hey1* mRNA expression levels in MVSCs compared to when cells were cultured in the presence of IgG-FC control with blank MNPs (Figure 6.9).

In order to further investigate whether DAPT loaded Fe_3O_4 PLGA/PVA-MNPs preserved their anti-myogenic differentiation effect, mMVSCs were treated with blank Fe_3O_4 PLGA/PVA-MNPs and DAPT loaded PLGA-MNPs in the presence of IgG-Fc Control and Jag-1-Fc before Cnn1 mRNA levels were assessed by qRT-PCR. Jag-1-Fc stimulation increased *Cnn1* mRNA expression levels in MVSCs compared to when cells were cultured in the presence of IgG-FC control with blank MNPs (Figure 6.10).

Parallel experiments assessed whether DAPT loaded Fe_3O_4 PLGA/PVA-MNPs attenuated Jag-1-Fc stimulated myogenic differentiation by measuring and the number of Myh-11 and Cnn1 positive cells following treatment with DAPT loaded-MNPs containing 150 µM DAPT. Cells were immunostained for Cnn1 and Myh-11 after seven days. Positive cells stained for Myh-11 filaments (green) and for Cnn1 filaments (red),

while the nuclei stained with blue (DAPI positive cells). There was a significant increase in the number of Cnn1$^+$ and Myh-11$^+$ cells following Jag-1-Fc treatment when compared to IgG-Fc control cells. This effect was diminished with DAPT-MNPs (80μM) (Figure 6.11 and 6.12).
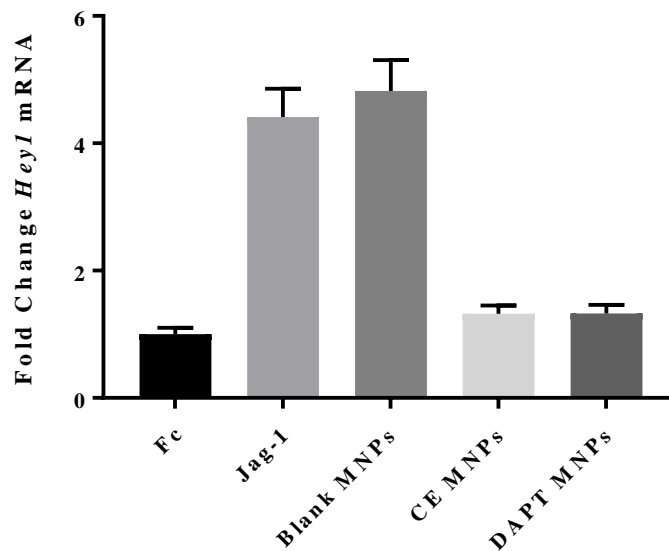
Figure 6.7. The effect of blank, DAPT- and Compound E loaded Fe$_3$O$_4$ PLGA/PVA-MNPs on Notch target gene expression in mSMCs. *Hey 1* mRNA relative levels were quantified by qRT-PCR. The mSMCs were seeded at 10^3 cells/well density and treated with IgG-Fc (500 ng/mL), Jag-1-Fc (500 ng/mL), Jag-1-Fc (500 ng/mL) plus Compound E-MNPs and Jag-1-Fc plus DAPT-MNPs for three days in the absence of an external magnetic field. Representative qRT-PCR analysis performed in triplicate was used to determine the fold change in Hey1 mRNA levels when compared to IgG-Fc control.
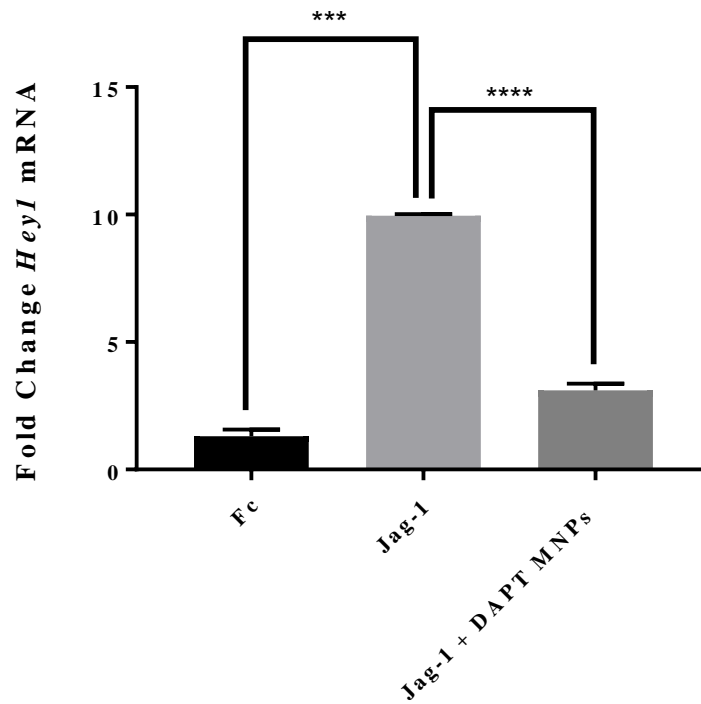
Figure 6.8. The effect of DAPT- loaded Fe₃O₄ PLGA/PVA-MNPs on Notch target gene expression. The mMVSCs were seeded at 10^5 cells/well density and treated with IgG-Fc (500 ng/mL), Jag-1-Fc (500 ng/mL) and Jag-1-Fc (500 ng/mL) plus DAPT-MNPs (150 µM) in maintenance medium for two days. qRT-PCR was used to analyse the fold change in *Hey 1* mRNA levels, compared to the IgG Fc control. Data analysis was performed by one-way ANOVA using the GraphPad Prism™ software and ***p<0.001 and ****p<0.0001were considered significant.
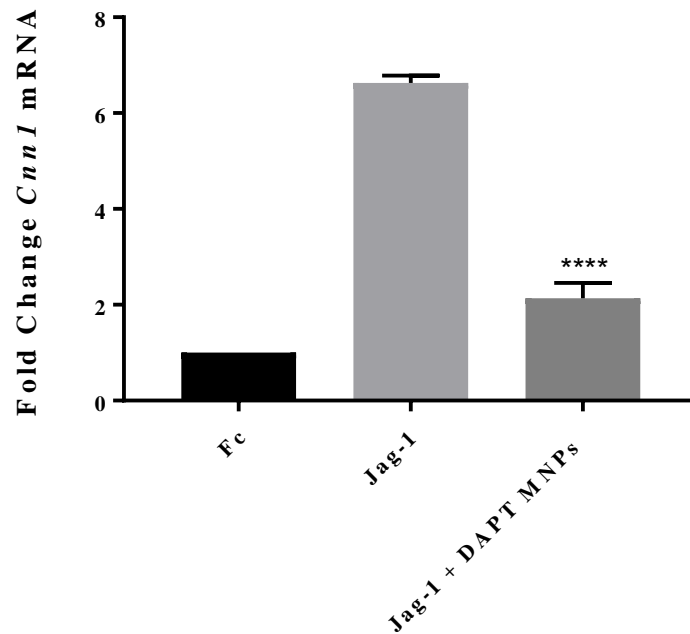
Figure 6.9.   The effect of DAPT- loaded Fe₃O₄ PLGA/PVA-MNPs on *Cnn1*
expression. The mMVSCs were seeded at 10^5 cells/well density and treated with IgG-Fc
(500 ng/mL), Jag-1-Fc (500 ng/mL) and Jag-1-Fc (500 ng/mL) plus DAPT-MNPs (150
µM) in maintenance medium for three days. qRT-PCR was used to analyse the fold
change in *Cnn1* mRNA levels, compared to the IgG Fc control. Data analysis was
performed by ANOVA using the GraphPad Prism™ software and ****$p<0.0001$ was
considered significant vs Jag-1.

(a)
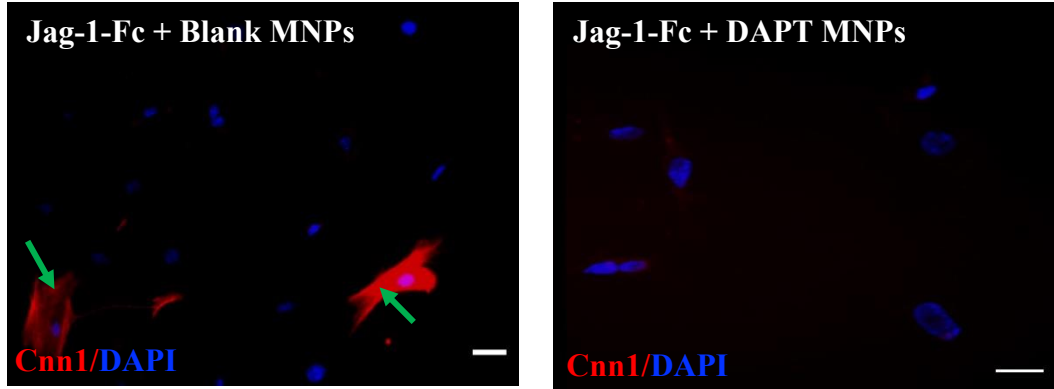
(b)
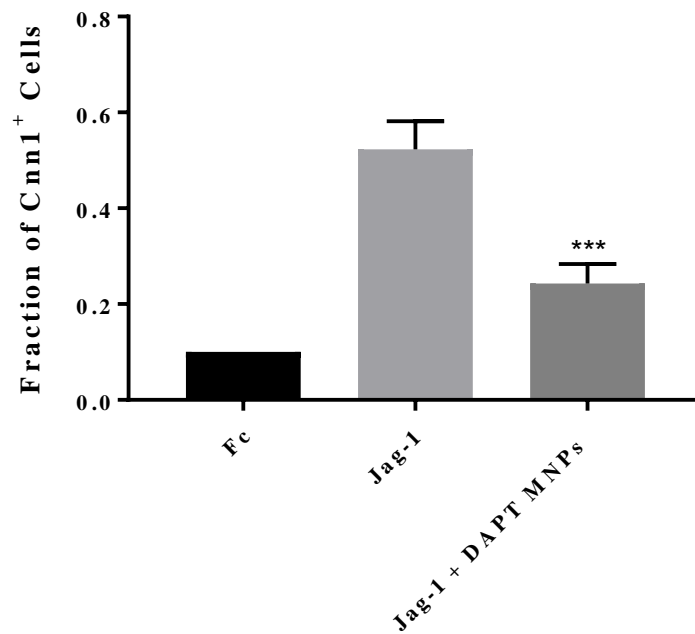
Figure 6.10. The effect of DAPT loaded MNPs on the number of Cnn1 positive MVSC cells. The mMVSCs were seeded at 2,500 cells/well density and treated with IgG-Fc (500 ng/mL), Jag-1-Fc (500 ng/mL) and Jag-1-Fc (500 ng/mL) in the presence of blank PLGA-MNPs and DAPT MNPs (150μM) in maintenance medium for seven days. (A) Immunocytochemistry was used to analyse the percentage of the positive cells. (B) Cnn1+ cells were counted and averaged. Data analysis was performed by ANOVA using the GraphPad Prism™ software and ***p<0.001 was considered significant vs Jag-1.

(a)
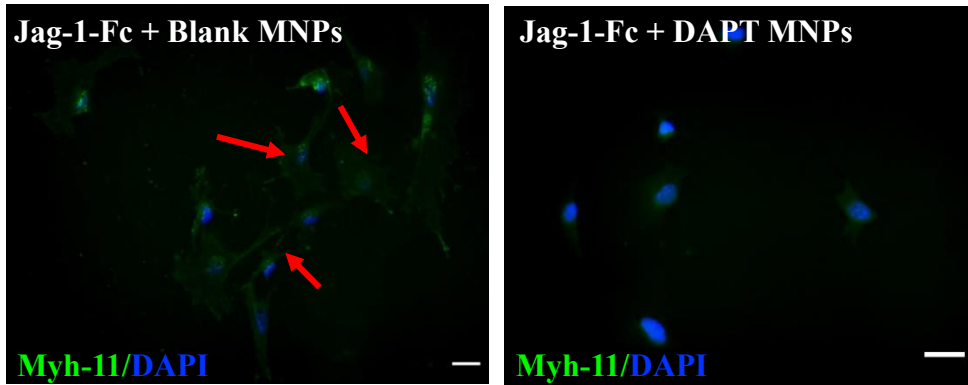
(b)
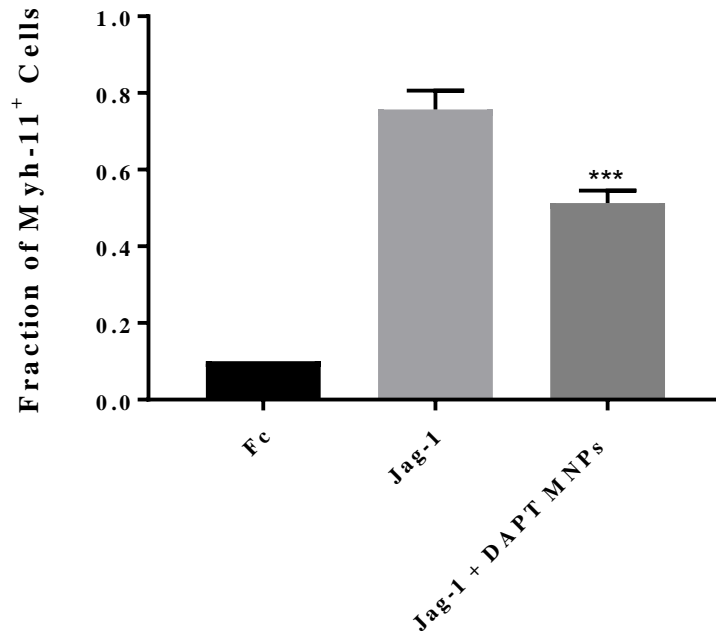
Figure 6.11. The effect of DAPT loaded MNPs on the number of Myh-11 positive mMVSC cells. The mMVSCs were seeded at 2,500 cells/well density and treated with IgG-Fc (500 ng/mL), Jag-1-Fc (500 ng/mL) and Jag-1-Fc (500 ng/mL) in the presence of blank PLGA-MNPs and DAPT MNPs (150 μM) in maintenance medium for seven days. (a) Immunocytochemistry was used to analyse the percentage of the positive cells. (b) Myh-11 positive cells were counted and averaged. Data analysis was performed by ANOVA using the GraphPad Prism™ software and ***$p < 0.001$ was considered significant vs Jag-1.

6.4.4 The effect of an external magnetic field on the functionality of DAPT and Compound E loaded MNPs

To determine whether the external magnetic field has an impact on the functionality of the DAPT and Compound E loaded MNPs, mouse MVSCs were cultured in maintenance medium (MM) before cells were treated with IgG-Fc and Jag-1-Fc in the absence or presence of drug-loaded MNPs (Compound E and DAPT) for three and seven days under magnetic and non-magnetic conditions. Following treatment, the expression level of the Notch target gene, *Hey1* and smooth muscle marker gene, *Myh-11* were assayed in triplicate and normalised to *HPRT* mRNA level.

In the absence of an external magnetic field, Jag-1-Fc increased the mRNA expression levels of *Hey1* when compared to IgG-Fc control. The extent of Jag-1-Fc stimulation of Notch target gene expression was similar when cells were treated with blank MNPs. However, exposure to the external magnetic field resulted in a reduction in Jag-1-Fc stimulation of *Hey 1* mRNA levels when compared the non-magnetic conditions for both Jag-1-Fc alone and following treatment with blank MNPs (Figure 6.13). Under both magnetic and non-magnetic conditions, the drug-loaded MNPs (Compound E and DAPT) significantly decreased the *Hey1* mRNA levels without a significant difference between magnetic and non-magnetic conditions (Figure 6.13).

Similarly, in the absence of an external magnetic field, Jag-1-Fc increased *Myh-11* mRNA levels when compared to IgG-Fc control. Jag-1-Fc stimulated *Myh-11* expression was similar when cells were treated with blank MNPs. However, the exposure to the external magnetic field also resulted in a reduction in Jag-1-Fc stimulation of *Myh-11* mRNA levels when compared the non-magnetic conditions for both Jag-1-Fc alone and following treatment with blank MNPs (Figure 6.13). Under both magnetic and non-magnetic conditions, the drug-loaded MNPs (Compound E and DAPT) significantly decreased the *Myh-11* mRNA levels without a significant difference between magnetic and non-magnetic conditions (Figure 6.14).
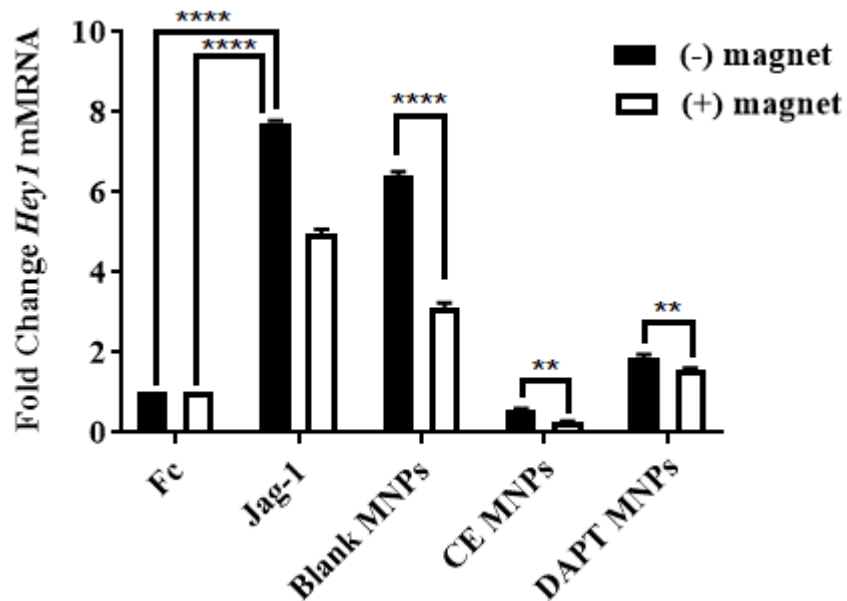
Figure 6.12. The effect of an external magnetic field on Jag-1-Fc stimulation of Notch target gene expression in the absence or presence of DAPT- and Compound E-loaded MNPs. The mMVSCs were seeded at 10^3 cells/well density and treated with IgG-Fc (500 ng/mL), Jag-1-Fc (500 ng/mL) and Jag-1-Fc (500 ng/mL) in the presence of DAPT- and Compound E-loaded MNPs for three days in the absence or presence of the external magnetic field. qRT-PCR was used to analyse the fold change in *Hey1* gene expression, compared to the IgG-Fc control. Data analysis was performed by two way ANOVA using the GraphPad Prism™ software and **p<0.005 and ****p<0.0001 was considered significant.

.
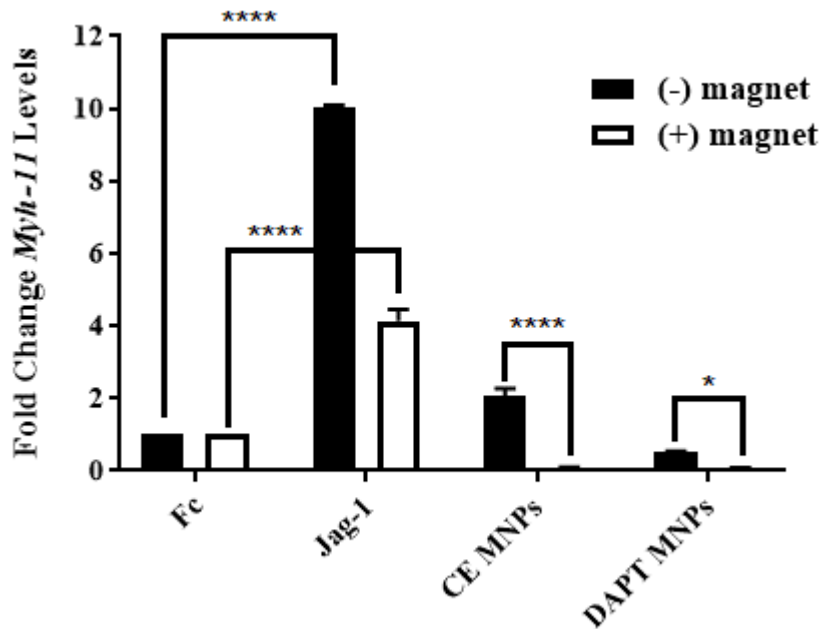
Figure 6.13. The effect of an external magnetic field on Jag-1-Fc stimulation of myogenic differentiation in the absence or presence of DAPT- and Compound E-loaded MNPs. The mMVSCs were seeded at 10^3 cells/well density and treated with IgG-Fc (500 ng/mL), Jag-1-Fc (500 ng/mL) and Jag-1-Fc (500 ng/mL) in the presence of DAPT- and Compound E-loaded MNPs for 14 days in the absence or presence of the external magnetic field. qRT-PCR was used to analyse the fold change in *Myh-11* gene expression, compared to the IgG-Fc control. Data analysis was performed by two way ANOVA using the GraphPad Prism™ software and *p<0.05 and ****p<0.0001 was considered significant.

.

### 6.4.5   Stent with IgGAlexa488-Fe$_3$O$_4$-PLGA-MNPs

To assess the ability of MNPs to bind bare-metal vascular stents under magnetic and non-magnetic conditions, fluorescently labelled IgG-Alexa488-Fe$_3$O$_4$-PLGA-MNPs and IgG-Alexa488 controls were incubated with vascular stents on 96-well plates in the absence or presence of an external magnetic field for 2 hrs before the stents were washed with H$_2$O and imaged using a fluorescent microscope. In parallel studies, FITC labelled Fe$_3$O$_4$-PLGA-MNPs were also incubated with vascular stents on 96-well plates in the absence or presence of an external magnetic field for 2 hours before the stents were washed with H$_2$O and imaged using a fluorescent microscope.

There was little binding of IgG-Alexa488 controls or IgG-Alexa488-Fe$_3$O$_4$-PLGA-MNPs to bare metal stents under non-magnetic conditions. However, there was a significant increase in IgG-Alexa488-Fe$_3$O$_4$-PLGA-MNPs binding when compared to IgG-Alexa488 controls under magnetic conditions (Figure 6.15).

Similarly, there was little binding of Fe$_3$O$_4$-PLGA-FITC-MNPs to bare metal stents under non-magnetic conditions. However, there was a significant increase in Fe$_3$O$_4$-PLGA-FITC-MNPs binding under magnetic conditions (Figure 6.16).
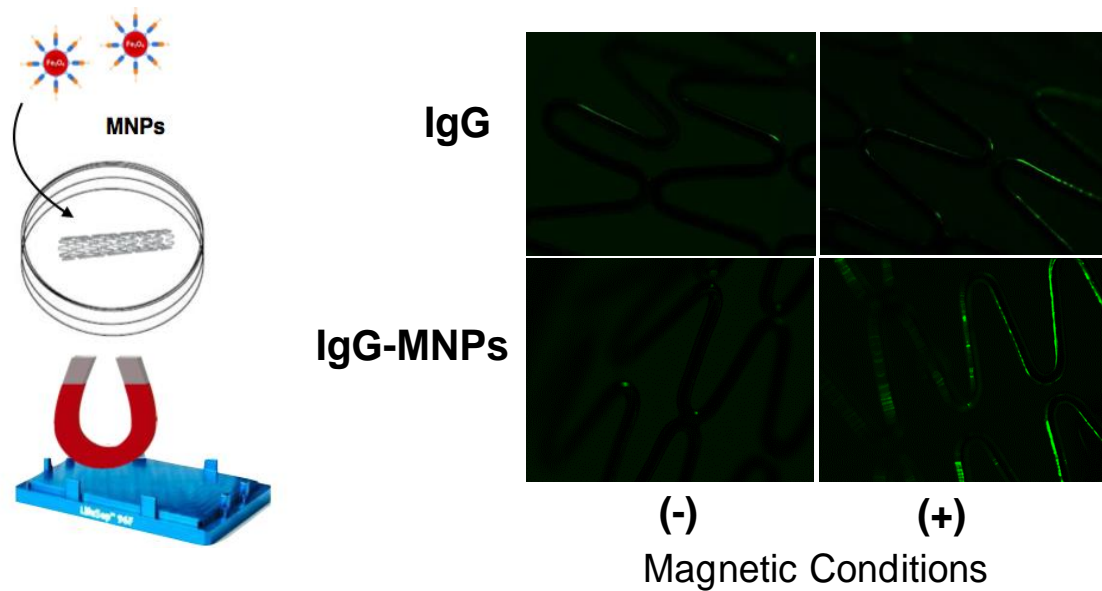
Figure 6.14. The effect of an external magnetic field on IgG-AlexaFluor488 labelled MNP binding to vascular stents under magnetic and non-magnetic conditions. Bare-metal Vascular stents were incubated with fluorescently labelled IgG-AlexaFluor488 blank MNPs for 2 hr in the absence or presence of a magnetic field before stents were washed and imaged. Data are representative of 3 experiments.
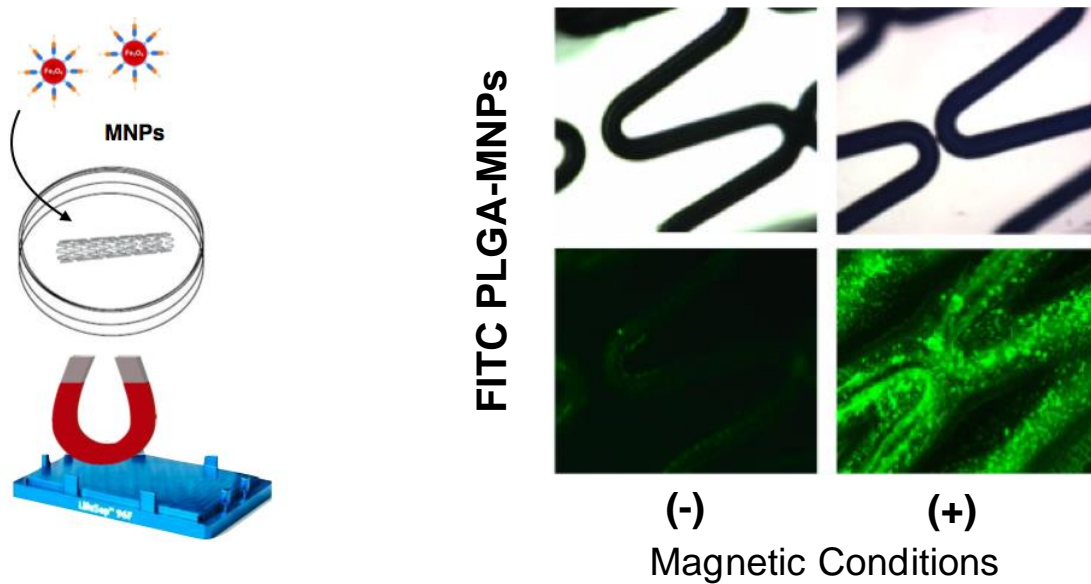
Figure 6.15. The effect of an external magnetic field on Fe₃O₄-PLGA-FITC-MNP binding to vascular stents under magnetic and non-magnetic conditions. Bare-metal vascular stents were incubated with labelled Fe₃O₄-PLGA-FITC-MNPs for 2 hr in the absence or presence of a magnetic field before stents were washed and imaged. Data are representative of 3 experiments.

6.5   Discussion

The main objective of this chapter was to determine the functionality of magnetic nanoparticles loaded with GSIs at inhibiting Notch signalling and attenuating Notch ligand-induced myogenic differentiation of resident vascular stem cells *in vitro* under magnetic and non-magnetic conditions. The data clearly demonstrate that DAPT-loaded Fe_3O_4 PLGA/PVA-MNPs and Compound E loaded Fe_3O_4 PLGA/PVA-MNPs both release a sufficient amount of active drug to control Notch target gene expression and Notch ligand control of myogenic differentiation of resident stem cells under both magnetic and non-magnetic conditions. Novel doxorubicin-loaded MNPs coated by poly (lactide-co-glycolide) have also been fabricated using a similar water-in oil-in-water emulsification method (F. Li et al., 2011) while several studies using MNPs prepared through iron oxide core oil-in-water emulsion technique have been deployed for cancer diagnostics, therapeutics and imaging (Jarzyna et al., 2009). Previous studies that addressed the effect of drug-free blank encapsulated MNPs on the level of apoptosis in target cells revealed that nanoparticles similar to those used here have no direct toxic effect on cells nor did they interfere with the mechanism of action of the loaded drug, paclitaxel (Bacso et al., 2000). In the current study, DAPI nuclear staining of cells revealed the effect of drug-free blank MNPs, DAPT-MNPs and Compound E-MNPs on the mMVSCs viability. Both DAPT-MNPs and Compound E-MNPs had a significant effect on cell viability since the number of cells decreased when compared to control Jag-1-Fc treated cells. Similar conclusions were reported for paclitaxel loaded MNPs (Danhier et al., 2009).

Jag-1-Fc stimulation of Notch target gene expression and myogenic differentiation was significantly attenuated following exposure of cells to DAPT and Compound E-loaded MNPs both in the absence or presence of a magnetic field and suggests that sufficient amounts of the active drug are released form the MNPs in aqueous media. Importantly, drug-free blank MNPs did not affect Jag-1-Fc stimulated cell number, Notch target gene expression or myogenic differentiation. This functionality of the DAPT and Compound E MNPs was greater in the presence of the magnetic field when compared to non-magnetic conditions and this has also been reported for transfection efficiency of anti-GFP siRNA in the cervical cancer HeLa cells using similar MNPs (Mykhaylyk et al.,

2007). This is most likely due to the initial burst of the drug released from the MNPs when the magnetic field is applied.

Interestingly, exposure of cells to a magnetic field in the absence of MNPs significantly attenuated Jag-1-Fc stimulated Notch target gene expression and myogenic differentiation and the reasons for this are not clear at present. Most magnetoception studies used a static magnetic field (Prijic and Sersa 2011) and despite compelling behavioural evidence that this sense exists, the cells, molecules, and mechanisms that mediate sensory transduction remain unknown (Nordmann et al., 2017). Notch receptors undergo dynamic spatial, chemical, mechanical, and structural changes, including receptor segregation, receptor clustering, force generation and receptor proteolysis. These events culminate in the release of the Notch intracellular domain, which traffics to the nucleus to affect gene transcription (Seo et al., 2016). Previous studies have suggested that varying the distance between samples and a fixed magnetic field can generate pulling forces that are applied to either a plate-tethered Negative Regulatory Region (NRR) domain or to Notch receptors expressed in live cells (Kovall et al., 2017). Indeed, previous studies have clearly shown that exposure to a magnetic field (MF) can impact cell signalling in epithelial and neuron cells whereby an MF signal is transformed into biological signal and transmitted along the signal transduction cascades (X. Wu et al., 2018).

The results in this chapter also clearly demonstrate the feasibility of site-specific delivery of GSI drug-loaded Fe_3O_4 MNPs to bare metal stents based on a uniform-field–induced magnetisation and targeting to the stent. Novel GSI-loaded MNPs used in these proof-of-concept experiments were designed with the following properties required for a safe and efficacious magnetic drug carrier: (1) strong magnetic responsiveness (2) delivery of chemically labile GSI drugs ($t_{1/2}$ ~12 h in aqueous solution at pH 7) and (3) sustained drug release properties and functional activity at inhibiting myogenic differentiation of vascular stem cells *in vitro*.

The biodegradable hydrophobic polyester, polylactide provided a sustained release depot for the encapsulated GSI drugs by maintaining the composite particle structure with the

multiple magnetite grains embedded in the solid polymeric matrix, thus enabling the high magnetic susceptibility of the formulation achieved without the loss of the superparamagnetic properties characteristic of ultra-small-sized crystallites confirmed by their ability to bind to bare metal stents under magnetic conditions. Both the duration of the magnetic exposure and the low dose of MNPs (1:2 corresponding theoretically to 150 µM for DAPT and 60 µM for Compound E) are likely to be advantageous in the context of anti-restenosis therapy.

The MNP distribution, as evident by fluorescence staining is relatively uniform along the stent with scant fluorescence noted in stents not exposed to the magnetic field. The intense MNP-associated fluorescence observed with magnetic targeting is likely due to the initial concentration of MNPs around the steel struts in the presence of a magnetic field. Although it is feasible that arterial wall uptake of MNPs may passively occur without a field exposure when deployed *in vivo*, the magnetic conditions facilitate a strong interaction of the MNP with the luminal surface of the stent since the MNPs still remain after washing.

It is also possible that higher rates of MNP capture in the presence of a uniform field could be achieved by extending the effective distance within which the magnetic force can act on the particles, thereby increasing the fraction of MNPs deposited on the stent surface. The magnetic responsiveness of an individual particle is proportionate to its magnetite content, which in turn is directly dependent on the particle size. Thus the lower size limit of the MNPs designed for the uniform field-controlled, magnetically targeted delivery is defined by the efficiency of the MNP–stent interaction (Yellen et al., 2005).

It is also notable that despite the initial distribution of a sizable fraction of initially captured MNPs, magnetic delivery resulted in their protracted presence at the target site even after several washes (Figure 6.15) at significantly higher levels compared to nonmagnetic control conditions. These higher local levels of retention of magnetically guided MNPs to bare metal stents would enhance any significant therapeutic effect, as opposed to a likely marginal effect observed without a magnetic exposure. Therefore,

stent loading can be accomplished *in situ* after the stent has been implanted. Since the deployed stent is freely accessible to blood flow, its surface can be actively targeted with therapeutic agents delivered to systemic or regional circulation, provided the targeting forces are strong enough to capture and retain a therapeutic agent on the stent surface. The concept of *in situ* stent loading with MNPs has recently been implemented using a magnetic targeting paradigm (Chorny et al., 2013). Indeed, stents made of magnetic alloys, when placed in a uniform magnetic field, such as that created within an MRI coil or induced by paired electromagnets generated strong highly localized magnetic forces due to steep field gradients between stent struts (Chorny et al., 2013). The same external magnetic source can be used to magnetise both stents and MNP, in particular, if stents are fabricated from magnetically responsive 304-grade stainless steel.

Chapter 7

Final Discussion

Final Discussion:

Cardiovascular disease (CVD), the leading cause of death and disability worldwide and is characterised by pathological structural changes to the blood vessel wall (Chistiakov et al., 2015). A hallmark is the accumulation of smooth muscle cell (SMC)-like cells leading to intimal medial thickening (IMT) and the obstruction to blood flow that can result in a heart attack or stroke (Bennett et al., 2016). The local origin of these SMC-like cells has been confirmed (B. Yu et al., 2018) yet their source remains controversial with de-differentiated SMCs (Chappell et al., 2016, Herring et al., 2014, Nemenoff et al., 2011), progenitor stem cell-derived myogenic progeny (F. Yuan et al., 2017, Kramann et al., 2016, Z. Tang et al., 2012b) and SMCs derived from endothelial to mesenchymal transition (EndoMT) (F. Yuan et al., 2017, Cooley et al., 2014) (Cooley et al., 2014; Yuan et al., 2017) all reported to play a contributory role. Importantly, irrespective of their origin, a transition to a more "plastic" mesenchymal stem cell (MSC)-like phenotype is considered a prerequisite before myogenic differentiation to a more synthetic neointimal SMC-like cell can progress (D. Klein 2018, F. Yuan et al., 2017, Chappell et al., 2016, Cooley et al., 2014, Z. Tang et al., 2012b).

Percutaneous angioplasty (PCTA) is widely used to treat atherosclerosis but has a major limitation called restenosis that is categorized by the unhindered accumulation of smooth muscle-like cells (SMC) and additional vascular inflammatory cells. As a solution, intracoronary stents were specifically developed to minimise restenosis, yet in-stent restenosis (ISR) may still persist in about 30% of stented coronary arteries (Woods and Marks 2004, Kasaoka et al., 1998). During ISR, vascular SMC-like cells accumulate within the neointima and can continue to proliferate following coronary angioplasty. The discovery of resident vascular stem cells within the blood vessel wall has raised the possibility that de-differentiated vascular SMC-like cells are derived from these stem cells (Z. Tang et al., 2012a). For this project, different types of stem cells were targeted using γ-secretase inhibitors of Notch signalling DAPT & Compound E, before these inhibitors were incorporated within functionalised MNPs as an alternative treatment for ISR.

7.1   Gamma secretase inhibitors and stem cell fate

The anti-proliferative activity of these drugs was first assessed using AlamarBlue® assay for viability activity, DAPI nuclear staining for cell growth and division and FACS analysis of apoptotic and necrotic cells, respectively. The efficiency of the AlamarBlue® assay at assessing cell viability and hence cell number was first addressed. Cells with different densities were grown in medium supplemented with 10 % FBS and a linear relationship between cell density and cell proliferation was confirmed and validated. Two chemically dissimilar γ −secretase inhibitors were then assessed for their ability to inhibit cell number and promote apoptosis/necrosis and thereby detect a dose of the drug that does not cause significant cell death or inhibit the proliferation for future myogenic differentiation studies.

The AlamarBlue® assay data clearly demonstrate that these GSI drugs have a significant effect on the growth of both mMSCs and mSMCs, particularly at high doses. Both cell lines had a similar response to drugs. The determined optimal drug dose for mSMCs and mMSCs were established as $80\mu M$ of DAPT and $25\mu M$ Compound E, respectively. These data were then confirmed by counting the number of DAPI nuclei under similar conditions. This could either be due to an anti-proliferative effect or a pro-apoptotic effect of the drugs. As a result, an evaluation of the apoptotic/necrotic properties of the drugs was established. The FACS analysis revealed little necrosis in response to the various doses due to any potential toxic effect. These data suggest that DAPT and Compound E are an anti-proliferative drug but not toxic. The anti-proliferative property of DAPT and Compound E may prove useful at the stent site because of their dual-functionality as they may inhibit the stem cell differentiation to smooth muscle cells at the site of injury while concomitantly inhibiting the proliferation of cells. The DAPI nuclei results confirmed that the suitable dose of DAPT for mMSCs and mSMCs is $80\mu M$ at the highest as almost 80% or more of the cells are still viable at this dose. In a similar manner, the dose of Compound E for mMSCs and mSMCs is 25μM at the highest since nearly 80% or more of the cells are viable at this dose. The FACS analysis also suggest that when the concentration of DAPT and Compound E is increased beyond these levels, they become be pro-apoptotic to the cells.

The differentiation of stem cells into smooth muscle cells (SMCs) (myogenic differentiation) plays an important role in vascular development and remodelling. In addition, stem cells represent a potential source of SMCs for regenerative medicine applications such as constructing vascular grafts. Previous studies have suggested that various biochemical factors, including transforming growth factor-beta (TGF-β1) and the Notch pathway, both found in serum, may play important roles in vascular differentiation (Kurpinski et al., 2010b). Notch signalling has been previously associated with neointimal formation (Doyle et al., 2015, Sakata et al., 2004, Gridley 2010, Caolo et al., 2011, Morrow et al., 2009) and has been shown to promote myogenic differentiation of various stem cells (Mooney et al., 2015b, Kurpinski et al., 2010b, Doi et al., 2006, Z. Tang et al., 2012b, Mack 2011).

Myogenic differentiation experiments performed on mMSC's following treatment with maintenance medium and myogenic differentiation medium in the absence or presence of 80μM of DAPT (the γ −secretase γ inhibitor) revealed that the initial increase in the number of Myh11$^+$ and Cnn1$^+$ cells after three days was markedly reduced when Notch signalling was blocked with the ɣ-secretase inhibitors, DAPT and Compound E. These data suggest that Notch ligands are present in FBS and increased the number of Myh-11$^+$ and Cnn1$^+$ cells when compared to maintenance medium. Moreover, as the percentage of FBS is increased, the number of MyH-11$^+$ and Cnn1$^+$ cells also increased, concomitant with an increase in cell number.

Using three discrete stem cell populations, bone-marrow-derived MSCs, embryonic C3H 10T½ MSC-like cells and resident multipotent vascular stem cells (MVSCs), the Notch ligand, Jagged1, increased myogenic differentiation in all three cells types. Moreover, inhibition of γ −secretase activity with DAPT and Compound E to attenuate Notch signalling decreased Notch target gene expression concomitant with a reduction in the percentage of the expression of *Myh11* and *Cnn1* cells, mRNA levels and overall myogenic differentiation. These data suggest that inhibition of Notch signalling with γ −secretase inhibitors might be a suitable candidate for functionalised MNPs targeted to bare-metal stents to attenuate ISR *in vivo*.

7.2 Nanoparticles Fabrication and Characterisation

The third main objective was to fabricate and characterise biodegradable magnetic nanoparticles (MNP's) that contain the γ −secretase inhibitors. Iron-oxide (Fe_3O_4) or magnetite is FDA approved and can be functionalised using polymers loaded with therapeutics that could potentially bind to the bare metal stent under a magnetic field to facilitate targeted drug-delivery (Revia and Zhang 2016). PLGA is FDA approved biodegradable polymer and was chosen to functionalised PLGA-Fe_3O_4-MNPs with γ −secretase inhibitors. The incorporation of the drugs within the MNP's, their size and uniformity and the release profile were all assessed (Y. Wang et al., 2016).

An oil emulsion technique was used to produce the PLGA-MNP's. PLGA was added to functionalize the MNPs for drug-loading, increase their stability and prevent the aggregation. PLGA has a very strong biodegradability and biocompatibility and it also has little systemic toxicity (Danhier et al., 2012, Panyam and Labhasetwar 2003). The use of MNP's as a drug delivery system has become increasingly popular. MNP's are ideal due to their small controllable size and ease with which they can be functionalised for drug-delivery. There are also further advantages such as prolongation of the half-life of drugs in circulation and specific targeting to the site of interest for more efficient drug use with limited side effects (Gangwar et al., 2012). In fact, chemotherapeutic drug targeting to tumours using MNP's has been widely reported (M. Wu and Huang 2017). However, concern remains about the toxic nature of MNPs as they may accumulate within organs and increase the risk of an inflammatory response. Therefore, novel drug-loaded MNPs require rigorous characterisation before considering *in vivo* studies (Markides et al., 2012).

To characterise the MNPs, dynamic light scattering (DLS) was used. Zetasizer nano Z system analysed the MNP samples and generated a Z-average for each MNP preparation. Under Rayleigh scattering, the volume of light scattered by a single particle is proportional to the sixth power of its radius (volume squared) (Strutt 1871). This situation leads the averaged hydrodynamic radius detected by DLS to be also weighted by volume squared and this averaged property is called the Z-average. The Z-average of the PLGA-MNPs was shown to be smaller than that of the DAPT MNPs and Compound E MNPs, 222.7 d.nm, 351.4 d.nm and 256.2 d.nm respectively. This indicated that the incorporation of DAPT and Compound E into the MNPs had been successfully achieved, and this was confirmed using HPLC. Moreover, (Yoo et al., 2000) have found as well

that the size and the zeta potential of the doxorubicin PLGA nanoparticles is a little higher than the blank PLGA nanoparticles and this increase in the doxorubicin PLGA nanoparticles is due to the encapsulation of the doxorubicin.

The size of MNPs must be large enough to avoid rapid leakage in blood capillaries but small enough to escape being captured by macrophages in the reticuloendothelial system (RES), such as the liver and spleen (Bamrungsap et al., 2012). DLS was also used to obtain a polydispersity index (PDI) value for all MNPs. PDI is a good indicator of variance between their peaks. A perfectly uniform sample would have a PDI of 0.01 (Bhattacharjee 2016). For the PLGA-MNPs, DAPT-loaded PLGA-MNPs and Compound E-loaded PLGA-MNPs, the PDI values of 0.299, 0.220 and 0.321 were achieved, respectively. These values display no suggestion of aggregation and suggest that both MNP samples were monodispersed systems. Therefore, to conclude that DAPT and Compound E loaded PLGA-MNPs were successfully generated and characterised. The DLS analysis indicated that the MNPs were round and relatively uniform in size.

Polydispersity Index (PDI) is dimensionless and scaled such that values smaller than 0.05 are rarely seen other than with highly monodisperse standards. Values greater than 0.7 indicate that the sample has a very broad size distribution and is probably not suitable for the DLS. Interestingly, the Z- an average of the iron oxide used in the MNP's preparation and its PDI were much higher than the blank and loaded magnetic nanoparticle with the size of 446.4 d.nm and PDI of 0.514. The lower PDI value, the closer to achieving monodisperse system; values less than 0.7 indicate greater stability for a nano-delivery/colloidal system (Bhattacharjee 2016). Additionally, it has been found that the size of ferric oxide (the magnet) could range between 200–800 nm (A. Lu et al., 2007). A reduction in the MNPs agglomeration has been observed due to the sonication step (Murdock et al., 2008). Therefore, all the data obtained indicate to achieving MNPs with no agglomeration for using sonication in the preparation procedure. In addition, due to the fact that magnetic nanoparticles can be attracted by an external magnetic field gradient, they should not be too small. However, it has been found that the particles which exhibit a diameter larger than 100nm are more likely to be caught by the cells an undergo mononuclear phagocytosis than smaller particles (Jurgons et al., 2006, Storm et al., 1995).

DLS also measured the size of the particles in the hydrated state (Tan et al., 2010). The hydrodynamic diameters are larger than those measured by TEM yet TEM confirmed that there was no damaging effect to the Fe_3O_4 nanocrystals following the encapsulation process. TEM is popular for imaging MNPs and in conjunction with image analysis software packages (e.g., ImageJ®) it is now possible to obtain size distributions of MNPs from TEM images with information on mean size, standard deviation and the overall estimation of PDI. However, such information from TEM images does not always corroborate with data obtained from DLS as the latter is an intensity-based technique whereas TEM is number-based making them fundamentally different (Bhattacharjee 2016). While the samples for DLS are solvated, TEM works on dry samples under UHV (ultrahigh vacuum) conditions. DLS measures the RH of the dispersed particles whereas TEM provides the projected surface area based on how much of the incident electrons were transmitted through the sample. Hence, the size obtained by DLS is usually bigger than TEM. An advantage with DLS is its capability to measure bigger number of particles (in millions) compared to TEM (few hundreds). Therefore, DLS provides more robust data on the size distribution and PDI.

To accomplish maximum therapeutic effectiveness while minimizing toxic side effects, accurate control over drug release from nanoparticles is critical. To achieve this, HPLC was also used to perform drug release kinetic studies. These studies were carried out at 4ºC and 22ºC to mimic storing environments that DAPT-loaded PLGA-MNPs and 37ºC to reflect physiological conditions. The entrapment and release kinetics of the GSI's from MNPs was assessed by HPLC. Standard curves for the varying concentrations of DAPT and Compound E were deployed to determine the level of DAPT and Compound E incorporation. The incorporation efficiency of DAPT and Compound E into the MNPs were approximately 68% and >90 % respectively which compared with a 90% drug incorporation using a single oil-emulsion method with doxorubicin (Jia et al., 2012). There was the minimal release of DAPT from the MNPs at any of the three temperatures examined over 24 hours. Hua et al., have published that PLGA-nanoparticles express early burst release of incorporated drug in two days (Hua et al., 2014). The amount DAPT released overtime under nonmagnetic conditions was time and temperature-dependent and suggests optimal release at 37^0C culminating in ~96% release after seven days in some instances. Under magnetic conditions, however, the release was around 40%. In

contrast, the release of Compound E was about 15 %. Even though a high incorporation efficiency for both drugs into the magnetic nanoparticles was observed, the drug release study suggested a low release rate for both drugs after seven days. The high incorporation efficiency and low release of DAPT and Compound E from the PLGA-MNPs might be as a result of the lactic acid-rich PLGA polymers as it makes the degradation rates of the drug release slower, or alternatively due to the formation of the covalent bonds in between the polymer and amine groups of the drugs (Lanao et al., 2013) thereby causing retention of the drug within the PLGAMNP. Another explanation might be the strategy of using the actual MNPs not their supernatants during the fabrication to determine drug release as it has done for other drug release and incorporation studies. Nevertheless, despite the low release rate for DAPT and Compound E, both drugs at these concentrations continued to be functional and decreased Notch target gene expression and attenuated Jag1 induced myogenic differentiation.

Dialysis is the most common method utilised to detect drug release kinetics from MNPs so this could be performed to increase the accuracy of the results (Zhou et al., 2016, Jia et al., 2012). Furthermore, while the incorporation of the drug was performed during the fabrication procedure, MNPs can also be functionalised by adsorption on the PLGA.PVA polymer after fabrication (Dorniani et al., 2012). Another factor is that sustained drug release properties may be more accurately evaluated under perfect sink conditions using an external sink drug release method (Chorny et al., 2002). Sink conditions are more reliable of the actual amount of drug released by avoiding distortion of the apparent release kinetics reported for hydrophobic compounds when a poor acceptor phase rapidly saturated with the drug is used as the release medium [non-sink release conditions] (Chorny et al., 2002).

7.3   Targeting DES with gamma-secretase inhibitors.

Angioplasty followed by stent placement is widely used to treat obstructive vascular disease but as a consequence of compliance mismatch (Colombo et al., 2013) triggers acute local inflammation due to disruption of the protective endothelial layer and infiltration of SMC-like cells and inflammatory cells to the site of arterial injury, in turn leading to in-stent restenosis (ISR) (Buccheri et al., 2016). The key role played by the accumulation of neointimal SMC-like cells provides a strong rationale for applying drug

targeting approaches as a way of improving outcomes by modulating the tissue healing processes. One important source of these cells is the niche of resident vascular S100β/Sox10 stem cells that reside within the adventitial and medial layers (Tang et al., 2012). Indeed, recent data from our group using S100β-CreERT2-Rosa26-tdTomato transgenic mice to track S100β progeny clearly demonstrates their putative role in contributing to the accumulation of SMC-like cells following vascular injury, typical of ISR (Fitzpatrick et al., 2018). Hence, pathway-targeted pharmacotherapy with cell-type specific delivery of small-molecule drugs formulated in biodegradable polymer-based nanoparticles is clearly desirable. The development of appropriate delivery systems and their evaluation in clinical trials and the potential utility of these novel therapeutics for other CVD applications are reviewed by (Aizik et al., 2018).

Indeed, new therapeutic approaches due to suboptimal effectiveness of existing treatment procedures for ISR in patients is fully warranted due to a growing number of patients unsuccessfully treated with drug-eluting stents (DES)—combination devices, which in recent years have largely replaced bare-metal stents as a strategy for treating the symptoms and consequences of obstructive vascular disease and for mitigating ISR. This arterial re-occlusion is still approached by repeat stenting ("stent sandwich" technique) in the absence of more effective treatment options. The recognized limitations of DES in clinical use include deterioration of their polymeric coating and the associated inflammatory response, as well as the non-selective mode of action of stent-eluted drugs, which together strongly increase the risk for stent thrombosis and neo-atherosclerosis, both contributing to eventual stent failure (Komiyama et al., 2015, Guagliumi et al., 2012, S. Park et al., 2012). Moreover, drug release kinetics that cannot be adjusted and poor compatibility of traditionally designed DES has been a major driver for new therapeutic strategies and DES modalities capable of addressing the limitations of existing DES.

Previous studies have demonstrated the feasibility of stents covered with non-polymeric coatings and providing site-specific delivery of immunosuppressants, anti-inflammatory and antithrombotic drugs, and other active compounds as single agents or in combination (Kommineni et al., 2018). Significant progress has also been made on advanced coating technologies for producing polymer-free DES (Kommineni et al., 2018). The side effects of currently used DES and their poor performance in a subgroup of patient cohorts at high clinical risk can potentially be addressed by acting on a set of molecular targets, which are readily accessible to small-molecule therapeutics. In this current study, DAPT and

Compound E loaded MNPs were successfully fabricated and shown to be functional at inhibiting resident vascular stem cell growth and myogenic differentiation *in vitro.* Moreover, these functionalised MNPs could be targeted to vascular stents under magnetic conditions. Hence, we have shown the feasibility of site-specific delivery of functionalised GSI-MNPs to bare metal stents based on a uniform-field–induced magnetisation and targeting to the stent. Both the duration of the magnetic exposure and the low dose of MNPs (1:2 corresponding theoretically to 150 µM for DAPT and 60 µM for Compound E) are likely to be advantageous in the context of anti-restenosis therapy *in vivo.* Indeed, the relevance of such an approach is clearly shown in studies that target the Notch signalling pathway *in vivo* using local pluronic gel delivery of siRNAs against the Notch1 receptor (Redmond et al., 2014). Therefore, molecular target-specific therapies using MNPs functionalised with small molecule inhibitors to block the restenotic cascade by interfering with early events in restenosis pathophysiology within resident vascular stem cells can offer an attractive, viable and effective alternative to traditional DES.

7.4   Future Work

The concept of using novel effective $\gamma-$secretase inhibitors (DAPT and Compound E) to target SMC-like cell accumulation during ISR by inhibiting myogenic differentiation of stem cells and accumulation of their myogenic progeny is novel and presents a clinically adaptable approach to precisely target the source of these cells *in vivo* through the administration of drug-loaded magnetic nanoparticles. While the proof-of-concept for this approach has been successfully demonstrated *in vitro*, the basic limitation of this work is the lack of validation *in vivo*. Additionally, the stem cells used were from animal cell culture, and thus may not reflect a similar response to the same treatment in human stem cells *in vivo*.

Magnetic targeting is based on two main components: a magnetically responsive carrier of therapeutics and a source of a magnetic field gradient (i.e., a magnetic force) responsible for the attraction or positioning of magnetically responsive carriers in organs or tissues. The use of the LifeSep™ 96F magnetic separator (Dexter Magnetic Technologies) to generate an external magnetic field *in vitro* was important for the proof-of-concept experiments and successfully demonstrated the ability to target vascular stents with these functionalised MNPs *in vitro.* There are two main classes of magnet systems

for magnetic targeting *in vivo* that have been proposed. In one class, magnets external to the body provide both the field to magnetize the carrier and field gradients for targeting (Alexiou et al., 2006, Lübbe et al., 2001). However, the use of external magnets imposes serious limitations in targeting deep tissues as their field strength and field gradient decrease exponentially with the distance from the surface. The other class is based on a combination of external magnets and magnets (or magnetizable devices) implanted local to the target region. In the second class of systems, the external magnet would typically provide the magnetizing field for the carrier, while the local magnet (or magnetizable implant) will provide the largest possible field gradients for targeting (Chorny, Fishbein et al., 2010, Polyak et al., 2008, Pislaru et al., 2006). The second type of magnet system can be of potential use for targeting deep tissues, including blood vessels where magnetizable implants can be placed.

In this context, the feasibility of site-specific drug delivery to implanted magnetisable stents by uniform field controlled targeting of MNPs with efficacy for in-stent restenosis has been reported (Chorny et al., 2010). These authors showed that local administration of MNPs applied to stented rat carotid arteries in the presence of a uniform magnetic field resulted in the fourfold higher initial number of MNPs associated with the stented region compared with non-magnetic control conditions. After removal of the uniform field, the stent and MNPs lose their magnetic moments and targeted MNPs are redistributed from the stented arterial segment over time. Interestingly, the number of MNPs measured in the arteries of magnetically treated animals remained 5.5- to 9.5-fold higher than in the non-magnetic control group up to five days post-treatment. Despite the redistribution of a sizable fraction of initially captured MNP, a significant reduction in the neointima-to-media ratio was revealed 14 days after surgery in the animals treated with paclitaxel-loaded particles in the presence of the uniform field, but not in control animals.

There is some disquiet regarding the toxicity of magnetic nanoparticles for cells and tissues *in vivo*, as MNPs can build-up in organs and interfere with cell-cell interactions and lead to particulate aggregation (Markides et al., 2012). The nanoparticles and the aggregation potential (zeta potential) of the nanoparticle fabrication was evaluated and emulated earlier *in vivo* work which was deemed acceptable (Chorny, Hood et al., 2010). Therefore, the DAPT-PLGA-MNPs and Compound E-PLGA-MNPs are suitable to proceed to *in vivo* studies.

Prior to applying this treatment *in vivo*, the use of a mock vascular phantom could further validate the benefit of this strategy for targeting functionalised MNPs to vascular stents. This novel mock vascular phantom system using Sylgard™ supports stent deployment and cell growth (Colombo et al., 2013). The stented region is associated with compliance mismatch and exaggerated SMC growth *in vitro,* mimics the hemodynamic microenvironments of circumferential strain and pressure and is associated with enhanced Notch signalling within the stented environment (Colombo et al., 2013). This technology could be adapted through seeding mMVSCs on the mock vascular phantom before the addition of DAPT-PLGA-MNPs and Compound E-PLGA-MNPs and targeting of the nanoparticles to the stent using an external magnetic field with the LifeSep™ 96F magnet, as described in Figure 7.1)
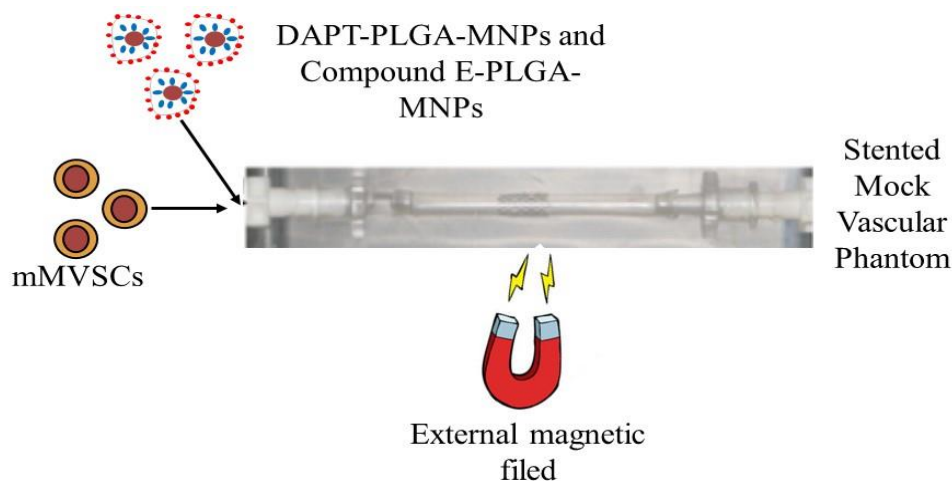
Figure 7.1. Mock vascular phantom system. Graphic representation of the mock vascular phantom seeded with MVSCs and perfused with DAPT-PLGA-MNPs or Compound E-PLGA-MNPs under magnetic and non-magnetic conditions through an external magnetic field.

7.5 Conclusion

Magnetic-based systems utilising magnetic nanoparticles and various configurations of magnetic fields and field gradients clearly provide for a range of new opportunities for a number of clinical applications. Localised therapy is highly desirable as it can enable administration of a significantly lower drug dose, thus minimizing systemic drug-induced toxicity. Magnetically mediated localisation of GSI's is a promising approach to improve the efficacy and safety of these therapies that may result in improved clinical outcomes. Furthermore, magnetic targeting can enable redosing or administration of an additional drug at the diseased site, which is highly desirable for the treatment of vascular lesions where DES are currently used to alleviate re-obstruction of the blood vessels but become depleted over time.

Targeting the Notch signalling pathway in resident vascular stem cells offers an opportunity to control stem cell self-renewal and myogenic differentiation using functionalised MNPs loaded with $\gamma-$secretase inhibitors. Generation of $\gamma-$secretase inhibitor-loaded magnetic nanoparticles could be a new potential platform alternative to current therapy with drug-eluting stents where the anti-proliferative drugs are depleted within 1 month of deployment.

In this project, the main goals were first to investigate the cytostatic effect of two pharmacological $\gamma-$secretase inhibitors, DAPT and compound E, on mouse smooth muscle cells (mSMC) and mouse mesenchymal stem cells (mMSC) and the results confirm the safety of using these drugs at low concentrations. The second goal was to evaluate the effect of DAPT and Compound E on the myogenic differentiation potential of various stem cell populations using differentiation medium supplemented with Jagged1 1 and TGF-β1. The data demonstrate a significant effect of these drugs on Notch control of myogenic differentiation at similar low concentrations. DAPT and Compound E were successfully incorporated into PLGA-MNPs and DLS/TEM was used to characterise the MNPs and ensure uniform nature of the particles so that they were of a similar size and small enough to be efficacious before their functionality at inhibiting Notch control of growth and myogenic differentiation of stem cells *in vitro* under magnetic and non-magnetic conditions were validated. An external magnetic field improved the performance of the DAPT- and Compound E-loaded MNPs and successfully targeted these MNPs to vascular stents. As a result, these proof-of-concept

studies clearly demonstrate that DAPT and Compound E-loaded MNPs are functional at affecting vascular stem cells *in vitro* and this effect is enhanced in the presence of the magnetic field which could be a potential alternative treatment for in-stent restenosis *in vivo*.

The manipulation and control of cell function and behaviour through MNP-based actuation is a relatively new strategy that has shown great potential for tissue engineering and regenerative medicine applications. Although promising results have been achieved demonstrating the potential of magnetic targeting of GSI-loaded MNP's, many challenges still exist in order to successfully translate this technology into clinical settings. Substantial improvements in both the magnetic carriers and the targeting magnet systems are likely to be necessary to make the magnetic targeting a viable clinical treatment modality. Upscaling magnetic drug delivery technology from in vitro studies to pre-clinical animals and laboratory models to humans will require the design of magnet systems enabling the pushing of a magnetic carrier inward in contrast to a conventional pulling of carriers, usually achieved using permanent magnets. The need to develop such carrier pushing-magnet systems has been recognized and work is ongoing in this direction.

Nevertheless, is clear the use of functionalised MNPs has great potential for clinical applications but more animal and clinical studies are necessary to fully realise the clinical potential of these magnetic-based systems.

Bibliography

Afilalo, J., Duque, G., Steele, R., Jukema, J.W., de Craen, A.J. & Eisenberg, M.J. 2008. Statins for secondary prevention in elderly patients: A hierarchical bayesian meta-analysis. *Journal of the American College of Cardiology,* 51(1), pp.37-45.

Ahn, E.H., Kim, Y., An, S.S., Afzal, J., Lee, S., Kwak, M., Suh, K., Kim, D. & Levchenko, A. 2014. Spatial control of adult stem cell fate using nanotopographic cues. *Biomaterials,* 35(8), pp.2401-2410.

Aizik, G., Grad, E. & Golomb, G. 2018. Monocyte-mediated drug delivery systems for the treatment of cardiovascular diseases. *Drug Delivery and Translational Research,* 8(4), pp.868-882.

Alexander, M.R.Owens, G.K. 2012. Epigenetic control of smooth muscle cell differentiation and phenotypic switching in vascular development and disease. *Annual Review of Physiology,* 74pp.13-40.

Alexiou, C., Schmid, R.J., Jurgons, R., Kremer, M., Wanner, G., Bergemann, C., Huenges, E., Nawroth, T., Arnold, W. & Parak, F.G. 2006. Targeting cancer cells: Magnetic nanoparticles as drug carriers. *European Biophysics Journal,* 35(5), pp.446-450.

Allen, T.M.Cullis, P.R. 2004. Drug delivery systems: Entering the mainstream. *Science (New York, N.Y.),* 303(5665), pp.1818-1822.

Ambesh, P., Campia, U., Obiagwu, C., Bansal, R., Shetty, V., Hollander, G. & Shani, J. 2017. Nanomedicine in coronary artery disease. *Indian Heart Journal,* 69(2), pp.244-251.

Arumugam, T.V., Chan, S.L., Jo, D., Yilmaz, G., Tang, S., Cheng, A., Gleichmann, M., Okun, E., Dixit, V.D. & Chigurupati, S. 2006. Gamma secretase–mediated notch signalling worsens brain damage and functional outcome in ischemic stroke. *Nature Medicine,* 12(6), pp.621.

Bacso, Z., Everson, R.B. & Eliason, J.F. 2000. The DNA of annexin V-binding apoptotic cells is highly fragmented. *Cancer Research,* 60(16), pp.4623-4628.

Bamrungsap, S., Zhao, Z., Chen, T., Wang, L., Li, C., Fu, T. & Tan, W. 2012. Nanotechnology in therapeutics: A focus on nanoparticles as a drug delivery system. *Nanomedicine,* 7(8), pp.1253-1271.

Bangs, L.B. 1996. New developments in particle-based immunoassays: Introduction. *Pure and Applied Chemistry,* 68(10), pp.1873-1879.

Barragan, P., Rieu, R., Garitey, V., Roquebert, P., Sainsous, J., Silvestri, M. & Bayet, G. 2000. Elastic recoil of coronary stents: A comparative analysis. *Catheterization and Cardiovascular Interventions,* 50(1), pp.112-119.

Barten, D.M., Meredith, J.E., Zaczek, R., Houston, J.G. & Albright, C.F. 2006. Γ-secretase inhibitors for alzheimer's disease. *Drugs in R&D,* 7(2), pp.87-97.

Bennett, M.R., Sinha, S. & Owens, G.K. 2016. Vascular smooth muscle cells in atherosclerosis. *Circulation Research,* 118(4), pp.692-702.

Bergheanu, S.C., Pons, D., Karalis, I., Özsoy, O., Verschuren, J.J., Ewing, M.M., Quax, P.H. & Jukema, J.W. 2011. Potential genetic determinants of adverse outcome after stent implantation: Results, limitations and perspectives. *Douwe Pons,* pp.21.

Bergheanu, S., Bodde, M. & Jukema, J. 2017. Pathophysiology and treatment of atherosclerosis. *Netherlands Heart Journal,* 25(4), pp.231-242.

Berne, B.Pecora, R. 2000. Dynamic light scattering. 1976. *USA, New York,*

Bhattacharjee, S. 2016. DLS and zeta potential–What they are and what they are not? *Journal of Controlled Release,* 235pp.337-351.

Bihel, F., Das, C., Bowman, M.J. & Wolfe, M.S. 2004. Discovery of a subnanomolar helical D-tridecapeptide inhibitor of γ-secretase. *Journal of Medicinal Chemistry,* 47(16), pp.3931-3933.

Bordonaro, M., Tewari, S., Atamna, W. & Lazarova, D.L. 2011. The notch ligand delta-like 1 integrates inputs from TGFbeta/activin and wnt pathways. *Experimental Cell Research,* 317(10), pp.1368-1381.

Borggrefe, T.Oswald, F. 2009. The notch signalling pathway: Transcriptional regulation at notch target genes. *Cellular and Molecular Life Sciences,* 66(10), pp.1631-1646.

Boucher, J.M., Gridley, T. & Liaw, L. 2012. Molecular pathways of notch signalling in vascular smooth muscle cells. *Frontiers in Physiology,* 3pp.81.

Boucher, J.M., Peterson, S.M., Urs, S., Zhang, C. & Liaw, L. 2011. The miR-143/145 cluster is a novel transcriptional target of jagged-1/notch signalling in vascular smooth muscle cells. *The Journal of Biological Chemistry,* 286(32), pp.28312-28321.

Boudi, B., Ahsan III, C., Compton, S. & Subhi, Y. 2013. Coronary artery atherosclerosis. *Medscape Reference,*

Brown, J., Pusey, P., Goodwin, J. & Ottewill, R. 1975. Light scattering study of dynamic and time-averaged correlations in dispersions of charged particles. *Journal of Physics A: Mathematical and General,* 8(5), pp.664.

Buccheri, D., Piraino, D., Andolina, G. & Cortese, B. 2016. Understanding and managing in-stent restenosis: A review of clinical data, from pathogenesis to treatment. *Journal of Thoracic Disease,* 8(10), pp.E1150-E1162.

Campos, A.H., Wang, W., Pollman, M.J. & Gibbons, G.H. 2002. Determinants of notch-3 receptor expression and signalling in vascular smooth muscle cells: Implications in cell-cycle regulation. *Circulation Research,* 91(11), pp.999-1006.

Caolo, V., Schulten, H.M., Zhuang, Z.W., Murakami, M., Wagenaar, A., Verbruggen, S., Molin, D.G. & Post, M.J. 2011. Soluble jagged-1 inhibits neointima formation by attenuating notch-Herp2 signalling. *Arteriosclerosis, Thrombosis, and Vascular Biology,* 31(5), pp.1059-1065.

Ceylan, H., Tekinay, A.B. & Guler, M.O. 2011. Selective adhesion and growth of vascular endothelial cells on bioactive peptide nanofiber functionalized stainless steel surface. *Biomaterials,* 32(34), pp.8797-8805.

Chadwick, K., Wang, L., Li, L., Menendez, P., Murdoch, B., Rouleau, A. & Bhatia, M. 2003. Cytokines and BMP-4 promote hematopoietic differentiation of human embryonic stem cells. *Blood,* 102(3), pp.906-915.

Chan, J.M., Rhee, J.W., Drum, C.L., Bronson, R.T., Golomb, G., Langer, R. & Farokhzad, O.C. 2011. In vivo prevention of arterial restenosis with paclitaxel-encapsulated targeted lipid-polymeric nanoparticles. *Proceedings of the National Academy of Sciences of the United States of America,* 108(48), pp.19347-19352.

Chappell, J., Harman, J.L., Narasimhan, V.M., Yu, H., Foote, K., Simons, B.D., Bennett, M.R. & Jorgensen, H.F. 2016. Extensive proliferation of a subset of differentiated, yet plastic, medial vascular smooth muscle cells contributes to neointimal formation in mouse injury and atherosclerosis models. *Circulation Research,* 119(12), pp.1313-1323.

Charles Molnar, J.G. 2015. Concepts of Biology *IN:* Anonymous

Chawla, J.S.Amiji, M.M. 2002. Biodegradable poly (ε-caprolactone) nanoparticles for tumour-targeted delivery of tamoxifen. *International Journal of Pharmaceutics,* 249(1-2), pp.127-138.

Chen, Y., Zheng, S., Qi, D., Zheng, S., Guo, J., Zhang, S. & Weng, Z. 2012. Inhibition of notch signalling by a γ-secretase inhibitor attenuates hepatic fibrosis in rats. *PloS One,* 7(10), pp.e46512.

Cherepanova, O.A., Gomez, D., Shankman, L.S., Swiatlowska, P., Williams, J., Sarmento, O.F., Alencar, G.F., Hess, D.L., Bevard, M.H. & Greene, E.S. 2016. Activation of the pluripotency factor OCT4 in smooth muscle cells is atheroprotective. *Nature Medicine,* 22(6), pp.657.

Cherng, S., Young, J. & Ma, H. 2008. HMG-CoA reductase (3-hydroxy-3-methyl-glutaryl-CoA reductase)(HMGR). *Journal of American Science,* 4(3), pp.62-64.

Chiba, S. 2006. Concise review: Notch signalling in stem cell systems. *Stem Cells,* 24(11), pp.2437-2447.

Chistiakov, D.A., Orekhov, A.N. & Bobryshev, Y.V. 2015. Extracellular vesicles and atherosclerotic disease. *Cellular and Molecular Life Sciences,* 72(14), pp.2697-2708.

Cho, K., Wang, X., Nie, S., Chen, Z.G. & Shin, D.M. 2008. Therapeutic nanoparticles for drug delivery in cancer. *Clinical Cancer Research : An Official Journal of the American Association for Cancer Research,* 14(5), pp.1310-1316.

Chorny, M., Fishbein, I., Adamo, R.F., Forbes, S.P., Folchman-Wagner, Z. & Alferiev, I.S. 2012. Magneticaly targeted delivery of therapeutic agents to injured blood vessels for prevention of in-stent restenosis. *Methodist DeBakey Cardiovascular Journal,* 8(1), pp.23-27.

Chorny, M., Fishbein, I., Danenberg, H.D. & Golomb, G. 2002. Study of the drug release mechanism from tyrphostin AG-1295-loaded nanospheres by in situ and external sink methods. *Journal of Controlled Release,* 83(3), pp.401-414.

Chorny, M., Fishbein, I., Tengood, J.E., Adamo, R.F., Alferiev, I.S. & Levy, R.J. 2013. Site-specific gene delivery to stented arteries using magnetically guided zinc oleate-based nanoparticles loaded with adenoviral vectors. *The FASEB Journal,* 27(6), pp.2198-2206.

Chorny, M., Fishbein, I., Yellen, B.B., Alferiev, I.S., Bakay, M., Ganta, S., Adamo, R., Amiji, M., Friedman, G. & Levy, R.J. 2010. Targeting stents with local delivery of paclitaxel-loaded magnetic nanoparticles using uniform fields. *Proceedings of the National Academy of Sciences,* 107(18), pp.8346-8351.

Chorny, M., Hood, E., Levy, R.J. & Muzykantov, V.R. 2010. Endothelial delivery of antioxidant enzymes loaded into non-polymeric magnetic nanoparticles. *Journal of Controlled Release,* 146(1), pp.144-151.

Chorny, M., Fishbein, I., Yellen, B.B., Alferiev, I.S., Bakay, M., Ganta, S., Adamo, R., Amiji, M., Friedman, G. & Levy, R.J. 2010a. Targeting stents with local delivery of paclitaxel-loaded magnetic nanoparticles using uniform fields. *Proceedings of the National Academy of Sciences of the United States of America,* 107(18), pp.8346-8351.

Chorny, M., Fishbein, I., Yellen, B.B., Alferiev, I.S., Bakay, M., Ganta, S., Adamo, R., Amiji, M., Friedman, G. & Levy, R.J. 2010b. Targeting stents with local delivery of paclitaxel-loaded magnetic nanoparticles using uniform fields. *Proceedings of the National Academy of Sciences of the United States of America,* 107(18), pp.8346-8351.

Cohn, W.E. 2010. Advances in surgical treatment of acute and chronic coronary artery disease. *Texas Heart Institute Journal,* 37(3), pp.328-330.

Colombo, A., Guha, S., Mackle, J.N., Cahill, P.A. & Lally, C. 2013. Cyclic strain amplitude dictates the growth response of vascular smooth muscle cells in vitro: Role in in-stent restenosis and inhibition with a sirolimus drug-eluting stent. *Biomechanics and Modeling in Mechanobiology,* 12(4), pp.671-683.

Conner, C., Ackerman, K.M., Lahne, M., Hobgood, J.S. & Hyde, D.R. 2014. Repressing notch signalling and expressing TNFalpha are sufficient to mimic retinal regeneration by inducing muller glial proliferation to generate committed progenitor cells. *The Journal of Neuroscience : The Official Journal of the Society for Neuroscience,* 34(43), pp.14403-14419.

Cooley, B.C., Nevado, J., Mellad, J., Yang, D., St Hilaire, C., Negro, A., Fang, F., Chen, G., San, H., Walts, A.D., Schwartzbeck, R.L., Taylor, B., Lanzer, J.D., Wragg, A., Elagha, A., Beltran, L.E., Berry, C., Feil, R., Virmani, R., Ladich, E., Kovacic, J.C. & Boehm, M. 2014. TGF-beta signalling mediates endothelial-to-mesenchymal transition

(EndMT) during vein graft remodelling. *Science Translational Medicine,* 6(227), pp.227ra34.

Costantini, F.Kopan, R. 2010. Patterning a complex organ: Branching morphogenesis and nephron segmentation in kidney development. *Developmental Cell,* 18(5), pp.698-712.

Crump, C. 2013. Target identification and mechanism of gamma-secretase modulators and inhibitors as Alzheier's disease theraeutics *IN:* AnonymousWeill Medical College of Cornell University,

Danenberg, H.D., Golomb, G., Groothuis, A., Gao, J., Epstein, H., Swaminathan, R.V., Seifert, P. & Edelman, E.R. 2003. Liposomal alendronate inhibits systemic innate immunity and reduces in-stent neointimal hyperplasia in rabbits. *Circulation,* 108(22), pp.2798-2804.

Danhier, F., Ansorena, E., Silva, J.M., Coco, R., Le Breton, A. & Préat, V. 2012. PLGA-based nanoparticles: An overview of biomedical applications. *Journal of Controlled Release,* 161(2), pp.505-522.

Danhier, F., Lecouturier, N., Vroman, B., Jérôme, C., Marchand-Brynaert, J., Feron, O. & Préat, V. 2009. Paclitaxel-loaded PEGylated PLGA-based nanoparticles: In vitro and in vivo evaluation. *Journal of Controlled Release,* 133(1), pp.11-17.

Davies, P.F. 2009. Hemodynamic shear stress and the endothelium in cardiovascular pathophysiology. *Nature Reviews Cardiology,* 6(1), pp.16.

Davis, C., Fischer, J., Ley, K. & Sarembock, I. 2003. The role of inflammation in vascular injury and repair. *Journal of Thrombosis and Haemostasis,* 1(8), pp.1699-1709.

Debbage, P.Jaschke, W. 2008. Molecular imaging with nanoparticles: Giant roles for dwarf actors. *Histochemistry and Cell Biology,* 130(5), pp.845-875.

Denizot, B., Tanguy, G., Hindre, F., Rump, E., Le Jeune, J.J. & Jallet, P. 1999. Phosphorylcholine coating of iron oxide nanoparticles. *Journal of Colloid and Interface Science,* 209(1), pp.66-71.

Ding, Z., Liu, S., Wang, X., Deng, X., Fan, Y., Sun, C., Wang, Y. & Mehta, J.L. 2015. Hemodynamic shear stress via ROS modulates PCSK9 expression in human vascular endothelial and smooth muscle cells and along the mouse aorta. *Antioxidants & Redox Signaling,* 22(9), pp.760-771.

Doi, H., Iso, T., Sato, H., Yamazaki, M., Matsui, H., Tanaka, T., Manabe, I., Arai, M., Nagai, R. & Kurabayashi, M. 2006. Jagged1-selective notch signalling induces smooth muscle differentiation via a RBP-jkappa-dependent pathway. *The Journal of Biological Chemistry,* 281(39), pp.28555-28564.

Domenga, V., Fardoux, P., Lacombe, P., Monet, M., Maciazek, J., Krebs, L.T., Klonjkowski, B., Berrou, E., Mericskay, M., Li, Z., Tournier-Lasserve, E., Gridley, T. &

Joutel, A. 2004. Notch3 is required for arterial identity and maturation of vascular smooth muscle cells. *Genes & Development,* 18(22), pp.2730-2735.

Dong, Y., Li, A., Wang, J., Weber, J.D. & Michel, L.S. 2010. Synthetic lethality through combined notch-epidermal growth factor receptor pathway inhibition in basal-like breast cancer. *Cancer Research,* 70(13), pp.5465-5474.

Dorans, K. 2010. Targeting drug delivery. pp.39.

Dorniani, D., Hussein, M.Z., Kura, A.U., Fakurazi, S., Shaari, A.H. & Ahmad, Z. 2012. Preparation of fe(3)O(4) magnetic nanoparticles coated with gallic acid for drug delivery. *International Journal of Nanomedicine,* 7pp.5745-5756.

Doyle, A.J., Redmond, E.M., Gillespie, D.L., Knight, P.A., Cullen, J.P., Cahill, P.A. & Morrow, D.J. 2015. Differential expression of hedgehog/notch and transforming growth factor-β in human abdominal aortic aneurysms. *Journal of Vascular Surgery,* 62(2), pp.464-470.

Dressler, G. 2008. Another niche for notch. *Kidney International,* 73(11), pp.1207-1209.

Egashira, K., Nakano, K., Ohtani, K., Funakoshi, K., Zhao, G., Ihara, Y., Koga, J., Kimura, S., Tominaga, R. & Sunagawa, K. 2007. Local delivery of anti-monocyte chemoattractant protein-1 by gene-eluting stents attenuates in-stent stenosis in rabbits and monkeys. *Arteriosclerosis, Thrombosis, and Vascular Biology,* 27(12), pp.2563-2568.

Everson-Rose, S.A.Lewis, T.T. 2005. Psychosocial factors and cardiovascular diseases. *Annu.Rev.Public Health,* 26pp.469-500.

Fang, J., Nakamura, H. & Maeda, H. 2011. The EPR effect: Unique features of tumour blood vessels for drug delivery, factors involved, and limitations and augmentation of the effect. *Advanced Drug Delivery Reviews,* 63(3), pp.136-151.

Farkouh, M.E., Domanski, M., Sleeper, L.A., Siami, F.S., Dangas, G., Mack, M., Yang, M., Cohen, D.J., Rosenberg, Y. & Solomon, S.D. 2012. Strategies for multivessel revascularization in patients with diabetes. *New England Journal of Medicine,* 367(25), pp.2375-2384.

Felton, C., Karmakar, A., Gartia, Y., Ramidi, P., Biris, A.S. & Ghosh, A. 2014. Magnetic nanoparticles as contrast agents in biomedical imaging: Recent advances in iron-and manganese-based magnetic nanoparticles. *Drug Metabolism Reviews,* 46(2), pp.142-154.

Fischer, A., Schumacher, N., Maier, M., Sendtner, M. & Gessler, M. 2004. The notch target genes Hey1 and Hey2 are required for embryonic vascular development. *Genes & Development,* 18(8), pp.901-911.

Fischman, D.L., Leon, M.B., Baim, D.S., Schatz, R.A., Savage, M.P., Penn, I., Detre, K., Veltri, L., Ricci, D. & Nobuyoshi, M. 1994. A randomized comparison of coronary-stent placement and balloon angioplasty in the treatment of coronary artery disease. *New England Journal of Medicine,* 331(8), pp.496-501.

Fishbein, I., Alferiev, I., Bakay, M., Stachelek, S.J., Sobolewski, P., Lai, M., Choi, H., Chen, I.W. & Levy, R.J. 2008. Local delivery of gene vectors from bare-metal stents by use of a biodegradable synthetic complex inhibits in-stent restenosis in rat carotid arteries. *Circulation,* 117(16), pp.2096-2103.

Fitzpatrick, E., Liu, W., Alshamrani, M., Helt, J., Hakimjavadi, R., Harman, S., Olayinka, A., Burtenshaw, D., Corcoran, E. & Di Luca, M. 2018. 8 HEDGEHOG responsive stem cell ANTIGEN-1/S100β resident vascular stem cells contribute to neointimal formationa.

Forte, A., Cipollaro, M., Cascino, A. & Galderisi, U. 2007. Pathophysiology of stem cells in restenosis. *Histology and Histopathology,* 22(4/6), pp.547.

Fox, E. 2014. Stable colloids of magnetic nanoparticles and nanoparticle assemblies with controlled size and magnetic resonance properties.

Fruchart, J.C., Nierman, M.C., Stroes, E.S., Kastelein, J.J. & Duriez, P. 2004. New risk factors for atherosclerosis and patient risk assessment. *Circulation,* 109(23 Suppl 1), pp.III15-9.

Fukuda, D., Aikawa, E., Swirski, F.K., Novobrantseva, T.I., Kotelianski, V., Gorgun, C.Z., Chudnovskiy, A., Yamazaki, H., Croce, K., Weissleder, R., Aster, J.C., Hotamisligil, G.S., Yagita, H. & Aikawa, M. 2012. Notch ligand delta-like 4 blockade attenuates atherosclerosis and metabolic disorders. *Proceedings of the National Academy of Sciences of the United States of America,* 109(27), pp.E1868-77.

Gangwar, M., Singh, R., Goel, R. & Nath, G. 2012. Recent advances in various emerging vescicular systems: An overview. *Asian Pacific Journal of Tropical Biomedicine,* 2(2), pp.S1176-S1188.

Gould, K.L., Johnson, N.P., Bateman, T.M., Beanlands, R.S., Bengel, F.M., Bober, R., Camici, P.G., Cerqueira, M.D., Chow, B.J. & Di Carli, M.F. 2013. Anatomic versus physiologic assessment of coronary artery disease: Role of coronary flow reserve, fractional flow reserve, and positron emission tomography imaging in revascularization decision-making. *Journal of the American College of Cardiology,* 62(18), pp.1639-1653.

Govender, T., Stolnik, S., Garnett, M.C., Illum, L. & Davis, S.S. 1999. PLGA nanoparticles prepared by nanoprecipitation: Drug loading and release studies of a water-soluble drug. *Journal of Controlled Release,* 57(2), pp.171-185.

GRANGE, R.W., Isotani, E., LAU, K.S., KAMM, K.E., HUANG, P.L. & STULL, J.T. 2001. Nitric oxide contributes to vascular smooth muscle relaxation in contracting fast-twitch muscles. *Physiological Genomics,* 5(1), pp.35-44.

Gridley, T. 2010. Notch signalling in the vasculature *IN:* Anonymous*Current topics in developmental biology.* Elsevier, pp.277-309.

Groth, C.Fortini, M.E. 2012. Therapeutic approaches to modulating Notch signalling: current challenges and future prospects *IN:* Anonymous*Seminars in cell & developmental biology.* Elsevier, pp.465-472.

Guagliumi, G., Sirbu, V., Musumeci, G., Gerber, R., Biondi-Zoccai, G., Ikejima, H., Ladich, E., Lortkipanidze, N., Matiashvili, A. & Valsecchi, O. 2012. Examination of the in vivo mechanisms of late drug-eluting stent thrombosis: findings from optical coherence tomography and intravascular ultrasound imaging. *JACC: Cardiovascular Interventions,* 5(1), pp.12-20.

Gummert, J.F., Opfermann, U., Jacobs, S., Walther, T., Kempfert, J., Mohr, F.W. & Falk, V. 2007. Anastomotic devices for coronary artery bypass grafting: Technological options and potential pitfalls. *Computers in Biology and Medicine,* 37(10), pp.1384-1393.

Gupta, A.K.Gupta, M. 2005. Synthesis and surface engineering of iron oxide nanoparticles for biomedical applications. *Biomaterials,* 26(18), pp.3995-4021.

Habara, S., Kadota, K., Shimada, T., Ohya, M., Amano, H., Izawa, Y., Kubo, S., Hyodo, Y., Otsuru, S. & Hasegawa, D. 2015. Late restenosis after paclitaxel-coated balloon angioplasty occurs in patients with drug-eluting stent restenosis. *Journal of the American College of Cardiology,* 66(1), pp.14-22.

Hahn, A.W., Resink, T.J., Kern, F. & Buhler, F.R. 1992. Effects of endothelin-1 on vascular smooth muscle cell phenotypic differentiation. *Journal of Cardiovascular Pharmacology,* 20 Suppl 12pp.S33-6.

Hansson, G.K. 2005. Inflammation, atherosclerosis, and coronary artery disease. *New England Journal of Medicine,* 352(16), pp.1685-1695.

Herring, B.P., Hoggatt, A.M., Burlak, C. & Offermanns, S. 2014. Previously differentiated medial vascular smooth muscle cells contribute to neointima formation following vascular injury. *Vascular Cell,* 6(1), pp.1.

Hirsch, A.T., Criqui, M.H., Treat-Jacobson, D., Regensteiner, J.G., Creager, M.A., Olin, J.W., Krook, S.H., Hunninghake, D.B., Comerota, A.J. & Walsh, M.E. 2001. Peripheral arterial disease detection, awareness, and treatment in primary care. *Jama,* 286(11), pp.1317-1324.

Hiruta, N., Maezawa, Y., Uchida, Y., Maezawa, Y. & Uchida, Y. 2013. Smooth muscle-like cells resident in the media participate in spasm-induced coronary intimal hyperplasia. *Experimental and Clinical Cardiology,* 18(1), pp.e65-70.

Ho, M., Chen, C., Wang, C., Chang, S., Hsieh, M., Lee, C., Wu, V. & Hsieh, I. 2016. The development of coronary artery stents: From bare-metal to bio-resorbable types. *Metals,* 6(7), pp.168.

Holčapek, M., Kolářová, L. & Nobilis, M. 2008. High-performance liquid chromatography-tandem mass spectrometry in the identification and determination of phase I and phase II drug metabolites. *Analytical and Bioanalytical Chemistry,* 391(1), pp.59-78.

Hoo, C.M., Starostin, N., West, P. & Mecartney, M.L. 2008. A comparison of atomic force microscopy (AFM) and dynamic light scattering (DLS) methods to characterize nanoparticle size distributions. *Journal of Nanoparticle Research,* 10(1), pp.89-96.

Hood, E. 2004. Nanotechnology: Looking as we leap. *Environmental Health Perspectives,* 112(13), pp.A740-9.

Hu, T., Yang, J., Cui, K., Rao, Q., Yin, T., Tan, L., Zhang, Y., Li, Z. & Wang, G. 2015. Controlled slow-release drug-eluting stents for the prevention of coronary restenosis: Recent progress and future prospects. *ACS Applied Materials & Interfaces,* 7(22), pp.11695-11712.

Hu, Y., Davison, F., Zhang, Z. & Xu, Q. 2003. Endothelial replacement and angiogenesis in arteriosclerotic lesions of allografts are contributed by circulating progenitor cells. *Circulation,* 108(25), pp.3122-3127.

Hua, X., Tan, S., Bandara, H., Fu, Y., Liu, S. & Smyth, H.D. 2014. Externally controlled triggered-release of drug from PLGA micro and nanoparticles. *PloS One,* 9(12), pp.e114271.

Huang, N.F.Li, S. 2008. Mesenchymal stem cells for vascular regeneration.

Huang, X.Brazel, C.S. 2001. On the importance and mechanisms of burst release in matrix-controlled drug delivery systems. *Journal of Controlled Release,* 73(2-3), pp.121-136.

Ikedo, H., Tamaki, K., Ueda, S., Kato, S., Fujii, M., Ten Dijke, P. & Okuda, S. 2003. Smad protein and TGF-β signalling in vascular smooth muscle cells. *International Journal of Molecular Medicine,* 11(5), pp.645-650.

Inoue, T.Node, K. 2009. Molecular basis of restenosis and novel issues of drug-eluting stents. *Circulation Journal,* pp.0903120300-0903120300.

Intengan, H.D.Schiffrin, E.L. 2001. Vascular remodelling in hypertension: Roles of apoptosis, inflammation, and fibrosis. *Hypertension (Dallas, Tex.: 1979),* 38(3 Pt 2), pp.581-587.

Iso, T., Hamamori, Y. & Kedes, L. 2003. Notch signalling in vascular development. *Arteriosclerosis, Thrombosis, and Vascular Biology,* 23(4), pp.543-553.

Jarzyna, P.A., Skajaa, T., Gianella, A., Cormode, D.P., Samber, D.D., Dickson, S.D., Chen, W., Griffioen, A.W., Fayad, Z.A. & Mulder, W.J. 2009. Iron oxide core oil-in-water emulsions as a multifunctional nanoparticle platform for tumour targeting and imaging. *Biomaterials,* 30(36), pp.6947-6954.

Jeromel, M., Milosevic, Z., Kocijancic, I., Lovric, D., Svigelj, V. & Zvan, B. 2013. Mechanical revascularization for acute ischemic stroke: A single-center, retrospective analysis. *Cardiovascular and Interventional Radiology,* 36(2), pp.338-345.

Jia, Y., Yuan, M., Yuan, H., Huang, X., Sui, X., Cui, X., Tang, F., Peng, J., Chen, J., Lu, S., Xu, W., Zhang, L. & Guo, Q. 2012. Co-encapsulation of magnetic Fe_3O_4 nanoparticles and doxorubicin into biodegradable PLGA nanocarriers for intratumoral drug delivery. *International Journal of Nanomedicine,* 7pp.1697-1708.

Jiang, L., Zhang, X., Du, P. & Zheng, J. 2011. Γ-secretase inhibitor, DAPT inhibits self-renewal and stemness maintenance of ovarian cancer stem-like cells in vitro. *Chinese Journal of Cancer Research,* 23(2), pp.140-146.

Jiang, J., Miao, Y., Xiao, S., Zhang, Z. & Hu, Z. 2014. DAPT in the control of human hair follicle stem cell proliferation and differentiation. *Postepy Dermatologii i Alergologii,* 31(4), pp.201-206.

Joner, M., Nakazawa, G., Finn, A.V., Quee, S.C., Coleman, L., Acampado, E., Wilson, P.S., Skorija, K., Cheng, Q. & Xu, X. 2008a. Endothelial cell recovery between comparator polymer-based drug-eluting stents. *Journal of the American College of Cardiology,* 52(5), pp.333-342.

Joner, M., Morimoto, K., Kasukawa, H., Steigerwald, K., Merl, S., Nakazawa, G., John, M.C., Finn, A.V., Acampado, E., Kolodgie, F.D., Gold, H.K. & Virmani, R. 2008b. Site-specific targeting of nanoparticle prednisolone reduces in-stent restenosis in a rabbit model of established atheroma. *Arteriosclerosis, Thrombosis, and Vascular Biology,* 28(11), pp.1960-1966.

Jordan, A., Scholz, R., Maier-Hauff, K., Johannsen, M., Wust, P., Nadobny, J., Schirra, H., Schmidt, H., Deger, S. & Loening, S. 2001. Presentation of a new magnetic field therapy system for the treatment of human solid tumours with magnetic fluid hyperthermia. *Journal of Magnetism and Magnetic Materials,* 225(1-2), pp.118-126.

Jovanovic, V.P., Sauer, C.M., Shawber, C.J., Gomez, R., Wang, X., Sauer, M.V., Kitajewski, J. & Zimmermann, R.C. 2013. Intraovarian regulation of gonadotropin-dependent folliculogenesis depends on notch receptor signalling pathways not involving delta-like ligand 4 (Dll4). *Reproductive Biology and Endocrinology,* 11(1), pp.43.

Jurgons, R., Seliger, C., Hilpert, A., Trahms, L., Odenbach, S. & Alexiou, C. 2006. Drug loaded magnetic nanoparticles for cancer therapy. *Journal of Physics: Condensed Matter,* 18(38), pp.S2893.

Kalampogias, A., Siasos, G., Oikonomou, E., Tsalamandris, S., Mourouzis, K., Tsigkou, V., Vavuranakis, M., Zografos, T., Deftereos, S. & Stefanadis, C. 2016. Basic mechanisms in atherosclerosis: The role of calcium. *Medicinal Chemistry,* 12(2), pp.103-113.

Kalanuria, A.A., Nyquist, P. & Ling, G. 2012. The prevention and regression of atherosclerotic plaques: Emerging treatments. *Vascular Health and Risk Management,* 8pp.549-561.

Kandaswamy, E.Zuo, L. 2018. Recent advances in treatment of coronary artery disease: Role of science and technology. *International Journal of Molecular Sciences,* 19(2), pp.424.

Kasaoka, S., Tobis, J.M., Akiyama, T., Reimers, B., Di Mario, C., Wong, N.D. & Colombo, A. 1998. Angiographic and intravascular ultrasound predictors of in-stent restenosis. *Journal of the American College of Cardiology,* 32(6), pp.1630-1635.

Khan, W., Farah, S. & Domb, A.J. 2012. Drug-eluting stents: Developments and current status. *Journal of Controlled Release,* 161(2), pp.703-712.

Klein, D. 2018. iPSCs-based generation of vascular cells: Reprogramming approaches and applications. *Cellular and Molecular Life Sciences,* pp.1-23.

Klein, A.M.Simons, B.D. 2011. Universal patterns of stem cell fate in cycling adult tissues. *Development (Cambridge, England),* 138(15), pp.3103-3111.

Knoblich, J.A. 2008. Mechanisms of asymmetric stem cell division. *Cell,* 132(4), pp.583-597.

Kobayashi, N., Yasu, T., Ueba, H., Sata, M., Hashimoto, S., Kuroki, M., Saito, M. & Kawakami, M. 2004. Mechanical stress promotes the expression of smooth muscle-like properties in marrow stromal cells. *Experimental Hematology,* 32(12), pp.1238-1245.

Komiyama, H., Takano, M., Hata, N., Seino, Y., Shimizu, W. & Mizuno, K. 2015. Neoatherosclerosis: Coronary stents seal atherosclerotic lesions but result in making a new problem of atherosclerosis. *World Journal of Cardiology,* 7(11), pp.776-783.

Kommineni, N., Saka, R., Khan, W. & Domb, A.J. 2018. Non-polymer drug-eluting coronary stents. *Drug Delivery and Translational Research,* 8(4), pp.903-917.

Kovacic, J.C., Mercader, N., Torres, M., Boehm, M. & Fuster, V. 2012. Epithelial-to-mesenchymal and endothelial-to-mesenchymal transition: From cardiovascular development to disease. *Circulation,* 125(14), pp.1795-1808.

Kovall, R.A., Gebelein, B., Sprinzak, D. & Kopan, R. 2017. The canonical notch signalling pathway: Structural and biochemical insights into shape, sugar, and force. *Developmental Cell,* 41(3), pp.228-241.

Kovtonyuk, L.V., Manz, M.G. & Takizawa, H. 2016. Enhanced thrombopoietin but not G-CSF receptor stimulation induces self-renewing hematopoietic stem cell divisions in vivo. *Blood,* 127(25), pp.3175-3179.

Kraemer, R.R., Francois, M. & Castracane, V.D. 2012. Estrogen mediation of hormone responses to exercise. *Metabolism,* 61(10), pp.1337-1346.

Kramann, R., Goettsch, C., Wongboonsin, J., Iwata, H., Schneider, R.K., Kuppe, C., Kaesler, N., Chang-Panesso, M., Machado, F.G. & Gratwohl, S. 2016. Adventitial MSC-like cells are progenitors of vascular smooth muscle cells and drive vascular calcification in chronic kidney disease. *Cell Stem Cell,* 19(5), pp.628-642.

Kurpinski, K., Lam, H., Chu, J., Wang, A., Kim, A., Tsay, E., Agrawal, S., Schaffer, D.V. & Li, S. 2010a. Transforming growth factor-β and notch signalling mediate stem cell differentiation into smooth muscle cells. *Stem Cells,* 28(4), pp.734-742.

Kurpinski, K., Lam, H., Chu, J., Wang, A., Kim, A., Tsay, E., Agrawal, S., Schaffer, D.V. & Li, S. 2010b. Transforming growth factor-β and notch signalling mediate stem cell differentiation into smooth muscle cells. *Stem Cells,* 28(4), pp.734-742.

Kzhyshkowska, J., Neyen, C. & Gordon, S. 2012. Role of macrophage scavenger receptors in atherosclerosis. *Immunobiology,* 217(5), pp.492-502.

Lanao, R.P.F., Jonker, A.M., Wolke, J.G., Jansen, J.A., van Hest, J.C. & Leeuwenburgh, S.C. 2013. Physicochemical properties and applications of poly (lactic-co-glycolic acid) for use in bone regeneration. *Tissue Engineering Part B: Reviews,* 19(4), pp.380-390.

Langer, R. 1990. New methods of drug delivery. *Science (New York, N.Y.),* 249(4976), pp.1527-1533.

Lanz, T.A., Karmilowicz, M.J., Wood, K.M., Pozdnyakov, N., Du, P., Piotrowski, M.A., Brown, T.M., Nolan, C.E., Richter, K.E., Finley, J.E., Fei, Q., Ebbinghaus, C.F., Chen, Y.L., Spracklin, D.K., Tate, B., Geoghegan, K.F., Lau, L.F., Auperin, D.D. & Schachter, J.B. 2006. Concentration-dependent modulation of amyloid-beta in vivo and in vitro using the gamma-secretase inhibitor, LY-450139. *The Journal of Pharmacology and Experimental Therapeutics,* 319(2), pp.924-933.

Laurent, S., Forge, D., Port, M., Roch, A., Robic, C., Vander Elst, L. & Muller, R.N. 2008. Magnetic iron oxide nanoparticles: Synthesis, stabilization, vectorization, physicochemical characterizations, and biological applications. *Chemical Reviews,* 108(6), pp.2064-2110.

Lee, B., Ryu, S. & Cui, J. 1999. Controlled release of dual drug-loaded hydroxypropyl methylcellulose matrix tablet using drug-containing polymeric coatings. *International Journal of Pharmaceutics,* 188(1), pp.71-80.

Lee, C.W., Simin, K., Liu, Q., Plescia, J., Guha, M., Khan, A., Hsieh, C. & Altieri, D.C. 2008. A functional notch–survivin gene signature in basal breast cancer. *Breast Cancer Research,* 10(6), pp.R97.

Lee, D.E., Ayoub, N. & Agrawal, D.K. 2016. Mesenchymal stem cells and cutaneous wound healing: Novel methods to increase cell delivery and therapeutic efficacy. *Stem Cell Research & Therapy,* 7(1), pp.1.

Lee, M.S., Tarantini, G., Xhaxho, J., Yang, T., Ehdaie, A., Bhatia, R., Favaretto, E. & Tobis, J. 2010. Sirolimus-versus paclitaxel-eluting stents for the treatment of cardiac allograft vasculopathy. *JACC: Cardiovascular Interventions,* 3(4), pp.378-382.

Lee, M., Kim, H.J., Kim, E., Rhee, S.B. & Moon, M.J. 1996. Effect of phase separation on ionic conductivity of poly (methyl methacrylate)-based solid polymer electrolyte. *Solid State Ionics,* 85(1-4), pp.91-98.

Lemos, P.A., Farooq, V., Takimura, C.K., Gutierrez, P.S., Virmani, R., Kolodgie, F., Christians, U., Kharlamov, A., Doshi, M. & Sojitra, P. 2013. Emerging technologies: Polymer-free phospholipid encapsulated sirolimus nanocarriers for the controlled release of drug from a stent-plus-balloon or a stand-alone balloon catheter. *EuroIntervention,* 9(1), pp.148-156.

Lewis, S.H., Salmela, H. & Obbard, D.J. 2016. Duplication and diversification of dipteran argonaute genes, and the evolutionary divergence of piwi and aubergine. *Genome Biology and Evolution,* 8(3), pp.507-518.

Li, F., Sun, J., Zhu, H., Wen, X., Lin, C. & Shi, D. 2011. Preparation and characterization novel polymer-coated magnetic nanoparticles as carriers for doxorubicin. *Colloids and Surfaces B: Biointerfaces,* 88(1), pp.58-62.

Li, X., Zhang, X., Leathers, R., Makino, A., Huang, C., Parsa, P., Macias, J., Yuan, J.X., Jamieson, S.W. & Thistlethwaite, P.A. 2009a. Notch3 signalling promotes the development of pulmonary arterial hypertension. *Nature Medicine,* 15(11), pp.1289.

Li, X., Zhang, X., Leathers, R., Makino, A., Huang, C., Parsa, P., Macias, J., Yuan, J.X., Jamieson, S.W. & Thistlethwaite, P.A. 2009b. Notch3 signalling promotes the development of pulmonary arterial hypertension. *Nature Medicine,* 15(11), pp.1289.

Li, Y., Takeshita, K., Liu, P.Y., Satoh, M., Oyama, N., Mukai, Y., Chin, M.T., Krebs, L., Kotlikoff, M.I., Radtke, F., Gridley, T. & Liao, J.K. 2009. Smooth muscle Notch1 mediates neointimal formation after vascular injury. *Circulation,* 119(20), pp.2686-2692.

Li, Y.M., Lai, M.T., Xu, M., Huang, Q., DiMuzio-Mower, J., Sardana, M.K., Shi, X.P., Yin, K.C., Shafer, J.A. & Gardell, S.J. 2000. Presenilin 1 is linked with gamma-secretase activity in the detergent-solubilized state. *Proceedings of the National Academy of Sciences of the United States of America,* 97(11), pp.6138-6143.

Lim, J., Yeap, S.P., Che, H.X. & Low, S.C. 2013. Characterization of the magnetic nanoparticle by dynamic light scattering. *Nanoscale Research Letters,* 8(1), pp.381.

Lin, C.Lue, T.F. 2013. Defining vascular stem cells. *Stem Cells and Development,* 22(7), pp.1018-1026.

Lincoff, A.M., Furst, J.G., Ellis, S.G., Tuch, R.J. & Topol, E.J. 1997. Sustained local delivery of dexamethasone by a novel intravascular eluting stent to prevent restenosis in the porcine coronary injury model. *Journal of the American College of Cardiology,* 29(4), pp.808-816.

Liu, J., Sato, C., Cerletti, M. & Wagers, A. 2010. Notch signalling in the regulation of stem cell self-renewal and differentiation *IN:* Anonymous*Current topics in developmental biology.* Elsevier, pp.367-409.

Liu, Z., Zhuge, Y. & Velazquez, O.C. 2009. Trafficking and differentiation of mesenchymal stem cells. *Journal of Cellular Biochemistry,* 106(6), pp.984-991.

Liu, Z., Turkoz, A., Jackson, E.N., Corbo, J.C., Engelbach, J.A., Garbow, J.R., Piwnica-Worms, D.R. & Kopan, R. 2011. Notch1 loss of heterozygosity causes vascular tumours and lethal hemorrhage in mice. *The Journal of Clinical Investigation,* 121(2), pp.800-808.

Livak, K.J.Schmittgen, T.D. 2001. Analysis of relative gene expression data using real-time quantitative PCR and the 2− ΔΔCT method. *Methods,* 25(4), pp.402-408.

Lloyd, R., Snyder, K., Joseph, J. & Dolan, J.W. 2010. Introduction to modern liquid chromatography *IN:* AnonymousWiley.,

Lu, A., Salabas, E.e. & Schüth, F. 2007. Magnetic nanoparticles: Synthesis, protection, functionalization, and application. *Angewandte Chemie International Edition,* 46(8), pp.1222-1244.

Lu, B., Huang, X., Mo, J. & Zhao, W. 2016. Drug delivery using nanoparticles for cancer stem-like cell targeting. *Frontiers in Pharmacology,* 7pp.84.

Lübbe, A.S., Alexiou, C. & Bergemann, C. 2001. Clinical applications of magnetic drug targeting. *Journal of Surgical Research,* 95(2), pp.200-206.

Mack, C.P. 2011. Signalling mechanisms that regulate smooth muscle cell differentiation. *Arteriosclerosis, Thrombosis, and Vascular Biology,* 31(7), pp.1495-1505.

Mackay, J.Mensah, G.A. 2004. The atlas of heart disease and stroke *IN:* AnonymousWorld Health Organization,

Mahdavi, M., Ahmad, M.B., Haron, M.J., Namvar, F., Nadi, B., Rahman, M.Z.A. & Amin, J. 2013. Synthesis, surface modification and characterisation of biocompatible magnetic iron oxide nanoparticles for biomedical applications. *Molecules,* 18(7), pp.7533-7548.

Majesky, M.W., Dong, X.R., Hoglund, V., Mahoney, W.M.,Jr & Daum, G. 2011. The adventitia: A dynamic interface containing resident progenitor cells. *Arteriosclerosis, Thrombosis, and Vascular Biology,* 31(7), pp.1530-1539.

Mäkinen, V., Civelek, M., Meng, Q., Zhang, B., Zhu, J., Levian, C., Huan, T., Segrè, A.V., Ghosh, S. & Vivar, J. 2014. Integrative genomics reveals novel molecular pathways and gene networks for coronary artery disease. *PLoS Genetics,* 10(7), pp.e1004502.

Maleki, H., Simchi, A., Imani, M. & Costa, B. 2012. Size-controlled synthesis of superparamagnetic iron oxide nanoparticles and their surface coating by gold for biomedical applications. *Journal of Magnetism and Magnetic Materials,* 324(23), pp.3997-4005.

Mamaeva, V., Rosenholm, J.M., Bate-Eya, L.T., Bergman, L., Peuhu, E., Duchanoy, A., Fortelius, L.E., Landor, S., Toivola, D.M. & Lindén, M. 2011. Mesoporous silica nanoparticles as drug delivery systems for targeted inhibition of notch signalling in cancer. *Molecular Therapy,* 19(8), pp.1538-1546.

Manabe, I.Owens, G.K. 2001. Recruitment of serum response factor and hyperacetylation of histones at smooth muscle-specific regulatory regions during differentiation of a novel p19-derived in vitro smooth muscle differentiation system. *Circulation Research,* 88(11), pp.1127-1134.

Margolis, J., McDonald, J., Heuser, R., Klinke, P., Waksman, R., Virmani, R., Desai, N. & Hilton, D. 2007. Systemic nanoparticle paclitaxel (nab-paclitaxel) for in-stent

restenosis I (SNAPIST-I): A first-in-human safety and dose-finding study. *Clinical Cardiology,* 30(4), pp.165-170.

Markides, H., Rotherham, M. & El Haj, A. 2012. Biocompatibility and toxicity of magnetic nanoparticles in regenerative medicine. *Journal of Nanomaterials,* 2012pp.13.

Marmur, J.D., Poon, M., Rossikhina, M. & Taubman, M.B. 1992. Induction of PDGF-responsive genes in vascular smooth muscle. implications for the early response to vessel injury. *Circulation,* 86(6 Suppl), pp.III53-60.

Matsumura, Y.Maeda, H. 1986. A new concept for macromolecular therapeutics in cancer chemotherapy: Mechanism of tumoritropic accumulation of proteins and the antitumor agent smancs. *Cancer Research,* 46(12 Pt 1), pp.6387-6392.

McBain, S., Griesenbach, U., Xenariou, S., Keramane, A., Batich, C., Alton, E. & Dobson, J. 2008. Magnetic nanoparticles as gene delivery agents: Enhanced transfection in the presence of oscillating magnet arrays. *Nanotechnology,* 19(40), pp.405102.

McBain, S.C., Yiu, H.H. & Dobson, J. 2008. Magnetic nanoparticles for gene and drug delivery. *International Journal of Nanomedicine,* 3(2), pp.169-180.

McCall, R.L.Sirianni, R.W. 2013. PLGA nanoparticles formed by single- or double-emulsion with vitamin E-TPGS. *Journal of Visualized Experiments: JoVE,* (82):51015. doi(82), pp.51015.

Meyer, V.R. 2013. Practical high-performance liquid chromatography *IN:* AnonymousJohn Wiley & Sons,

Milano, J., McKay, J., Dagenais, C., Foster-Brown, L., Pognan, F., Gadient, R., Jacobs, R.T., Zacco, A., Greenberg, B. & Ciaccio, P.J. 2004. Modulation of notch processing by γ-secretase inhibitors causes intestinal goblet cell metaplasia and induction of genes known to specify gut secretory lineage differentiation. *Toxicological Sciences,* 82(1), pp.341-358.

Miller, R.A., Brady, J.M. & Cutright, D.E. 1977. Degradation rates of oral resorbable implants (polylactates and polyglycolates): Rate modification with changes in PLA/PGA copolymer ratios. *Journal of Biomedical Materials Research,* 11(5), pp.711-719.

Min, K.A., Shin, M.C., Yu, F., Yang, M., David, A.E., Yang, V.C. & Rosania, G.R. 2013. Pulsed magnetic field improves the transport of iron oxide nanoparticles through cell barriers. *ACS Nano,* 7(3), pp.2161-2171.

Miniati, D., Jelin, E.B., Ng, J., Wu, J., Carlson, T.R., Wu, X., Looney, M.R. & Wang, R.A. 2009. Constitutively active endothelial Notch4 causes lung arteriovenous shunts in mice. *American Journal of Physiology-Lung Cellular and Molecular Physiology,* 298(2), pp.L169-L177.

Moghimi, S.M., Hunter, A.C. & Murray, J.C. 2005. Nanomedicine: Current status and future prospects. *The FASEB Journal,* 19(3), pp.311-330.

Molina, C.A. 2010. A call to improve the selection of patients for revascularization. *Futile Recanalization in Mechanical Embolectomy Trials: A Call to Improve Selection of Patients for Revascularization,*

Mooney, C.J., Hakimjavadi, R., Fitzpatrick, E., Kennedy, E., Walls, D., Morrow, D., Redmond, E.M. & Cahill, P.A. 2015a. Hedgehog and resident vascular stem cell fate. *Stem Cells International,* 2015pp.468428.

Mooney, C.J., Hakimjavadi, R., Fitzpatrick, E., Kennedy, E., Walls, D., Morrow, D., Redmond, E.M. & Cahill, P.A. 2015b. Hedgehog and resident vascular stem cell fate. *Stem Cells International,* 2015pp.468428.

Moore, K.J.Tabas, I. 2011. Macrophages in the pathogenesis of atherosclerosis. *Cell,* 145(3), pp.341-355.

Mori, M., Miyamoto, T., Yakushiji, H., Ohno, S., Miyake, Y., Sakaguchi, T., Hattori, M., Hongo, A., Nakaizumi, A. & Ueda, M. 2012. Effects of N-[N-(3, 5-difluorophenacetyl-L-alanyl)]-S-phenylglycine t-butyl ester (DAPT) on cell proliferation and apoptosis in ishikawa endometrial cancer cells. *Human Cell,* 25(1), pp.9-15.

Morohashi, Y., Kan, T., Tominari, Y., Fuwa, H., Okamura, Y., Watanabe, N., Sato, C., Natsugari, H., Fukuyama, T., Iwatsubo, T. & Tomita, T. 2006. C-terminal fragment of presenilin is the molecular target of a dipeptidic gamma-secretase-specific inhibitor DAPT (N-[N-(3,5-difluorophenacetyl)-L-alanyl]-S-phenylglycine t-butyl ester). *The Journal of Biological Chemistry,* 281(21), pp.14670-14676.

Morrow, D., Cullen, J.P., Liu, W., Guha, S., Sweeney, C., Birney, Y.A., Collins, N., Walls, D., Redmond, E.M. & Cahill, P.A. 2009. Sonic hedgehog induces Notch target gene expression in vascular smooth muscle cells via VEGF-A. *Arteriosclerosis, Thrombosis, and Vascular Biology,* 29(7), pp.1112-1118.

Morrow, D., Guha, S., Sweeney, C., Birney, Y., Walshe, T., O'brien, C., Walls, D., Redmond, E.M. & Cahill, P.A. 2008. Notch and vascular smooth muscle cell phenotype. *Circulation Research,* 103(12), pp.1370-1382.

Morrow, D., Hatch, E., Hamm, K., Cahill, P.A. & Redmond, E.M. 2014. Flk-1/KDR mediates ethanol-stimulated endothelial cell notch signalling and angiogenic activity. *Journal of Vascular Research,* 51(4), pp.315-324.

Murdock, R.C., Braydich-Stolle, L., Schrand, A.M., Schlager, J.J. & Hussain, S.M. 2008. Characterization of nanomaterial dispersion in solution prior to in vitro exposure using dynamic light scattering technique. *Toxicological Sciences,* 101(2), pp.239-253.

Mykhaylyk, O., Antequera, Y.S., Vlaskou, D. & Plank, C. 2007. Generation of magnetic nonviral gene transfer agents and magnetofection in vitro. *Nature Protocols,* 2(10), pp.2391.

Naahidi, S., Jafari, M., Edalat, F., Raymond, K., Khademhosseini, A. & Chen, P. 2013. Biocompatibility of engineered nanoparticles for drug delivery. *Journal of Controlled Release,* 166(2), pp.182-194.

Naghavi, M., Wang, H., Lozano, R., Davis, A., Liang, X., Zhou, M., Vollset, S.E., Ozgoren, A.A., Abdalla, S. & Abd-Allah, F. 2015. Global, regional, and national age-sex specific all-cause and cause-specific mortality for 240 causes of death, 1990-2013: A systematic analysis for the global burden of disease study 2013. *Lancet,* 385(9963), pp.117-171.

Nakano, K., Egashira, K., Masuda, S., Funakoshi, K., Zhao, G., Kimura, S., Matoba, T., Sueishi, K., Endo, Y. & Kawashima, Y. 2009. Formulation of nanoparticle-eluting stents by a cationic electrodeposition coating technology: Efficient nano-drug delivery via bioabsorbable polymeric nanoparticle-eluting stents in porcine coronary arteries. *JACC: Cardiovascular Interventions,* 2(4), pp.277-283.

Nakazawa, G., Otsuka, F., Nakano, M., Vorpahl, M., Yazdani, S.K., Ladich, E., Kolodgie, F.D., Finn, A.V. & Virmani, R. 2011. The pathology of neoatherosclerosis in human coronary implants: Bare-metal and drug-eluting stents. *Journal of the American College of Cardiology,* 57(11), pp.1314-1322.

Nemenoff, R.A., Horita, H., Ostriker, A.C., Furgeson, S.B., Simpson, P.A., VanPutten, V., Crossno, J., Offermanns, S. & Weiser-Evans, M.C. 2011. SDF-1alpha induction in mature smooth muscle cells by inactivation of PTEN is a critical mediator of exacerbated injury-induced neointima formation. *Arteriosclerosis, Thrombosis, and Vascular Biology,* 31(6), pp.1300-1308.

Newman, A.A., Baylis, R.A., Hess, D.L., Griffith, S.D., Shankman, L.S., Cherepanova, O.A. & Owens, G.K. 2018. Irradiation abolishes smooth muscle investment into vascular lesions in specific vascular beds. *JCI Insight,* 3(15), pp.10.1172/jci.insight.121017. eCollection 2018 Aug 9.

Nishizawa, T., Kanter, J.E., Kramer, F., Barnhart, S., Shen, X., Vivekanandan-Giri, A., Wall, V.Z., Kowitz, J., Devaraj, S. & O'Brien, K.D. 2014. Testing the role of myeloid cell glucose flux in inflammation and atherosclerosis. *Cell Reports,* 7(2), pp.356-365.

Niwa, T., Takeuchi, H., Hino, T., Kunou, N. & Kawashima, Y. 1994. In vitro drug release behaviour of D, l-lactide/glycolide copolymer (PLGA) nanospheres with nafarelin acetate prepared by a novel spontaneous emulsification solvent diffusion method. *Journal of Pharmaceutical Sciences,* 83(5), pp.727-732.

Nordmann, G.C., Hochstoeger, T. & Keays, D.A. 2017. Magnetoreception—a sense without a receptor. *PLoS Biology,* 15(10), pp.e2003234.

Nowak, H. 2007. Magnetism in medicine: a handbook *IN:* AnonymousJohn Wiley & Sons,

Oda, T., Elkahloun, A.G., Pike, B.L., Okajima, K., Krantz, I.D., Genin, A., Piccoli, D.A., Meltzer, P.S., Spinner, N.B. & Collins, F.S. 1997. Mutations in the human Jagged1 gene are responsible for alagille syndrome. *Nature Genetics,* 16(3), pp.235.

Olsauskas-Kuprys, R., Zlobin, A. & Osipo, C. 2013a. Gamma secretase inhibitors of notch signalling. *OncoTargets and Therapy,* 6pp.943.

Olsauskas-Kuprys, R., Zlobin, A. & Osipo, C. 2013b. Gamma secretase inhibitors of notch signalling. *OncoTargets and Therapy,* 6pp.943-955.

Owens, G.K., Kumar, M.S. & Wamhoff, B.R. 2004. Molecular regulation of vascular smooth muscle cell differentiation in development and disease. *Physiological Reviews,* 84(3), pp.767-801.

P Imbimbo, B.AM Giardina, G. 2011. Γ-secretase inhibitors and modulators for the treatment of alzheimer's disease: Disappointments and hopes. *Current Topics in Medicinal Chemistry,* 11(12), pp.1555-1570.

Palekar, R. 2015. Molecularly Targeted Nanoparticles for Modulation of Inflammatory Mediators in Atherosclerosis *IN:* AnonymousWashington University in St. Louis,

Pankhurst, Q.A., Connolly, J., Jones, S. & Dobson, J. 2003. Applications of magnetic nanoparticles in biomedicine. *Journal of Physics D: Applied Physics,* 36(13), pp.R167.

Panyam, J.Labhasetwar, V. 2003. Biodegradable nanoparticles for drug and gene delivery to cells and tissue. *Advanced Drug Delivery Reviews,* 55(3), pp.329-347.

Panyam, J., Zhou, W., Prabha, S., Sahoo, S.K. & Labhasetwar, V. 2002. Rapid endo-lysosomal escape of poly (DL-lactide-co-glycolide) nanoparticles: Implications for drug and gene delivery. *The FASEB Journal,* 16(10), pp.1217-1226.

Park, S., Kang, S., Virmani, R., Nakano, M. & Ueda, Y. 2012. In-stent neoatherosclerosis: A final common pathway of late stent failure. *Journal of the American College of Cardiology,* 59(23), pp.2051-2057.

Park, H.Y., Lim, H., Yoon, Y.J., Follenzi, A., Nwokafor, C., Lopez-Jones, M., Meng, X. & Singer, R.H. 2014. Visualization of dynamics of single endogenous mRNA labelled in live mouse. *Science (New York, N.Y.),* 343(6169), pp.422-424.

Peister, A., Mellad, J.A., Larson, B.L., Hall, B.M., Gibson, L.F. & Prockop, D.J. 2004. Adult stem cells from bone marrow (MSCs) isolated from different strains of inbred mice vary in surface epitopes, rates of proliferation, and differentiation potential. *Blood,* 103(5), pp.1662-1668.

Peterson, S.M., Turner, J.E., Harrington, A., Davis-Knowlton, J., Lindner, V., Gridley, T., Vary, C.P. & Liaw, L. 2018. Notch2 and proteomic signatures in mouse neointimal lesion formation. *Arteriosclerosis, Thrombosis, and Vascular Biology,* 38(7), pp.1576-1593.

Pislaru, S.V., Harbuzariu, A., Agarwal, G., Witt AAS CVT LATG, Tyra, Gulati, R., Sandhu, N.P., Mueske AA, C., Kalra, M., Simari, R.D. & Sandhu, G.S. 2006. Magnetic forces enable rapid endothelialization of synthetic vascular grafts. *Circulation,* 114(1_supplement), pp.I-314-I-318.

Polyak, B., Fishbein, I., Chorny, M., Alferiev, I., Williams, D., Yellen, B., Friedman, G. & Levy, R.J. 2008. High field gradient targeting of magnetic nanoparticle-loaded

endothelial cells to the surfaces of steel stents. *Proceedings of the National Academy of Sciences of the United States of America,* 105(2), pp.698-703.

Portet, D., Denizot, B., Rump, E., Lejeune, J. & Jallet, P. 2001. Nonpolymeric coatings of iron oxide colloids for biological use as magnetic resonance imaging contrast agents. *Journal of Colloid and Interface Science,* 238(1), pp.37-42.

Powers, K.W., Brown, S.C., Krishna, V.B., Wasdo, S.C., Moudgil, B.M. & Roberts, S.M. 2006. Research strategies for safety evaluation of nanomaterials. part VI. characterization of nanoscale particles for toxicological evaluation. *Toxicological Sciences,* 90(2), pp.296-303.

Prijic, S.Sersa, G. 2011. Magnetic nanoparticles as targeted delivery systems in oncology. *Radiology and Oncology,* 45(1), pp.1-16.

Proweller, A., Pear, W.S. & Parmacek, M.S. 2005. Notch signalling represses myocardin-induced smooth muscle cell differentiation. *The Journal of Biological Chemistry,* 280(10), pp.8994-9004.

Puranik, A.S., Dawson, E.R. & Peppas, N.A. 2013. Recent advances in drug-eluting stents. *International Journal of Pharmaceutics,* 441(1-2), pp.665-679.

Qiao, L., Xie, L., Shi, K., Zhou, T., Hua, Y. & Liu, H. 2012. Notch signalling change in pulmonary vascular remodelling in rats with pulmonary hypertension and its implication for therapeutic intervention. *PLoS One,* 7(12), pp.e51514.

Radtke, F.Raj, K. 2003. The role of notch in tumorigenesis: Oncogene or tumour suppressor? *Nature Reviews Cancer,* 3(10), pp.756.

Raiser, D.M., Zacharek, S.J., Roach, R.R., Curtis, S.J., Sinkevicius, K.W., Gludish, D.W. & Kim, C.F. 2008. Stem cell biology in the lung and lung cancers: Using pulmonary context and classic approaches. *Cold Spring Harbor Symposia on Quantitative Biology,* 73pp.479-490.

Rajendran, P., Rengarajan, T., Thangavel, J., Nishigaki, Y., Sakthisekaran, D., Sethi, G. & Nishigaki, I. 2013. The vascular endothelium and human diseases. *International Journal of Biological Sciences,* 9(10), pp.1057-1069.

Räthel, T., Mannell, H., Pircher, J., Gleich, B., Pohl, U. & Krötz, F. 2012. Magnetic stents retain nanoparticle-bound antirestenotic drugs transported by lipid microbubbles. *Pharmaceutical Research,* 29(5), pp.1295-1307.

Redmond, E.M., Guha, S., Walls, D. & Cahill, P.A. 2011. Investigational notch and hedgehog inhibitors–therapies for cardiovascular disease. *Expert Opinion on Investigational Drugs,* 20(12), pp.1649-1664.

Redmond, E.M., Liu, W., Hamm, K., Hatch, E., Cahill, P.A. & Morrow, D. 2014. Perivascular delivery of notch 1 siRNA inhibits injury-induced arterial remodelling. *PLoS One,* 9(1), pp.e84122.

Regan, J.N. 2010. *Regulation of Adventitia-Resident Progenitor Cells,*

Renna, N.F., de las Heras, N. & Miatello, R.M. 2013. Pathophysiology of vascular remodelling in hypertension. *International Journal of Hypertension,* 2013

Revia, R.A.Zhang, M. 2016. Magnetite nanoparticles for cancer diagnosis, treatment, and treatment monitoring: Recent advances. *Materials Today,* 19(3), pp.157-168.

Rizzo, P.Ferrari, R. 2015. The notch pathway: A new therapeutic target in atherosclerosis? *European Heart Journal Supplements,* 17(suppl_A), pp.A74-A76.

Roca, C.Adams, R.H. 2007. Regulation of vascular morphogenesis by Notch signalling. *Genes & Development,* 21(20), pp.2511-2524.

Roger Véronique L, Go, A.S., Lloyd-Jones, D.M., Benjamin, E.J., Berry, J.D., Borden, W.B., Bravata, D.M., Dai, S. & Ford, E.S. 2012. Executive summary: Heart disease and stroke statistics—2012 update: A report from the american heart association. *Circulation,* 125(1), pp.188-197.

Rosen, E.D.Spiegelman, B.M. 2000. Molecular regulation of adipogenesis. *Annual Review of Cell and Developmental Biology,* 16(1), pp.145-171.

Rossant, J.Howard, L. 2002. Signalling pathways in vascular development. *Annual Review of Cell and Developmental Biology,* 18(1), pp.541-573.

Saito, N., Fu, J., Zheng, S., Yao, J., Wang, S., Liu, D.D., Yuan, Y., Sulman, E.P., Lang, F.F. & Colman, H. 2014. A high notch pathway activation predicts response to γ secretase inhibitors in proneural subtype of glioma Tumor-Initiating cells. *Stem Cells,* 32(1), pp.301-312.

Sakata, Y., Xiang, F., Chen, Z., Kiriyama, Y., Kamei, C.N., Simon, D.I. & Chin, M.T. 2004. Transcription factor CHF1/Hey2 regulates neointimal formation in vivo and vascular smooth muscle proliferation and migration in vitro. *Arteriosclerosis, Thrombosis, and Vascular Biology,* 24(11), pp.2069-2074.

Sans, S., Kesteloot, H. & Kromhout, D.o. 1997. The burden of cardiovascular diseases mortality in europe: Taskforce of the european society of cardiology on cardiovascular mortality and morbidity statistics in europe. *European Heart Journal,* 18(8), pp.1231-1248.

Segev, A., Aviezer, D., Safran, M., Gross, Z. & Yayon, A. 2002. Inhibition of vascular smooth muscle cell proliferation by a novel fibroblast growth factor receptor antagonist. *Cardiovascular Research,* 53(1), pp.232-241.

Seo, D., Southard, K.M., Kim, J., Lee, H.J., Farlow, J., Lee, J., Litt, D.B., Haas, T., Alivisatos, A.P. & Cheon, J. 2016. A mechanogenetic toolkit for interrogating cell signalling in space and time. *Cell,* 165(6), pp.1507-1518.

Serruys, P.W., de Jaegere, P., Kiemeneij, F., Macaya, C., Rutsch, W., Heyndrickx, G., Emanuelsson, H., Marco, J., Legrand, V. & Materne, P. 1994. A comparison of balloon-

expandable-stent implantation with balloon angioplasty in patients with coronary artery disease. *New England Journal of Medicine,* 331(8), pp.489-495.

Shah, M.M., Zerlin, M., Li, B.Y., Herzog, T.J., Kitajewski, J.K. & Wright, J.D. 2013. The role of notch and gamma-secretase inhibition in an ovarian cancer model. *Anticancer Research,* 33(3), pp.801-808.

Shahriyari, L.Komarova, N.L. 2013. Symmetric vs. asymmetric stem cell divisions: An adaptation against cancer? *PloS One,* 8(10), pp.e76195.

Sharif, F., Hynes, S.O., Cooney, R., Howard, L., McMahon, J., Daly, K., Crowley, J., Barry, F. & O'brien, T. 2008. Gene-eluting stents: Adenovirus-mediated delivery of eNOS to the blood vessel wall accelerates re-endothelialization and inhibits restenosis. *Molecular Therapy,* 16(10), pp.1674-1680.

Sheiban, I., Villata, G., Bollati, M., Sillano, D., Lotrionte, M. & Biondi-Zoccai, G. 2008. Next-generation drug-eluting stents in coronary artery disease: Focus on everolimus-eluting stent (xience V). *Vascular Health and Risk Management,* 4(1), pp.31-38.

Shimizu, K., Sugiyama, S., Aikawa, M., Fukumoto, Y., Rabkin, E., Libby, P. & Mitchell, R.N. 2001. Host bone-marrow cells are a source of donor intimal smooth-muscle–like cells in murine aortic transplant arteriopathy. *Nature Medicine,* 7(6), pp.738.

Simper, D., Stalboerger, P.G., Panetta, C.J., Wang, S. & Caplice, N.M. 2002. Smooth muscle progenitor cells in human blood. *Circulation,* 106(10), pp.1199-1204.

Singh, R., Artaza, J.N., Taylor, W.E., Gonzalez-Cadavid, N.F. & Bhasin, S. 2003. Androgens stimulate myogenic differentiation and inhibit adipogenesis in C3H 10T1/2 pluripotent cells through an androgen receptor-mediated pathway. *Endocrinology,* 144(11), pp.5081-5088.

Song, X., Zhao, Y., Wu, W., Bi, Y., Cai, Z., Chen, Q., Li, Y. & Hou, S. 2008. PLGA nanoparticles simultaneously loaded with vincristine sulfate and verapamil hydrochloride: Systematic study of particle size and drug entrapment efficiency. *International Journal of Pharmaceutics,* 350(1-2), pp.320-329.

Stanisławska, A. 2014. Biomaterials and implants in cardiac and vascular surgery-review. *Advances in Materials Science,* 14(3), pp.5-17.

Storm, G., Belliot, S.O., Daemen, T. & Lasic, D.D. 1995. Surface modification of nanoparticles to oppose uptake by the mononuclear phagocyte system. *Advanced Drug Delivery Reviews,* 17(1), pp.31-48.

Strutt, J.W. 1871. LVIII. on the scattering of light by small particles. *The London, Edinburgh, and Dublin Philosophical Magazine and Journal of Science,* 41(275), pp.447-454.

Sun, C., Lee, J.S. & Zhang, M. 2008. Magnetic nanoparticles in MR imaging and drug delivery. *Advanced Drug Delivery Reviews,* 60(11), pp.1252-1265.

Sun-Wada, G., Manabe, S., Yoshimizu, T., Yamaguchi, C., Oka, T., Wada, Y. & Futai, M. 2000. Upstream regions directing heart-specific expression of the GATA 6 gene during mouse early development. *The Journal of Biochemistry,* 127(4), pp.703-709.

Sweeney, C., Morrow, D., Birney, Y.A., Coyle, S., Hennessy, C., Scheller, A., Cummins, P.M., Walls, D., Redmond, E.M. & Cahill, P.A. 2004. Notch 1 and 3 receptor signalling modulates vascular smooth muscle cell growth, apoptosis, and migration via a CBF-1/RBP-jk dependent pathway. *The FASEB Journal,* 18(12), pp.1421-1423.

Tan, H., Xue, J.M., Shuter, B., Li, X. & Wang, J. 2010. Synthesis of PEOlated Fe_3O_4@ SiO2 nanoparticles via bioinspired silicification for magnetic resonance imaging. *Advanced Functional Materials,* 20(5), pp.722-731.

Tang, H., Babicheva, A., McDermott, K.M., Gu, Y., Ayon, R.J., Song, S., Wang, Z., Gupta, A., Zhou, T. & Sun, X. 2017. Endothelial HIF-2α contributes to severe pulmonary hypertension by inducing endothelial-to-mesenchymal transition. *American Journal of Physiology-Lung Cellular and Molecular Physiology,*

Tang, Z., Wang, A., Yuan, F., Yan, Z., Liu, B., Chu, J.S., Helms, J.A. & Li, S. 2012a. Differentiation of multipotent vascular stem cells contributes to vascular diseases. *Nature Communications,* 3pp.875.

Tang, Z., Wang, A., Yuan, F., Yan, Z., Liu, B., Chu, J.S., Helms, J.A. & Li, S. 2012b. Differentiation of multipotent vascular stem cells contributes to vascular diseases. *Nature Communications,* 3pp.875.

Tang, Z., Wang, A., Yuan, F., Yan, Z., Liu, B., Chu, J.S., Helms, J.A. & Li, S. 2012c. Differentiation of multipotent vascular stem cells contributes to vascular diseases. *Nature Communications,* 3pp.875.

Tang, H., Brennan, J., Karl, J., Hamada, Y., Raetzman, L. & Capel, B. 2008. Notch signalling maintains leydig progenitor cells in the mouse testis. *Development (Cambridge, England),* 135(22), pp.3745-3753.

Tang, Z., Wang, A., Wang, D. & Li, S. 2013. Smooth muscle cells: To be or not to be? response to nguyen et al. *Circulation Research,* 112(1), pp.23-26.

Tartaj, P., del Puerto Morales, M., Veintemillas-Verdaguer, S., González-Carreño, T. & Serna, C.J. 2003. The preparation of magnetic nanoparticles for applications in biomedicine. *Journal of Physics D: Applied Physics,* 36(13), pp.R182.

Taylor, S.M.Jones, P.A. 1979. Multiple new phenotypes induced in 10T12 and 3T3 cells treated with 5-azacytidine. *Cell,* 17(4), pp.771-779.

Thomas, C.R., Ferris, D.P., Lee, J., Choi, E., Cho, M.H., Kim, E.S., Stoddart, J.F., Shin, J., Cheon, J. & Zink, J.I. 2010. Noninvasive remote-controlled release of drug molecules in vitro using magnetic actuation of mechanized nanoparticles. *Journal of the American Chemical Society,* 132(31), pp.10623-10625.

Thömmes, K.B., Hoppe, J., Vetter, H. & Sachinidis, A. 1996. The synergistic effect of PDGF-AA and IGF-1 on VSMC proliferation might be explained by the differential activation of their intracellular signalling pathways. *Experimental Cell Research,* 226(1), pp.59-66.

Tomei, L.D., Shapiro, J.P. & Cope, F.O. 1993. Apoptosis in C3H/10T1/2 mouse embryonic cells: Evidence for internucleosomal DNA modification in the absence of double-strand cleavage. *Proceedings of the National Academy of Sciences of the United States of America,* 90(3), pp.853-857.

Tran, P.H., Tran, T.T., Van Vo, T. & Lee, B. 2012. Promising iron oxide-based magnetic nanoparticles in biomedical engineering. *Archives of Pharmacal Research,* 35(12), pp.2045-2061.

Ulbrich, K., Hola, K., Subr, V., Bakandritsos, A., Tucek, J. & Zboril, R. 2016. Targeted drug delivery with polymers and magnetic nanoparticles: Covalent and noncovalent approaches, release control, and clinical studies. *Chemical Reviews,* 116(9), pp.5338-5431.

van der Giessen, Willem J, Lincoff, A.M. & Schwartz, R.S. 1997. Marked inflammatory sequelae to implantation of biodegradable and nonbiodegradable polymers in porcine coronary arteries. *Journal of Vascular & Interventional Radiology,* 8(3), pp.488.

van Es, J.H.Clevers, H. 2005. Notch and wnt inhibitors as potential new drugs for intestinal neoplastic disease. *Trends in Molecular Medicine,* 11(11), pp.496-502.

van Es, J.H., van Gijn, M.E., Riccio, O., van den Born, M., Vooijs, M., Begthel, H., Cozijnsen, M., Robine, S., Winton, D.J. & Radtke, F. 2005. Notch/γ-secretase inhibition turns proliferative cells in intestinal crypts and adenomas into goblet cells. *Nature,* 435(7044), pp.959.

Vangijzegem, T., Stanicki, D. & Laurent, S. 2019. Magnetic iron oxide nanoparticles for drug delivery: Applications and characteristics. *Expert Opinion on Drug Delivery,* 16(1), pp.69-78.

Veiseh, O., Gunn, J.W. & Zhang, M. 2010. Design and fabrication of magnetic nanoparticles for targeted drug delivery and imaging. *Advanced Drug Delivery Reviews,* 62(3), pp.284-304.

Villablanca, A.C., Jayachandran, M. & Banka, C. 2010. Atherosclerosis and sex hormones: Current concepts. *Clinical Science (London, England : 1979),* 119(12), pp.493-513.

Wait, M.A. 2000. Treatment of coronary heart disease with minimally invasive surgery *IN:* Anonymous*Baylor University Medical Center Proceedings.* Taylor & Francis, pp.121-127.

Wakeyama, T., Ogawa, H., Iida, H., Takaki, A., Iwami, T., Mochizuki, M. & Tanaka, T. 2003. Intima-media thickening of the radial artery after transradial intervention: An

intravascular ultrasound study. *Journal of the American College of Cardiology,* 41(7), pp.1109-1114.

Wang, C., Cherng, W., Yang, N., Kuo, L., Hsu, C., Yeh, H., Lan, Y., Yeh, C. & Stanford, W.L. 2008. Late-outgrowth endothelial cells attenuate intimal hyperplasia contributed by mesenchymal stem cells after vascular injury. *Arteriosclerosis, Thrombosis, and Vascular Biology,* 28(1), pp.54-60.

Wang, F., Cao, Y., Ma, L., Pei, H., Rausch, W.D. & Li, H. 2018. Dysfunction of cerebrovascular endothelial cells: Prelude to vascular dementia. *Frontiers in Aging Neuroscience,* 10pp.376.

Wang, X., Wang, L., He, X., Zhang, Y. & Chen, L. 2009. A molecularly imprinted polymer-coated nanocomposite of magnetic nanoparticles for estrone recognition. *Talanta,* 78(2), pp.327-332.

Wang, Y., Wen, Q. & Choi, S. 2016. FDA's regulatory science program for generic PLA/PLGA-based drug products. *Am Pharm Rev,* 19(4), pp.5-9.

Wang, G., Jacquet, L., Karamariti, E. & Xu, Q. 2015. Origin and differentiation of vascular smooth muscle cells. *The Journal of Physiology,* 593(14), pp.3013-3030.

Waugh, A.Grant, A. 2007. Ross and Wilson: Anatomy and physiology in health and illness. (french).

Weber, C.Noels, H. 2011. Atherosclerosis: Current pathogenesis and therapeutic options. *Nature Medicine,* 17(11), pp.1410.

WHO *Cardiovascular diseases (CVDs)* [Online]. Available from: http://www.who.int/mediacentre/factsheets/fs317/en/

Wilfinger, W.W., Mackey, K. & Chomczynski, P. 1997. Effect of pH and ionic strength on the spectrophotometric assessment of nucleic acid purity. *BioTechniques,* 22(3), pp.474-481.

Williams, D.N., Ehrman, S.H. & Holoman, T.R.P. 2006. Evaluation of the microbial growth response to inorganic nanoparticles. *Journal of Nanobiotechnology,* 4(1), pp.3.

Wilson, M.W., Kerlan Jr, R.K., Fidelman, N.A., Venook, A.P., LaBerge, J.M., Koda, J. & Gordon, R.L. 2004. Hepatocellular carcinoma: Regional therapy with a magnetic targeted carrier bound to doxorubicin in a dual MR imaging/conventional angiography suite—initial experience with four patients. *Radiology,* 230(1), pp.287-293.

Wong, M.M., Winkler, B., Karamariti, E., Wang, X., Yu, B., Simpson, R., Chen, T., Margarita, A. & Xu, Q. 2013. Sirolimus stimulates vascular stem/progenitor cell migration and differentiation into smooth muscle cells via epidermal growth factor receptor/extracellular signal-regulated kinase/beta-catenin signalling pathway. *Arteriosclerosis, Thrombosis, and Vascular Biology,* 33(10), pp.2397-2406.

Woods, T.C.Marks, A.R. 2004. Drug-eluting stents. *Annu.Rev.Med.,* 55pp.169-178.

Wormuth, K. 2001. Superparamagnetic latex via inverse emulsion polymerization. *Journal of Colloid and Interface Science,* 241(2), pp.366-377.

Wu, C., Tang, Z., Jiang, L., Li, X., Jiang, Z. & Liu, L. 2012. PCSK9 siRNA inhibits HUVEC apoptosis induced by ox-LDL via bcl/Bax–caspase9–caspase3 pathway. *Molecular and Cellular Biochemistry,* 359(1-2), pp.347-358.

Wu, K., Zhang, L., Lin, Y., Yang, K. & Cheng, Y. 2014. Inhibition of γ-secretase induces G2/M arrest and triggers apoptosis in renal cell carcinoma. *Oncology Letters,* 8(1), pp.55-61.

Wu, M.Huang, S. 2017. Magnetic nanoparticles in cancer diagnosis, drug delivery and treatment. *Molecular and Clinical Oncology,* 7(5), pp.738-746.

Wu, X., Du, J., Song, W., Cao, M., Chen, S. & Xia, R. 2018. Weak power frequency magnetic fields induce microtubule cytoskeleton reorganization depending on the epidermal growth factor receptor and the calcium-related signalling. *PloS One,* 13(10), pp.e0205569.

Wu, Y., Cain-Hom, C., Choy, L., Hagenbeek, T.J., de Leon, G.P., Chen, Y., Finkle, D., Venook, R., Wu, X. & Ridgway, J. 2010. Therapeutic antibody targeting of individual Notch receptors. *Nature,* 464(7291), pp.1052.

Xu, R.N., Fan, L., Rieser, M.J. & El-Shourbagy, T.A. 2007. Recent advances in high-throughput quantitative bioanalysis by LC-MS/MS. *Journal of Pharmaceutical and Biomedical Analysis,* 44(2), pp.342-355.

Xue, G., Zippelius, A., Wicki, A., Mandalà, M., Tang, F., Massi, D. & Hemmings, B.A. 2015. Integrated Akt/PKB signalling in immunomodulation and its potential role in cancer immunotherapy. *JNCI: Journal of the National Cancer Institute,* 107(7),

Xue, Y., Gao, X., Lindsell, C.E., Norton, C.R., Chang, B., Hicks, C., Gendron-Maguire, M., Rand, E.B., Weinmaster, G. & Gridley, T. 1999. Embryonic lethality and vascular defects in mice lacking the Notch ligand Jagged1. *Human Molecular Genetics,* 8(5), pp.723-730.

Yamamoto, H., Kuno, Y., Sugimoto, S., Takeuchi, H. & Kawashima, Y. 2005. Surface-modified PLGA nanosphere with chitosan improved pulmonary delivery of calcitonin by mucoadhesion and opening of the intercellular tight junctions. *Journal of Controlled Release,* 102(2), pp.373-381.

Yang, X., Klein, R., Tian, X., Cheng, H., Kopan, R. & Shen, J. 2004. Notch activation induces apoptosis in neural progenitor cells through a p53-dependent pathway. *Developmental Biology,* 269(1), pp.81-94.

Yellen, B.B., Forbes, Z.G., Halverson, D.S., Fridman, G., Barbee, K.A., Chorny, M., Levy, R. & Friedman, G. 2005. Targeted drug delivery to magnetic implants for therapeutic applications. *Journal of Magnetism and Magnetic Materials,* 293(1), pp.647-654.

Yin, L., Velazquez, O.C. & Liu, Z. 2010. Notch signalling: Emerging molecular targets for cancer therapy. *Biochemical Pharmacology,* 80(5), pp.690-701.

Yin, R.X., Yang, D.Z. & Wu, J.Z. 2014. Nanoparticle drug- and gene-eluting stents for the prevention and treatment of coronary restenosis. *Theranostics,* 4(2), pp.175-200.

Yoo, H.S., Lee, K.H., Oh, J.E. & Park, T.G. 2000. In vitro and in vivo anti-tumour activities of nanoparticles based on doxorubicin–PLGA conjugates. *Journal of Controlled Release,* 68(3), pp.419-431.

Yu, B., Chen, Q., Le Bras, A., Zhang, L. & Xu, Q. 2018. Vascular stem/progenitor cell migration and differentiation in atherosclerosis. *Antioxidants & Redox Signaling,* 29(2), pp.219-235.

Yu, S., Zhang, R., Liu, F., Wang, H., Wu, J. & Wang, Y. 2012. Notch inhibition suppresses nasopharyngeal carcinoma by depleting cancer stem-like side population cells. *Oncology Reports,* 28(2), pp.561-566.

Yuan, F., Wang, D., Xu, K., Wang, J., Zhang, Z., Yang, L., Yang, G. & Li, S. 2017. Contribution of vascular cells to neointimal formation. *PloS One,* 12(1), pp.e0168914.

Yuan, X., Wu, H., Xu, H., Xiong, H., Chu, Q., Yu, S., Wu, G.S. & Wu, K. 2015. Notch signalling: An emerging therapeutic target for cancer treatment. *Cancer Letters,* 369(1), pp.20-27.

Zavadil, J., Cermak, L., Soto-Nieves, N. & Bottinger, E.P. 2004. Integration of TGF-beta/Smad and Jagged1/notch signalling in epithelial-to-mesenchymal transition. *The EMBO Journal,* 23(5), pp.1155-1165.

Zhang, L., Gu, F., Chan, J., Wang, A., Langer, R. & Farokhzad, O. 2008. Nanoparticles in medicine: Therapeutic applications and developments. *Clinical Pharmacology & Therapeutics,* 83(5), pp.761-769.

Zhou, Y., He, C., Chen, K., Ni, J., Cai, Y., Guo, X. & Wu, X.Y. 2016. A new method for evaluating actual drug release kinetics of nanoparticles inside dialysis devices via numerical deconvolution. *Journal of Controlled Release,* 243pp.11-20.